Systems analysis of the host response to *Clostridium difficile* toxins

A Dissertation

presented to the faculty of the School of Engineering and Applied Science
in partial fullfillment of the requirements for the degree of

Doctor of Philosophy

by Kevin Michael D'Auria

May 2014

Department of Biomedical Engineering
University *of* Virginia

APPROVAL SHEET

This dissertation is in partial fulfillment of the requirements for the degree of Doctor of Philosophy in Biomedical Engineering

Kevin Michael D'Auria
Author

This dissertation has been read and approved by the examining committee:

Jason Papin, Ph.D.
Dissertation Advisor
Department of Biomedical Engineering

Shayn Peirce-Cottler, Ph.D.
Committee Chair
Department of Biomedical Engineering

Erik Hewlett, M.D.
Committee Member, Division of Infectious Diseases and International Health

Alison Criss, Ph.D.
Committee Member
Department of Microbiology

Kevin Janes, Ph.D.
Committee Member
Department of Biomedical Engineering

Accepted for the School of Engineering and Applied Science:

James H. Ayl

Jaymes H. Aylor, Ph.D.
Dean, School of Engineering and Applied Science

Contents

Acknowledgements **xi**

Preface **xiii**

0.1 Me, a biomedical engineer . . . xiii
0.2 Me, a computational systems biologist . . . xiii
0.3 My dissertation as systems biologist . . . xiv

1 Introduction **1**

1.1 Abstract . . . 1
1.2 A preview of this dissertation . . . 2

2 Choosing transcriptomics analyses **4**

2.1 Background . . . 4
2.1.1 mRNA as a measure of cell state . . . 4
2.1.2 Measuring mRNA levels with microarrays . . . 5
2.2 Microarray preprocessing . . . 6
2.2.1 Steps of data preprocessing . . . 6
2.3 Choosing preprocessing techniques . . . 8
2.3.1 What are the best preprocessing steps? . . . 8
2.3.2 Which workflow do I use? . . . 12
2.4 Differential expression . . . 12
2.4.1 Types of statistical tests . . . 13
2.4.2 What test should I use? . . . 16
2.5 Caveats of microarrays and alternatives . . . 17
2.6 Reproducibile analyses . . . 17
2.6.1 Why bother? . . . 17
2.6.2 Are microarrays reproducible? . . . 18
2.7 Transcriptomics analyses in this dissertation . . . 19

3 miRNA Transcriptomics of melanoma **20**

3.1 Motivation . . . 20
3.2 Introduction . . . 21
3.3 Methods . . . 22
3.3.1 miRNA quantification . . . 22
3.4 Results . . . 23
3.4.1 miRNA expression of all samples . . . 23
3.4.2 miRNA expression changes after treatment . . . 25
3.4.3 Different miRNA expression changes between responders and non-responders 25

3.5 Conclusions . . . 28

4 Functional transcriptomics of toxin response 29
4.1 *C. difficile*: a dangerous pathogen . . . 30
4.1.1 Historical significance . . . 30
4.1.2 Toxin molecular biology . . . 31
4.1.3 Physiological toxin responses . . . 31
4.2 Functional transcriptomics: enrichment . . . 32
4.2.1 Gene set enrichment analysis . . . 33

5 Toxins A and B disrupt the cell cycle 35
5.1 Synopsis . . . 35
5.2 Background . . . 36
5.3 Methods . . . 37
5.3.1 Cell Culture . . . 37
5.3.2 Microarrays . . . 37
5.3.3 Flow Cytometry . . . 38
5.3.4 Quantitative real time PCR . . . 39
5.3.5 Western Blots . . . 39
5.4 Results . . . 40
5.4.1 Transcriptional Responses . . . 40
5.4.2 Functions associated with differentially expressed genes . . . 42
5.4.3 Effects of TcdA and TcdB on the Regulation of Cell Cycle . . . 47
5.5 Discussion . . . 50
5.6 Conclusion . . . 52
5.7 Acknowledgements . . . 52

6 In vivo toxin responses 53
6.1 From in vitro to in vivo host responses . . . 53
6.2 Synopsis . . . 54
6.3 Introduction . . . 54
6.4 Methods . . . 57
6.4.1 Cecal injection . . . 57
6.4.2 Cell culture . . . 58
6.4.3 Blood counts . . . 58
6.4.4 Histology . . . 58
6.4.5 Isolation of cells from cecal tissue . . . 59
6.4.6 Flow cytometry . . . 59
6.4.7 Antibody-mediated neutralization of chemokines . . . 59
6.4.8 Microarray procedure . . . 60
6.4.9 Statistical analysis . . . 60
6.4.10 Microarray preprocessing . . . 60
6.4.11 Determining differentially expressed genes . . . 61
6.4.12 Gene set enrichment . . . 62
6.4.13 Cytopathic effects on a mouse, cecal, epithelial cell line . . . 64
6.5 Results . . . 65
6.5.1 Dose-response to TcdA cecal injection . . . 65
6.5.2 Survival after cecal injection . . . 66

6.5.3 Physiological results of toxin cecal injection 66
6.5.4 Host transcription altered by toxin injection 69
6.5.5 Comparisons of gene and protein expression of cytokines 78
6.5.6 CXCL1 and CXCL2 neutralization alters the host response to TcdA cecal injection 80
6.5.7 *In vivo* transcriptome response *versus in vitro* transcriptome and proteome responses 82
6.6 Discussion 84
6.7 Acknowledgements 89

7 Responses of multiple cell types 91
7.1 From transcriptomics of the epithelial-layer to the roles of different cell types in the epithelial layer 91
7.2 Synopsis 92
7.3 Introduction 93
7.4 Methods 95
7.4.1 Cell Culture 95
7.4.2 Electrical impedance assay 95
7.4.3 Analyses 96
7.5 Results 96
7.5.1 Quantification of the cytopathic effects elicited by TcdA and TcdB 96
7.5.2 Epithelial and endothelial cells: similar characteristic responses but different sensitivities to TcdA and TcdB 98
7.5.3 Macrophages: rapid, sensitive, complex concentration-dependent responses to TcdA and TcdB 99
7.5.4 Glucosyltransferase-deficient TcdB alters the effects of TcdA and TcdB on macrophages and epithelial cells 100
7.6 Discussion 104
7.7 Acknowledgements 109

8 Multi-well time course analyses 110
8.1 Concise annotation of multiple wells 110
8.2 Selecting and modifying wells 111
8.3 Visualization 113
8.4 Independent wells 114
8.5 Data transformations 115
8.6 Interpolation and smoothers 117
8.7 Custom metrics 119
8.8 Future plans 121

9 Future directions: toxin responses and metabolism 122
9.1 Toxins alter expression of many metabolic genes 122
9.2 Integrating and visualizing transcriptional changes within a metabolic network . . . 122
9.3 Synopsis 123
9.4 Glossary 123
9.5 Systems biology and pathogen metabolism 126
9.6 Reconstructing metabolic networks 129
9.7 Drug targets in metabolic networks 136

9.7.1 Metabolite essentiality . . . 140
9.7.2 Combination gene and reaction perturbations . . . 140
9.7.3 Groups of targets and network topology . . . 141
9.7.4 Environment and conditional essentiality . . . 141
9.8 From target to drug and the development of model guided pipelines for drug discovery 142
9.9 A host cell perspective . . . 143
9.10 Next steps . . . 145
9.11 Concluding remarks . . . 146
9.12 Acknowledgements . . . 147

Appendices **181**

A Reproducing in vivo analyses **182**
A.1 Introduction . . . 182
A.2 Preparing software, files, and folders . . . 182
A.2.1 Directory structure . . . 182
A.2.2 R and R packages . . . 183
A.2.3 Downloading the microarray data . . . 183
A.3 Loading and organizing microarray data . . . 183
A.4 Preprocessing microarray data . . . 184
A.5 Microarray and gene annotation . . . 184
A.5.1 Background . . . 184
A.5.2 Annotation sources . . . 185
A.5.3 Generating annotation lists in R . . . 186
A.5.4 Transitive mapping . . . 188
A.5.5 Many probes to many genes mapping . . . 189
A.6 Analyzing differential expression . . . 190
A.7 Gene set enrichment . . . 191
A.7.1 Competitive . . . 191
A.7.2 Self-contained . . . 192
A.8 Analysis of previous *in vitro* data . . . 193
A.9 Comparisons to other transcriptomic and proteomic data . . . 193
A.10 Cytotoxicity assay . . . 194
A.11 Scripts for generating figures and tables . . . 194
A.12 Notes on formatting . . . 194
A.13 Acknowledgements . . . 195

B Reproducing time-course analyses **196**
B.1 Introduction . . . 196
B.2 References from Chapter 7 . . . 196
B.2.1 Reference 1 . . . 196
B.2.2 Reference 2 . . . 197
B.3 Reproducing Figures . . . 197
B.3.1 Figure 1 . . . 198
B.3.2 Figure 2 . . . 198
B.3.3 Figure 3 . . . 201
B.3.4 Figure 4 . . . 202
B.3.5 Figure 5 . . . 203

B.4 Exploring the data . . . 204
B.4.1 Plate summaries . . . 205
B.4.2 HCT8 cells . . . 206
B.4.3 CHO cells . . . 209
B.4.4 IMCE cells . . . 210
B.4.5 HUVECs . . . 210
B.4.6 T84 cells . . . 211
B.4.7 J774 cells . . . 211
B.4.8 PMN leukocytes . . . 213
B.4.9 Plate Layouts . . . 216

List of Figures

3.1 miRNA expression profiles pre- and post-treatment 24
3.2 Effect size and statistical significance of post- versus pre-treatment miRNA expression 26
3.3 Different miRNA expression between responders and non-responders 27

4.1 An oversimplified view of *C. difficile* infection 30
4.2 Sequence, structure, and functioin of TcdA and TcdB 32

5.1 Overall transcriptional response of HCT-8 cells to TcdA and TcdB 41
5.2 qRT-PCR validation of and genes with high differential expression 42
5.3 Gene ontology categories associated with differentially expressed genes 43
5.4 Gene set enrichment of biological processes and cellular components 44
5.5 The altered gene expression of G_1 phase cell cycle regulators at 6h and changes in the distribution of cells within the cell cycle 46
5.6 Timing of RAC1 glucosylation and expression of cyclin-related genes and proteins in subconfluent and confluent cultures. 47
5.7 Distribution of apoptotic versus non-apoptotic cells within the cell cycle and characteristics of G_2/M phase, toxin-treated cells 49

6.1 Study workflow 55
6.2 Cytopathic effects of TcdA and TcdB on a mouse epithelial cell line. 64
6.3 Histopathology 6h after cecal injection with TcdA. 66
6.4 Physiological and gene expression changes post toxin injection 68
6.5 The concentration of circulating blood cells was altered during intoxication 69
6.6 Cell type proportions as determined by flow cytometry 71
6.7 Gene expression changes post toxin injection 72
6.8 Biological functions associated with gene-expression changes 76
6.9 Expression changes of inflammation associated and immune regulatory genes 77
6.10 Cytokine gene and protein expression 79
6.11 Antibody neutralization of CXCL1 and CXCL2 81
6.12 *Cxcl1* and *Cxcl2* expression after Cxcl1 & Cxcl2 neutralization 82
6.13 Neutrophil infiltration 6h after TcdA cecal injection of mice pretreated with neutralizing antibodies 83
6.14 Correlations between *in vitro* and *in vivo* responses to toxins 83
6.15 Similarly expressed genes *in vitro* and *in vivo* 84

7.1 Measurement of toxins' cytopathic effects by tracking electrical impedance across the surface of a cell culture 97
7.2 SQuantification of cytopathic effects 98

7.3 Macrophage responses to TcdA and TcdB . . . 101
7.4 Response of HCT8 epithelial cells to gdTcdB, TcdA+gdTcdB, and TcdB+gdTcdB . 102
7.5 Response of J774 macrophages to gdTcdB, TcdA+gdTcdB, and TcdB+gdTcdB . . . 103

9.1 The iterative process of model building and refinement . . . 128
9.2 Drug targeting in metabolic networks . . . 138

A.1 Batch corrected HCT8 transcriptional data . . . 194

List of Tables

3.1 Patient outcomes and availability of miRNA data 22

6.1 Survival in cecal injection experiments 67
6.2 Infiltration of immune cells 6h and 16h after cecal injection 70
6.3 Genes with significantly altered expression 2h after TcdA or TcdB injection 73
6.4 Biological functions and gene sets associated with gene expression changes 2h after TcdA or TcdB injection 74
6.5 Molecular functions associated with gene expression changes 16h after TcdA injection 75

8.1 Example metadata file 111

9.1 Drug targeting-related analysis of pathogen metabolic networks 127

A.1 Annotation scripts and variables. “Affy”=Affymetrix Mouse 430 2.0 probeset ID. “Entrez”=Entrez gene ID, “Ensembl”=Ensembl gene ID 187
A.2 Annotation scripts and variables for Hgu133 Plus 2.0 chip 188
A.3 Scripts for producing tables and figures 195

Acknowledgements

First and foremost, I would like to thank my family for their love and continued support during my graduate education. Throughout my work in the past few years, I have finally begun to realize the extent of the dedication of my parents, Mike and Jennifer, to my sister and me. I thank my sister and best friend, Wendy, for showing me how to survive and always keeping my spirits up.

I would not be adequately equipped for my research if it weren't for the faculty, students, and researchers in Biomedical Engineering and the Biomedical Sciences at UVa. As an engineer, I have had the incredible opportunity to work day in and day out with biologists, learning how to develop and contextualize my work. At the same time, the faculty in Biomedical Engineering have developed my intuition for applying models to practical problems. I've been fortunate to "grow up" in this multilingual scientific community, unknowingly becoming fluent in different "scientific languages".

My dissertation would not exist if it wasn't for collaborations and help from colleagues and friends. The students with whom I've worked with the longest—Arvind, Edik, Paul, Phil, Anna, Jennie and Matt—have provided constant critical feedback that has improved my work and kept me focused. I'd especially like to thank Arvind Chavali, a colleague with whom I collaborated with many times, but even more a friend who showed me the ropes, and has and I'm sure will continue to provide advice for years to come. I've been very fortunate to have fellow students that have made these past five years so enjoyable, whether it be cheering for the 'Hoos or discovering Charlottesville's most interesting locations.

I'm indebted to the handful of researchers with whom I have worked most closely since my first day of graduate school. Mary Gray and Gina Donato, who always happily answered my many questions, taught me most everything I know at the bench. Without their instruction, I would surely have spent many months of frustration troubleshooting every problem I encountered. Cirle Warren, in our group's weekly meetings, has helped me put my research into clinical context. Glynis Kolling has been a tremendous resource, showing me what is and is not possible experimentally and helping me choose the best path to follow based on my many crazy ideas. I've had the privilege to work side by side with this group of researchers, at the bench and at the whiteboard hammering out ideas and manuscripts.

Finally, I'd like to thank those on my dissertation committee: Shayn Peirce-Cottler, Kevin Janes, Alison Criss, Erik Hewlett, and Jason Papin. My discussions with them have shown me their genuine interest in my career. They have pushed me far beyond my comfort zone as only a clever engineering to become a better thinker, to step back and understand the broader goals.

Erik Hewlett has graciously been an unofficial secondary advisor. After every experiment, presentation, and paper, he has been right there excited to hear how things are going, ready to provide encouragement and criticism. As someone from an engineering background, he has helped me contextualize my work. I am also appreciative for his introductions that have allowed me to work with many other great people.

Jason Papin has been a great mentor and advisor, helping me develop as a scientist and leader. I try to emulate him as I mentor others. I credit much of my progression from a fault-finding cynic to more of a forward-thinking optimist to his influence. I am most thankful for his genuine interest in my personal and career goals. He has given me the freedom to think independently, to fail and to succeed on my own.

Preface

0.1 Me, a biomedical engineer

I don’t label myself an engineer in the traditional sense; I don’t design things to be manufactured. I also dislike being called a scientist because of the visual it may provoke; most of my time isn’t spent in a long white coat at a bench. Though others might think me one, I don’t consider myself a statistician, computer scientist, or biologist either.

I am a scientist in that I’m curious about nature, especially health and medicine. I’m an engineer in that I’m curious about translating scientific understanding to ideas and tools that will improve others’ quality of life. To do this, I use and invent tools in mathematics, statistics, computer science, and the biological sciences. There is no formal and universally accepted definition of a “biomedical engineer” and likely never will be. However, these dual interests in basic and translational science and medicine are what, I believe, defines a biomedical engineer, and I think many would agree.

0.2 Me, a computational systems biologist

As a biomedical engineer in the information age, trillions of data points are available. In this dissertation alone, I gather data from dozens of expression states of the 3.3-billion letter human genome or 2.8-billion letter mouse genome. Tens of thousands of megapixel images of individual cells are captured at different wavelengths of light. Tissue and blood samples from hundreds of mice under different stresses are analyzed microscopically and by molecular assays to quantify pathology, the proportion of different cells (e.g., epithelial, white blood cell, etc.), and the amounts of dozens of proteins.

However, these data points independent of each other are of little use. As an example, consider a mouse that ingests a toxin. If we then observe inflammation in the mouse's intestine, we wonder about the cause. After dissecting tissue sections, we then find that a particular gene is expressed prior to inflammation. Is this gene responsible for inflammation? Are there other genes whose regulation is linked to this gene of interest? How does expression of this gene translate to the amount of its gene product, the protein that physically interacts with the cells' environment? Is this inflammation only due to local events? What about the brain and the nervous system? What happens after inflammation? Are there any changes throughout the body from the local injury in the intestine (e.g., in the blood)? Where did the toxin go? The questions go on, but it is apparent that there are many levels of data and interactions, a **system**, that determine the apparent clinical manifestation. **Systems biology** aims to consider biological systems as a whole and answer how one or many changes affects the state or output of the entire system.

Systems biology requires computational tools just so data can be managed, so the term **computational systems biology** is somewhat redundant. The term's definition will change from person to person. As I use it in this dissertation, it is distinct from "systems biology" in that computational tools are used to make insights and comparisons that would be experimentally impossible, or would at least be prohibitively difficult. Computational systems biology may take well-designed, simple, comparative experiments that are the core of good scientific research (e.g., think null versus alternate hypotheses and p-values) and then go one step further by presenting the data in novel ways and by making formal, rigorous predictions.

0.3 My dissertation as a biomedical engineer and computational systems biologist

As I described above, Biomedical Engineering and Computational Systems Biology include aspects of many different fields (biology, medicine, engineering, etc.). Therefore, this dissertation includes new contributions and tools to these fields, allowing for better descriptions and reliable, repeatable predictions from biological data. The unifying element to these contributions and tools is one research question: why do a bacterium's toxins make us sick and what are ways to make us better once we're sick? More specifically, I show how multi-level, systems biology data improves our understanding of host cell responses to the two principal virulence factors of *Clostridium difficile*, toxins A and B. This understanding suggests new treatments and diagnostics, but also reveals entirely new ways of thinking that offer leads to promising targets for future treatments.

Chapter 1

Introduction

1.1 Abstract

Toxins A and B, two highly potent protein toxins, are the essential virulence factors of *C. difficile*, a bacterium which infects 300,000+ people in the US every year [1]. Since the extent to which a persons body overreacts to the toxins determines disease severity, controlling the host response is critical for improving treatments. Given the manifestations of diarrhea and colitis, nearly all research to date has predictably focused on known inflammatory pathways and related cellular responses. However, 40 years after the toxins' discovery, the fatality rate has continued to rise. A different approach is needed. In this dissertation, I present a holistic approach, profiling the physiological and transcriptional changes of host cells to toxins in vitro and in vivo. I determine the most appropriate statistical methods for identifying genes and pathways affected by toxins, leading to discovery of an unrecognized cell-cycle disruption of epithelial cells treated with toxins. I then extend the approach to investigate epithelial-layer cells in mice with toxin injected into their intestines, identifying pathways altered only in vivo. These pathways offer new therapeutic targets, as is shown by antibody neutralization experiments showing that the levels of two cytokines are predictive of survival. I again extend the systems approach to analyze toxin sensitivity and dynamic, morphological changes of cell types in addition to epithelial cells. Sensitivities of macrophages, epithelial, and endothelial cells indicate that epithelial cells may not be the critical cell type for initiating disease and show that the most well-studied toxin molecular activity (glucosylation) is not required for all toxin-induced cellular responses. In addition to these novel findings, this work

presents new ways of thinking about host responses to *C. difficile* toxins that can be investigated in the future with mechanistic models and reductionist experiments.

1.2 A preview of this dissertation

In Chapter 2, I explain the experimental and computational methods at the core of the findings in all subsequent chapters. A short primer explains the biological concepts of mRNA and transcriptomics studies. The advantages and pitfalls of the many possible data processing techniques that together form the analytical workflow are described in context of the data presented in Chapter 5 and Chapter 6. The importance of reproducibility, a special concern of mine, is also discussed. Chapter 3 presents my transcriptomics analysis of samples from a clinical trial for a combination melanoma therapy. These methods set the stage for the primary focus of this dissertation, the host response to *C. difficile* toxins.

Chapter 4 gives the scientific background and clinical significance of *C. difficile* infections, the known roles of *C. difficile* toxins in infection, and the importance of the host response to pathogenesis. The basic concepts, advantages, and pitfalls of functional genomics and systems biology methods such as gene set enrichment that come after the methods in Chapter 2 are briefly described. These systems biology methods are then used in Chapter 5 to analyze the transcriptional responses of an epithelial cell line, revealing disruptions in cell cycle that block cell growth without inducing complete cell death.

Chapter 6 presents physiological and transcriptional responses to *C. difficile* toxins in a mouse intoxication model. Changes in the expression of pathways and gene sets that are characteristic of the response are described and compared to the in vitro responses in Chapter 5. Follow-up experiments neutralizing two cytokines within these gene sets proved that the systemic levels of the two cytokines correlated with disease severity and could be used to predict survival.

Epithelial cells are the focus of the in vitro and in vivo transcriptional studies, yet the data indicate that other cell types are also important. Therefore, in Chapter 7 the dynamic, morphological changes responses of macrophage, endothelial cells, and epithelial cells are measured precisely with electrical impedance. With this experimental framework, I also investigate the necessity of the toxins' glucosyltransferase activity to these responses. Software that I developed for managing and visualizing time course data from multi-well data is presented in Chapter 8.

The last chapter, Chapter 9, reviews metabolic network analyses. Although not directly related to the methods in the previous chapters, it is presented as an example of additional analyses that could be performed to gain more mechanistic insight.

Chapter 2

Reliable, reproducible transcriptomics analyses

Throughout this dissertation, I present analyses of the expression of the genomes of human cells or tissues of mice that have been treated with *C. difficile* toxins A and B (TcdA and TcdB) in order to determine the pathogenic responses of the host at the cellular level. In deciding how to process this type of data, I encountered many limitations and misunderstandings in common gene expression analyses. In this chapter, I summarize the principles of these analyses that form the base of this dissertation, and explain some important considerations for interpreting sometimes very different results produced by different data analyses, an overlooked problem in the majority of gene expression studies.

2.1 Background

2.1.1 mRNA as a measure of cell state

Our genomes are a sequence of ∼3-billion "letters" from a four-letter alphabet of nucleobase molecules (*bases*) [2]. Each of our ∼20,000 genes is pieced together from, on average, 5 physically separate sequences called *exons*. Exons, which range from ∼20 to 1,600 bases, are contained within one of the 46 strands of DNA in our cells [3].

The central dogma of molecular biology is DNA → RNA → protein [4]. In each cell, exons are copied (*transcribed*) and spliced into portable messenger RNA (mRNA). mRNA is then *translated* to strings of amino acids that arrange themselves into shapes with chemical properties that perform specific tasks. These amino acid strings, or proteins, are the primary functional units that execute the instructions in our DNA.

When a protein is needed, a cell's "circuitry" triggers a gene (the DNA encoding that protein) to be transcribed to mRNA that is then translated to the protein. Specific amounts of proteins are produced in response to different stimuli. Since the proteins will alter the physical state of cells and consequently the body's overall physiological responses, many scientists have striven to understand the arrangement and logic of this regulatory circuitry.

Most of this circuit's components were identified soon after the sequencing of the human genome in 2003 [5, 6]. This and decades of previous biological research provided a very basic view of connections within the cell, yet many of the studies delineating functions were limited to small sets of genes and proteins. To be able to understand how all the components affect each other, there had to be a way to take snapshots of the levels of thousands more mRNAs or proteins.

In 1982, technology to simultaneously measure genome-wide gene expression (i.e., the levels of mRNA in a cell) from a collection of cells was already being developed [7]. Current RNA sequencing technologies can now count individual mRNA molecules (*transcripts*) from a collection of cells for $1000 or less.

2.1.2 Measuring mRNA levels with microarrays

DNA molecules consist of two, connected, parallel strands, each strand containing a sequence of nucleobases along a sugar backbone. The four bases (adenosine (A), thymine (T), cytosine (C), guanine (G)) join to each other by hydrogen bonds. A only pairs with T; C only pairs with G. Two strands *hybridize* when their base pairs are aligned.

Strand-specific hybridization can be used to identify DNA sequences from uncharacterized samples. For example, single-stranded DNA with a known sequence can be fixed to a substrate or surface, and DNA from an unknown source can then be labeled and washed over that surface. If DNA from the two sources have matching strands (i.e., they *complement* one another), the labeled DNA will hybridize and be detected. The first "gene arrays" that could detect multiple sequences in this way were built by attaching DNA to hundreds of spots (*probes*) on glass plates or slides [7, 8]. Each probe contained thousands or millions of DNA molecules with the same sequence so that one gene was detected per probe.

Since hybridization requires two DNA samples, mRNA must be reverse transcribed back to DNA if it is to be measured on a gene array. The resulting complementary DNA (cDNA) can then be labeled and detected. Signal intensities from the probes indicate the relative amounts of each mRNA in a sample.

Microarrays, very small gene arrays, were introduced in 1995 [9]. Although microarrays require more sophisticated manufacturing, they are based on the principles of older gene arrays.

2.2 Microarray preprocessing techniques

The most commonly used microarrays over the past decade have been made by Affymetrix. I described here many methods designed for these arrays, yet the principles can be extended to most other microarray technologies and even sequencing data.

2.2.1 Steps of data preprocessing

Affymetrix microarrays

In less than one square inch, Affymetrix arrays fit over one million probes, enough to measure genome-wide expression (the *transcriptome*). Since exons are longer than the 25-nucleotide probes, *probe sets* of ten to fifteen probes are designed to hybridize one gene or exon.

Nonspecific hybridization

For each probe sequence, Affymetrix made a *mismatch* probe with the 13$^{\text{th}}$ base changed. The mismatch probes are placed directly beside the corresponding mismatch probes and were intended to measure how many other transcripts bind to a similar sequence as the targeted mRNA (the perfect match probe sequence).

Hence, by subtracting the mismatch signal from the *perfect-match* signal, *nonspecific hybridization* (*cross-hybrdization* from other transcripts) may be estimated (*perfect-match correction*). However, mismatch hybridization is complex. Usually, more than one third of mismatch probes have a higher signal than their perfect match probes [10]. This should theoretically never happen, but presumably is due to nonspecific binding of other transcripts or low signal to noise ratios. Several have proposed hierarchical models with nonlinear terms that better account for mismatch probes [11–14], yet algorithms that ignore mismatch probes perform equally well or better [10, 15, 16].

Background correction

Since mismatch probes cannot be used and there is no empty space on high-density arrays, background signals must be estimated from many probes. Affymetrix first proposed splitting an array into zones and calculating background signals from low intensity probes. This approach systematically corrects large sections of the array, yet it does not address probe-specific background signals.

Irizarry et al. observed the distribution of all observed probe signals (O) could be approximated by a mixture of an exponential distribution (S) and a normal distribution (B) [10]. S and B were considered the true signal and background signal, respectively ($O = S + B$). After the mean and variance of S and B are estimated from the data, the background-corrected signal can be calculated as $\mathrm{E}[S|O = o]$ by the robust multi-array average (RMA) procedure in [10]. Wu et al. introduced gcRMA, which improved upon RMA by accounting for sequence-specific probe affinities that were determined from previous experiments ($O = S + B + N$ where N is the differences in hybridization due to sequence-specific probe affinities) [17]. gcRMA also modeled mismatch probes by making two equations, one for O_{mismatch} and one for O_{perfect}, with one common term, the true signal S. Similarly, other model-based expression value calculations have the option to include or ignore mismatch probes (e.g.,[11, 12]).

Probe set summarization

To estimate a gene's expression, the probes in a probe set must be summarized. Since outliers are common, robust statistics (e.g., median) are preferred. Affymetrix first recommended the Tukey bi-weight statistic, calculating probe set values one microarray at a time. However, many probes have similar effects across all microarrays (e.g., different affinities), and these *probe effects* can be modeled and removed as was shown by Li and Wong ([11, 18] is often called the "Li-Wong method"). The most popular summarization, "median polish", places a probe set's expression values a_{ij} in a matrix (i indicates the probe an j indicates the array). The row and column medians are iteratively subtracted to estimate an error matrix. Probe effects and expression values are calculated from the sum of the subtracted row and column medians, respectively, minus the medians of both vector sums [10, 19]. Chen et al.'s "distribution-free, weighted" summarization accounts for probe effects primarily by assuming that low-variability probes are high-quality and should be weighted more than other probes [15]. Hochreiter et al. assume perfect match probes are normally distributed, enabling them to perform 'factor analysis' where the 'factors' are mRNA concentrations [16]. Even more complex models may incorporate background correction, perfect-match correction, and probe set summarization into one step (e.g. [13, 20]), yet each step is typically performed separately.

Normalization

Systematic differences between arrays must be normalized if they are to be compared. The simplest normalization procedures center all array values by mean, median, or some other measure, yet centering doesn't account for different ranges of values. Quantile normalization forces two arrays to have the exact same statistical distribution [21]. Li and Wong's normalization iteratively searches for a group of "housekeeping genes" (the invariant set of probes) that will be forced to the same expression values in all arrays, and all other probes are adjusted accordingly [18]. Huber et al. found that the inverse hypberbolic sine transformation made probe variance less dependent on probe mean [22]. This variance stabilization—in combination with a nonlinear model fit to find scaling factors and offsets for each microarray—is used for normalization. Loess normalization applies a smoother to an 'MA plot' which plots the differences between two arrays ($M = log_2(x_1/x_2) = log_2(x_1) - log_2(x_2)$) versus the average signal of two arrays ($A = \frac{1}{2}log_2(x_1x_2) = \frac{1}{2}(log_2(x_1) + log_2(x_2))$). The smoother is subtracted from each point so that the plot is centered around the A-axis. Loess normalization thus makes offset adjustments that are dependent on the intensity of the signal.

2.3 Choosing preprocessing techniques

2.3.1 What are the best preprocessing steps?

Usually, the answer is "we're not sure" or "it depends". Hundreds of methods have been published. Which ones are chosen depends on if the methods' assumptions match the experimental design.

Selecting the full sequence of steps (the *workflow*) is daunting. The techniques in 2.2.1 are a subset of the many choices. For each step (background correction, normalization, perfect-match correction, and probe set summarization), there are ten or more possible algorithms making at least $10^4 = 10,000$ possible workflows. However, each algorithm has at least one, sometimes three or four arbitrarily or heuristically chosen parameters, making for over ten million possible workflows (actually real number parameters make for infinite workflows). Since there are no general guidelines, I present some illustrative examples below.

Background correction and perfect-match correction

Background correction algorithms decompose the observed signal into two signals: the noise and true signal. They are most helpful then for low-signal probes where the signal to noise ratio is lowest. If researchers are uninterested in low-abundance transcripts, they might consider skipping background correction.

Background correction is the least understood step because “there is currently no way to design an oligonucleotide microarray such that the probes have fully predictable hybridization” [23]. gcRMA and PDNN use sequence data to try and infer complex probe affinities from sequence data yet are not much better than some that do not [10, 17, 20]. Affymetrix’s MAS5.0 background correction and perfect-match corrections are not model based, making simple assumptions on how low-intensity probes or mismatch probes should adjust surrounding perfect-match probes. Although there is no clear, universal support of one method over another, it is commonly accepted that mismatch signals should be ignored or modeled in some way as contributing to the observed signal.

Normalization

If one is sure of impeccable sample isolation and reproducibility, they might decide against normalization. However, since even the slightest differences in one of many experimental factors (e.g., scanner reproducibility, mRNA concentration calculations, hybridization temperatures) cause systematic errors, there should be strong justification for skipping normalization.

If researchers believe that only a few dozen of thousands of transcripts vary between arrays, then the distribution of expression values should be similar among all arrays. Quantile normalization would then be appropriate. If treatment systematically increases the total mRNA per cell, quantile normalization would incorrectly mean-center all arrays (though uncommon, cells may need to be counted before RNA isolation [24]). Loess normalization might be better since it modifies each array's values according to similarly expressed probes on other arrays, allowing for slightly different distributions. If the primary problem is high variance of low-signal probes, variance stabilization may be best. If 10 "housekeeping" genes are known or can be trusted to be found algorithmically, invariant set normalization would work. However, since invariant set normalization assumes probe affinities are similar, probe values must be corrected in background correction. Treatment groups may be so different that no normalization cannot be justified. The treatment groups might then be separately normalized, although subsequent comparisons may be difficult to interpret.

Probe set summarization

There are no general rules for probe set summarization, yet there are mistakes to be avoided. Outliers are common in microarrays so robust measures of center are used. It is recommended to choose summaries that "borrow" information from all arrays to identify probe effects. Though different summarization techniques may produce significantly different expression values, no technique is necessarily incorrect. However, the artifacts introduced by some techniques may cause incorrect interpretations in downstream analyses (see 2.3.1).

Summarization reduces 10+ probes to one value, so 90% of the data is lost. Therefore, before summarization, one might use the distribution of probe values to perform more powerful statistical tests or to propogate error through subsequent steps [12, 13]. Nevertheless, probe set summarization must eventually be performed at some level if one wants to study genes, not 25-nucleotide stretches of DNA.

The order of steps

There is no required order for each step of the workflow, yet there are limitations. For instance, if probe set summarization were done first, probe values would not be available to estimate the background signal. Perfect-match correction also wouldn't be possible. Normalization can be applied before and/or after summarization. There is no strong evidence supporting one choice over the other. It is also unclear if normalization should be done for all arrays at once or separately for subsets (e.g., control and treatment groups).

With few exceptions, each preprocessing method is modular, compatible with any other method.

However, very few have explored the effects effects of combining algorithms. For example, it may be the case that a background correction invalidates assumptions for some normalization procedures.

Different choices for different goals

Different analyses work better for different problems. For example, Zhang et al claimed their PDNN model was superior to dChip (”Li-Wong” method) and MAS5.0 (Affymetrix default) [20]. However, Wu and Irizzary commented that their RMA and gcRMA methods performed as well or better for predicting mRNA concentrations [25]. Zhang et al. responded that their concentration predictions are off by a predictable scale factor, and that the ability to detect differentially expressed genes was better than RMA and gcRMA [26]. They were also unable to reproduce results supporting Wu and Irizarry's claims. It was unclear what the goal should be: accurate predictions of mRNA levels or differentially expressed genes?

If the goal of a study is to compare the profiles of many genes or samples, one must be aware of artifacts introduced by probe set summarization algorithms that severely overestimate correlations. Lim et al. observed, with gcRMA, an average correlation coefficient of 0.4 among randomly generated, uncorrelated arrays [27]. Since correlation measures are essential for reverse engineering regulatory networks, previous network studies that used gcRMA were flawed. Giorgi et al. identified that the median polish algorithm introduces high inter-sample correlations among randomly generated arrays [28]. Their solution was to transpose the matrix of probe intensities for each probe set, thereby transferring the error so that probes would be overly correlated, not samples. Therefore, if a study's goal is to classify patients by a clustering algorithm, one should use the median polish algorithm very carefully. If the goal is only to detect differentially expressed genes, then the algorithm will not cause critical errors.

Gold standards?

To once and for all determine the best preprocessing methods, Choe et al. spiked in 5,700 transcripts at various concentrations on 18 arrays (called “Golden Spike” [29]) By quantifying the accuracy of predicted differentially expressed genes, they defined one best performing workflow, though several others performed similarly well. Several authors noted flaws in the experimental design and analysis causing unrealistic conclusions [30–35], and a “Platinum Spike” data set was generated to address the flaws [36]. Conflicting recommendations from various authors that stemmed from these data suggests that there will likely never be one "best" workflow, yet the analyses made possible by these data sets highlighted advantages and pitfalls each method (many of which are discussed in 2.3.1) and led to the invention of new techniques.

2.3.2 Which workflow do I use?

The previous sections have shown that I or anyone else cannot definitively choose the right workflow. Instead, I would recommend an exploratory approach tailored for each data set. For example, one could analyze there data set with ten or more different workflows and compare the results using diagnostic tools (e.g., correlation matrices, clustering, principal components analysis (PCA), and MA plots). For example, one may find, as I did in one case, that invariant set normalization causes outlier arrays (identified by PCA) because of the automatically selected "housekeeping genes". Using an MA plot, they may then notice extraordinarily high variance in the fold changes of low-signal probes, and then decide on a workflow (e.g., mmGmos) that propagates this error to statistical tests for differential expression. If expression levels from arrays will be used as parameters in another model (e.g., a model of metabolic flux where expression levels indicate the presence of different enzymes), then the high-variance, low-signal expression values might all be set to a common threshold. Interactive, easy-to-use diagnostic visualizations that allow for these decisions are desperately lacking. Although developing visualizations is a tremendous technical challenge, there is a great opportunity for improvement in this area.

2.4 Detecting differentially expressed genes

After preprocessing, it is common to identify genes that are differentially expressed (DEGs) between two treatment groups. Like preprocessing, there are many methods with different assumptions (reviewed in [37–45]). This further expands the number of possible workflows to well over 100 million.

Conceptually, significance tests for DEGs are simple. For each gene, two groups can be compared with a t-test. However, significant p-values are usually found for too many lowly expressed transcripts with small effect sizes because of very small variances near the microarray detection limit. Therefore, filtering of low-abundance transcripts is common, yet newer statistical tests can adjust for errors in low-signal probes without excluding the probes from subsequent analyses.

2.4.1 Types of statistical tests

Modified t-tests

In Student's t-test, a t statistic is the difference in expression between conditions (effect size) divided by the amount of variability in the data (standard error). The distribution of t-statistics with different sample sizes is known, so how unusual (or how significant) a t-statistic is can be calculated as a p-value. Since the standard error of probes is what causes too many significant transcripts, a simple solution is to add a "fudge factor" to the standard error, thus making a modified t-statistic.

$$t_{\text{modified}} = \frac{\text{Effect size}}{\text{fudge factor} + \text{standard error}} \tag{2.1}$$

The goal of several bioinformatics studies has been to how to best estimate the fudge factor. Tusher et al. heuristically chose a constant that minimized the variation of the standard error across all expression values [46]. Efron et al. chose the constant to be the 90$^{\text{th}}$ percentile of the standard error for all transcripts [47, 48]. Baldi and Speed's cyberT method adds "pseudo-replicate" arrays for which the standard deviation is estimated as the average standard deviation of similarly expressed genes on the real arrays [49]. The variance of expression values is therefore "shrunk" towards the variance of similarly expressed genes. Fox et al. instead calculate the variance of pseudoreplicates using the sum-squared differences of similarly expressed genes [50]. Demissie et al. show how to use a similar fudge factor but for a Welch test (a t-test where groups have unequal variance) [51].

Bayesian statistics

cyberT improves upon a regular t-test by incorporating information we know (or guessed) to be true, namely that the sample variance of low-signal probes is usually greater than observed. "Bayesian statistics" is the field of statistics that allows one to make such prior assumptions (called *priors*) in a mathematically rigorous way to reduce the set of possible outcomes (the sample space). The reduced sample space allows us to make new, *posterior* probabilities *given* the prior information. For example, my guess of the average height of people in a room (perhaps 5'6") would change dramatically if I were told prior that everyone was 2 years old (a subset of the population–the reduced sample space). Bayesian statistics are common in microarray analyses. Since formulas for prior and posterior probabilities can be esoteric, I will only mention the assumptions on which the priors are based.

Lonnstedt et al. derived a statistic equal to the log of the probability a gene is a DEG divided by the probability the gene is not a DEG [52]. To do so, they made the prior assumptions that (1) only a small proportion, p, of genes are DEG, (2) all log fold changes of transcripts are normally distributed, and (3) the variances of expression values follow an inverse gamma distribution. The parameters for prior distributions (e.g. the mean and variance of the normal distribution) are called hyperparameters. Lonnstedt et al. guessed p and estimated the other hyperparameters using the data. Efron et al. assumed a prior distribution of a modified t-statistic based on random permutations of microarrays. This "empirical Bayes" procedure has been used in several other DEG tests [48]. As researchers have continued to learn about microarray chemistry so that we may make better prior assumptions, Bayes statistics for DEG detection have continued to be published. See the aforementioned reviews and citations for more examples [53–61].

Linear models

Linear models are a natural extension to t-tests when an experiment has multiple factors that describe the samples (e.g., treatment group, gender, RNA isolation protocol). Analysis of variance (ANOVA) is used to estimate how much of the experiment-wide variance is due to each factor. Instead of a t-statistic, ANOVA finds an F-statistic which compares these variances. Like the modified t-tests in 2.4.1 , there are several modified F-tests, some of which use Bayesian statistics to estimate fudge factors (reviewed in [37]). For example, the IBMT method extends cyberT's assumptions to linear models [62]. Perhaps the most common DEG test, "linear models for microarray data" (LIMMA), builds a linear model based on multiple factors that are then reduced to another linear model calculating specific contrasts (effect sizes) [63, 64]. Limma extends the bayesian moderated t-statistic from Lonnstedt et al. to calculate the signifcance of the contrasts for each gene [52].

Rank-based metrics

t-tests and linear models (types of parametric tests) assume the expression values for each gene are normally distributed. However, the assumption may not be justified; there usually aren't enough samples to know. Additionally, the assumption required by the t-test that the mean and variance are independent is usually not true in microarray data. Nevertheless, parametric tests are often chosen for practical reasons. Expensive microarray experiments have small sample sizes, and parametric tests are needed to gain enough statistical power to find DEGs.

However, several non-parametric tests have been developed which make fewer assumptions [65]. The Wilcoxan rank sums test uses combinatorics to calculate how unusual the rankings of microarrays are for each gene. In another approach called RankProd, genes are ranked by fold change for all two-array treatment group comparisons (e.g., $3 \times 3 = 9$ comparisons for triplicate samples in two treatment groups) [66–68]. For each gene, the product of its ranking in all comparisons is calculated. To determine if a rank product is unusual (significant), samples are permuted between treatment groups many times to estimate the usual distribution of rank products (the null distribution).

Permutation tests

Many other statistical tests use permutations to avoid making inappropriate assumptions about the data (e.g., [48, 69]). The most popular DEG test (by citation count) is Significant Analysis of Microarrays (SAM) [46]. SAM calculates moderated t-statistics for each permutation and compares this to the actual moderated t-statistic to estimate which genes fall below a specified false discovery rate (FDR). The greatest limitation of permutation tests is that they require much larger sample sizes than is typical in costly microarray experiments. For example, the minimum two-sided p-value for an 8-sample permutation test with quadruplicates is only $2/\binom{8}{4} = 0.03$. Hence although permutation tests are possible with moderate sample sizes, it is better to have at least ten arrays where the minimum p-value is 0.008.

Machine learning-based tests

Many of the previously introduced statistics such as the modified t-statistic violate the assumptions on which the significance tests are based, or the test statistics are no longer in forms that can be used in statistical tests. Although these methods depart from the statistical theory, they are still useful for ranking and prioritizing genes. In this spirit, some statisticians have used machine learning algorithms to prioritize genes even though the numbers from the algorithms are difficult to interpret. For example, Lu et al performed PCA on the probes in a probe set to determine which probe sets to filter as as not differentially expressed [70]. They used the loading on the first principal component relative to all other loadings to set a filtering cutoff. Clark et al. use linear discriminant analysis to find a hyperplane in n-dimensional space (where n is the number of transcripts) that separates treatment groups [71]. The angle between each transcript's axis and the hyperplane is used to define how much that gene contributes to the overall differential expression between treatment groups.

Fold change-based tests

The MAQC project found that irreproducibility between microarrays was largely due to the analyses, not due to the technology or experimental variability [72]. The most basic ranking statistic they tested, the fold change, was the most consistent between laboratories performing the same protocols. Other statistics they used such as limma have the problem discussed in the previous sections that many low-signal probes are ranked among the most significant DEGs. It may be that many complex significance tests are biased to the data sets on which they were tested. Several statistical methods that are based on fold change, yet do not disregard the variability in the data, are potential compromises (e.g. [43, 73–79]).

2.4.2 What test should I use?

Like with preprocessing, I recommend an exploratory approach with significance testing, looking at the results from several tests. The different gene rankings from the same data will put into perspective the confidence one should have in any follow-up experiments. Since probes with low signals are problematic (see previous sections), I also recommend reporting expression values and fold changes along with any p-values or statistical measures.

2.5 Caveats of microarrays and alternatives

As discussed, many of the problems with microarrays are low-intensity probes (low-abundance transcripts). The number of statistical tests to correct for this problem is exasperating, yet very few studies have focused on experimental methods to improve the dynamic range of arrays.

Next generation sequencing of RNA (RNA-seq) is the next step to improving variability. RNA-seq offers great potential for reducing the uncertainty in transcript levels because transcripts are counted. With microarrays, relative abundances can only be estimated indirectly. However, RNA-seq presents new challenges. For instance, many of the sequenced reads cannot be mapped to the genome. There also is not a standard way to quantify expression levels of entire genes based off of many different transcripts.

A major hindrance to any research with microarrays or sequencing is the availability and reproducibility of analyses. I have taken a special interest in reproducible research and will now discuss it briefly.

2.6 Reproducibile analyses

2.6.1 Why bother?

Irreproducible analyses are dangerous, perhaps bordering on unethical negligence. Dave et al. in the *New England Journal of Medicine* reported a marker for follicular lymphoma [80]. In letters to the editor, Tibshirani and Hong et al. stated they could not reproduce the analyses [81]. Dave et al. rectified the discrepancy as a misunderstanding in how their data was interpreted. This is just one of a handful of public disputes in the literature about gene expression analyses (two mentioned in previous paragraphs). Authors of disputed studies are most always well-intentioned, yet irreproducible analyses or poorly presented data raise suspicions.

In my opinion, analysts shouldn't fear being wrong. As researchers, we must speculate and make hypotheses that, when tested, are very often found to be wrong. Instead, researchers should fear being overconfident or misleading. By making data and code open to criticism, scientists protect their integrity and intellectual property in the same way that lab notebooks do. They protect their colleagues whose careers are dependent on their analyses as well as the patients whose health decisions are affected by their research. Finally, they increase their chance for mutually beneficial collaborations.

2.6.2 Are microarrays reproducible?

Thre has been great concern about inter-lab repeatability of gene expression experiments (see example of poor reproducibility in [82–85]). Rather than discrediting microarray analysis, one should also consider that microarrays may reveal differences in *seemingly* identical experimental protocols. For example, with the data presented in this dissertation, arrays from replicate experiments on different days were clearly different when visualized with principal components analysis. However, the differences were systematic and could be corrected.

Problems may also arise from overexpectations and misunderstandings of what expression values can predict. For example, comparisons of microarray classification studies (e.g., [86–98]) with non-microarray studies have indicated predictive cancer markers or profiles may not be as reliable as hoped [99–102]. Hundreds or even thousands of microarrays may be necessary to accurately predict cancer outcomes [103–106]. However, a more rigorous re-evaluation of a pessimistic study claiming that microarray studies cannot predict cancer markers found that markers can indeed be found (see [104, 107–109] for the debate). One shouldn't jump to conclusions from any one or even a few analytical workflows. For instance, two studies may find very different list of differentially expressed genes, yet the correlation between the data sets may be strong. Alternatively, two studies may predict two different results that are both correct [110, 111].

Several studies raise concerns about experimental reproducibility between experimental platforms [112–118]. Many irreproducibility claims were incorrect, first dismissed by scientists at the FDA [119]. The FDA and EPA coordinated a Microarray Quality Control (MAQC) project to set standards and resolve outstanding questions [120–123]. With careful quality assurance and analyses, microarray data were similar between laboratories [124–129] and platforms [130–138].

2.7 Transcriptomics analyses in this dissertation

In my dissertation, the first set of challenges have been solving engineering problems—ensuring the reliability and reproducibility of all analyses. This behind the scenes work is not highlighted in all of the following chapters, yet it is central to achieving the goals of each chapter. In developing the best analytical strategies, I worked through several previous publications. The greatest challenge I and others have faced is reproducing these results. I have made special efforts to make all computational analyses repeatable.

The next chapter describes a transcriptomics analysis where that I have included to ensure reproducibility of a clinical trial for which I analyzed the results.

As the hundreds of publications about microarray preprocessing and significance tests have shown, engineers and statisticians have been very interested in techniques and optimization. However, the most difficult part of microarray studies comes after the data processing, when biological interpretations need to be made. For example, new techniques may improve the accuracy of DEG detection from 80% to 90%, but is that better accuracy more helpful? Would a biologist find it useful that 9/10 of genes in a list are correct, not just 8/10? Maybe. Maybe not.

The following chapters focus on this transition from statistics to biological understanding. In particular, transcriptomics analyses of host cells to *C. difficile* toxins are used to elucidate changes in the replication of cells and proteins that contribute to or are markers of pathogenesis.

Chapter 3

Transcriptomics characterize responses to melanoma treatment

3.1 Motivation

Computational models that use millions of data points often require complex, multi-step analyses that few can implement or understand completely, yet the end goal is most always to find simple, fundamental relationships that anyone can intellectually grasp. Simple, well-designed summaries and descriptions of the data are, arguably, of equal importance if not more important than a predictive or mechanistic model. Transitioning from a computer and data to logic and understanding is a bottleneck for the sharing ideas with a larger community that can derive new interpretations to advance medicine. Visual summaries allow us to take advantage of the best analytical tool we have, the human intellect. Here, I present a phase II clinical trial in which I guided the analyses and presentation of the data after the completion of the treatment period [139]. Through this example, I show how appropriate visualizations identified errors in previous analyses and enabled new interpretations and new hypotheses to be generated.

The clinical trial was directed by Dr. Craig Slingluff at the University of Virginia. Aubrey Wagenseller, the first author on the associated publication [139], drafted the manuscript and led follow-up experiments. A more general and briefer background of that given in the manuscript is provided below. My analysis as presented in the publication (figures and results) are also presented in this section. In addition, a more in depth description of the methods are also presented. This important addition allows one to understand the choice of methods and also reproduce the results shown in the publication, a process which is not possible from the supplemental data provided in the published manuscript.

3.2 Introduction

A metastatic melanoma (more formally ‘stage IV melanoma’) is a type of cancer in which melanocytes (cells that produce the pigment melanin that is found in the skin, eye, inner ear, etc.) grow improperly or uncontrollably and spread to other parts of the body. Even with current treatments, the two-year survival rate is under 20%, so there is a need for new therapeutics or improvements upon current therapies [140, 141]. To find more potent, target-specific drugs, several studies have targeted molecular pathways known to be disregulated in many melanomas [142]. Clinical trials with many of these monotherapies have had variable results: 3% response rate in a Temsirolimus (targeting PI3K-AKT-mTOR pathway) trial and 0% and 17% response rates in two Bevaczimub (targeting VEGF) trials [143–145]. However, combination therapies that simultaneously target multiple pathways have potential to succeed where single drugs have failed. For example, Molhoek et al. found that dual targeting of VEGF and mTOR with bevacizumab and sirolimus synergistically reduced growth and caused death in VEGFR-2^{+}, patient-derived, melanoma cell lines [146]. In a follow-up phase II trial with 17 patients treated with temsirolimus+bevaczimub, three patients partially responded, nine had stable disease after eight weeks, four had progressive disease, and one patient could not be evaluated (Table 3.1) [147]. In this clinical study, additional miRNA data was taken from patients before and after treatment. This analysis aimed to identify (1) if pre-treatment miRNA expression profiles correlate with treatment response or (2) if any post- versus pre-treatment changes in miRNA expression correlate with the treatment effectiveness.

Patient	Pre-tx	Post-tem	Post-combo	BRAF^{V600E}	Outcome
1			+	ND	Stable disease
2	+	+	+	Y	Stable disease
3	+	+	ND	Y	Stable disease
4	+	+	+	Y	Stable disease
5	+	+	+	Y	Progressive disease
6	+	+	ND	N	Partial response
7	+	+	+	N	Progressive disease
8	+	+	+	Y	Progressive disease
9	+	+	+	N	Partial response
10	+	+	+	N	Not evaluable
11	+	+	ND	N	Stable disease
12	+	+	+	N	Stable disease

Table 3.1: Patient outcomes and availability of miRNA data. A '+' indicates that miRNA was measured from biopsies before treatment (Pre-tx), after temsirolimus treatment (Post-tem), or after bevacizumab+temsirolimus treatment (Post-combo). All patients received each treatment unless denoted with ND (not done). Blank entries indicate where ample RNA could not be obtained.

3.3 Methods

3.3.1 miRNA quantification

500 ng of total RNA was extracted from formalin-fixed, paraffin-embedded tissue sections and labeled with the dye Hy3. A universal reference sample was labeled with Hy5. After image processing, the local *median* background signal was subtracted from the *median* signal of each spot on the array. The log of the ratio of these background-corrected signals (log(Hy3/Hy5)) was then normalized using LOWESS fits (fitting log(Hy3/Hy5) versus log(Hy3 $\times$ Hy5)/2). These intra-array normalized ratios were denoted as the 'log median ratio' (LMR). Inter-array normalization was not performed because of the built-in normalization provided by the universal reference sample. The LMR metric will be unfamiliar to most researchers who use popular single-channel, high-density RNA microarrays (e.g. Affymetrix). However, the universal reference sample in this experimental design better accounts for errors from cross-hybridization or probe-specific affinities. The raw data processing was performed by the manufacturer of the arrays. The images of the scanned arrays are not publicly available. The raw data files publicly available online (GEO #GSE37131) only include the signal intensities for one channel, which makes it impossible to reproduce the data normalization. The processed data (the LMR values provided to me) are available online as an

XML file. The code for parsing and analyzing this XML file is provided online in my public code repository. For more information about experimental methods, see Wagenseller et al. [139].

3.4 Results

3.4.1 miRNA expression of all samples

Figure 3.1 summarizes the miRNA data from tumors that could be bioposied and profiled (14 of the 17 patients). The row of colors above the heatmap indicate the patient from which miRNA samples came. The shapes above each column of the heatmap represent the time at which the sample was obtained. Lines indicate pre-treatment samples. Filled circles represent samples from patients one day after temsirolimus treatment (day 1). Patients then received bevacizumab+temsirolimus (day 8) and then temsirolimus (day 15). “Double-circles” indicate post-combination treatment samples that were obtained on day 23. The heatmap colors show the expression of each miRNA relative to a universal reference sample.

The dendrogram in Figure 3.1 shows a hierarchical clustering of miRNA samples based on correlation coefficients. This clustering shows that the strongest factor distinguishing the tumors is the patient. In other words, patient to patient variability is greater than variability from any other factor such as pre- versus post-treatment. The tight clustering of technical replicates (shaded gray) showed that variations were due experimental or human error. In the initial analysis, there were only four samples from patient 7 (there are five samples shown in Figure 3.1). However, the clustering suggested that one of the pre-treatment samples for patient 7, which had been annotated as patient 6, was mislabeled. After checking lab notebooks and shipping documents, we rectified the problem. After correcting the annotations, the variance of samples from patients 6 and 7 decreased greatly. This, in turn, increased statistical power so that additional differentially expressed miRNAs could be detected.

This initial profiling provided a general understanding of the structure and scale of the data. However, because the patient-to-patient variability so strongly dominated the overall variability, we performed statistical tests to focus on treatment effects.

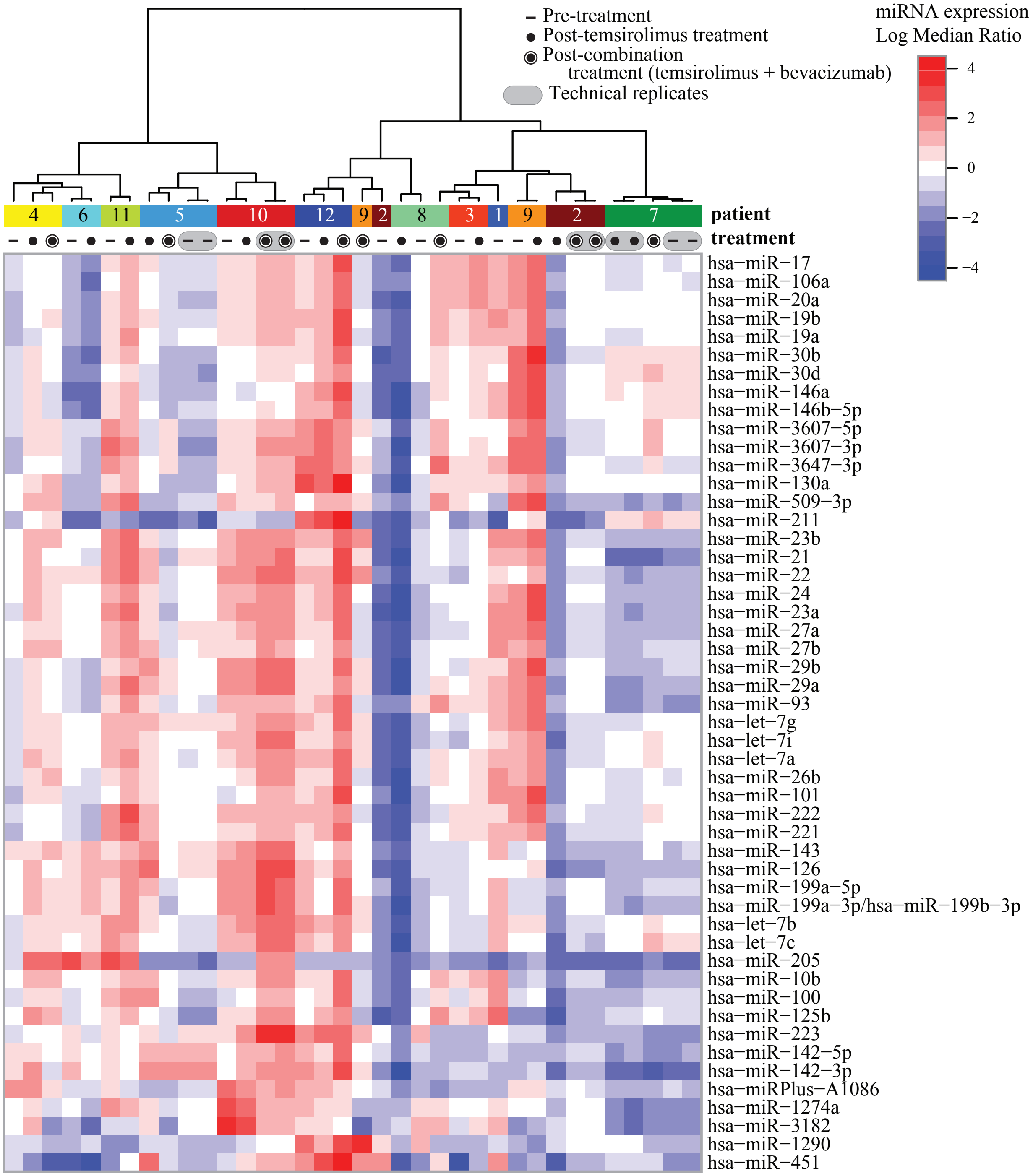

Figure 3.1: miRNA expression profiles pre- and post-treatment The 50 miRNAs with the greatest variance across all samples are shown.

3.4.2 miRNA expression changes after treatment

To identify differentially expressed miRNAs, paired t-tests were performed by comparing pre- and post-treatment groups (samples from the same patient were paired). Figure 3.2 plots the p-values from these tests against the effect size (shown as dLMR = $\text{LMR}_{\text{post-treatment}} - \text{LMR}_{\text{pre-treatment}}$). These "volcano plots" helps identify differences that are statistically significant (y-axis) while the x-axis helps identify large effects sizes that are often interpreted as more biologically significant. miRNAs with low p-values and large effects sizes are in the upper left and upper right corners of the plot. The samples used in the comparisons can be seen in Figure 3.1 or Table 3.1. This visualization revealed a technical error in previous analyses that was to be used for publication before I joined the study. There was an unusual distribution of p-values with an overabundance of values close to 1.0, which appeared to be an artifact of the code used to calculate the statistics.

The volcano plots were used to select miRNAs of interest, with the cutoffs being $|dLMR| > 0.5$ and $p < 0.01$ (gray lines in Figure 3.2). No miRNAs met these cutoffs in the post-temsirolimus treatment versus pre-treatement comparison. However, there were 15 miRNAs of interest when comparing post-combination treatment versus pre-treatment. One concern from this analysis may be that the t-test is inappropriate if the effect sizes are not normally distributed. I therefore performed a permutation based statistical test ('Significant Analysis of Microarrays') and found the same 15 miRNAs as the most significant. Such close agreement between statistical tests is rare. The same findings with two statistical tests further supports these miRNAs as truly differentially expressed. The expression of the 15 miRNAs was validated by qRT-PCR. Several of the selected miRNAs have predicted targets that are known to be oncogenic. For a discussion of these targets, see Wagenseller et al. [139].

3.4.3 Different miRNA expression changes between responders and non-responders

Last, we investigated if there are miRNAs or sets of miRNAs whose pre-treatment expression would separate the responders from the non-responders (patients with 'progressive disease'). This is a two-class classification problem (10 total samples) with 1,300 features (1,300 miRNAs). Any linear model with 10 of the miRNAs will be guaranteed to perfectly predict responders. The problem is then to identify which 10 or fewer miRNAs most reliably predict responders versus non-responders.

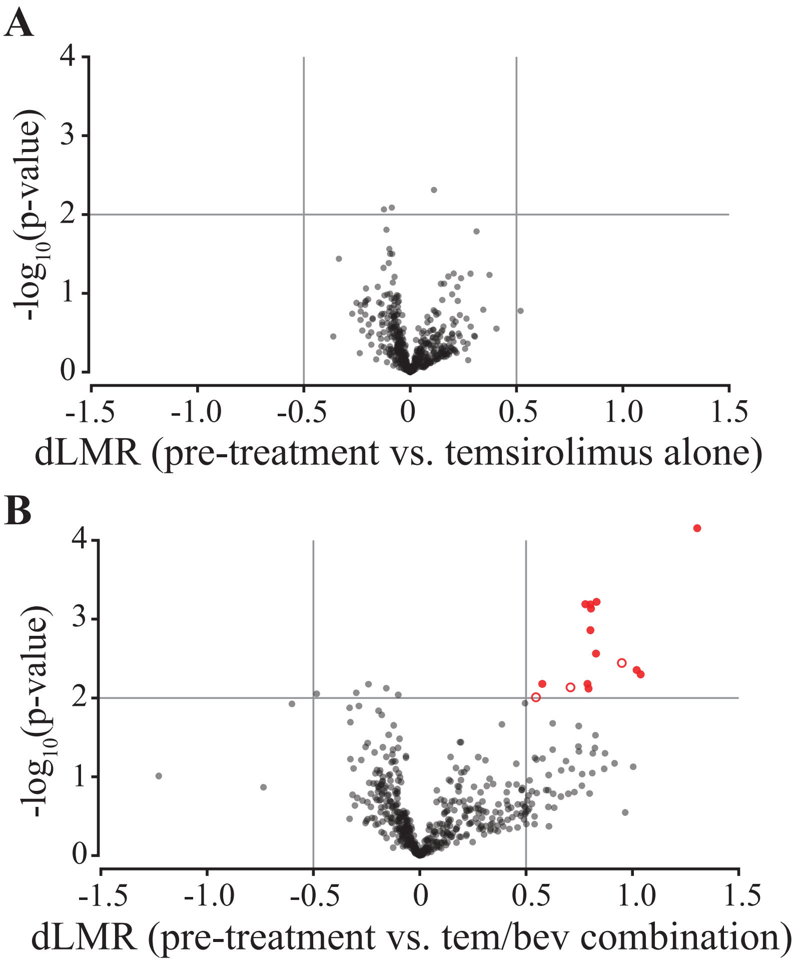

Figure 3.2: Effect size and statistical significance of post- versus pre-treatment miRNA expression Black circles represent individual miRNAs. Red circles indicate miRNAs of interest. Closed red circles are putative tumor suppressors.

Backwards subtraction selection of features finds many possible sets of miRNAs that perfectly predict responders. The problem of many possible models remains. Often, miRNAs are correlated to each other so that the independence assumption of linear models are violated. I investigated regularized linear models (lasso and ridge regression), yet there was still no clear best set of miRNAs that predicted responders. Cross-validation of many models worked 100% of the time. Other predictive models (e.g. support vector machines and decision trees) had similar problems. After conceding that there is no 'best' model given the miRNA data, I decided to present the four miRNAs with $p < 0.01$ and |dLMR| > 0.5 (Figure 3.3A). The heatmap shows that any one of these miRNAs, with an appropriately selected cutoff, are capable of predicting responders versus non-responders. Figure 3.3B shows miRNAs with |dLMR| > 0.5 and $p < 0.04$ when comparing post-combination treatment to pre-treatment expression. Finally, BRAF^{V600E}, BRAF^{WT}, melanomas are treatable with vemurafenib. Since the effectiveness of temsirolimus and bevacizumab are dependent on BRAF status, we also tried to distinguish miRNAs that differ between BRAF^{V600E} and BRAF^{WT}. The separation of samples based on mutational status is more difficult (Figure 3.3C). However, there are a collection of miRNAs that warrant further investigation.

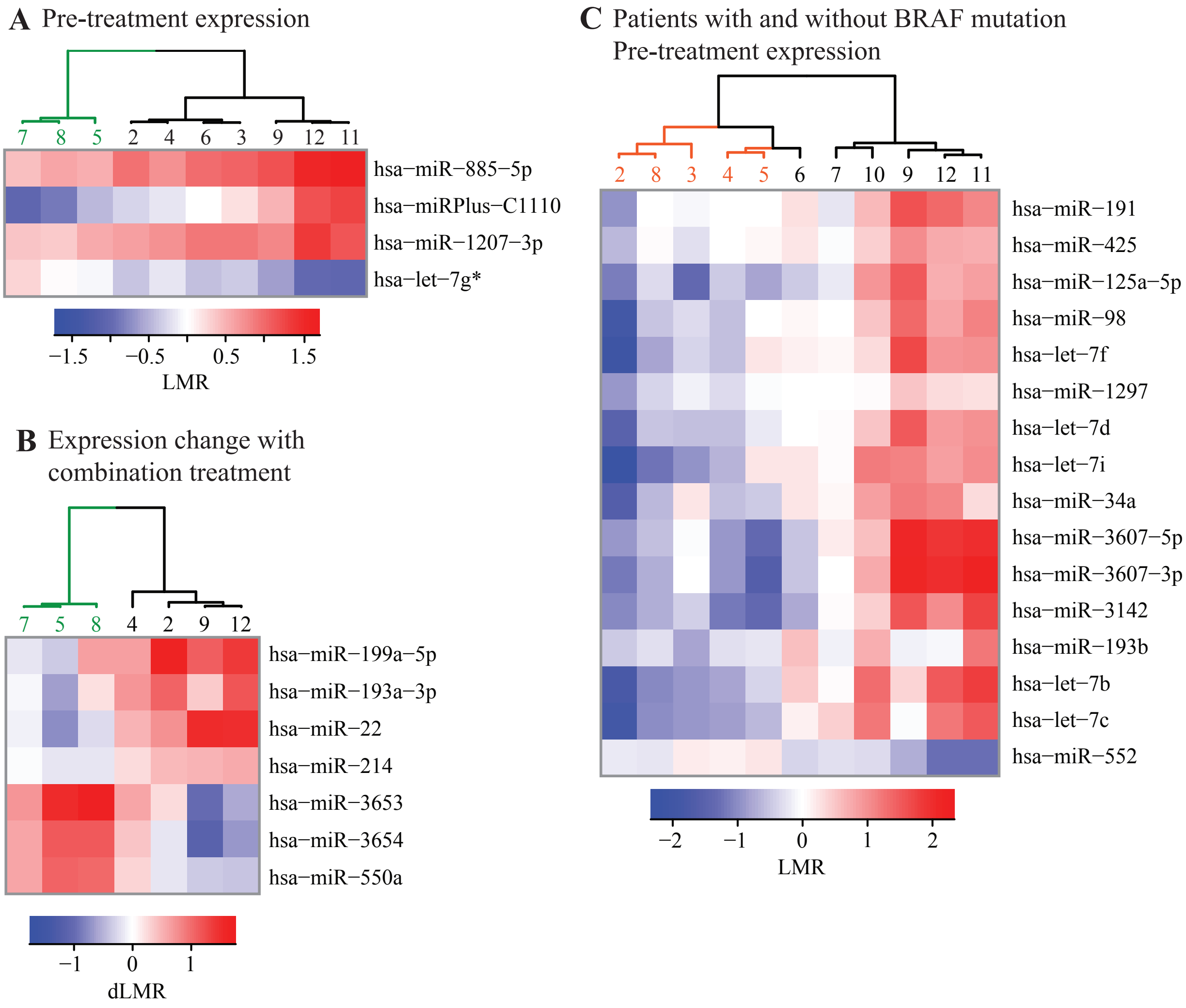

Figure 3.3: Different miRNA expression between responders and non-responders. Green numbers and branches indicate non-responders. Red numbers and branches indicate BRAF^{V600E} tumors.

3.5 Conclusions

Proper use of simple statistical tests and well-designed visualizations corrected for small, but critical errors in the analyses of high throughput biological data obtained from a clinical trial (Figure 3.1).

Bevacizumab+temsirolimus treatment affects miRNA expression more than temsirolimus treatment alone, suggesting that the two drugs are at least additive in their effects on melanoma miRNA expression (Figure 3.2). This is in line with their synergistic growth-reducing effects in melanoma cell lines [146].

The pre-treatment expression of small sets of miRNA predicted the success of bevacizumab+temsirolimus treatment (Figure 3.3A). The expression changes of 7 miRNAs could classify responders versus non-responders; these miRNAs may play a role in the response to treatment (Figure 3.3B).

Chapter 4

Functional transcriptomics of the host response to *C. difficile* toxins

C. difficile causes 300,000+ reported infections and ∼20,000 deaths in the US every year, indirectly costing the healthcare system over $8 billion [1]. Infections indicate worsened health due to *Clostridium difficile*, not normal colonization of C. difficile that occurs in healthy individuals. *C. difficile* strains are only pathogenic if they release toxin A or toxin B (TcdA and TcdB). The basic structure and enzymatic activities of the toxins are understood but the complex host response to the toxins is not [148–153]. Since the severity of illness is determined by the the host and not the extent of infection or the number of bacteria in the host, it is critical to understand detrimental host responses [154].

Taking a systems biology approach, I show how transcriptomics can be used to infer previously unidentfied host cell responses. The field of functional genomics (or functional transcriptomics) overlaps with systems biology. They both aim to determine functions from genetic data and characterize interactions between genes and proteins. In this chapter's last section, I discuss the concept of "enrichment" to identify groups of genes or pathways that are altered.

4.1 *C. difficile*: a dangerous pathogen

4.1.1 Historical significance

In 1935, Hall and O'Toole isolated a novel gram-positive bacterium from infants which they named *Bacillus difficilis* because it was a rod (*Bacillus*) and was an anaerobe that was difficult to grow (*difficilis*). They also identified a *B. difficilis* toxin that killed mice. In 1943, the first rodent model of infection was made unintentionally when penicillin induced inflammation in the cecum [155]. Remarkably, these findings from 70 years ago summarize much of what we now know: *C. difficile* infection occurs when the flora is disrupted by antibiotics and the pathogenic effects are due to toxins. Even more interesting, several studies over 50 years ago suggested that the most effective treatment could be the restoration of the bacterial flora, which in the past few years has proved to be the most effective treatment (reviewed in [156]).

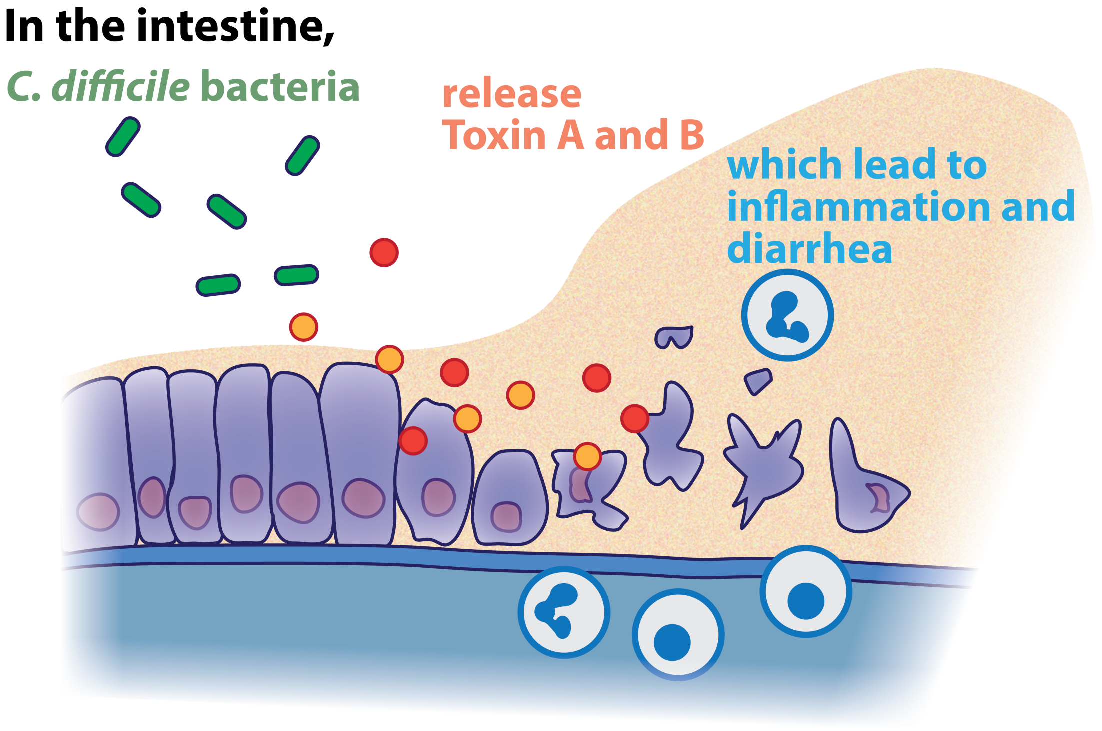

Figure 4.1: An oversimplified view of *C. difficile* infection

After the advent of antibiotics, "pseudomembranous colitis" (PMC), a condition manifesting as inflammation and diarrhea, became associated with antibiotic treatment [156, 157]. The etiology of PMC remained unknown for several years until a rapid succession of experiments between 1977 and 1981 found *C. difficile* and its two large protein toxins (TcdA and TcdB) to be the primary cause of PMC [158–167]. With increased antibiotic usage and improved surveillance, the incidence of *C. difficile* infections has increased nearly every year since [1]. From 1981 to 1995, studies characterized the broad physiological toxin effects, many of which are discussed in the following chapters.

4.1.2 Toxin molecular biology

TcdA and TcdB are extremely potent. They are not small molecules like other toxins such as arsenic or cyanide. As proteins, they are more similar to other toxins such as ricin, anthrax toxin, tetanus toxin, and botulinum toxin (Botox).

The enzymatic activity of TcdA and TcdB which is responsible for their cytopathic effects was discoverd in 1995 by Just et al. [151, 152]. Both TcdA and TcdB, with 63% amino acid homology [168], have N-terminal domains that glucosylate Rho family proteins, disabling them from entering their GTP-bound, active state [151, 152]. The C-terminal of both toxins consists of many "clostridial repetitive oligopeptides" (CROPs) that are present in other clostridial and streptococcal species [169, 170] that are important for cell binding and entry [171–173]. However, it is unclear if the CROPs are entirely necessary for cell entry or if the CROPs can alone cause cytopathic effects [174, 175]. Both toxins enter cells by endocytosis and rearrange structurally in the acidic endosome [176, 177]. After translocating N-terminal domains to the cytosol through self-formed pore in the endosome, a cysteine protease domain cleaves off the glucosyltransferase domain into the cytosol [150, 178, 179]. Although much remains to be understood about the toxins' functions on the molecular level (e.g., no toxin receptors are known and a large middle portion of the toxins has no known function), there are even more unknowns about the disease pathogenesis that is most critical to clinical outcome.

4.1.3 Physiological toxin responses

The external manifestations of *C. difficile* infection are diarrhea, abdominal pain, and sometimes fever. Internally, pseudomembranous colitis is characterized by an inflamed colon covered with yellow, volcano-shaped pseudomembranes made of cellular debris, exudate, and inflammatory cells

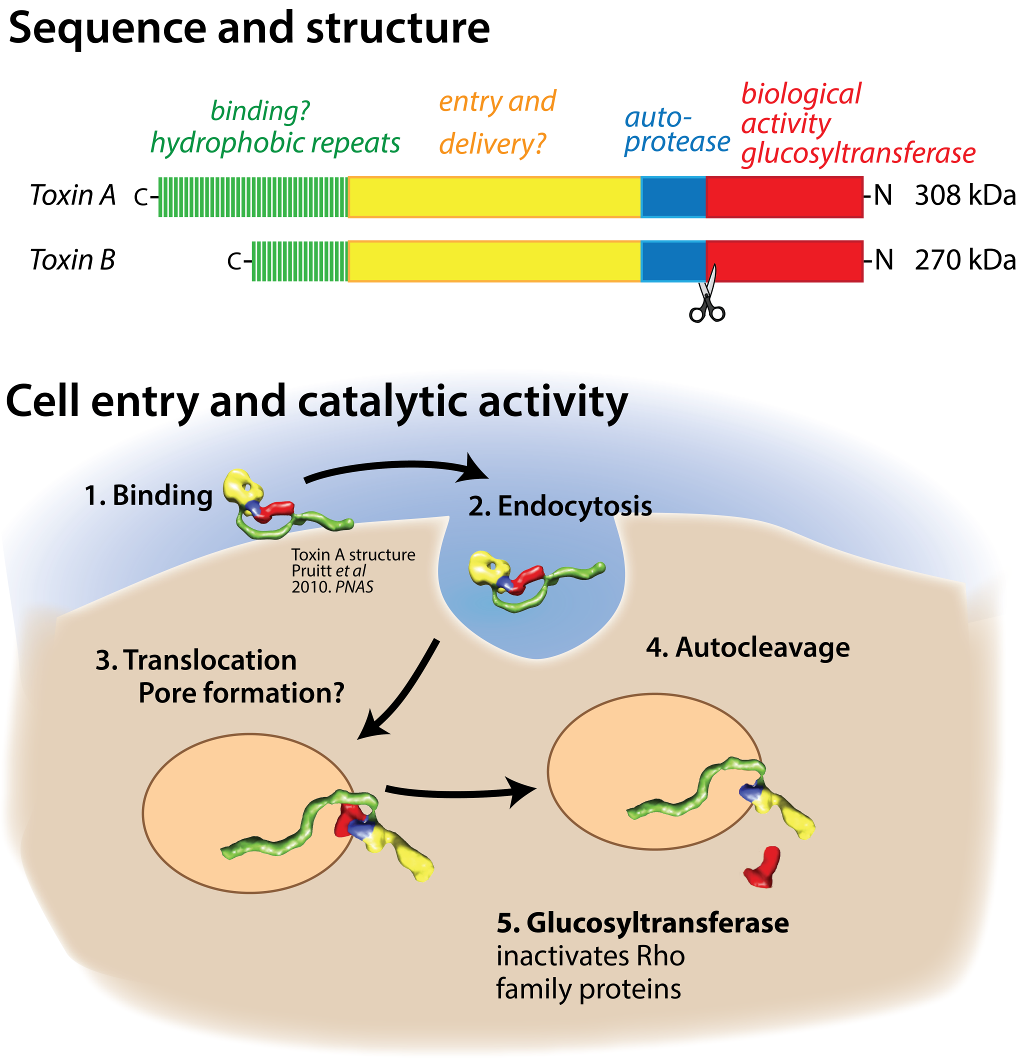

Figure 4.2: Sequence, structure, and functioin of TcdA and TcdB

[157]. Histology reveals an abundance of neutrophils and loss of epithelial barrier integrity [180, 181]. Accordingly, many of the hypotheses for *C. difficile* and toxin studies have been centered around known inflammatory markers. However, how these markers interact together is unknown. It is also unknown if any other cell functions (e.g., regulation of metabolism) contribute to the pathogenesis or the healing process.

4.2 Functional transcriptomics: enrichment

This dissertation presents a systems biology approach to the host response to *C. difficile* toxins, using genome-wide expression to reveal altered cellular functions. Appropriate data processing techniques were chosen to calculate expression values and differentially expressed genes (Chapter 2).

Many network based algorithms can be used to reconstruct regulatory networks and gene interactions. However, many of these methodologies are unproven or still in the formative stages. The approach in this dissertation is to present the differentially expressed genes using exploratory analyses that enable novel hypotheses.

4.2.1 Gene set enrichment analysis

One of the simplest yet most helpful questions from transcriptomics data is 'what types of genes changed'. For example, is the number of differentially expressed chemokines greater than expected? If so, then one could say that the data set is *enriched* with highly expressed chemokines. Alternatively, it is common to say that chemokine genes or chemokine functions are *enriched*.

These questions lead to a hypothesis tests in which the significance of the difference between two different proportions is determined. For example, is there a significantly greater proportion of chemokines in the list of DEGs compared to the list of non-DEGs? The Fisher exact test calculates the significance of such proportions, and it is ubiquitous in gene expression studies. The enrichment of hundreds of predefined sets of genes from public biological databases can be used.

The Fisher test as well as the χ^2 and other tests of proportions require a threshold to define DEGs, and the results of the test are very sensitive to the threshold chosen. A handful of algorithms have tried to solve the problem by scanning many thresholds, but they have had little success. These proportion tests usually assume that genes within the gene set are independent, which usually incorrect.

Like with DEG significance tests, the choices are numerous. In trying to find the appropriate test, I evaluated over 130 articles introducing new tests and software tools to perform enrichment tests, and there are probably one hundred more. Reviews of these methods can usually discuss a portion of the possible tests [182–186]. Also similar to DEG tests, there are many different categories (e.g., parametric tests, permutation tests, machine learning algorithms) that make different statistical assumptions.

Enrichment methods are even more complicated because the hypotheses are ill defined. For instance, are there more genes in a gene set than all genes outside the gene set? Is the fold change of gene in a gene set, on average, different than 1? The first question is more restrictive than the second, but neither are wrong questions to ask.

In later chapters, I describe some more details of different tests and give reasoning to the enrichment tests chosen for the transcriptomics data. The tests were chosen based on exploration of many methods to find the most consistent lists of highly ranked gene sets.

Chapter 5

Toxins A and B disrupt the cell cycle

5.1 Synopsis

Toxins A and B (TcdA and TcdB) are *Clostridium difficile*'s principal virulence factors, yet the pathways by which they lead to inflammation and severe diarrhea remain unclear. Also, the relative role of either toxin during infection and the differences in their effects across cell lines is still poorly understood. To better understand their effects in a susceptible cell line, we analyzed the transciptome-wide gene expression response of human ileocecal epithelial cells (HCT-8) after 2, 6, and 24 hr of toxin exposure. We show that toxins elicit very similar changes in the gene expression of HCT-8 cells, with the TcdB response occurring sooner. The high similarity suggests differences between toxins are due to events beyond transcription of a single cell-type and that their relative potencies during infection may depend on differential effects across cell types within the intestine. We next performed an enrichment analysis to determine biological functions associated with changes in transcription. Differentially expressed genes were associated with response to external stimuli and apoptotic mechanisms and, at 24 hr, were predominately associated with cell-cycle control and DNA replication. To validate our systems approach, we subsequently verified a novel G_1/S and known G_2/M cell-cycle block and increased apoptosis as predicted from our enrichment analysis. This study shows a successful example of a workflow deriving novel biological insight from transcriptome-wide gene expression. Importantly, we do not find any significant difference between TcdA and TcdB besides potency or kinetics. The role of each toxin in the inhibition of cell growth and proliferation, an important function of cells in the intestinal epithelium, is characterized.

5.2 Background

C. difficile, a Gram-positive, spore-forming anaerobe, colonizes the human gut and causes infections leading to pseudomembranous colitis. This opportunistic pathogen flourishes in antibiotic-treated and immunocompromised patients and is frequently spread in hospitals, although community-acquired *Clostridium difficile* infection (CDI) cases have also increased [187]. The emergence of hypervirulent strains that possess more robust toxin production and increased sporulation has been correlated with outbreaks across Europe and North America [188]. In most areas, the number of cases has increased in the past decade. The number of patients hospitalized in the US with CDI doubled to approximately 250,000/year (from year 2000 to 2003) and fatalities increased at a similar rate [189]. The US healthcare costs for CDI are estimated to be over $1 billion/year [190]. As TcdA and TcdB appear to be responsible for many of the clinical manifestations of CDI, understanding the intracellular and systemic effects of each toxin is critical to developing and improving strategies for treatment and prevention.

In light of the multiple events and pathways involved in the development of CDI, we chose to examine the toxins' effects from a systems perspective, focusing on epithelial cells in vitro. Both TcdA and TcdB bind to cells [173], enter an endosome by clathrin-mediated endocytosis [176], translocate and then cleave their catalytic domain into the cytosol which glucosylates and so inactivates Rho family proteins [178]. The disruption of these crucial signaling regulators begins to explain cytotoxic effects such as deregulation of the cytoskeleton and the breakdown of the epithelial barrier [191]. However, other processes are likely affected by the trafficking and processing of these toxins. In addition, secondary effects of Rho glucosylation in relation to pathologies of CDI have not been fully elucidated.

We therefore investigated the transcriptional profile of HCT-8 [192] cells treated with TcdA or TcdB and identified pathways and cellular functions associated with differentially expressed genes. With respect to toxins, in vitro analyses of gene expression in host cells have been performed with type A botulinum neurotoxin, lethal toxin [193] and edema toxin [194] from *Bacillus anthracis*, pertussis toxin [195], Shiga toxin type 1 [196], and several others. Such studies provide lists of differentially expressed genes or classes of genes that serve as a resource for the generation of new hypotheses. In this regard, we used bioinformatics analyses to identify cellular functions altered by TcdA and TcdB that are relevant to pathogenicity. The correct identification of the majority of functions found to be affected in previous research regarding TcdA and TcdB confirmed our analysis and experimental design, and experiments reported herein validated changes in cell function that were suggested by altered gene expression.

Among the genes that TcdA and TcdB affect, many are involved in the regulation of the cell cycle and induction of apoptosis. Bacterial factors such as cytotoxic necrotizing factor and cytolethal distending toxins that disrupt normal cell cycle progression have been described as "cyclomodulins" [197]. In addition to effects of TcdA and TcdB on cells in the G_2/M phase which have been described previously [198–201], we found that TcdA and TcdB affect expression of cyclins and cyclin-dependent kinase (CDK) inhibitors controlling the G_1−S transition. Our experiments establish that alterations of cell cycle implicated in our analysis of gene expression do, in fact, occur in toxin-treated cells. In addition to effects on cell cycle, we also present the other cellular functions associated with differentially expressed genes, some of which enable novel hypotheses on the cellular activity and function of these toxins.

5.3 Methods

5.3.1 Cell Culture

HCT-8 cells were cultured in RPMI-1640 supplemented with 10% heat-inactivated fetal bovine serum (Gibco) and 1mM sodium pyruvate (Gibco). The cultures were maintained at 37°C/5% CO_2 up to passage 35. Toxin A and Toxin B, isolated from strain VPI-10643, were a generous gift from David Lyerly (TECHLAB Inc., Blacksburg, VA).

5.3.2 Microarrays

HCT-8 cells (5 x 106/flask) were grown overnight at 37°C/5% CO_2. Media were replaced with 2.5 ml fresh media and toxin was added (100 ng/ml). At the end of the indicated incubation period, cells were washed with 5 ml PBS (Sigma) and total RNA was isolated using the QIAshredder and RNeasy mini kits (Qiagen), according to the manufacturer's instructions. An RNase inhibitor was added (RNasin, Promega) and samples were stored at -80°C. RNA integrity was assessed using an Agilent 2100 BioAnalyzer prior to cDNA synthesis and RNA labeling using either the 3′ IVT expression or one-cycle target labeling methods (Affymetrix). Biotin-labeled RNA was hybridized to Human Genome U133 Plus 2.0 chips, washed, stained and scanned using a GeneChip System 3000 7G (Affymetrix). Data from three independent microarray experiments were deposited into the NCBI Gene Expression Omnibus repository (GSE29008).

Microarray signal intensities were normalized using the gcrma package [17]. Treatment and control groups were contrasted with linear models; a Benjamini-Hochberg correction was applied across all the probes and the nestedF method within the limma software package was used for multiple testing across all contrasts [63, 64]. The Gene Ontology (GO) annotation database was used to map gene symbols to GO categories [202]. A gene symbol was considered differentially expressed if at least one of the probe sets annotated to it was significant. A probe set was considered significant if the $p<0.1$ and the magnitude of the fold change was above 1.5. Enriched GO categories were identified with the topGO package using Fisher's exact test to calculate p-values and the elim algorithm [203].

5.3.3 Flow Cytometry

HCT-8 cells were grown overnight to 50% confluence, media were removed and replaced with fresh media, and toxin was added at the concentrations denoted in the text and figures. At 24h and 48h, non-adherent cells were removed and saved on ice. Adherent cells were treated with 1mL of 0.25% trypsin and 1 mL of Accutase with EDTA for 30 min at room temperature and joined with the non-adherent cells in 5 mL PBS. After centrifugation, resuspension for counting cells, and another round of centrifugation, the dissociated cells were resuspended to 2×10^6 cells/mL and 0.5 mL was added to 5mL of 70% ice-cold ethanol for fixation. Afterward, the fixed cells were resuspended in 5 ml PBS with 2% Bovine Serum Albumin and then resuspended and incubated for 30 min in a solution to stain DNA (PBS with 10% Triton X-100, 2% DNasefree RNase, 0.02% propidium iodide(PI)). Single-cell fluorescence was measured with a Becton Dickinson FACSCalibur flow cytometer. The proportion of cells in each stage of the cell cycle was calculated using ModFit cell cycle analyzer. The 24h-samples were imaged with an Amnis Imagestream imaging flow cytometer, which photographs the bright field and fluorescent channels from every cell individually [204]. Using Amnis software, a bivariate gate—based on the contrast of the brightfield image and the area of nuclear stain—differentiated apoptotic and non-apoptotic cells [205]. All other image features were taken from the Amnis software.

5.3.4 Quantitative real time PCR

For each gene examined, primers were designed from the target sequences retrieved from the RefSeq Sequence Database, using the Primer Express 3.0 software (Applied Biosystems). Primers were then custom made through Invitrogen Oligo Program. RNA quality control was carries out using an Agilent 2100 BioAnalyzer. Approximately 2 µg of each RNA sample was converted to cDNA. Quantitative PCRs were carried out in triplicates using equal amounts of each cDNA sample approximately equivalent to 50 ng of starting total RNA. Power SYBR Green Master Mix (Applied Biosystems, PN 4367660) was used with the respective forward and reverse primers at the optimized concentrations. Amplifying PCR and monitoring of the fluorescent emission in real time were performed in the ABI Prism 7900HT Sequence Detection System (Applied Biosystems) as described (ABI SYBR Green Protocol). To verify that only a single PCR product was amplified per transcript, dissociation curve data was analyzed through the 7900HT Sequence Detection Software (SDS). To account for differences in starting material, quantitative PCR was also carried out for each cDNA sample using housekeeping genes synthesized in-house, human glyceraldehyde-3-phosphate dehydrogenase (GAPDH) and hypoxanthine phosphoribosyltransferase I (HPRT1). The data collected from these quantitative PCRs defined a threshold cycle number (Ct) of detection for the target or housekeeping genes in each cDNA sample. The relative quantity (RQ) of target, normalized to geometric means of the housekeeping genes and relative to a calibrator (the Rox reference dye in this case), is given by $RQ = 2–\Delta\Delta Ct$ where $\Delta\Delta Ct$ represents the difference in Ct between the transcript and the housekeeping gene for the same RNA sample. The ratio of the RQs for the treated sample and the experiment sample was used to derive the fold change.

5.3.5 Western Blots

After toxin treatment, non-adherent cells were removed and centrifuged. The adherent cells were then treated with 200 µL of homogenization buffer: 10 mM HEPES pH 7.4, 150 mM NaCl, 10 mM sodium pyrophosphate, 10 mM NaF, 10 mM EDTA, 4mM EGTA, 0.1 mM PMSF, 2 g/mL CLAP (Chymostatin, Leupeptin, Antipain, and Pepstatin), and 1% Triton X-100. Each well was scraped and the sample with homogenization buffer was added to the resuspended non-adherent cells. This was centrifuged at 15,000 rpm for 5 min at 4°C and the supernatant was boiled for 5 min, placed on ice for 5 min, boiled again for 5 min, and stored at -20°C. Samples containing equal amounts of protein were loaded into each lane of a 12.5% polyacrylamide gel. Gels were electrophoresed, transferred to PVDF, and the membranes were blocked with 5% skim milk in PBS, 0.1% Tween-20 for 2h. Primary antibodies (Cyclin D1 #2922, Cyclin E2 #4132, p57 Kip2 #2557, p27 Kip1 #2552 from Cell Signaling and Cyclin A sc-751 from Santa Cruz Biotechnology) were added to the blocking solution and membranes were incubated overnight at 4°C on a platform shaker. The membranes were then washed six times in PBS-Tween 20. The appropriate secondary antibodies, either anti-mouse or anti-rabbit HRP-linked antibodies (#7076, #7074, Cell Signaling), were added and the membranes were incubated for 2h on a platform shaker. The membranes were subsequently washed 6 times and proteins were detected by chemiluminescence with ECL reagents (Amersham). To strip antibodies, the membranes were incubated in 50 mM Tris, 2% SDS, 0.7% -mercaptoethanol at 50°C for 30 min. The membranes were then washed 6 times, blocked, and reprobed with a GAPDH antibody (ab8245 from Abcam) as described above.

5.4 Results

5.4.1 Transcriptional Responses

Overall, the changes in gene expression are consistent as time progresses, but the number of differentially expressed genes increases (Figure 5.1A). Specifically, at 2h and 6h, there are 4 and 134 probe sets differentially expressed (relative to control) for TcdA and 57 and 294 for TcdB, respectively (Figure 5.1C). Many more are differentially expressed by 24h—1,155 and 1,205 in TcdA- and TcdB-treated cells, respectively. In order to validate these data, qRT-PCR was performed on 10 representative genes (r=0.89 by Pearson correlation; Figure 5.2A). Since the glucosylation of Rho family proteins occurs within one hour of toxin treatment [206], many of the differentially expressed genes at 24h may reflect secondary effects from the initial toxin action or possibly other unknown activities and processing of the toxin.

Though the transcriptional responses to the two toxins are similar overall, a notable difference between the two toxins is that TcdB-induced changes occur more rapidly (Figure 5.1A). At the later time points, however, the overall transcriptional response induced by TcdA becomes more similar

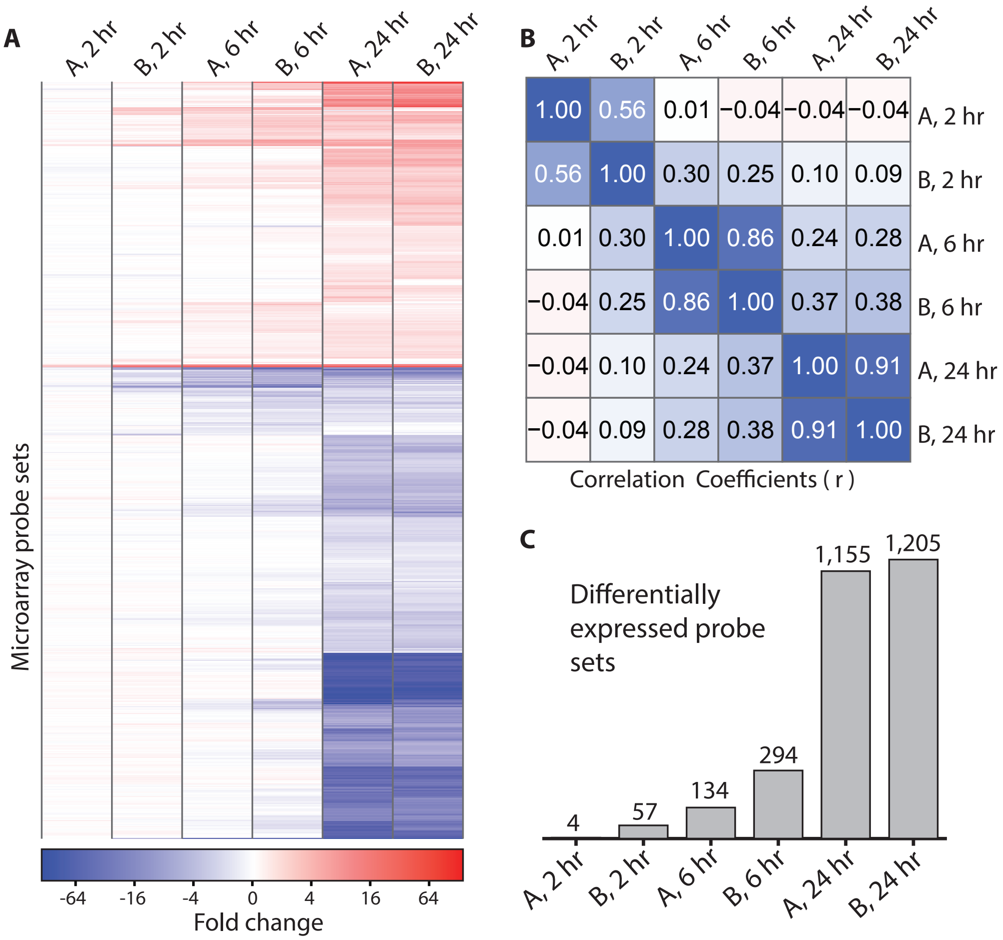

A, 2 hr	B, 2 hr	A, 6 hr	B, 6 hr	A, 24 hr	B, 24 hr	
1.00	0.56	0.01	−0.04	−0.04	−0.04	A, 2 hr
0.56	1.00	0.30	0.25	0.10	0.09	B, 2 hr
0.01	0.30	1.00	0.86	0.24	0.28	A, 6 hr
−0.04	0.25	0.86	1.00	0.37	0.38	B, 6 hr
−0.04	0.10	0.24	0.37	1.00	0.91	A, 24 hr
−0.04	0.09	0.28	0.38	0.91	1.00	B, 24 hr

Correlation Coefficients (r)

Figure 5.1: Overall transcriptional response of HCT-8 cells to TcdA and TcdB. (A) A heatmap shows the number of differentially expressed probe sets at 2h, 6h, and 24h. The color scale represents the fold change (binary log scale) of genes relative to untreated cells at the same time point. "A, 2hr" indicates the gene expression of cells after 2h of TcdA treatment. TcdA and TcdB concentration is 100 ng/ml. **(B)** The correlation of transcriptional profiles between TcdA and TcdB at the indicated time points are displayed in a correlation matrix. The values represent the Pearson correlation coefficient calculated from the fold change of all the probe sets within the microarray. **(C)** The number of differentially expressed genes used to identify enriched GO categories was determined from a linear model (see 5.3.2).

to the TcdB-induced transcriptional changes (see correlations in Figure 5.1B). Among the most affected genes, immediate early-response genes such as JUN, KLF2, and RHOB are upregulated 2h after toxin treatment and remain increased compared to untreated cells through 24 hr (Figure 5.2B). While identification of the most-affected genes provides important insight, focusing on a small subset risks overlooking other toxin effects key to the disease process. We therefore analyzed the expression data in the context of broad functional categories.

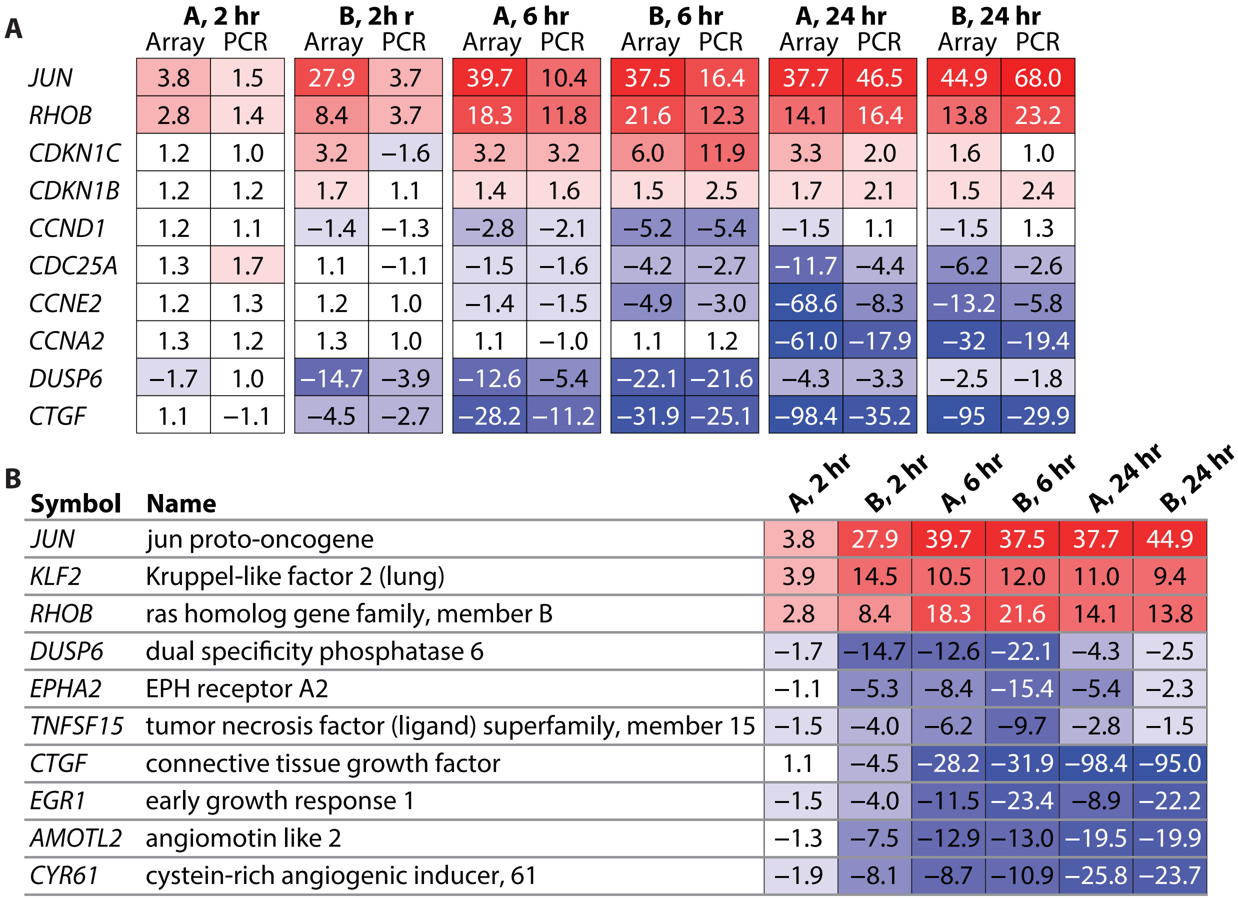

A

	A, 2 hr		B, 2h r		A, 6 hr		B, 6 hr		A, 24 hr		B, 24 hr	
	Array	PCR	Array	PCR	Array	PCR	Array	PCR	Array	PCR	Array	PCR
JUN	3.8	1.5	27.9	3.7	39.7	10.4	37.5	16.4	37.7	46.5	44.9	68.0
RHOB	2.8	1.4	8.4	3.7	18.3	11.8	21.6	12.3	14.1	16.4	13.8	23.2
CDKN1C	1.2	1.0	3.2	−1.6	3.2	3.2	6.0	11.9	3.3	2.0	1.6	1.0
CDKN1B	1.2	1.2	1.7	1.1	1.4	1.6	1.5	2.5	1.7	2.1	1.5	2.4
CCND1	1.2	1.1	−1.4	−1.3	−2.8	−2.1	−5.2	−5.4	−1.5	1.1	−1.5	1.3
CDC25A	1.3	1.7	1.1	−1.1	−1.5	−1.6	−4.2	−2.7	−11.7	−4.4	−6.2	−2.6
CCNE2	1.2	1.3	1.2	1.0	−1.4	−1.5	−4.9	−3.0	−68.6	−8.3	−13.2	−5.8
CCNA2	1.3	1.2	1.3	1.0	1.1	−1.0	1.1	1.2	−61.0	−17.9	−32	−19.4
DUSP6	−1.7	1.0	−14.7	−3.9	−12.6	−5.4	−22.1	−21.6	−4.3	−3.3	−2.5	−1.8
CTGF	1.1	−1.1	−4.5	−2.7	−28.2	−11.2	−31.9	−25.1	−98.4	−35.2	−95	−29.9

B

Symbol	Name	A, 2 hr	B, 2 hr	A, 6 hr	B, 6 hr	A, 24 hr	B, 24 hr
JUN	jun proto-oncogene	3.8	27.9	39.7	37.5	37.7	44.9
KLF2	Kruppel-like factor 2 (lung)	3.9	14.5	10.5	12.0	11.0	9.4
RHOB	ras homolog gene family, member B	2.8	8.4	18.3	21.6	14.1	13.8
DUSP6	dual specificity phosphatase 6	−1.7	−14.7	−12.6	−22.1	−4.3	−2.5
EPHA2	EPH receptor A2	−1.1	−5.3	−8.4	−15.4	−5.4	−2.3
TNFSF15	tumor necrosis factor (ligand) superfamily, member 15	−1.5	−4.0	−6.2	−9.7	−2.8	−1.5
CTGF	connective tissue growth factor	1.1	−4.5	−28.2	−31.9	−98.4	−95.0
EGR1	early growth response 1	−1.5	−4.0	−11.5	−23.4	−8.9	−22.2
AMOTL2	angiomotin like 2	−1.3	−7.5	−12.9	−13.0	−19.5	−19.9
CYR61	cystein-rich angiogenic inducer, 61	−1.9	−8.1	−8.7	−10.9	−25.8	−23.7

Figure 5.2: qRT-PCR validation of and genes with high differential expression (A) Fold changes of gene expression relative to controls as measured by microarray were validated by qRT-PCR. To summarize multiple probe sets within a microarray that were annotated to the same gene, the value for the probe set with the greatest fold change is shown. The notation "A, 2hr" indicates the expression of genes treated with TcdA for 2 hr. **(B)** This list consists of genes that were among the top 25 differentially expressed genes (according to fold change) in at least 3 of the 6 conditions.

5.4.2 Functions associated with differentially expressed genes

We employed the GO database, which contains extensive annotation of biological functions associated with specific genes, to identify cellular phenotypes associated with changes in gene expression. The terms in this database are separated into three ontologies: Molecular Functions, Cellular Components, and Biological Processes (detailed descriptions at http://www.geneontology.org). A GO category—here defined as all the genes associated with a single GO term—with a proportion of differentially expressed genes greater than would be expected by chance is considered overrepre-

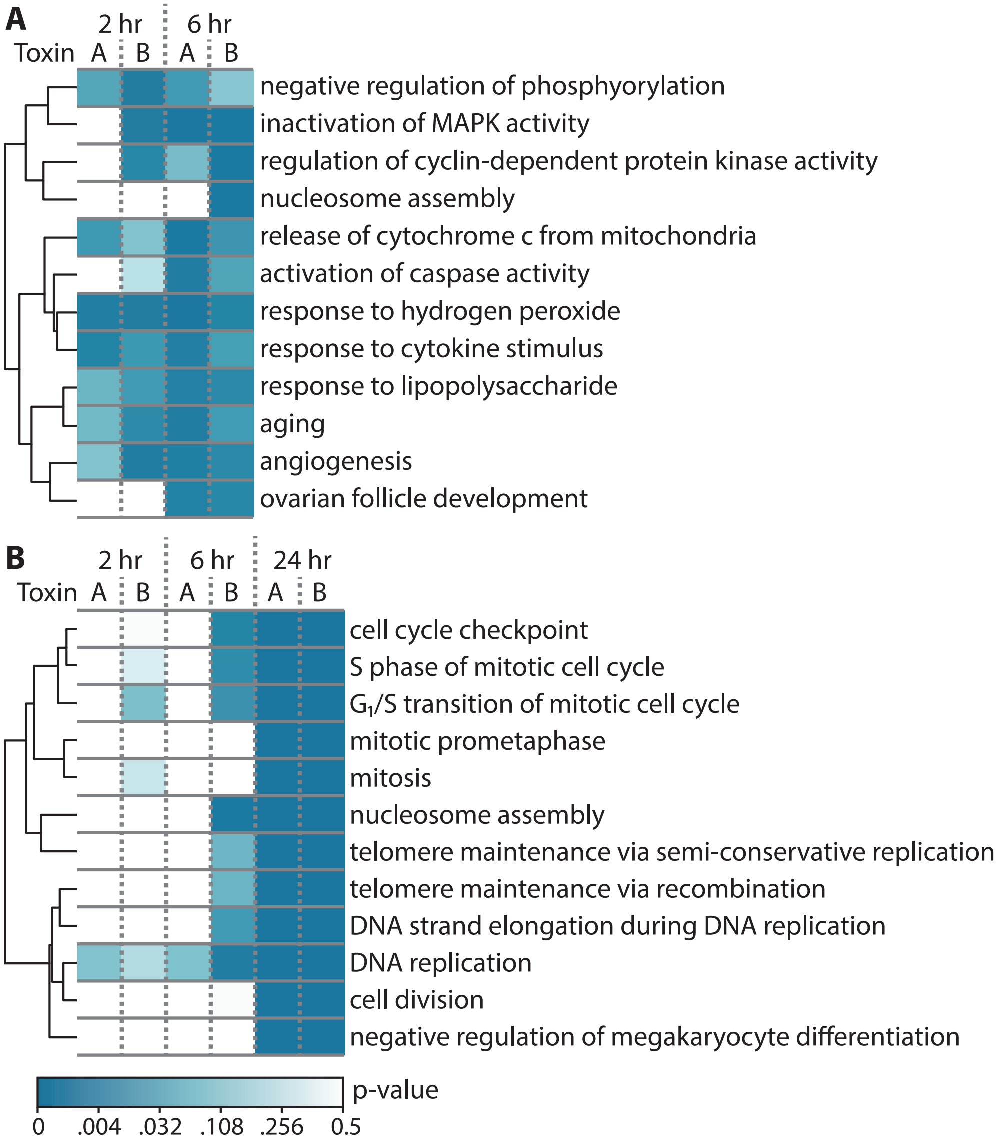

Figure 5.3: Gene ontology categories associated with differentially expressed genes. **(A)** The most significantly enriched GO categories (Fisher Exact Test, topGO elim algorithm [203], see 5.3.2) at 2h and 6h are displayed in a heat map. The color intensity in each cell corresponds to the p-value (Fisher Exact Test) for the GO category that is enriched. The dendrograms were generated from a hierarchical clustering of GO Groups according to Resnik similarity [207]. **(B)** The most significantly enriched GO categories at 24h were determined similarly

sented or enriched (see 5.3.2). While some enriched categories might have been anticipated, others provide novel insights. Within the Biological Processes ontology, the most significantly enriched categories at 2 and 6 hr are listed in Figure 5.3A. Within the Cellular Component ontology, the mitochondrial outer membrane and the apical junction complex category are enriched most significantly at 6h (Figure 5.4A). Interestingly, many of the functions related to the enriched categories

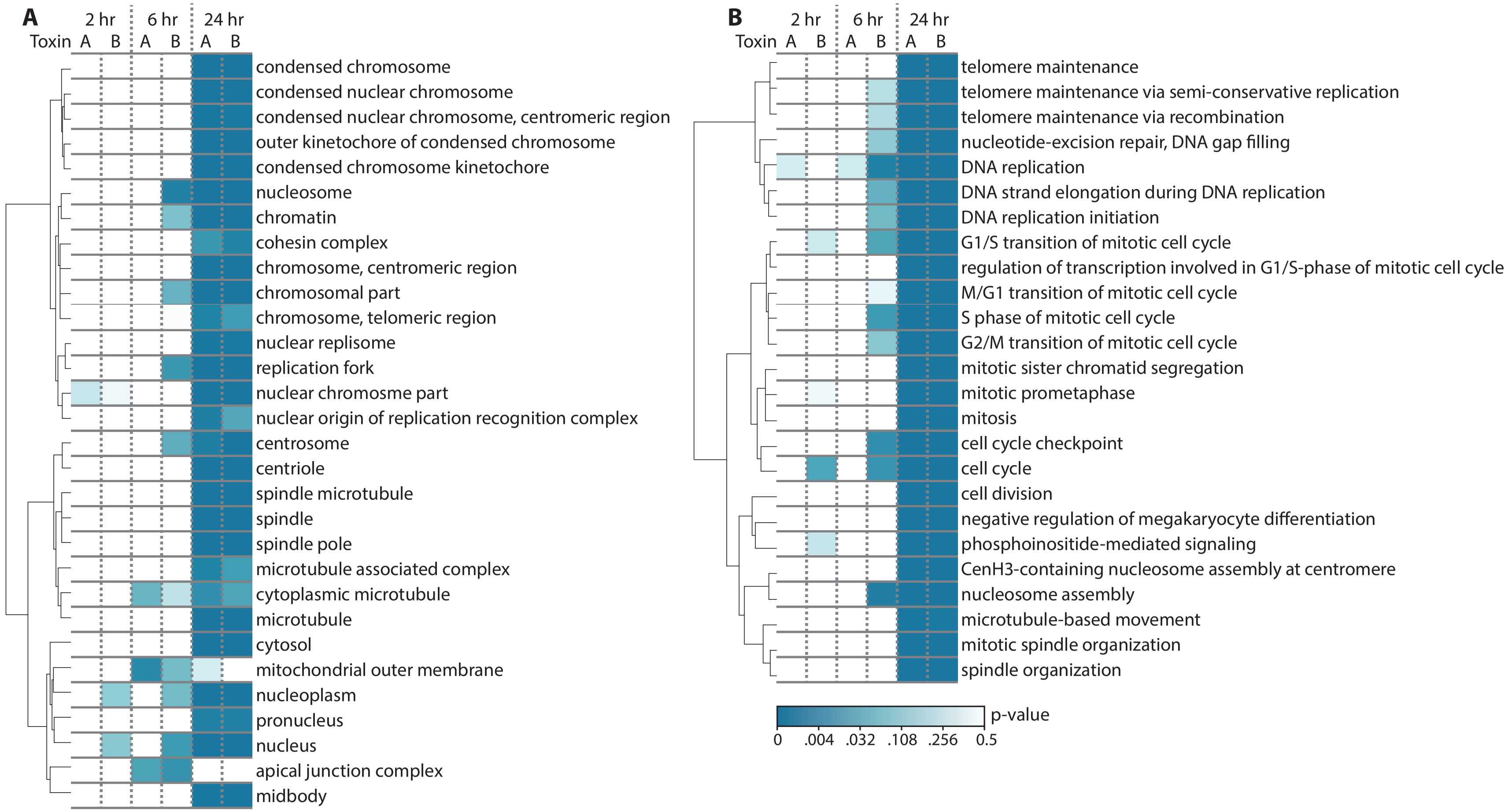

Figure 5.4: Gene set enrichment of biological processes and cellular components. **(A)** Cellular Component GO categories with $p < 10^{-3}$ across all time points are shown. Criteria for calculating p values and GO categories were the same as in Figure 2. **(B)** The 25 most significant GO Biological Processes at 24 hr were selected by the criteria described in Figure 5.3.

have been linked with toxin treatment in previous work. One or both of the toxins induce activation of caspases [200, 208–210], damage mitochondria and cause the release of cytochrome c [211, 212], increase oxygen radicals and expression of cytokines [213–215], alter MAPK signaling [216–218], and disrupt the organization of tight junctions [191]. Hence, our analysis of gene expression as summarized in Figure 5.3 is consistent with the previously reported cellular responses to these toxins.

The most significantly enriched categories for each toxin at the later time points are related to cell cycle and DNA replication (Figure 5.3B). Categories such as telomere maintenance and nucleosome assembly provide more specific connections between the toxins and changes in DNA replication. A more extensive list reveals that several categories related to microtubule organization during cell division are also enriched (Figure 5.4B). By 24 hr, there are changes related to virtually all elements of the cell cycle, but those controlling G_1 and S phases are more significantly affected. Though many of the genes within the enriched categories were not among the most differentially expressed genes, the abundance of differentially expressed genes involved in the same functions provides evidence for toxin effects on control of cell cycle at the G_1 phase. Cyclins and other proteins necessary for progression from the G_1 phase into and through the S phase are downregulated (Figure 5.5A). Cyclin proteins expressed at different points are central in coordinating entry into or exit from different phases. They specifically bind and activate particular CDKs which then phosphorylate downstream targets effecting progression [219]. Inhibitors of cyclin-CDK complexes from the INK4 family (p15, p16, p18, and p19) and Cip/Kip family (p21, p27, and p57) may suppress cyclin-CDK signaling [220]. Expression of many of these and other genes, such as CDC6 and CDC25A that are required for progression from G_1 to the S phase, is altered by TcdA and TcdB. The decreased expression of G_1 cyclins along with the increased expression of inhibitors of G_1-associated cyclin-CDK complexes suggest altered regulation of the cell cycle specifically in G_1. We also measured expression of genes and proteins (Figure 5.6) after 6 and 24 hr of treatment with 0.1, 1, and 10 ng/ml of TcdA or TcdB in confluent and subconfluent cultures, which confirmed a consistent alteration of cell cycle genes and proteins across a variety of conditions.

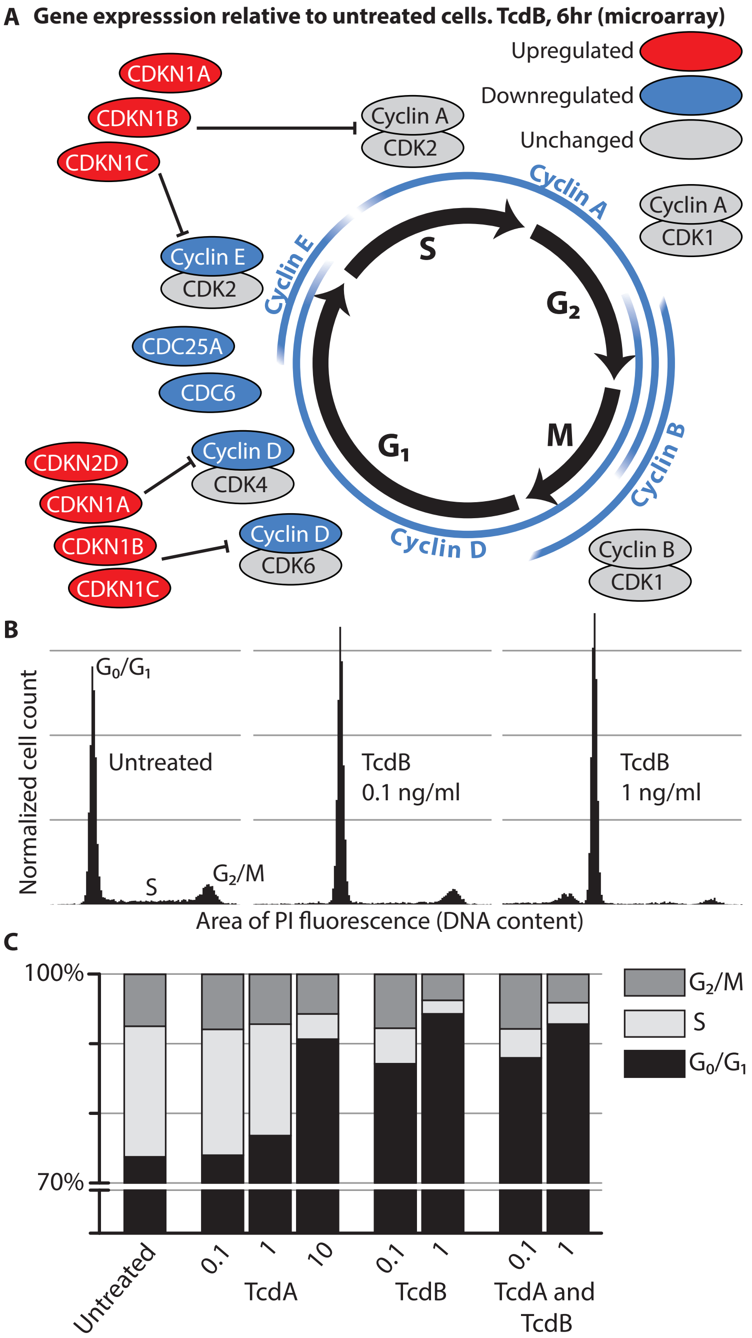

Figure 5.5: The altered gene expression of G_1 phase cell cycle regulators at 6h and changes in the distribution of cells within the cell cycle. **(A)** A schematic of cell cycle regulation with proteins placed next to the phase of cell cycle with which they are associated (p19 and p21 are the products of the CDKN2D and CDKN1A genes, respectively). Gray, blue, and red indicate genes with unchanged, increased, or decreased expression, respectively, post toxin treatment. **(B)** Cells in a subconfluent culture were treated with the indicated concentrations of toxin for 24h. The DNA content of cells in each condition was quantified by PI fluorescence. The histograms of the area of PI fluorescence are normalized to the total number of cells (denoted as normalized cell count) in the sample such that the area under each histogram is equal to 1. In this way, the proportions of cells in each phase of the cell cycle may be compared for different size samples. The scale of the vertical axis is the same in each histogram. **(C)** The percentage of cells in each phase of the cell cycle was calculated using ModFit LT software. Sub-G_0/G_1 cells were not included in the calculations.

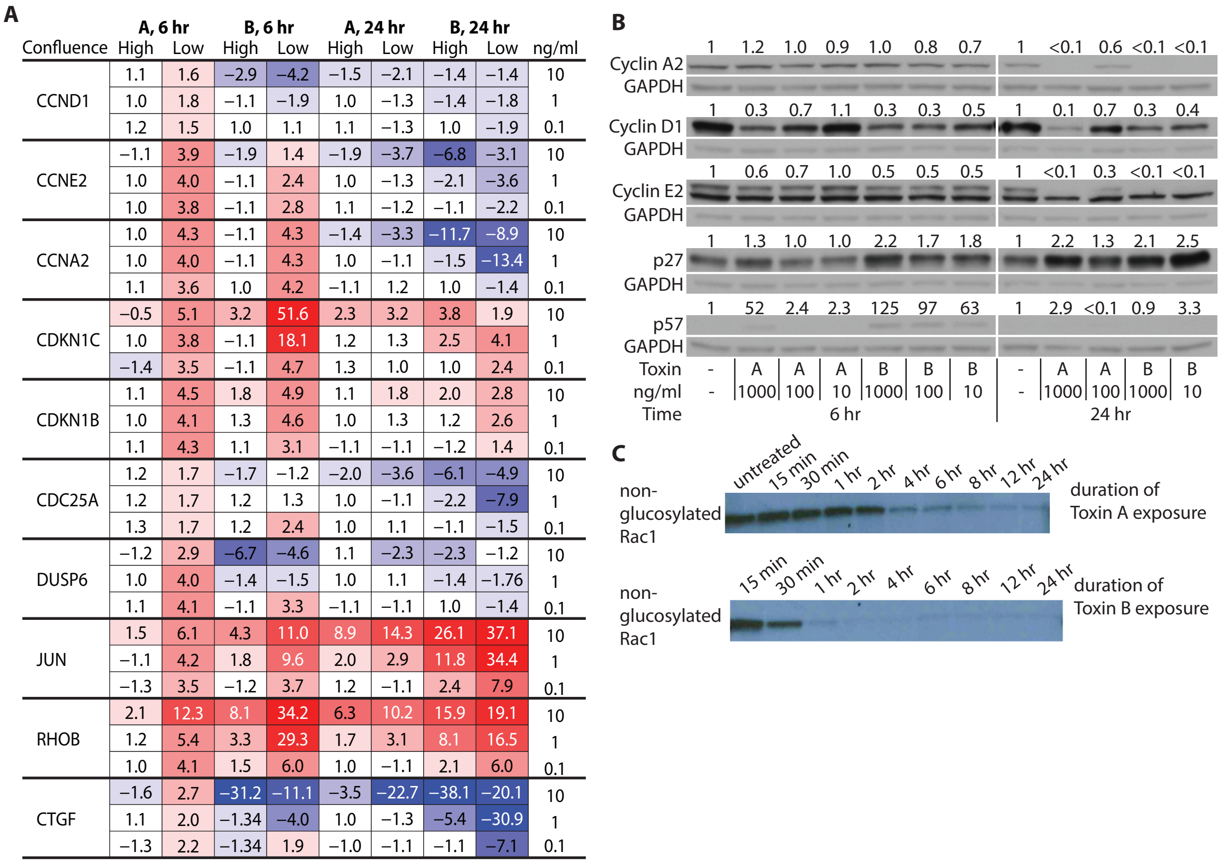

A

	A, 6 hr		B, 6 hr		A, 24 hr		B, 24 hr		
Confluence	High	Low	High	Low	High	Low	High	Low	ng/ml
CCND1	1.1	1.6	−2.9	−4.2	−1.5	−2.1	−1.4	−1.4	10
	1.0	1.8	−1.1	−1.9	1.0	−1.3	−1.4	−1.8	1
	1.2	1.5	1.0	1.1	1.1	−1.3	1.0	−1.9	0.1
CCNE2	−1.1	3.9	−1.9	1.4	−1.9	−3.7	−6.8	−3.1	10
	1.0	4.0	−1.1	2.4	1.0	−1.3	−2.1	−3.6	1
	1.0	3.8	−1.1	2.8	1.1	−1.2	−1.1	−2.2	0.1
CCNA2	1.0	4.3	−1.1	4.3	−1.4	−3.3	−11.7	−8.9	10
	1.0	4.0	−1.1	4.3	1.0	−1.1	−1.5	−13.4	1
	1.1	3.6	1.0	4.2	−1.1	1.2	1.0	−1.4	0.1
CDKN1C	−0.5	5.1	3.2	51.6	2.3	3.2	3.8	1.9	10
	1.0	3.8	−1.1	18.1	1.2	1.3	2.5	4.1	1
	−1.4	3.5	−1.1	4.7	1.3	1.0	1.0	2.4	0.1
CDKN1B	1.1	4.5	1.8	4.9	1.1	1.8	2.0	2.8	10
	1.0	4.1	1.3	4.6	1.0	1.3	1.2	2.6	1
	1.1	4.3	1.1	3.1	−1.1	−1.1	−1.2	1.4	0.1
CDC25A	1.2	1.7	−1.7	−1.2	−2.0	−3.6	−6.1	−4.9	10
	1.2	1.7	1.2	1.3	1.0	−1.1	−2.2	−7.9	1
	1.3	1.7	1.2	2.4	1.0	1.1	−1.1	−1.5	0.1
DUSP6	−1.2	2.9	−6.7	−4.6	1.1	−2.3	−2.3	−1.2	10
	1.0	4.0	−1.4	−1.5	1.0	1.1	−1.4	−1.76	1
	1.1	4.1	−1.1	3.3	−1.1	−1.1	1.0	−1.4	0.1
JUN	1.5	6.1	4.3	11.0	8.9	14.3	26.1	37.1	10
	−1.1	4.2	1.8	9.6	2.0	2.9	11.8	34.4	1
	−1.3	3.5	−1.2	3.7	1.2	−1.1	2.4	7.9	0.1
RHOB	2.1	12.3	8.1	34.2	6.3	10.2	15.9	19.1	10
	1.2	5.4	3.3	29.3	1.7	3.1	8.1	16.5	1
	1.0	4.1	1.5	6.0	1.0	−1.1	2.1	6.0	0.1
CTGF	−1.6	2.7	−31.2	−11.1	−3.5	−22.7	−38.1	−20.1	10
	1.1	2.0	−1.34	−4.0	1.0	−1.3	−5.4	−30.9	1
	−1.3	2.2	−1.34	1.9	−1.0	−1.1	−1.1	−7.1	0.1

B

Cyclin A2 / GAPDH	1	1.2	1.0	0.9	1.0	0.8	0.7	1	<0.1	0.6	<0.1	<0.1
Cyclin D1 / GAPDH	1	0.3	0.7	1.1	0.3	0.3	0.5	1	0.1	0.7	0.3	0.4
Cyclin E2 / GAPDH	1	0.6	0.7	1.0	0.5	0.5	0.5	1	<0.1	0.3	<0.1	<0.1
p27 / GAPDH	1	1.3	1.0	1.0	2.2	1.7	1.8	1	2.2	1.3	2.1	2.5
p57 / GAPDH	1	52	2.4	2.3	125	97	63	1	2.9	<0.1	0.9	3.3
Toxin	-	A	A	A	B	B	B	-	A	A	B	B
ng/ml	-	1000	100	10	1000	100	10	-	1000	100	1000	10
Time	6 hr							24 hr				

Figure 5.6: Timing of RAC1 glucosylation and expression of cyclin-related genes and proteins in subconfluent and confluent cultures. (A) The expression of 10 genes in both subconfluent and confluent toxin-treated cells was measured by qRT-PCR. Fold changes shown are relative to untreated samples. (B) Densitometry was performed on immunoblots of lysates from toxin-treated, confluent cells. The intensity of each band was normalized to the intensity of GAPDH, the loading control. The values above each row indicate the amount of protein relative to the amount in untreated cells. The relative intensity for p57 was not calculated because the protein was not detectable in untreated cells. The blots show the presence of p57 after toxin treatment. (C) A Rac1 antibody (BD#610650) that recognizes non-glucosylated Rac1 (protein that has not been glucosylated by either toxin) shows the activity of TcdA and TcdB in HCT-8 cells.

5.4.3 Effects of TcdA and TcdB on the Regulation of Cell Cycle

The functional changes suggested by altered gene and protein expression were then investigated by quantifying the proportion of cells in each phase of the cell cycle before and after toxin treatment. To focus on actively growing cells and avoid the effects of contact inhibition, subconfluent cultures were used. After 24 hr of 0.1 or 1 ng/ml TcdB treatment, the distribution of cells across the cell cycle changes significantly, with only a small increase in the proportion of cells with less than a G_0/G_1 amount of DNA—cells that are presumably dead or dying (Figure 5.5B). In agreement with our gene expression analysis, the percentage of G_0/G_1 cells increased from 67% in untreated cells to 91% and 94% in cultures treated with 10 ng/ml TcdA and 1 ng/ml TcdB, respectively (Figure 5.5C). The magnitude of increase in the G_0/G_1 proportion is also concentration-dependent. The effect on cell cycle by the combination of TcdA and TcdB is comparable to those produced by TcdB alone (Figure 5.5C), indicating that,with respect to their influence on cell-cycle arrest, the toxins are neither synergistic nor antagonistic. As with gene and protein expression, TcdB is more potent or faster-acting than TcdA. Taken together, these data establish that the toxin-induced alterations in genes associated with cell cycle correlate with a block at the G_1–S interface. In other studies, a G_2/M arrest has been reported in human cell lines treated with different concentrations of TcdA or TcdB [199–201]. This G_2/M arrest has been linked with a deregulation of the cell structure resulting in an inability of cells to complete cytokinesis [221]. We therefore investigated the cell cycle effects and morphology of cells treated for 24 hr with higher concentrations of TcdA (100 ng/ml) and TcdB (10 and 100 ng/ml).

Our analysis of single-cell images from toxin-treated cultures reveals two unanticipated observations: (1) a biphasic distribution of apoptotic cells with respect to stage of cell cycle and (2) two populations of cells at the G_2/M interface. Cells with a high-contrast bright-field image and a low area of PI fluorescence are classified as apoptotic (Figure 5.7A). Typically, apoptotic cells are associated with a PI fluorescence level less than that of the G_0/G_1 population. Here, a significant portion of the toxin-treated cells between the G_0/G_1 and G_2/M cell populations (typically associated with/attributed to the S-phase) are apoptotic (Figure 5.7B). Thus, the accumulation of toxin-treated cells with S-phase levels of PI-fluorescence is not the result of progression from G_1 but rather the apoptosis of G_2/M cells. Even 24 hr after the addition of 100 ng/ml of TcdB, apoptosis does not dominate or override effects on cell cycle. At the highest concentration tested (100 ng/ml), 68.6% of TcdB-treated cells are still classified as non-apoptotic (Figure 5.7B). Of the total number of non-apoptotic cells, the proportion in the G_2/M phase increases as the concentrations of either TcdA or TcdB increases, indicating an inhibition of progression from G_2/M phase, in addition to the G_1-S block discussed above.

In order to understand the differences between toxin-treated and control cells in G_2/M, we determined several cellular characteristics (circumference, area, and others) of individual cells using an imaging flow cytometer. The feature that best distinguishes toxin-treated from untreated cells

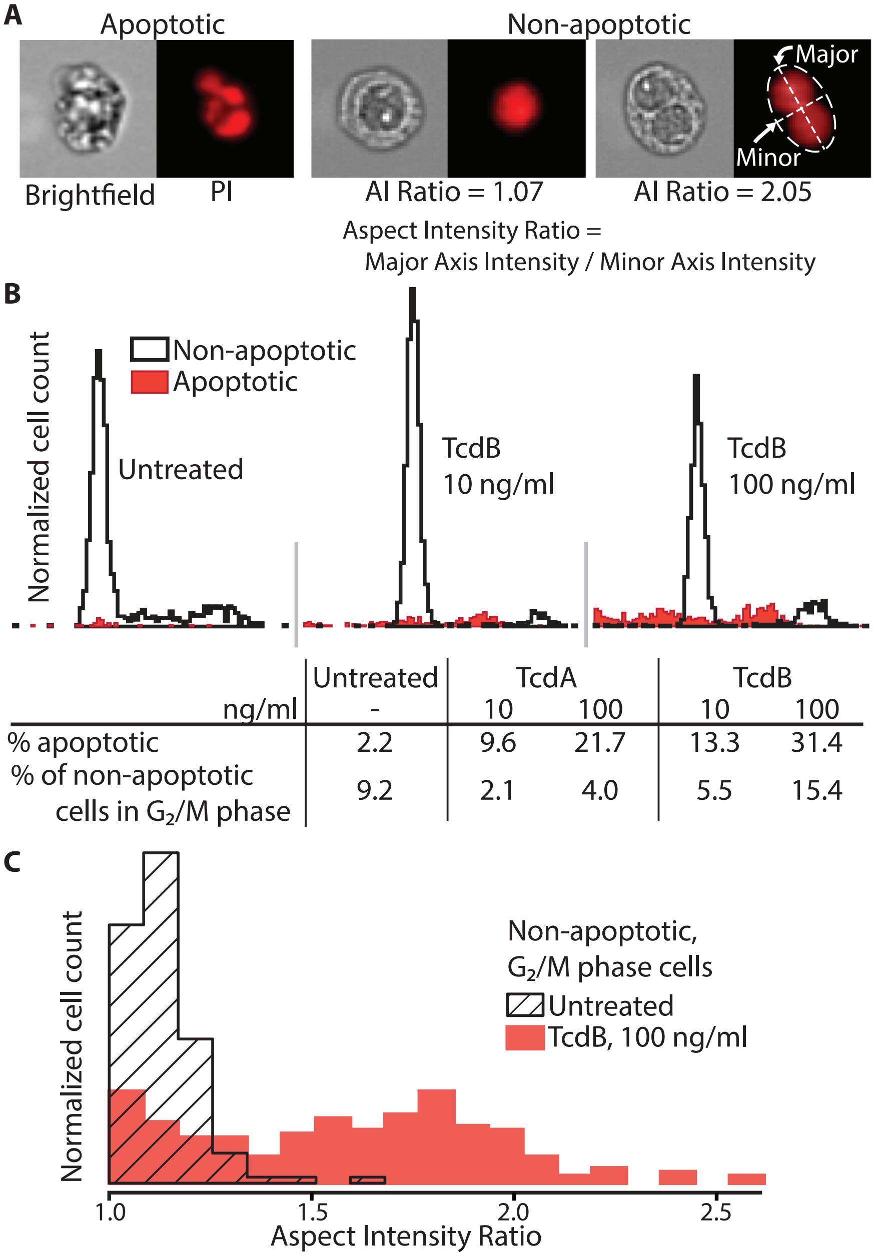

	Untreated	TcdA		TcdB	
ng/ml	-	10	100	10	100
% apoptotic	2.2	9.6	21.7	13.3	31.4
% of non-apoptotic cells in G_2/M phase	9.2	2.1	4.0	5.5	15.4

Figure 5.7: Distribution of apoptotic versus non-apoptotic cells within the cell cycle and characteristics of G_2/M phase, toxin-treated cells. (A) Cells were classified as either apoptotic or non-apoptotic based on the contrast of their brightfield image and the area of PI fluorescence. Representative images of a cell in each class are shown (100 ng/ml TcdB). **(B)** Histograms of the area of PI fluorescence of each cell show the location of apoptotic and non-apoptotic cells within the cell cycle. The percentage of G_2/M cells represents the proportion of non-apoptotic cells with a G_2/M level of DNA. **(C)** Non-apoptotic G_2/M phase cells were analyzed to determine the number of distinct nuclei. For this analysis only, cells with an area of PI fluorescence 1.85 times greater than the PI fluorescence area at the G_0/G_1 peak were considered to be G_2/M cells. The major and minor axis intensity values are the length of the axis weighted by the intensity of the image along the axis.

is the intensity-weighted aspect ratio of the PI fluorescence image. When an ellipse is fit around the image, an aspect ratio near one indicates a circular nucleus and a higher aspect ratio indicates an elliptical nucleus or multiple nuclei (Figure 5.7A). Upon visual inspection, a high aspect ratio is due typically to binucleation. The higher proportion of binucleated cells in toxin-treated cells (Figure 5.7C) indicates that the G_2/M block is attributable to a failure to complete cytokinesis [221]. Therefore, in addition to demonstration of a G_1-S block, our results show an inhibition of progression at the G_2-M transition, which is congruent with previous findings [198–201] in other cell types treated with different toxin concentrations. Importantly, these G_2/M effects were observed at the same concentration of toxin used for microarray analysis (100 ng/ml). Again, TcdA elicited a similar response to TcdB at the same concentration, yet to a lesser extent, thus showing consistency from gene and protein expression to cell function.

5.5 Discussion

Understanding the differences between these two toxins is particularly relevant in determining their roles in *C. difficile* infection. Toxin A appears to be the dominant virulence factor in animal studies, yet Toxin B has higher enzymatic activity in vitro and is more potent when injected into Don cells and for human cells studied in vitro [206, 222]. In a hamster model, Kuehne et al. found that strains of *C. difficile* producing only TcdA or TcdB are comparable in their virulence, while Lyras et al used a TcdA mutant to show that TcdB was the key virulence factor [223, 224]. In this study, we used a systems approach to understand the effects of TcdA and TcdB on a human colonic epithelial cell line. We observed that the responses to these two toxins are strikingly similar, with the response to TcdB occurring more rapidly. Investigation of one of the biological consequences of these changes in gene expression revealed toxin effects at both the G_1-S and the G_2-M transitions.

In order to explore the interactions between *C. difficile* and intestinal epithelial cells, Janvilisri et al. examined the transcriptional responses of Caco-2 cells and *C. difficile* organisms during an in vitro infection [225]. Because expression was measured at no more than 2 hr post-infection, most of the changes in gene expression were slight, yet they identified functions such as cell metabolism and transport associated with affected genes. We focused on cells treated with TcdA or TcdB at a concentration and time course in which the cell morphology is strongly affected. The effects of

TcdA and TcdB on gene expression in host cells have been interrogated in other studies focusing on individual pathways, but until now, an analysis of the comprehensive global transcriptional response induced by either TcdA or TcdB alone had not been performed.

Our systems approach identified a disruption of the cell cycle not readily apparent from a ranked list of genes. This approach overcame difficulties in deciphering the particular relevance of genes known to be induced by several stimuli or genes whose expression leads to many possible cellular phenotypes. JUN is overall the most differentially expressed gene in our data, and, considering TcdA or TcdB as a cellular stress, its dramatic increase in expression is consistent with it being characterized as a stress-response gene. However, increased JUN expression has also been associated with the promotion of G_1 progression, protection from apoptosis after ultraviolet radiation, and even induction of apoptosis [226]. Clearly, multiple events may lead to the same changes in expression of an individual gene. The identification of functions associated with many of the differentially expressed genes thus provides better evidence of actual biological functions important to the toxin response.

These results have clarified the effects of TcdA and TcdB at each stage of the cell cycle. In studying Rho signaling, Welsh et al. showed that combined Rho, Rac, and Cdc42 inhibition by TcdA (200 ng/ml) in fibroblasts led to decreased cyclin D1 expression and an inability of serum-starved cells, stimulated with fetal calf serum and treated with toxin, to progress past the G_1 phase [227]. Importantly, we show that a strong G_1 arrest occurs in unsynchronized, proliferating epithelial cells. Only when treated with higher concentrations (100 ng/ml TcdA, 10 ng/ml TcdB) of toxin did we begin to observe the inhibition of cell division at the G_2/M phase in a significant proportion of cells. With regard to cell death, others have shown an increased susceptibility of S-phase cells to toxin treatment [228]. We did observe an increase in the proportion of apoptotic S or G_2/M phase cells. At low concentrations (10 ng/ml TcdA, 1 ng/ml TcdB), the decrease in the proportion of S-phase cells, however, could not be entirely accounted for by death of cells at a particular point in the growth cycle. Rather, many non-apoptotic cells remained in the G_0/G_1 phase.

5.6 Conclusion

Our results have several implications in reference to the role of these toxins in pathogenicity. In a host, the gut epithelial cells normally turn over every 2-3 days [229]. Disruption of this cellular renewal process, and therefore cell cycle, impairs the maintenance of the epithelial barrier. The ability of both TcdA and TcdB to arrest growth at the G_0/G_1 phase and the G_2-M transition, by likely different mechanisms (G_1 arrest occurs even at low toxin concentrations and is associated with altered protein signaling; G_2 arrest is likely associated with disorganization of the cytoskeleton), places each toxin in the category of cyclomodulins. As has been previously shown however, control of cell proliferation is certainly not their only or necessarily primary effect (e.g., inflammation, disruption of tight junctions). The high similarity in the gene expression induced by these two toxins indicates that, qualitatively, their effects and the overall cellular responses are comparable. The rate of internalization and/or the rapidity of inactivation of Rho-family proteins in different hosts may partially account for the different rates in the onset of gene expression. Though we did not observe synergy or antagonism between the two toxins, it is possible that each could differentially bind various cell types and therefore act synergistically within a host. Clearly, the response to each toxin is a complex process involving the activation and inhibition of several pathways in different cell types. The integration and use of the data we present here have and will continue to aid the organization of these multiple effects into a central framework for interrogating toxin activity.

5.7 Acknowledgements

This entire chapter is taken from Kolling, G. L., D'Auria, K. M., Donato, G. M., Gray, M. C., Warren, C. A., Cave, L. M., Solga, M. D., Lannigan, J. A., Papin, J. A. & Hewlett, E. L. Systems analysis of the transcriptional response of human ileocecal epithelial cells to Clostridium difficile toxins and effects on cell cycle control. *BMC Systems Biology* **6,** 2 (2012). I would like to thank all the co-authors. I am also grateful to David Lyerly, Ph.D., and TechLab, Inc., Blacksburg, VA, for the generous gift of Toxins A and B.

Chapter 6

In vivo physiological and transcriptional profiling of Toxins A and B

6.1 From in vitro to in vivo host responses

The cell cycle is disrupted in HCT8 epithelial cells, but does something a similar thing happen to epithelial cells in the intestines? To answer this, we isolated epithelial cells from mice injected with toxins. There was no significant difference in the proportions of cells in each stage of the cell cycle when comparing treatment groups (data not shown). This may have been because most of the epithelial cells in the intestines are no longer growing. The cell cycle is already stopped. We therefore performed immunohistochemistry for changes in cell growth markers Ki67 and PCNA at the base of intestinal crypts (the locations where cells are still dividing). The results were not definitive (data not shown), but did indicate that their might be changes in cell cycle for the small minority of epithelial cells that are actively dividing and growing. Better techniques will be required to isolate changes in specific cell types [231, 232]. For example, one could use transgenic Fucci mice, whose cells fluoresce red or green depending on their stage in the cell cycle [233]. In addition to cell cycle regulators, many other genes were altered in HCT8 cells, but their relevance in the pathogenesis of disease could not be assessed in vitro. In this chapter, I present altered gene expression induced by TcdA and TcdB in a mouse intoxication model. Several novel responses were identified, and comparisons between in vitro and in vivo experiments are discussed in the last sections.

6.2 Synopsis

Toxin A (TcdA) and toxin B (TcdB) of *Clostridium difficile* cause gross pathologic changes (e.g., inflammation, secretion, and diarrhea) in the infected host, yet the molecular and cellular pathways leading to observed host responses are poorly understood. To address this gap, we evaluated the effects of single doses of TcdA and/or TcdB injected into the ceca of mice and several endpoints were analyzed, including tissue pathology, neutrophil infiltration, epithelial-layer gene expression, chemokine levels, and blood-cell counts—2, 6, and 16h after injection. In addition to confirming TcdA's gross pathologic effects, we found that both TcdA and TcdB resulted in neutrophil infiltration. Bioinformatics analyses identified altered expression of genes associated with the metabolism of lipids, fatty acids, and detoxification; small GTPase activity; and immune function and inflammation. Further analysis revealed transient expression of several chemokines (e.g., Cxcl1 and Cxcl2). Antibody neutralization of CXCL1 and CXCL2 did not affect TcdA-induced local pathology or neutrophil infiltration, but it did decrease the peripheral blood neutrophil count. Additionally, low serum levels of CXCL1 and CXCL2 corresponded with greater survival. Though TcdA induced more pronounced transcriptional changes than TcdB and the upregulated chemokine expression was unique to TcdA, the overall transcriptional responses to TcdA and TcdB were strongly correlated, supporting differences primarily in timing and potency rather than differences in the type of intracellular host response. In addition, the transcriptional data revealed novel toxin effects (e.g., altered expression of GTPase-associated and metabolic genes) underlying observed physiological responses to *C. difficile* toxins.

6.3 Introduction

The toxins TcdA and TcdB are two key virulence factors of *C. difficile*, an intestinal, opportunistic pathogen responsible for more than 300,000 infections in the US per year (2009 data) with several estimates of annual cost between $433 million and $8.2 billion [1, 234–236]. Clinical manifestations

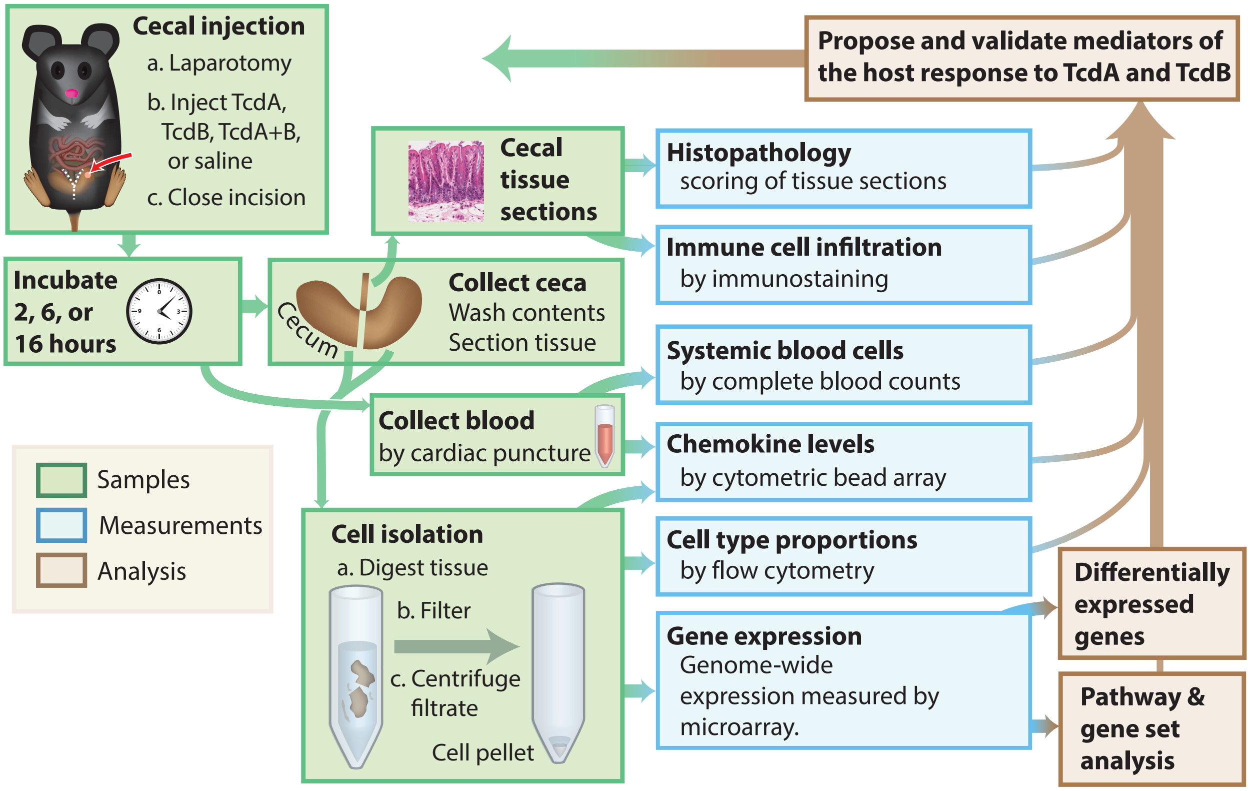

Figure 6.1: Study workflow.

include leukocytosis and diarrhea. The importance of TcdA and TcdB is underlined by the facts that strains without either toxin colonize but do not cause disease and that intoxication causes similar manifestations as infection [223, 224, 237]. TcdA and TcdB are similar in size, amino acid sequence, and enzymatic specificity, yet exhibit different enzymatic activities and in vivo potencies [163, 168, 206]. Furthermore, much remains unknown about common and divergent cellular pathways leading to toxin-mediated host responses [238, 239].

Determining the relative roles of TcdA and TcdB in pathogenesis has proven difficult in part because of variable findings within and between animal models as well as species-specific responses. Clinically, strains lacking TcdA are commonly isolated from infected patients, and no TcdA+/TcdB- clinical strain has ever been reported [240]. Toxin effects in the context of infection have typically been studied using animal models in which an antibiotic regimen and subsequent disruption of intestinal flora must precede infection with *C. difficile* [165, 241]. By generating mutant strains, Lyras et al. found that TcdB but not TcdA was essential for hamster infection, yet Kuehne et al. found, in a similar hamster infection model, that either toxin was sufficient [223, 224]. Investigating toxin effects more directly, multiple intoxication models have demonstrated TcdA to be enterotoxic, while TcdB caused little to no pathology [163, 237, 242]. However, epithelial damage in human xenografts in mice is greater with TcdB than TcdA, suggesting that many differences in toxin effects may be species-specific [243]. The ability of either toxin to bind, enter, and/or activate intestinal cells may also explain differential effects of TcdA and TcdB. The sequences differ most in the C-terminal binding domain. TcdB has been shown to be incapable of binding the brush border membranes of hamsters, although TcdB has been found to further damage bruised ceca, synergize with TcdA, and contribute to pathogenesis during infection [224, 242, 244]. Multiple receptors for TcdA have been proposed or identified, yet the roles of these receptors in different organisms, animal models, and cell types are unclear [245–250]. TcdB weakly binds various trisaccharides and oligosaccharides, yet no functional receptor for TcdB has been identified [251]. It is also possible that differences in intracellular actions of TcdA versus TcdB are responsible for differences in the host response. Though a similar dose of TcdA or TcdB may result in different gross pathologies, it is unclear if entirely different pathways are activated or repressed or if the same overall functions are affected to different degrees. We previously analyzed the transcriptional response of a human, ileocecal, epithelial cell line (HCT8) to TcdA and TcdB and showed that the toxins induce very similar transcriptional signatures, yet the effects of TcdB occurred earlier [230]. In addition, we found altered regulation of many genes involved in cell growth and division but no overwhelming expression of inflammatory markers or other genes associated with physiological changes in vivo. The in vivo effects of these toxins have not been investigated by measuring genome-wide responses, and many of the links between cellular responses and physiological changes remain unknown. We therefore used an in vivo system, intracecal injection of toxin into mice, and collected samples to characterize the genome-wide cellular responses and gross physiological effects of each toxin over a 16h time course.

It has been difficult to tease apart the aspects of the host response to TcdA and TcdB because of the important interactions among the many tissues, cell types, and signals involved [153, 252]. The intestinal epithelium, the initial barrier to these toxins, continuously interacts with surrounding cells throughout the development and resolution of disease. We therefore focused on the transcriptional response of epithelial-layer cells to toxin and other toxin-related effects. Given the importance of surrounding tissues and with recent evidence of systemic dissemination of toxins, we chose cecal injection of toxin, an open system, as opposed to closed ileal loop models or ex vivo systems that may restrict toxin to a limited area [253]. Additionally, previous studies have focused on separate facets of the host response, typically with only one toxin per study [181, 254–259]. To address these deficits in the knowledge of this illness, we measured genome-wide expression from epithelial-layer cells exposed to TcdA and TcdB to simultaneously capture effects of each toxin.

Using this approach, we identify several genes differentially expressed after toxin treatment that serve as specific candidates to investigate further. Additionally, we employ currently available bioinformatic methods and also introduce novel methods to identify groups of regulated genes associated with known biological functions. Our measurements were taken on several biological levels to link changes in one set of variables (e.g., gene expression) to changes in others (e.g., pathology and blood counts). These linkages serve as tools to validate previous findings as well as identify novel functions affected by TcdA or TcdB. Of the many linkages that could be explored, we further investigated chemokine expression and the role of two chemokines in the response to TcdA cecal injection with respect to changes in pathology, neutrophil recruitment, and survival. In addition to the comparison between toxins and identification of differentially expressed genes, these associations and concepts serve as a basis for further probing the host response to these toxins in the context of *C. difficile* infection.

6.4 Methods

6.4.1 Cecal injection

All procedures involving animals were conducted in accordance with the guidelines of the University of Virginia IACUC (Protocol #3626). Purified TcdA and TcdB were generously provided by Dr. David Lyerly at TECHLAB, Inc. Mice (male C57BL/6J, 8 w.o. from Jackson Laboratories) were anesthetized with ketamine/xylazine in preparation for surgery. A midline laparotomy was performed to locate the cecum, and 20 µg of toxin in 100 µL of 0.9% normal saline was injected into the distal tip. Incisions were sutured, and animals were monitored during recovery. Sham injected animals received only 100 µL of saline. If an animal became moribund (i.e., hunched posture, ruffled coat, or little to no movement), they were immediately euthanized.

6.4.2 Cell culture

An immortalized, C57BL/6 mouse, cecal epithelial cell line (passage 9) was provided from the laboratory of Dr. Eric Houpt and maintained as described by Becker et al. [260]. Toxin cytopathicity was assessed by measuring changes in cell adherence and morphology using a multi-well, continuous, electrical impedance assay (xCelligence; ACEA Biosciences). In each well, 20x solutions of TcdA or TcdB (prepared in media) were added 34h after seeding 21,000 cells yielding the indicated concentrations.

6.4.3 Blood counts

Blood was collected using cardiac puncture and complete blood counts were measured using a HEMAVET 950FS (Drew Scientific). Serum was analyzed for levels of systemic chemokines using MILLIPLEX MAP beads, and the signal was measured using a Luminex 100 IS System (UVA Flow Cytometry Core Facility).

6.4.4 Histology

A cross section from the middle of each cecum was dissected and fixed. The tissues were paraffin-embedded, sectioned, and stained by the UVA histology core. H&E sections were coded and scored by a blinded observer using parameters to assess inflammation, luminal exudates, mucosa thickening, edema, and epithelial erosions [261]. Each of these five parameters was scored between zero and three yielding total pathology scores between zero and fifteen. Eosinophils were detected in tissue using Congo Red Staining [262]. Tissues for H&E, MPO, and eosinophil staining were fixed in Bouin's solution; tissues for other measurements were fixed in 4% paraformaldehyde. Immunohistochemistry was performed by the Biorepository and Tissue Research Facility at the University of Virginia. Monocytes/macrophages, dendritic cells, and neutrophils were separately identified using the markers F4/80 (clone CI:A3-1; AbD Serotec), Ly75 (EPR5233; Abcam), and myeloperoxidase (MPO; rabbit-anti-MPO; Novus Biologicals), respectively. The presence of neutrophils was quantified by averaging the number of positive cells associated with epithelial and subepithelial layers in ten random fields (40x objective). Monocytes/macrophages and dendritic cell staining was scored by analyzing each section for the number of positive cells and overall staining intensity. Samples were assigned scores of 1 (few cells/weak staining), 2 (moderate staining), or 3 (many cells/intense staining).

6.4.5 Isolation of cells from cecal tissue

The remaining two sections of each cecum were opened longitudinally, rinsed with Hank's Balanced Salt Solution (HBSS, Gibco), and shaken at 250 rpm for 30 minutes at 37°C in HBSS containing 50mM EDTA and 1mM DTT in order to remove epithelial layer cells. The digested tissue was strained with a 100-µm cell strainer, and the filtrate was centrifuged (1,000×g, 4°C, 10 min). Cells were resuspended in red-cell lysis buffer (150 mM NH4Cl, 10mM NaHCO3, 0.1 mM EDTA) and centrifuged again. The pelleted cells were used immediately for flow cytometry or stored at -80°C until RNA isolation. RNA was isolated using the RNeasy mini kit (Qiagen) with on-column DNase digestion according to manufacturer's instructions. Protein was collected from cell lysate supernatants, which were made using a lysis buffer containing 50 mM HEPES, 1% Triton-X100, and HALT protease inhibitor. The lysate was incubated on ice for 30 minutes and centrifuged (13,000×g, 4°C, 10 min). Clarified supernatants were stored at -80°C.

6.4.6 Flow cytometry

Epithelial layer cells were isolated from mice 16h after injection with TcdA (n=2), TcdB (n=3), or saline control (n=3). The cell preparations were stained with markers including CD3 (BV421; BioLegend), cytokeratin (PE; Novus Biologicals), CD11b (APC-Cy7; BioLegend), B220 (FITC; BD Bioscience), and CD45 (V500; BD Bioscience) to detect different populations. Samples were analyzed on the CyAn ADP analyzer; 50,000 events were collected and subsequently analyzed using FlowJo software.

6.4.7 Antibody-mediated neutralization of chemokines

For each antibody, 100 µg was administered by intraperitoneal injection 16h before sham/toxin injection. Mice received a combination of anti-CXCL1 (clone 48415) and anti-CXCL2 (clone 40605) or the relevant isotype controls (clones 54447 and 141945). All antibodies were purchased from R&D systems and resuspended according to the manufacturer's directions. Decreased levels of CXCL1 and CXCL2 in the serum of mice receiving neutralizing antibody (compared to isotype controls) were indicative that the neutralization was successful.

6.4.8 Microarray procedure

An Agilent 2100 BioAnalyzer was used to assess RNA integrity. cDNA was synthesized, biotin labeled, and hybridized to Affymetrix Mouse Genome 430 2.0 GeneChip according to the manufacturer's instructions. Arrays were scanned with a GeneChip System 3000 7G (Affymetrix).

6.4.9 Statistical analysis

Unless otherwise stated, each two-sample test is a two-sided Mann-Whitney U test.

6.4.10 Microarray preprocessing

Multiple steps are involved in processing the raw data of microarrays to a matrix of signal intensity values. We first introduce the usual steps and then describe the methods we chose for each step.

Possible steps in processing microarrays

Except for probe set summarization, each one of the steps below is optional. The order of some steps may be alternated, though this is not typical.

1. *Background correction*: Each array is corrected for background intensity.
2. *Probe level normalization*: All arrays are normalized to each other based on the probe level data.
3. *Mismatch correction*: The signal intensity of perfect-match probes is corrected based on the signal from corresponding mismatch probes.
4. *Probe set summarization*: The probes in each probe set are summarized into one probe set signal intensity

Each step has about four to ten different computational methods that can be used. Many of the methods have several optional parameters. Hence, the number of ways to process microarrays is vast.

Steps taken in processing microarrays

In the list below are the computatonal methods we chose for the microarray processing steps described in the last section. Instead of presenting the lengthy comparative analysis of the many sequences of methods that we examined, we provide only a brief description of either why a method was chosen or why others were not.

1. *Background correction* [10]: gcRMA[17] was not used since it has been shown to cause artificially high gene-gene correlation which would affect our gene set enrichment tests [27]. Instead, RMA normalization was used.

2. *Probe level normalization*: Cyclic loess normalization was used over quantile normalization because of quantile normalization's assumption that the probes on each microarray have the exact same distribution [263]. Invariant set normalization caused some microarrays to become outliers, which we observed using principal components analysis [18]. A second cyclic loess normalization was applied at the probe set level.

3. *Perfect match correction*: Only perfect match probes were used. Although several model-based processing techniques have shown that mismatch probes provide useful information, the precise way in which mismatch probes should be used to correct for the signal from the corresponding perfect match probes remains unclear [264].

4. *Probe set summarization*: Median polish was used as opposed to Tukey's Bi-Weight algorithm to better account for differences in probe affinities [265, 266].

6.4.11 Determining differentially expressed genes

As with processing raw microarray data, there are many methods and options for determining the significance of a probe set's change in expression between two sample groups. We analyzed the results from many available methods, but only briefly explain some of the findings that led us to the statistical test which we chose. Though permutation tests such as significance analysis of microarrays are advantageous because they are less sensitive to outliers, we did not use such tests because our low sample numbers did not allow many permutations to be generated [46]. We did not use simple fold change cutoffs because they do not account for variation among replicates. We also considered limma's moderated t-statistic [64]. We found that many of the significant probe sets identified by limma had low intensity values but very small expression differences between sample groups. This was due to the near zero standard errors of some probe sets which we believed to occur for mostly technical, not biological reasons. We therefore used cyberT, which, in practice, adjusts the standard deviation for a probe set depending on the signal intensity of that probe set [49].

The next problem is deciding what p-value cutoff to use for determining which probe sets are "significant". To help with this, various "p-value adjustments" or "FDR corrections" use the p-value distribution to estimate the false discovery rate (FDR). FDR corrections generate q values that describe the false discovery rate for a group of genes. For instance, if the tenth ranked gene has a q value of 0.2, then 2 of the top ten genes should be false positives and the other 8 should be true positives. We chose to use the Benjamini-Hochberg p-value adjustment instead of other more conservative methods such as the Bonferroni correction which controls the family-wise error rate [267]. This helps conceptually, yet still leaves an arbitrary choice of what q-value cutoff to use. We chose a cutoff of $q<0.01$ for mostly the practical reason that the number of significant genes it led to was manageable.

Of the many statistical tests that we analyzed, we found that the number of differentially expressed genes varied from test to test. However, for each test, the number of differentially expressed genes for one comaparison relative to another comparison was similar. For instance, if statistical test A, relative to test B, found double the number of differentially expressed genes for the TcdA versus sham comparison at 2h, then test A also found about double the number of differentially expressed genes in all other comparisons. Also, the ranking of the genes was fairly consistent for different statistical tests. Hence, in our next analysis of gene set enrichment, we sought enrichment methods which use expression values or test statistics, not those that require genes to be set as "differentially expressed" or "not differentially expressed".

6.4.12 Gene set enrichment

As briefly mentioned in the manuscript, gene set enrichment methods help to understand the biological functions associated with changes in gene expression data. To define gene sets, we used gene function annotations from the Gene Ontology and Reactome databases.

Much of the bioinformatics literature has categorized different enrichment methods by the type of hypothesis tested [182].

Competitive

One possible hypothesis tested in the "competitive" gene set enrichment method CAMERA, developed by Wu *et al.*, is whether the mean t-statistic for the genes in a gene set is significantly different than the genes not in the gene set [268]. In other words, it tests whether or not the genes in a gene set are more differentially expressed than the genes outside of the gene set. As this type of test compares the differential expression of two competing groups of genes (genes in the set versus not in the set), it has come to be named a "competitive" test. CAMERA was written to use the moderated t-statistic from limma [64]. We wrote a modified version of CAMERA to instead use the cyberT t statistic, the same statistic used in our differential gene expression analysis [49].

Self-contained

Another important and common null hypothesis is that the genes in the gene set are not differentially expressed at all. Since this type of test requires only data from genes in the gene set, it has been coined a "self-contained" test. Our self-contained method tests whether the avearge t-statistic for the genes in a gene set is zero.

To describe our self-contained test, we use the notations from the CAMERA manuscript [268]. Consider a gene-wise statistic, z_i for gene i in a gene set with m genes. In our self-contained test, this statistic is the standard normal deviate which has the same quantile as the cyberT t-statistic; a similar transformation is also performed with CAMERA. Under the null hypothesis that the average of the gene expression differences between the two sample groups is zero, the gene set's mean test statistic, $\bar{z}$, is normally distributed with $\mu = 0$ and

$$Var(\bar{z}) = \frac{1}{m^2}\left(\sum_{i=1}^{m}\sigma_i^2 + \sum_{i<j}\sigma_i\sigma_j\rho_{ij}\right). \tag{6.1}$$

Since $z_i \sim \mathcal{N}(0,1)$ for all i,

$$Var(\bar{z}) = \frac{1}{m} + \frac{m-1}{m}\bar{\rho} \tag{6.2}$$

where $\bar{\rho}$ is the average correlation between genes in the gene set. Note for large m, $Var(z) \approx \bar{\rho}$. If $\bar{z}_k$ is the mean test statistic for gene set k calculated from the data, then a p-value is calculated using location of $\bar{z}_k$ in the cumulative distribution function of $\bar{z}$. This novel method improves upon another published, parametric gene set enrichment method, namely PAGE [269].

6.4.13 Cytopathic effects on a mouse, cecal, epithelial cell line

The cytopathic effects (e.g. cell rounding) of TcdA and TcdB were confirmed using an immortalized, mouse, cecal epithelial cell line (Methods). These effects were quantified by continuously measuring

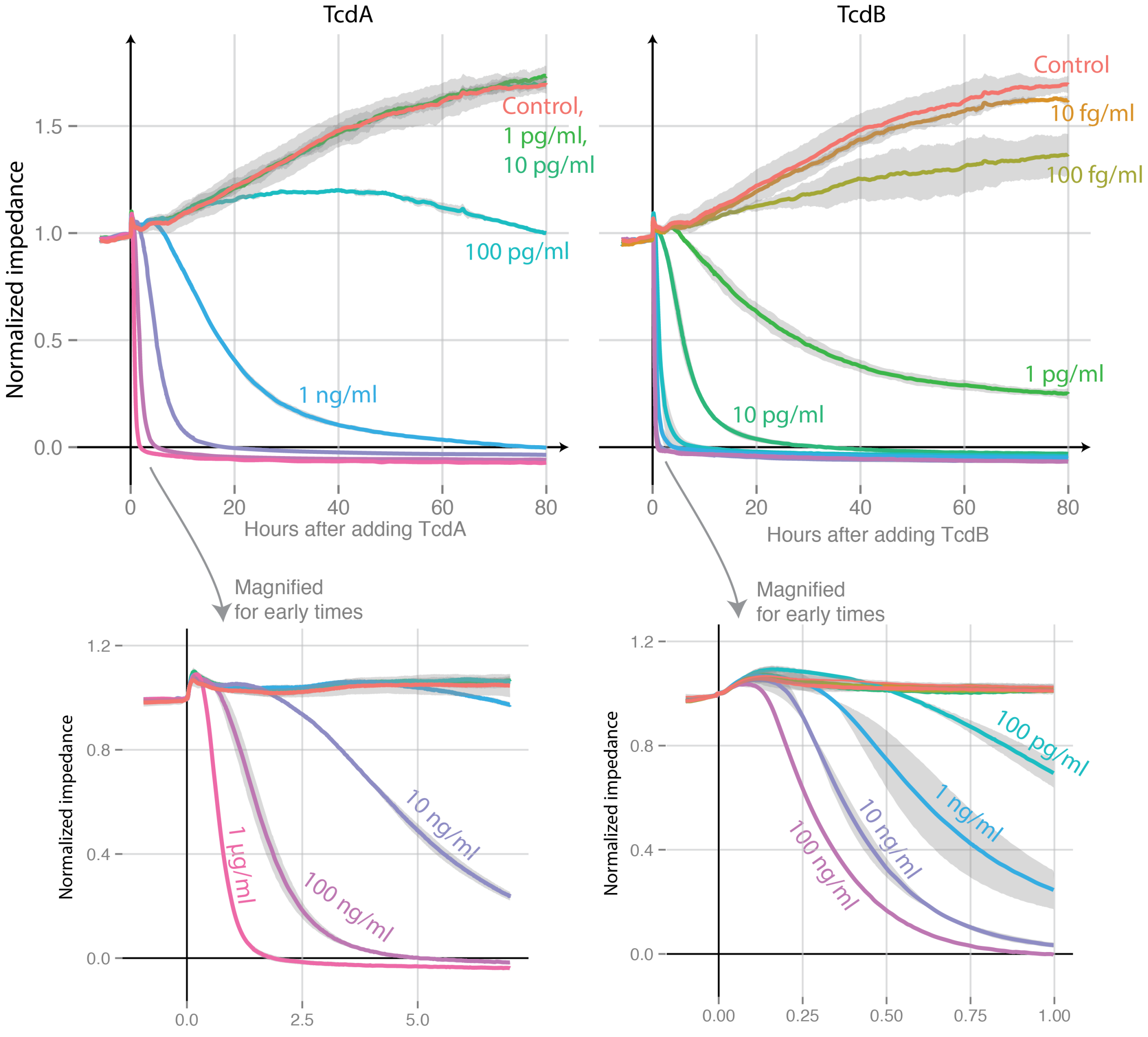

Figure 6.2: Cytopathic effects of TcdA and TcdB on a mouse epithelial cell line.

the impedance across the surface of electrode-embedded wells (ACEA Biosciences). Similar methods and instrumentation have been used previously in an ultrasensitive assay to detect TcdA and TcdB. [270] Changes in impedance represent changes in cell adherence, morphology, and number. Our visual observations of cell rounding corresponded with changes in impedance.

Figure 6.2 shows impedance before and after toxin addition. All readings are normalized to the impedance at the time the toxin was added. Gray ribbons surrounding the lines represent the standard deviation (n=2 per concentration, n=3 for control). If ribbons are not visible, this is because the replicates are highly similar. An impedance of zero is the impedance of media before cells were seeded.

The minimum concentration of TcdA needed to alter an impedance profile (as shown in Figure 6.2) is between 10 and 100 pg/ml (in a volume of 210.5 µl); the concentration for TcdB is approximately 10 fg/ml. Hence, TcdB is at least 1,000 times more potent than TcdA *in vitro* with immortalized epithelial cells from a mouse cecum. Interestingly, our results clearly show that TcdA more potently induces inflammation and tissue damage *in vivo*. The initial concentration in our cecal injection experiments was 20µg/100µl=200µg/ml. Nevertheless, the preparations of TcdA and TcdB used in this study affect mouse cells rapidly (e.g. <10min for TcdB at 100 ng/ml, Figure 6.2) at concentrations comparable to and even far lower than the initial concentrations in our *in vivo* experiments.

6.5 Results

6.5.1 Dose-response to TcdA cecal injection

To understand the potency of TcdA in a cecal injection system, a dose-response experiment was performed with histopathology as the measured outcome. Five histopathology parameters were scored from zero to three, for a total possible score between zero and fifteen (Methods). Excluding the largest dose (40 µg), TcdA dose was positively correlated with the parameters “Architecture and epithelial erosions”, “Congestion and luminal exudates”, and “Inflammation” (Figure 6.3). The total histopathology score was similarly correlated. The 20 µg dose led to the highest scores; the scores with the 40 µg dose were similar to the scores for the 5 or 10 µg dose. A slight correlation between toxin dose and the “Edema” and ”Mucosal thickening” parameters may be observed from

Figure 6.3, yet this possible correlation is unclear due to Sham mice scoring similar to all other toxin doses. TcdA thus affects aspects of histopathology at 5 µg, the lowest dose tested. Maximal effects occur with 20 µg, the dose used in all our other experiments.

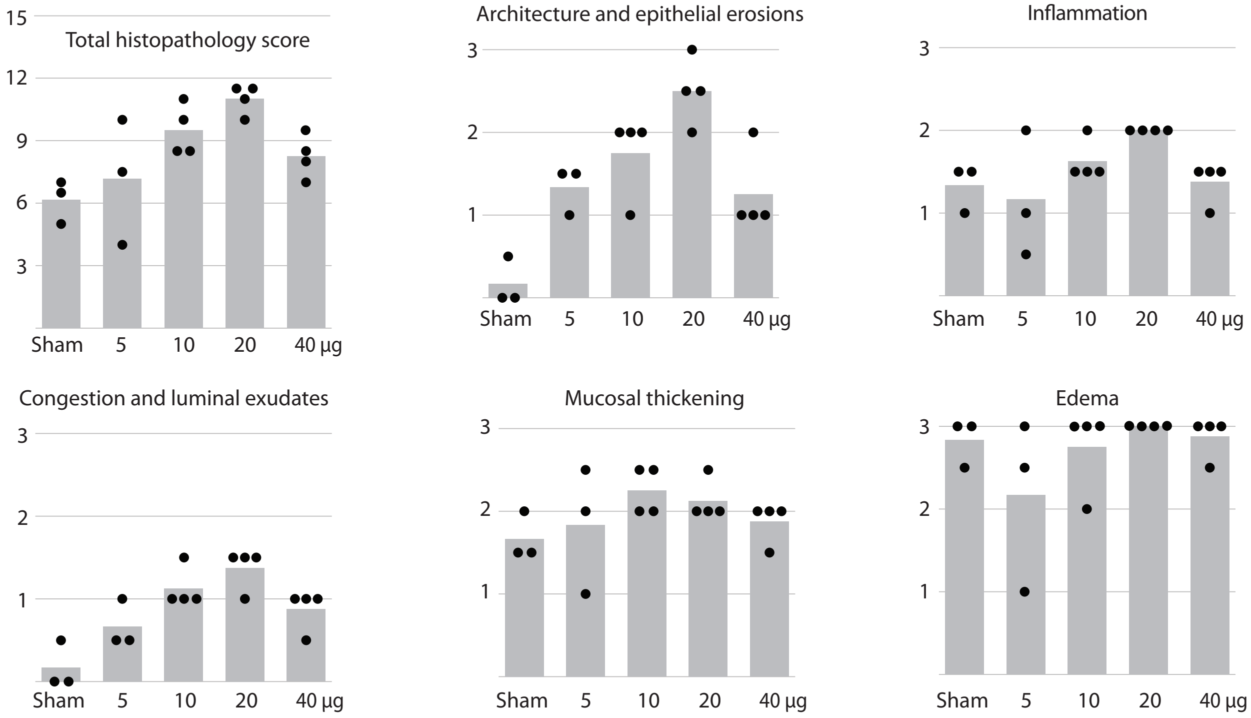

Figure 6.3: Histopathology 6h after cecal injection with TcdA.

6.5.2 Survival after cecal injection

In addition to the dose-response experiment, three cecal injection experiments were performed, each on different days (Table 6.1).

6.5.3 Physiological results of toxin cecal injection

TcdA, TcdB, or TcdA and TcdB (TcdA+B) were injected into the cecum to study an anatomical site affected during infection (Figure 6.1). The TcdA dose (20 µg/animal) and incubation periods (2, 6, and 16h) were chosen based on our in vitro data and dose-response experiments (Figure 6.3) in order to capture the early effects from a single dose of toxin [230]. The biological activities of TcdA and TcdB were confirmed using an immortalized, mouse, cecal epithelial cell line (Figure 6.2).

Relative to sham controls, TcdA-challenged mice had greater total pathology scores (more

	2 hours				6 hours				16 hours			TcdA	TcdB
Toxin:	A	B	A+B	Sham	A	B	A+B	Sham	A	B	Sham	Lot #	Lot #
Dose-response	—	—	—	—	15/16*	—	—	3/3	—	—	—	0810123	—
Exp. 1	3/3	5/5	3/3	3/3	3/3	3/3	1/3	3/4	3/3	2/3	3/3	0909101	0209165
Exp. 2	3/4	4/4	—	4/4	3/4	3/4	—	3/4	5/5	4/5	5/5	0909101	0209165
Exp. 3	—	—	—	—	—	—	—	—	2/5	3/4	3/3	0810123	0209165
Totals	6/7	9/9	3/3	7/7	10/11	6/7	1/3	9/11	10/13	9/12	11/11		
	86%	100%	100%	100%	91%	86%	33%	82%	77%	75%	100%		

Table 6.1: Survival in cecal injection experiments The "15/16*" in the table are the mice shown in Figure 6.3. Only four of these mice were given 20 μg, and only these four are included in the "Totals". The one mouse that did not survive in the dose-response experiment was given 5μg of TcdA. The TECHLAB® lot numbers of the toxins used are given in the last two columns. Mice used for microarrays and all protein measurements were from experiments 1 and 2. The numbers give the fraction of survivors in each sample group (# survivors/total mice).

severe pathology) at 2, 6, and 16h (Figure 6.4A and Figure 6.4B), with higher scores for all five measured parameters at 16h ($p<0.01$), all but mucosa thickening at 6h ($p<0.03$), and all but luminal exudates at 2h ($p<0.02$). In contrast, the average total pathology score for TcdB-challenged mice was significantly higher than sham mice at only 16h ($p<0.05$). At 2h, TcdA+B led to mucosal thickening, inflammation, and edema ($p<0.04$). Mice challenged with TcdA experienced diarrhea at intermediate and late time points based on visual observations of wet tail and clumped cage bedding. We also examined the colons of mice 16h after TcdA, TcdB, or sham challenge in order to determine if there are distant effects from the cecal injection. Using the same scoring system, no significant differences in histopathology scores were noted throughout the colon (data not shown).

The complete blood counts and infiltration of immune cells are also altered by TcdA and TcdB. In blood drawn by cardiac puncture 16h after injection of TcdB, there was an increased concentration of several cell types (Figure 6.5). At 16h, TcdA slightly increased the concentration of monocytes ($p<0.1$), but decreased the concentrations of lymphocytes and platelets ($p<0.05$). The increased systemic concentration of monocytes after TcdA challenge is reflected in their infiltration into the cecal submucosa 6 and 16h after injection (based on immunohistochemistry staining using F4/80, Table 6.2). In addition, increases in dendritic cells were also evident in the submucosa 6h and 16h after TcdA challenge. Relative to sham, TcdA and TcdB increased neutrophil infiltration at 16h ($p\leq0.02$, using MPO staining), and at 6h, neutrophil infiltration in four of the six animals challenged with TcdA was greater than neutrophil infiltration in any sham mouse (Figure 6.4C).

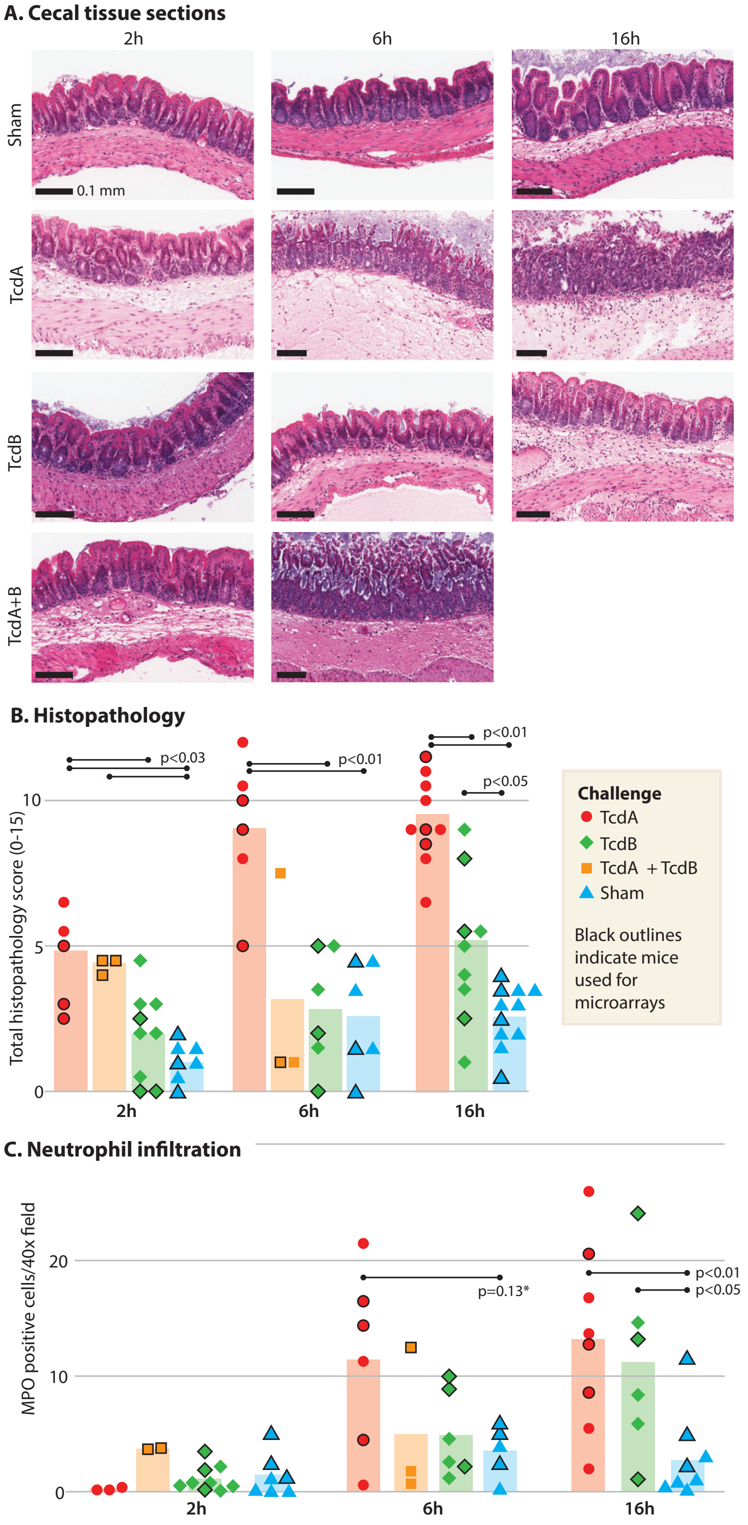

Figure 6.4: Physiological changes post toxin injection. Panels A, B, and C include data combined from four independent experiments with 7, 39, 36, and 12 mice. In total, 10 of 94 mice did not survive until the experimental end point: one TcdA-treated mouse did not survive to 2h, six mice did not survive to 6h (1 TcdA, 2 TcdA+B, 1 TcdB, 2 Sham), and six mice did not survive to 16h (3 TcdB, 3 TcdA; Table 6.1). The data points displayed in the figure were used for each statistical test. The horizontal lines above the bar charts which connect two sample groups indicate a two-sample statistical tests. The p-values for these tests are indicated beside the lines. **(A)** Representative examples of H&E-stained cecal tissue sections from the eleven indicated sample groups. **(B)** Total histopathology score (see 6.4.4) from cecal-tissue sections. Except for the two mice injected with TcdA+B (two mice not used for microarrays), histopathology scores were not measured for mice that did not survive. Since two of three mice injected with TcdA+B did not survive to six hours in our first experiment, we dedicated more mice for TcdA and TcdB at 16h so that no samples were obtained for TcdA+B at 16h. All subsequent experiments also excluded the 16h time point for injection of TcdA+B. **(C)** The number of cells within the mucosa and immediate submucosa which were positive for MPO after immunohistochemical staining. *p=0.055 by the two-sided t test.

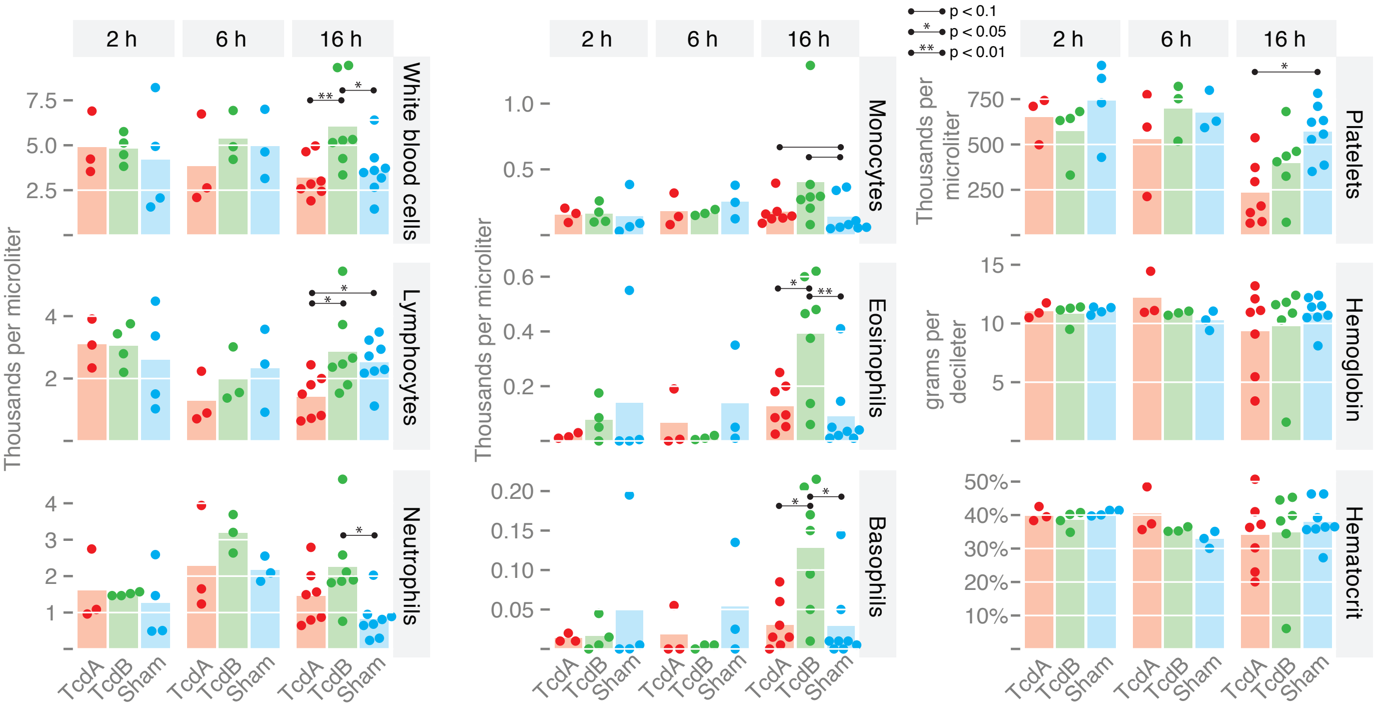

Figure 6.5: The concentration of circulating blood cells is altered during intoxication Blood was drawn by cardiac puncture immediately after mice were euthanized. Only measurements for mice which survived to the end point are represented in the figure. Sufficient blood to measure complete blood counts was not capable of being drawn from every mouse. The mean corpuscular volume (MCV), mean corpuscular hemoglobin (MCH), MCH concentration (MCHC), red blood cell distribution width (RDW), and mean platelet volume (MPV) were similar across all three sample groups and are not shown.

6.5.4 Host transcription altered by toxin injection

We evaluated gene expression changes in the epithelial layer to characterize the host-cell responses to TcdA and TcdB. To determine the proportions of cell types within our epithelial-layer isolation, we used flow cytometry to analyze cells from mice 16h after TcdA, TcdB, and sham challenge (Figure 6.6). The percentage of epithelial cells (cytokeratin+) was similar across all experimental conditions, averaging 85%. Approximately half of the remaining non-epithelial fraction in each experimental condition was leukocytes (CD45+). However, the number of leukocytes was slightly greater for TcdA-challenged mice over sham controls (p=0.06). Within the leukocyte fraction, there was no significant difference between experimental conditions in the percentage of CD3+ cells (average of 40%, T cell marker) or CD11b+ cells (average of 59%, marker for myeloid lineage). However, the percentage of leukocytes positive for B220, a common B cell marker, was greater

Cell type:	Macrophages	Dendritic Cells	Eosinophils	
Marker:	F4/80	Ly75	Congo Red	*n*
Sham, 6h:	+	+	+	4
TcdA, 6h:	+++	++	+	8 (4 for F4/80)
Sham, 16h:	+	+	+	4
TcdA, 16h:	+++	+++	+	7

Table 6.2: Infiltration of immune cells 6h and 16h after cecal injection To determine if monocytes/macrophages, dendritic cells, and eosinophils infiltrate the epithelial layer after cecal injection of toxin, we used immunohistochemistry markers (Methods). Cecal tissue sections were scored by analyzing each section for the number of positive cells and overall staining intensity. Samples were assigned scores of + (few cells/weak staining), ++ (moderate staining), or +++ (increased cell/intense staining).

in TcdB samples than sham samples (60% versus 34%, $p<0.01$). The remaining non-epithelial fraction, an average of 7.5% of all cells, was not characterized by the markers used. The same epithelial-layer isolation procedure was used for all gene expression measurements.

For both toxins, a small set of genes is affected at 2h and, at 6h and 16h, hundreds or thousands are differentially expressed. A more pronounced TcdA transcriptional response, compared to TcdB, is consistent with TcdA's greater pathophysiological effects in vivo (Figure 6.4B). However, many of the expression changes induced by TcdA and TcdB are similar. Over 50% and 90% of the genes that are differentially expressed after TcdB treatment, at 6h and 16h respectively, are also differentially expressed after TcdA treatment (Figure 6.7A). Comparing challenge with individual toxins versus TcdA+B challenge, the transcriptional response induced by TcdA+B is very similar to that induced by TcdA alone. For instance, at 2h, 12 of the 20 genes with a significant change in expression after TcdA challenge were also differentially expressed after TcdA+B challenge. Although the degree of pathology and magnitude of transcriptional changes are significantly different between TcdA and TcdB, the overall transcriptional responses to TcdA and TcdB are highly correlated (Figure 6.7B). Hence, in general, gene expression that is affected by TcdA is also affected by TcdB but to a lesser extent, suggesting broadly similar in vivo cellular responses to TcdA and TcdB.

For an initial perspective of which genes are affected, we present genes differentially expressed 2h post toxin challenge (Table 6.3). These include several transcription factors (Atf3, Egr1, and Jun) and an mRNA binding protein (Zfp36). Consistent with the observed pathology, several of the affected genes at 2h are related to the regulation of inflammation (C3, Cxcl1, Cxcl10, Dusp1, Egr1, etc.). Increased expression of Sprr1a and Atf3, markers of neuronal damage, is interesting

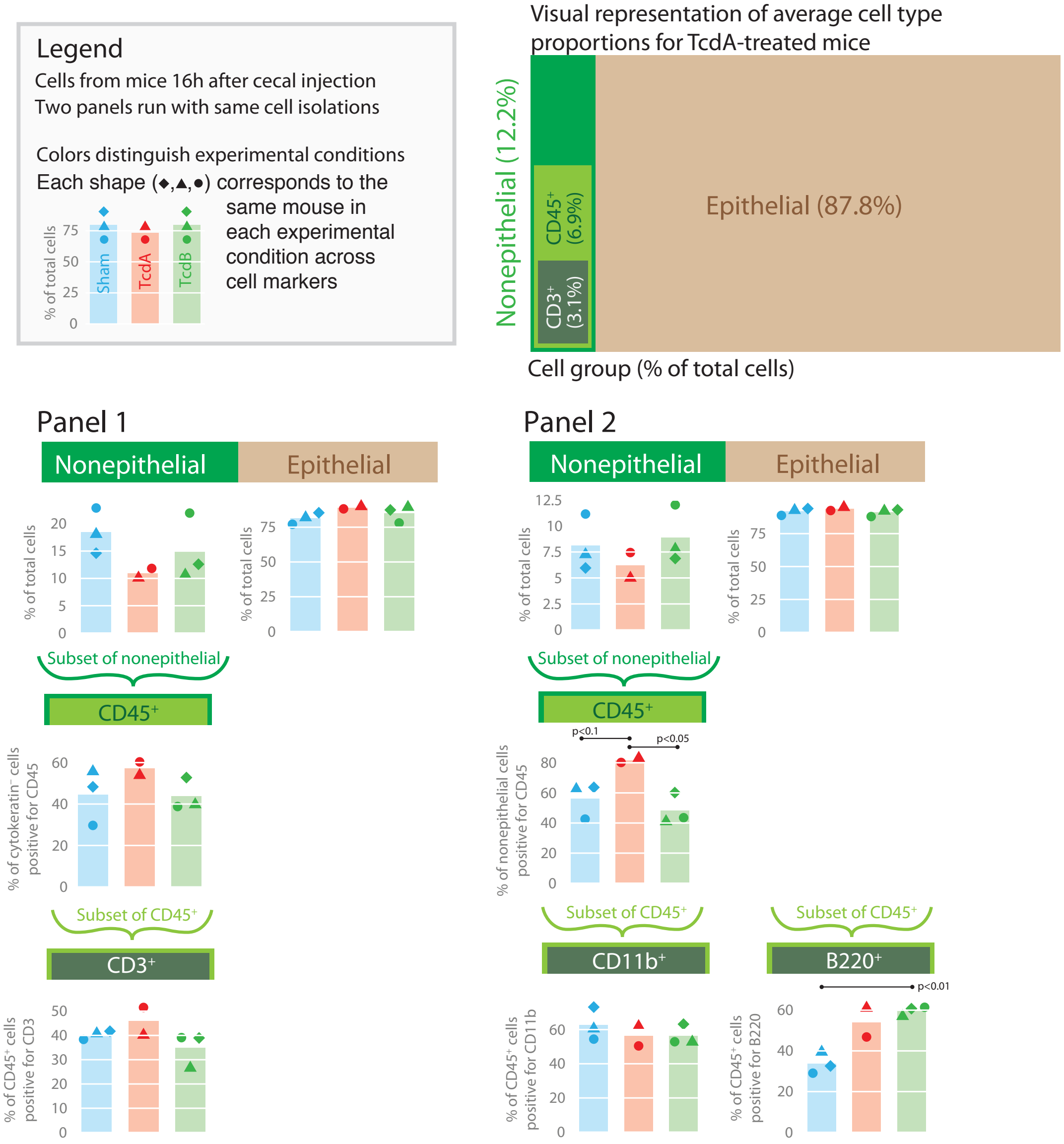

Figure 6.6: Cell type proportions as determined by flow cytometry The cell type proportions within the epithelial-layer cell isolation were determined by flow cytometry. Two separate flow cytometry panels were used. For each sample, 50,000 events, or particles, were captured. For both panels, all particles were initially gated using pulse width and forward scatter-area to select for single cells, or singlets. Events in this gate were then separated by forward scatter and side scatter to identify epithelial and non-epithelial fractions. Epithelial cells were then validated using cytokeratin positivity in the first panel. The non-epithelial fractions from both panels were further characterized with CD45, a leukocyte marker. Finally, the leukocytes were further characterized using CD3 (a T cell marker), CD11b (a myeloid lineage marker), and B220 (a primarily B cell marker).

with respect to previous findings implicating involvement of the enteric nervous system in the host response [271, 272]. Rhob, upregulated in our and others' previous in vitro studies, is also

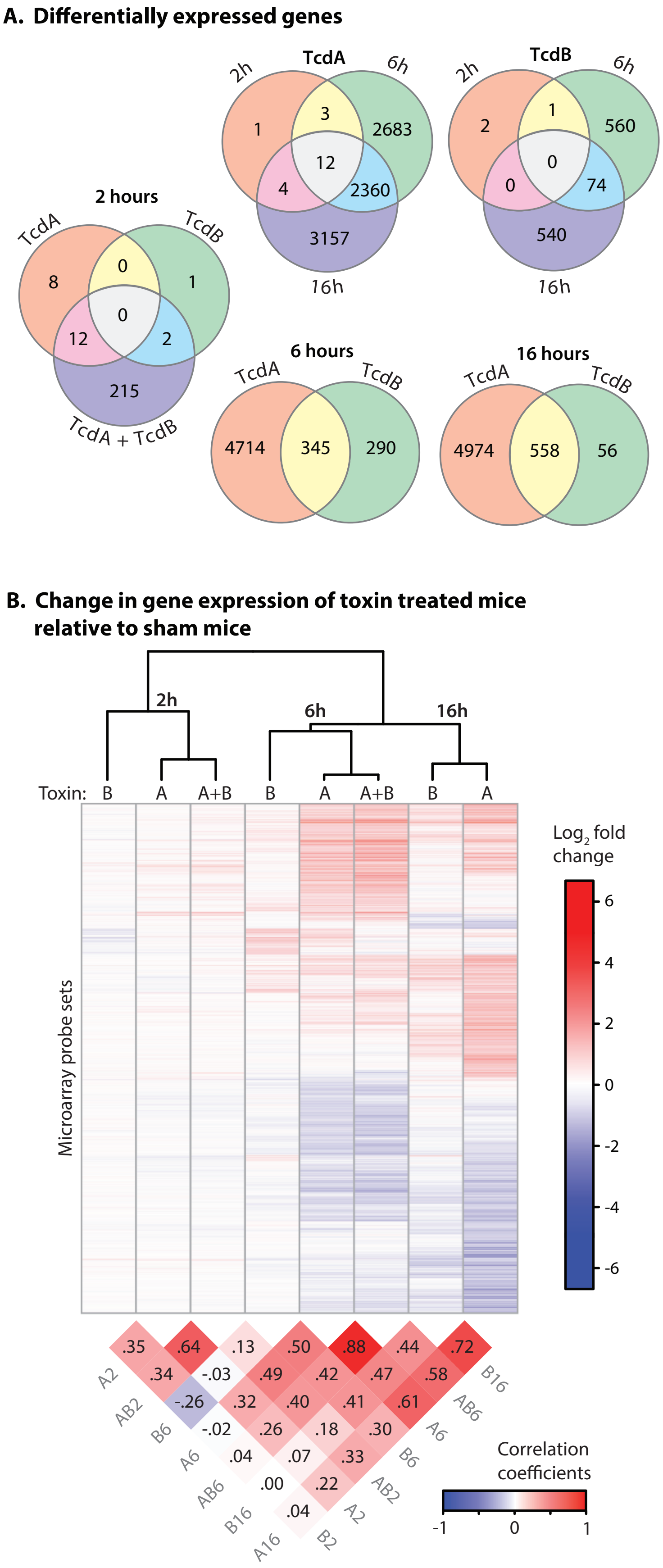

Figure 6.7: Gene expression changes post toxin injection. **(D)** Venn diagrams show the overlap of which microarray probe sets are differentially expressed (comparing toxin-challenged mice versus Sham-challenged mice using a cutoff of q<0.01, see 6.4.10). All microarray probes are annotated into 45,501 probe sets, each of which represents the expression of one gene or multiple similarly related genes. Since only one microarray was used for TcdA+B at 6h, statistical tests could not be used to determine differentially expressed genes for that sample group. **(E)** All probe sets which were differentially expressed for at least one time point were included in the heat map. The Pearson correlation coefficients below the heat map are generated by comparing the log fold changes between each sample group. The dendrogram above the heatmap is a hierarchical clustering of the sample groups, using the correlation coefficients as the distance metric.

upregulated in these experiments [230, 273]. Manually scanning large lists of differentially expressed genes provides novel and interesting findings, yet is impractical when the list includes thousands of genes as is the case at 6 and 16h. This manual approach also overlooks groups of genes that are only slightly regulated, but in a coordinated fashion. Therefore, we performed bioinformatics analyses to identify other potentially important yet not readily apparent associations that could reflect important functional relationships.

Time	2 hours			6 hours			16 hours	
Toxin	A	B	A+B	A	B	A+B	A	B
Differentially expressed genes after TcdA challenge								
Dusp1	4.8	1.3	4.4	6.4	-1.0	10.1	1.9	1.1
Rhob	4.2	1.2	3.8	4.0	1.5	4.8	2.2	1.3
Atf3	4.0	1.4	3.5	2.7	-1.2	4.0	1.2	2.0
Sprr1a	3.4	1.5	3.7	4.9	-1.1	8.8	-1.6	-1.4
C3	2.8	1.6	1.2	2.2	1.6	3.2	5.7	1.9
Areg	2.6	-1.1	2.5	12.8	2.4	15.5	14.9	5.1
Cxcl10	2.6	2.0	6.8	11.3	1.3	13.3	4.7	2.2
Insig1	2.5	1.5	1.8	-1.9	-1.1	-1.4	-2.3	-1.5
Errfi1	2.5	1.1	2.2	3.4	-1.0	5.5	-1.2	-1.4
Egr1	2.3	-1.1	1.5	2.5	1.9	5.0	3.7	1.4
Zfp36	2.2	1.1	2.0	2.9	1.8	3.4	2.2	1.2
Hmgcs1	1.8	1.2	1.6	-1.2	1.0	-1.1	2.4	1.5
Jun	1.8	1.3	1.6	1.4	1.2	1.6	-1.9	-1.1
Gm11545	1.6	1.1	1.7	7.3	1.9	8.2	5.6	3.8
1700006J14Rik	-1.8	-1.3	-1.2	-1.3	1.4	-1.1	-1.6	-1.1
H3f3b	-2.0	-1.5	-1.3	1.1	2.0	1.4	1.8	1.4
Lrrtm1	-2.3	-2.0	-2.2	-2.3	-1.5	-2.5	-1.9	-1.9
Slc8a1	-2.3	-1.3	-1.7	-3.4	1.4	-2.7	-2.9	1.0
Differentially expressed genes after TcdB challenge								
Cxcl1	4.4	2.2	6.5	9.7	1.1	8.1	3.3	1.6
Mtch2	-1.5	-2.0	-1.7	-1.1	2.0	-1.6	-1.5	-1.2
Slc20a1	-1.9	-2.1	-2.5	-2.5	1.7	-2.7	-4.4	-1.5

Table 6.3: Genes with significantly altered expression 2h after TcdA and TcdB injection Average fold changes relative to sham are shown (values of -1.1 and +1.1 imply a 10% decrease and increase, respectively, in gene expression). The cutoff for determining a differentially expressed gene is q<0.01 (see 6.4.10).

Many statistical tools, termed "enrichment methods", can be used to determine if the transcription of predefined sets of genes is significantly altered or "enriched"; this approach allows for the characterization of cellular processes (instead of individual genes) that are affected. Given our experimental design, we carefully chose two enrichment methods. In our implementation of a "competitive" enrichment method named CAMERA, which was developed by Wu et al., we test whether the genes in a set are more differentially expressed than those outside the set [268]. We also developed a "self-contained" test, inspired by CAMERA, to determine if the average change in gene expression within each gene set is different than zero. Whereas the "competitive" hypothesis may find a gene set (with several differentially expressed genes) to be insignificant because many genes outside the set are also differentially expressed, the self-contained hypothesis would find the same set to be significant. The self-contained test identified enriched functions for all samples; for TcdA and TcdB samples at 2h, which have few differentially expressed genes, multiple gene sets are enriched (Table 6.4). Using the competitive test for TcdA samples, no functions are enriched at 6h ($q<0.2$) but several are enriched at 16h (Table 6.5). The genes within these groups are presented below.

TcdA	$-log_{10}(p)$	q	Database
Interleukin-1-mediated signaling pathway	5.3	0.003	BP
Cellular response to hydrogen peroxide	5.1	0.003	BP
Positive regulation of fatty acid biosynthetic process	4.0	0.026	BP
Cholesterol metabolic process	3.7	0.042	BP
Hormone activity	4.2	0.021	MF
Innate immunity signaling	3.9	0.047	Reactome
TcdB			
Negative regulation of the Notch signaling pathway	5.7	0.002	BP
Nuclear envelope lumen	3.6	0.045	CC
Genes involved in apoptotic cleavage of cellular proteins	4.0	0.037	Reactome
Membrane trafficking	3.6	0.043	Reactome

Table 6.4: Biological functions and gene sets associated with gene expression changes 2h after TcdA or TcdB injection Our self-contained enrichment test was run on multiple databases separately, and gene sets with $q<0.05$ are shown. The logarithms of the p-values from the enrichment test are shown. The Gene Ontology database is separated into three ontologies: molecular functions (MF), biological processes (BP), and cellular components (CC). Mouse genes were mapped to human orthologs so that the Reactome database could be used.

One of the most striking upregulated sets of genes includes those encoding proteins which bind to GTP or GTPases (Table 6.5). These expression changes are most evident for TcdA at 16h, though a similar pattern is observed at earlier time points and with TcdB (Figure 6.8A). The expression of interferon-inducible GTPase genes is increasingly affected from 2h to 16h with either toxin. To a lesser extent, the expression of several small GTPase genes, not directly tied to interferons or

TcdA	$-log_{10}(p)$	q
Cell surface binding	3.5	0.102
Rho GTPase binding	3.3	0.102
GTPase activity	3.1	0.107
GTP binding	2.9	0.107
Protein N-terminus binding	2.5	0.205
Glutathione transferase activity	2.3	0.205
Steroid binding	2.3	0.205
Carboxylase activity	2.2	0.205
RNA polymerase II core promoter sequence-specific DNA binding	2.2	0.205
Protein complex binding	2.1	0.205
Heme binding	2.1	0.205
Thiolester hydrolase activity	2.1	0.205
Fibronectin	2.1	0.205
Cholesterol binding	2.1	0.205
Histone deacetylase activity	2.1	0.205
Triglyceride lipase activity	2.0	0.210
Selenium binding	2.0	0.210
Aromatase activity	2.0	0.210
Beta-tubulin binding	1.9	0.210
Actin binding	1.9	0.210

Table 6.5: Molecular functions associated with gene expression changes 16h after TcdA injection. The top 20 competitively enriched gene sets from the molecular function ontology of the Gene Ontology database are shown.

immune function, is also altered. These small GTPases include members of several subfamilies from the Ras protein superfamily. Genes encoding proteins which interact or bind with Rho family proteins were also upregulated. Hence, in addition to the toxins' glucosylation of small GTPases, the in vivo transcription of many GTP and GTPase binding proteins with a wide range of functions is clearly altered in response to TcdA and TcdB.

We also found an abundance of differentially expressed genes associated with cell metabolism (Table 6.4 and Table 6.5). More specifically, many enzymes involved in fatty acid breakdown and beta-oxidation were downregulated. Four other classes of enzymes were also downregulated: cytochrome P450 enzymes, glutathione S-transferases, carboxylesterases, and sulfotransferases (Figure 6.8B). These genes span several metabolic pathways, yet there is a strong commonality in their substrates, most of which include lipid and fatty acids or related compounds; xenobiotics; or both. In addition to the conspicuous toxin-induced pathology and inflammation, recognition of the altered expression of detoxification enzymes and fatty acid metabolic enzymes introduces an

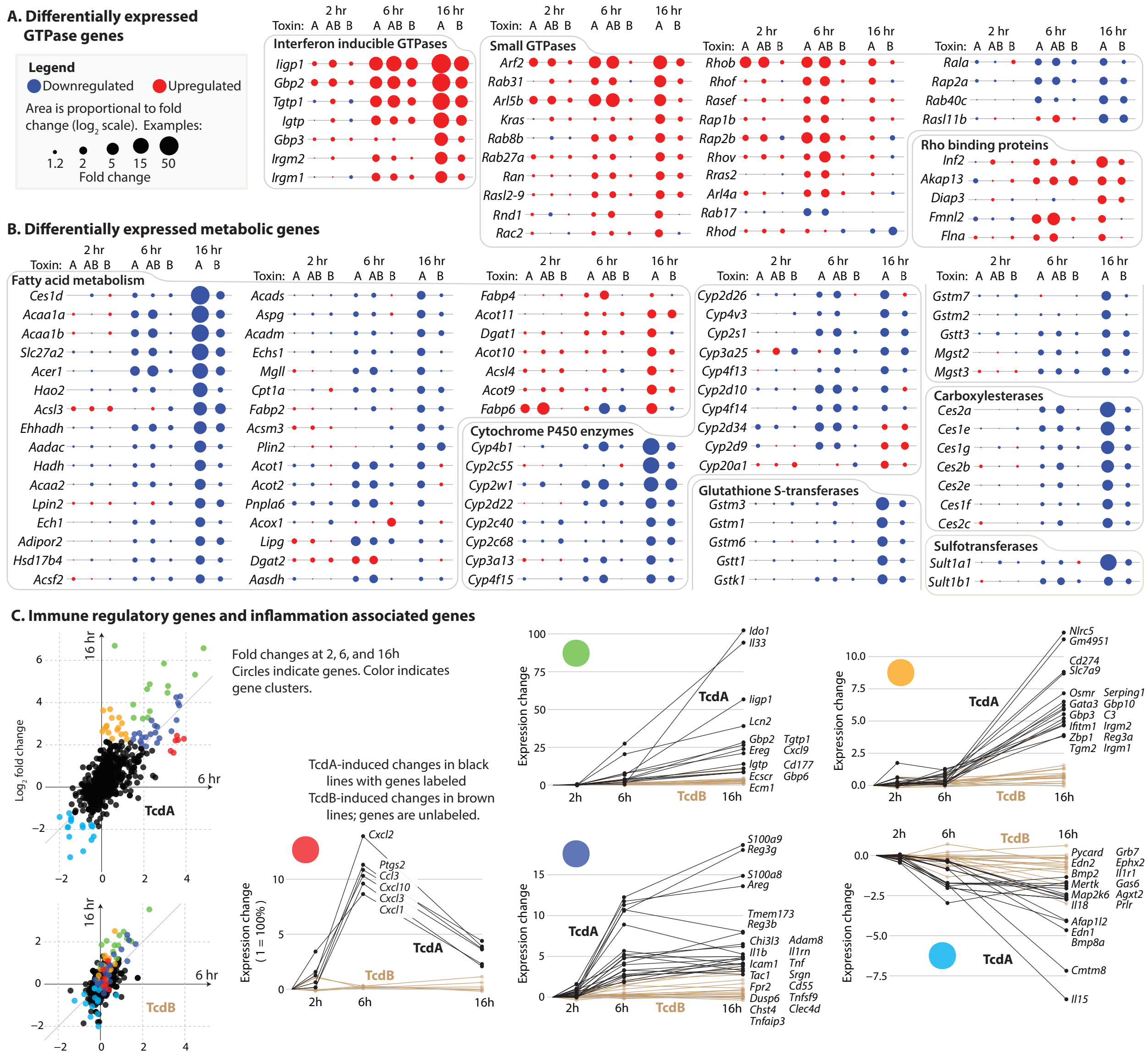

Figure 6.8: Biological functions associated with gene-expression changes. The expression data was generated from the mice indicated in Figure 6.4B. **(A)** The fold changes of differentially expressed GTPase and GTPase-binding genes. Only genes with greater than a two-fold change in expression are shown. **(B)** Similar to (A), but instead showing genes associated with metabolic functions associated with gene expression changes. **(C)** Expression changes and clustering of genes annotated as being associated with immune regulation or inflammation. Genes were clustered based on expression changes 6 and 16h after TcdA injection. In the scatterplots, black circles indicate genes with low expression changes; these genes are not included in the line plots.

unexplored aspect of the host response to TcdA and TcdB.

Inflammation is a clear pathophysiological manifestation of toxin injection, and many inflammation-associated genes are differentially expressed (Table 6.3, Figure 6.8C). However, at 6 and 16h, genes

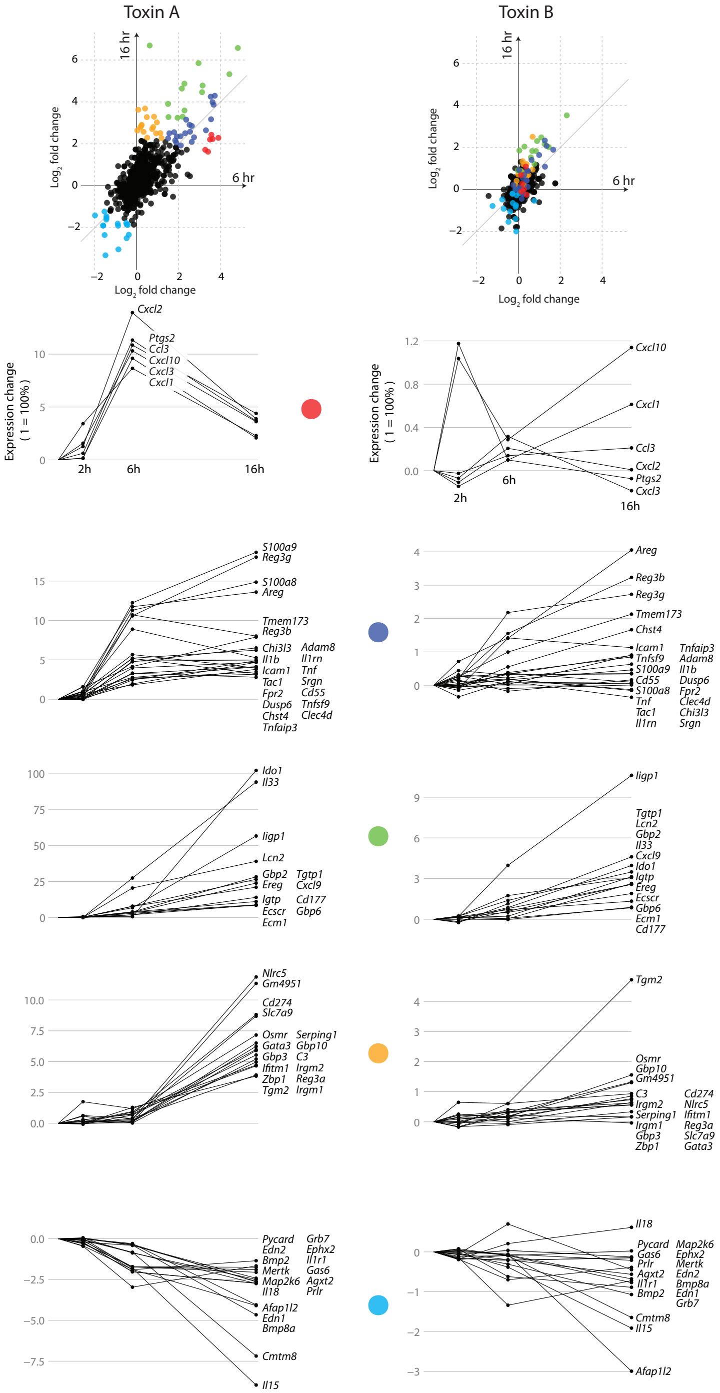

Figure 6.9: Expression changes of inflammation associated and immune regulatory genes This figure extends Figure 6.8C to also show TcdB-induced and TcdA-induced expression changes on separate, side-by-side plots.

associated with inflammation are not expressed to a greater extent than genes associated with several other functions (see Table 6.5). Competitive enrichment tests did find “inflammatory response” and “chemotaxis” among the top six enriched functions for TcdA at 6h, but the enrichment of these groups is not significant (q=0.32). Given the importance of inflammation in our physiological measurements at 6 and 16h, yet no remarkable regulation of only inflammation-associated genes at these times, we further investigated the expression of genes known to be linked with inflammation and related physiological effects.

To identify temporal expression patterns, we clustered genes associated with immune regulation and inflammation according to their change in expression over time (Figure 6.8C). Several of these genes are upregulated at 6h and still at 16h, which may represent transcription that perpetuates the inflammatory response or has anti-inflammatory effects. For TcdA, expression of five chemokine genes (Cxcl1, Cxcl2, Cxcl3, Cxcl10, and Ccl3) is strongly upregulated at 6h (coinciding with increased neutrophil infiltration) but subsides by 16h. The gene expression of several of these chemokines also correlates with protein expression (r=0.67, TcdA at 6h, Figure 6.10). Though the 6h peak in chemokine gene expression does not occur with TcdB, TcdA-induced and TcdB-induced gene expression changes are correlated for all other inflammatory genes (Figure 6.9). Hence, except for the aforementioned chemokines, TcdA and TcdB similarly regulate inflammation-associated and immune-regulatory genes, although TcdA-induced changes are on average two and three times greater at 6 and 16h, respectively.

6.5.5 Comparisons of gene and protein expression of cytokines

To test the common assumption that gene expression correlates with protein expression, we compared the microarray data for chemokines to the intracellular protein expression. After mapping microarray probes to the appropriate Ensembl gene IDs, we found that TcdA-induced changes in gene expression correlated to changes in protein expression (r=0.67, Figure 6.10A).

Figure 6.10B compares our measurements of changes in the gene expression of cecal epithelial cells (Toxin A+B versus Sham at 6h; cecal injection) to protein concentration changes in mouse colonic tissue lysates as measured by Hirota *et al.* (Toxin A+B versus Sham at 4h; intrarectal instillation) [274]. Figure 6.10C compares cecal epithelial layer protein expression (Toxin A versus Sham at 6h) to the same Hirota *et al.* data. Overall, the changes in the protein concentrations of

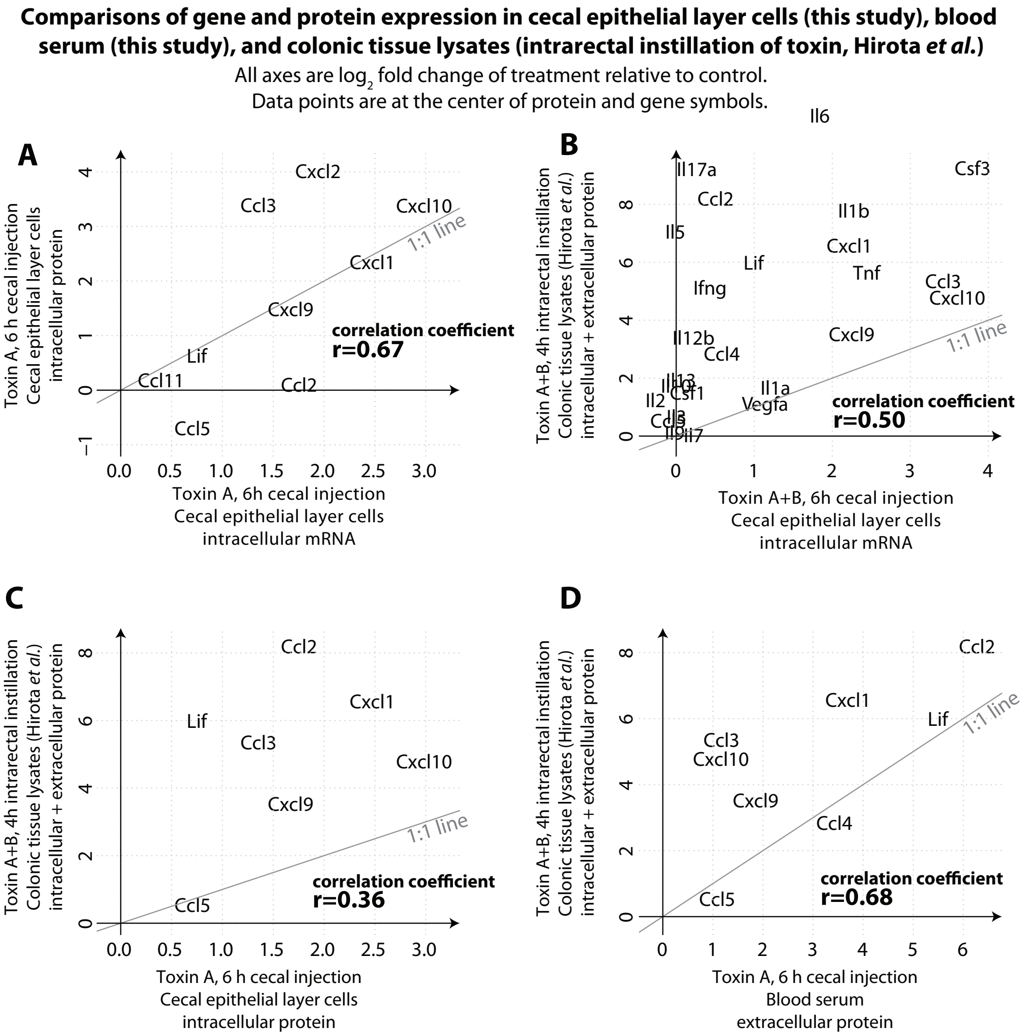

Comparisons of gene and protein expression in cecal epithelial layer cells (this study), blood serum (this study), and colonic tissue lysates (intrarectal instillation of toxin, Hirota *et al.*)

All axes are $\log_2$ fold change of treatment relative to control.
Data points are at the center of protein and gene symbols.

Figure 6.10: Cytokine gene and protein expression Our data for Ccl4 is not shown in Figure 6.10A because the protein concentration measurements were at or below the detection limit of our assay. The Ccl4 concentration from three mice treated with toxin A were 0.8, 0.8, and 4.8 pg/ml; the concentrations from three sham mice were 0.8, 0.8, and 14.72 pg/ml. Cell lysates were obtained as described in the Methods of the Manuscript. Cytokine levels in serum and lysates were measured by using MILLIPLEX® MAP beads and the signal was measured using a Luminex 100 IS System.

colonic tissue were greater than measurements of gene or protein expression from cecal cells.

In addition to differences in the location of the intestine and differences in the biological molecules being measured, the Hirota *et al.* samples were obtained from a different source, colonic tissue. The colonic tissue presumably includes proteins from intracellular and extracellular proteins, while many of our measurements included only intracellular protein or mRNA. Nevertheless, Figure 6.10B and Figure 6.10C show correlation between the colonic tissue data and cecal epithelial layer gene expression (r=0.5) and protein expression (r=0.36). Additionally, our measurements of changes in blood serum cytokines after 6h of TcdA injection correlated best with the data from Hirota *et al.* (Figure 6.10D).

6.5.6 CXCL1 and CXCL2 neutralization alters the host response to TcdA cecal injection

To investigate the role of these acutely expressed chemokine genes in response to TcdA challenge, we administered neutralizing antibodies against CXCL2 and the closely related CXCL1. In addition to the high expression of Cxcl2, we also chose Cxcl1 because it is another important primary neutrophil chemoattractant. Anti-CXCL1 and anti-CXCL2 (or corresponding isotypes) were administered by intraperitoneal injection (100 µg/antibody/animal) 16h prior to TcdA cecal injection. TcdA-induced increases in the serum levels of CXCL1 and CXCL2 is significantly reduced in mice pretreated with anti-CXCL1 and anti-CXCL2, demonstrating that systemic levels were effectively neutralized compared to isotype controls (Figure 6.11A; $p<0.01$ for CXCL1, $p<0.02$ for CXCL2). To test if neutralization of CXCL1 and CXCL2 alters expression of Cxcl1 and Cxcl2, we isolated mRNA from epithelial-layer cells. We found that neutralization does not eliminate the 6h-peak in Cxcl1 and Cxcl2 expression caused by TcdA (Figure 6.12). In addition, pathology and neutrophil infiltration in the cecum is not affected by administration of anti-CXCL1 and anti-CXCL2 (Figure 6.11C, Figure 6.13). However, 16h after TcdA injection, systemic neutrophil levels are reduced by neutralization (Figure 6.11B). A larger percentage of mice survived after CXCL1 and CXCL2 neutralization, though the experiment was not designed to assess survival and more samples would be necessary to determine statistical significance (Figure 6.11D). However, higher sera levels of CXCL1 and CXCL2 correlate with a moribund state and administration of anti-CXCL1 and anti-CXCL2 reduces those chemokine elevations.

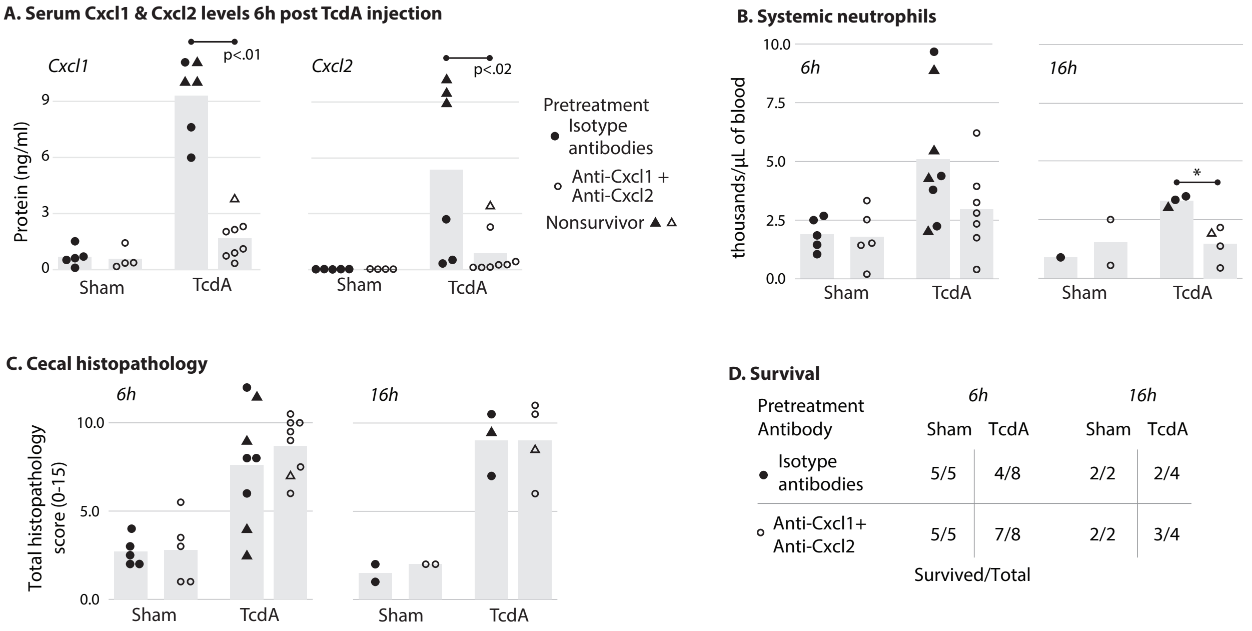

Pretreatment Antibody	6h Sham	6h TcdA	16h Sham	16h TcdA
● Isotype antibodies	5/5	4/8	2/2	2/4
○ Anti-Cxcl1+ Anti-Cxcl2	5/5	7/8	2/2	3/4

Survived/Total

Figure 6.11: Antibody neutralization of CXCL1 and CXCL2. In each panel, the four sample groups are defined by two binary factors: (1) TcdA injection or sham injection and (2) pretreatment with isotype antibodies or anti-CXCL1 and anti-CXCL2 antibodies. The data in all panels are combined from two independent experiments, one with 24 mice and another with 14 mice (**??**). Missing values in panels A and B are due to the limited volume of blood that could be drawn from some mice. The data points displayed in the figure were used for each statistical test. Statistical tests are indicated with horizontal lines as described in the caption to Figure 6.4. **(A)** Concentration of CXCL1 and CXCL2 in the sera of mice 6h after cecal injection of TcdA. **(B)** Concentration of neutrophils in blood obtained by cardiac puncture. *p=0.057 by the Mann-Whitney U test; using this nonparametric, two-sided test with three samples in one group and four in the other, the minimum possible p-value is 0.057. p<0.02 by the two-sided t test. **(C)** Total histopathology score (see 6.4.4) from cecal tissue sections. **(D)** Survival of mice after cecal injection. Mice were monitored so that moribund mice were sacrificed and are counted as having not survived (nonsurvivors).

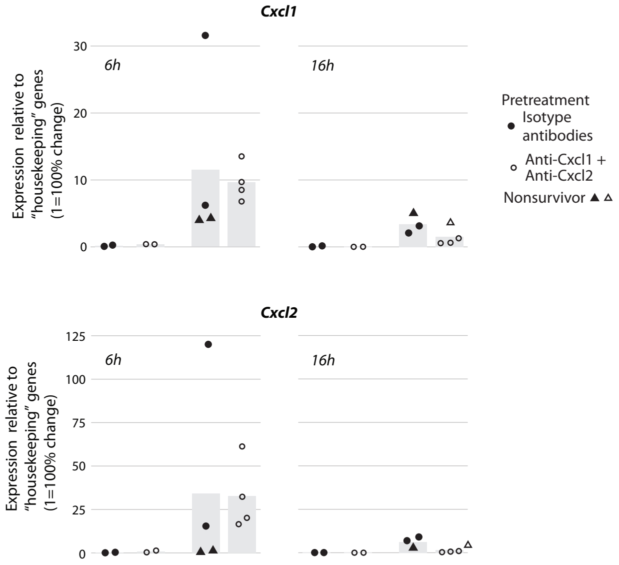

Figure 6.12: *Cxcl1* and *Cxcl2* expression after Cxcl1 & Cxcl2 neutralization Aside from any possible feedback and regulatory mechanisms, i.p. administration of anti-Cxcl1 and anti-Cxcl2 were predicted to neutralize extracellular proteins and not directly affect *Cxcl1* and *Cxcl2* expression. Using qRT-PCR to measure mRNA in epithelial-layer cells, we found that antibody neutralization did not block the transient increase in *Cxcl1* and *Cxcl2* expression that we previously measured by microarray. *Actb* and *Hprt* were used as "housekeeping" genes. The quantity of each transcript was calculated as $2^{-\Delta\Delta Ct}$ where $\Delta\Delta Ct$ is the difference in cycle threshold between the transcript and the geometric mean of the housekeeping genes).

6.5.7 *In vivo* transcriptome response *versus in vitro* transcriptome and proteome responses

In previous studies with epithelial cell lines, the response to TcdA and/or TcdB has been analyzed with transcriptomic and proteomic techniques. In order to merge the data in this present study to our previous data from a human ileocecal epithelial cell line (HCT8 cells) treated with TcdA or TcdB, we mapped orthologous mouse and human genes [230]. These genes were further mapped to human proteins in order to be compared to a recent proteomics study by Zeiser *et al.* who treated Caco-2 cells with TcdA [275].

The fold changes of sample groups relative to control groups were compared using nonparametric correlation coefficients (Figure 6.14). The values in cells of the figure are the correlation coefficients squared (the square of the Pearson correlation coefficient is the coefficient of determination, or R^2 value). The colors of the cells correspond to the correlation coefficients. Negative

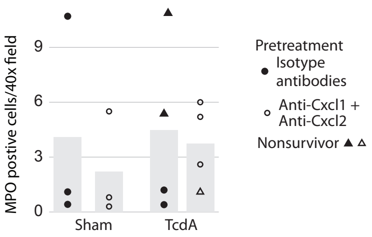

Figure 6.13: Neutrophil infiltration 6h after TcdA cecal injection of mice pretreated with neutralizing antibodies We hypothesized that neutralization of Cxcl1 and Cxcl2 would inhibit neutrophil infiltration in the cecum. We found that our neutralization did not affect the amount of infiltration after injection of TcdA (Figure 6.13). The high variability for these limited samples, however, makes it difficult to claim that isotype, anti-Cxcl1, and anti-Cxcl2 antibodies do or do not have an effect on neutrophil infiltration 6h after cecal injection—at least with the method in which we administered the antibodies.

correlations are blue; positive correlations are red. One-to-one orthologs were used to compare the two transcriptional data sets (19,643 genes). The proteomics data set was merged separately since data is available for many fewer proteins than genes (4,090 gene-protein pairs).

As seen above, there is little correlation between different studies and experimental systems. In Figure 6.15, we show 13 of the most differentially expressed genes that were similarly expressed in both our *in vivo* and *in vitro* data sets.

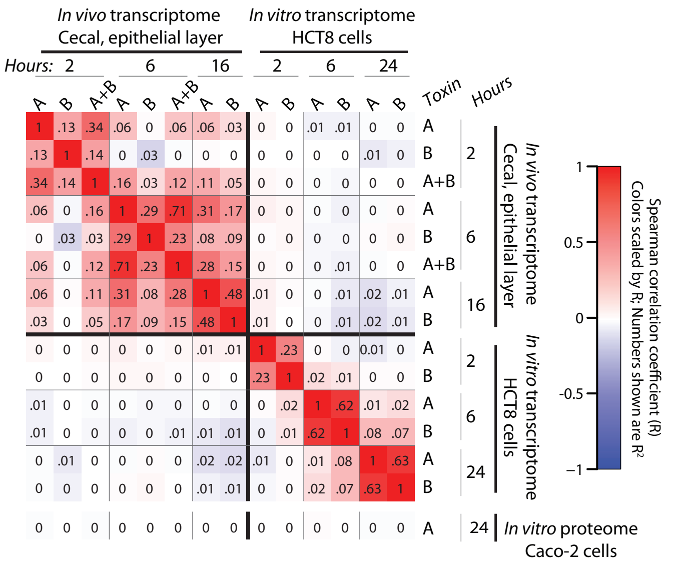

			In vivo transcriptome Cecal, epithelial layer								*In vitro* transcriptome HCT8 cells					
		Hours:	2			6			16		2		6		24	
	Hours	Toxin	A	B	A+B	A	B	A+B	A	B	A	B	A	B	A	B
In vivo transcriptome Cecal, epithelial layer	2	A	1	.13	.34	.06	0	.06	.06	.03	0	0	.01	.01	0	0
		B	.13	1	.14	0	.03	0	0	0	0	0	0	0	.01	0
		A+B	.34	.14	1	.16	.03	.12	.11	.05	0	0	0	0	0	0
	6	A	.06	0	.16	1	.29	.71	.31	.17	0	0	0	0	0	0
		B	0	.03	.03	.29	1	.23	.08	.09	0	0	0	0	0	0
		A+B	.06	0	.12	.71	.23	1	.28	.15	0	0	0	.01	0	0
	16	A	.06	0	.11	.31	.08	.28	1	.48	.01	0	0	.01	.02	.01
		B	.03	0	.05	.17	.09	.15	.48	1	.01	0	0	.01	.02	.01
In vitro transcriptome HCT8 cells	2	A	0	0	0	0	0	0	.01	.01	1	.23	0	0	0.01	0
		B	0	0	0	0	0	0	0	0	.23	1	.02	.01	0	0
	6	A	.01	0	0	0	0	0	0	0	0	.02	1	.62	.01	.02
		B	.01	0	0	0	0	.01	.01	.01	0	.01	.62	1	.08	.07
	24	A	0	.01	0	0	0	0	.02	.02	.01	0	.01	.08	1	.63
		B	0	0	0	0	0	0	.01	.01	0	0	.02	.07	.63	1
In vitro proteome Caco-2 cells	24	A	0	0	0	0	0	0	0	0	0	0	0	0	0	0

Figure 6.14: Correlations between *in vitro* and *in vivo* responses to toxins

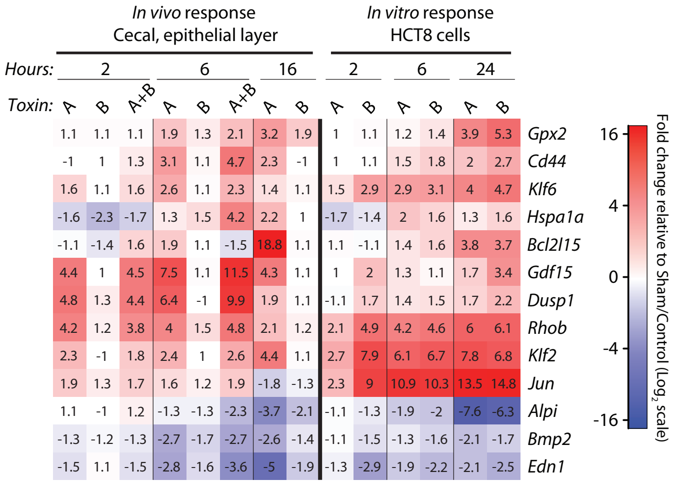

	In vivo response Cecal, epithelial layer								*In vitro* response HCT8 cells					
Hours:	2			6			16		2		6		24	
Toxin:	A	B	A+B	A	B	A+B	A	B	A	B	A	B	A	B
Gpx2	1.1	1.1	1.1	1.9	1.3	2.1	3.2	1.9	1	1.1	1.2	1.4	3.9	5.3
Cd44	-1	1	1.3	3.1	1.1	4.7	2.3	-1	1	1.1	1.5	1.8	2	2.7
Klf6	1.6	1.1	1.6	2.6	1.1	2.3	1.4	1.1	1.5	2.9	2.9	3.1	4	4.7
Hspa1a	-1.6	-2.3	-1.7	1.3	1.5	4.2	2.2	1	-1.7	-1.4	2	1.6	1.3	1.6
Bcl2l15	-1.1	-1.4	1.6	1.9	1.1	-1.5	18.8	1.1	1.1	-1.1	1.4	1.6	3.8	3.7
Gdf15	4.4	1	4.5	7.5	1.1	11.5	4.3	1.1	1	2	1.3	1.1	1.7	3.4
Dusp1	4.8	1.3	4.4	6.4	-1	9.9	1.9	1.1	-1.1	1.7	1.4	1.5	1.7	2.2
Rhob	4.2	1.2	3.8	4	1.5	4.8	2.1	1.2	2.1	4.9	4.2	4.6	6	6.1
Klf2	2.3	-1	1.8	2.4	1	2.6	4.4	1.1	2.7	7.9	6.1	6.7	7.8	6.8
Jun	1.9	1.3	1.7	1.6	1.2	1.9	-1.8	-1.3	2.3	9	10.9	10.3	13.5	14.8
Alpi	1.1	-1	1.2	-1.3	-1.3	-2.3	-3.7	-2.1	-1.1	-1.3	-1.9	-2	-7.6	-6.3
Bmp2	-1.3	-1.2	-1.3	-2.7	-1.7	-2.7	-2.6	-1.4	-1.1	-1.5	-1.3	-1.6	-2.1	-1.7
Edn1	-1.5	1.1	-1.5	-2.8	-1.6	-3.6	-5	-1.9	-1.3	-2.9	-1.9	-2.2	-2.1	-2.5

Figure 6.15: Similarly expressed genes *in vitro* and *in vivo*

6.6 Discussion

This is the first study to characterize the genome-wide transcriptional response to TcdA and TcdB in vivo. Additionally, several other parallel measurements were assessed to quantify changes at the cellular and tissue levels. The overall dynamics of the host responses to TcdA include rapid changes in cecal pathology, neutrophil infiltration, and gene expression. Conversely, TcdB elicits a delayed transcriptional response and causes significantly less pathology yet still recruits neutrophils and induces histopathological changes by 16h. The combined effects of TcdA and TcdB (20 µg/toxin) on histopathology at 2h and the overall transcriptional response at 2h and 6h are not additive. However, two of three mice injected with TcdA+B did not survive to our 6h time point, so we do not rule out potential synergism at later times. For example, Hirota et al., using lower doses (5 µg/toxin), found that TcdA and TcdB may act synergistically 4h after both toxins are introduced intrarectally [274]. As for TcdB alone, several studies have found that TcdB does not damage hamster or mouse intestines, nor does TcdB bind to hamster brush border membranes [242, 244]. However, Lyerly et al. showed that, when the cecum was bruised before intragastric administration of TcdB, all mice became ill [242]. Hence, it is possible that the experimental procedure of cecal injection may allow or enhance the TcdB-induced pathology we observe at 16h. In line with our findings that TcdB has pathologic effects, Libby et al. found that 16 of 16 hamsters died within 36h of cecal injection of 60 µg of TcdB and found that 35 µg of TcdA resulted in epithelial lesions, edema, and neutrophil infiltration [237]. We were able to quantify separate aspects of these host responses over time, revealing the relative responses to TcdA and TcdB, individually altered genes and markers of intoxication, and regulated gene sets associated with pathways that function at the intracellular and extracellular levels.

This study builds on our previous analysis of the transcriptional response of a human ileocecal, epithelial cell line (HCT8) to TcdA or TcdB (2, 6, and 24h after toxin treatment). After mapping all orthologous genes, we found that the overall transcriptional response of HCT8 cells is poorly correlated to the responses of the cecal epithelial layer cells in vivo ($r^2 < 0.03$ for all comparisons, Figure 6.14). Some of these dissimilarities are presumably due to the different experimental systems and mRNA sources (in vitro vs. in vivo and human vs. mouse). Many differences may also represent important responses primarily observed in an in vivo experimental system. For instance, transient expression of chemokines and increased expression of several other cytokines was not observed in HCT8 cells. Also, the altered expression of many metabolic genes did not occur in HCT8 cells. Conversely, cell-cycle and DNA damage-associated gene sets were not enriched in vivo as they were with HCT8 cells. Selecting for expression that is similar between the data sets, ten genes are commonly upregulated (Rhob, Klf2, Klf6, Jun, Dusp1, Gdf15, Hspa1a, Dusp1, Bcl2l15, and Gpx2) and a few are commonly downregulated (Edn1, Alpi, and Bmp2; Figure 6.15). In another high-throughput analysis of the host cell response to TcdA, Zeiser et al. analyzed the changes in the proteome of Caco2 cells 24h after TcdA exposure [275]. By mapping transcripts to proteins, we found that the proteomics data was poorly correlated with transcriptional changes in HCT8 cells and our in vivo data ($r^2 < 0.01$ for all comparisons). However, similar to our previous study and this current study, Zeiser et al. did note changes in the amount of many cell-cycle associated proteins and several proteins involved in lipid and cholesterol metabolism.

Aside from the quantitative and temporal differences of the physiological responses, many transcriptional similarities exist between the host response to TcdA and TcdB. For both toxins, the immediate transcriptional response, indicative of initial or acute toxin effects, is represented by altered expression of a small set of genes. By 6h, the number of differentially expressed genes for both toxins increases 200 fold, coinciding with changes in pathology including neutrophil infiltration. TcdA challenge leads to approximately ten-fold more differentially expressed genes at 2, 6, and 16h; however, there is significant overlap in the genes affected by TcdA and TcdB (Figure 6.7). Though TcdA-induced changes were greater in magnitude, correlation coefficients (which are scale invariant) between TcdA and TcdB demonstrate strong overall similarity in gene expression signatures (Figure 6.7B). This difference in scale between the toxin responses may result from differences in molecular functions and/or the number, type, and sensitivity of cells affected. Which and how many cells are affected might also originate from the differential abilities of TcdA and TcdB to bind and enter intestinal cells. In line with our results showing that TcdB caused significantly less pathology than TcdA, Rolfe found little to no TcdB adsorption relative to TcdA on hamster brush border membranes [244]. The location and transport of toxins within the gut, which is very poorly understood, may also partly explain the extent of pathology in intoxicated mice. After cecal injection of TcdA or TcdB, we did not observe any significant pathology in the colon. Hence, the effects of the toxins which we measured were restricted to the cecum. Nevertheless, other systemic effects emanating from local insult may contribute to overall pathology. Multiple animal studies have observed increased mucosal permeability after TcdA intoxication, and Steele et al. demonstrated systemic dissemination of both TcdA and TcdB during severe infection in mice and piglets [253]. Despite the various explanations for the lesser effects we observe with TcdB, a change in transcription after injection of TcdB is distinct even at 2h and 6h when changes in histopathology and many other variables are not apparent. Furthermore, this transcriptional response is highly correlated with the response to TcdA. Hence, the transcriptional analysis reveals that overall intracellular responses of epithelial-layer cells to TcdA and TcdB are largely similar though the magnitudes of the gross observed pathologies may differ.

Beyond piecemeal identification of genes with altered expression, the transcriptional data as a whole reflects the cellular responses to underlying molecular interactions. Our analyses identified the upregulation of several genes encoding Rho binding proteins and small GTPases that are known to be affected by TcdA and TcdB. We also identified strong upregulation of many interferon-inducible GTPases. These interferon-inducible GTPases have been implicated in several mechanisms of cell-autonomous immunity such as inflammasome activation, recognition of pathogens in vacuoles, assembly of defense complexes, and autophagy [276]. Though the transcription of interferon genes is unaltered in the epithelial-layer cells we isolated, the GTPase upregulation suggests the functional presence of interferons. Consistent with this, Ishida et al. found increased transcription of IFN-γ in whole tissue and increased production of IFN-γ by infiltrating neutrophils after injection of TcdA into ligated ileal loops of mice [256]. In the same analysis, “beta-tubulin binding” and "histone deacytelase activity" were also enriched. Though the relevance of these associations may seem at first unclear, Nam et al. have recently shown that inhibition of histone deacytelase 6 blocks TcdA-induced tubulin acetylation and subsequent mucosal damage [277]. Hence, our analysis corroborates previous data and suggests that our transcriptional data reflects other functions that are affected in parallel with or prior to transcription. For example, a novel set of toxin-induced genes identified in our analysis includes several metabolic genes. At 2h, multiple genes associated with cholesterol and steroid synthesis (specifically the mevalonate pathway) are slightly upregulated, whereas, at 6 and 16h, genes associated with fatty acid metabolism and detoxification of xenobiotics are downregulated. The expression of several of these genes is known to be controlled directly or indirectly by nuclear receptors. In light of the finding that gp96 (a paralogue to heat shock protein 90, Hsp90) serves as a receptor for TcdA in vitro, these transcriptional changes may also result from Hsp90 interactions (e.g. Hsp90 proteins bind xenobiotic response elements and steroid hormone receptors) [250].

In addition to the above intracellular effects, several genes previously associated with toxin-mediated pathophysiology are altered. For instance, our self-contained enrichment test identified the "interleukin-1 mediated signaling pathway" as the most enriched gene set 2h after TcdA injection. More specifically, TcdA increases proinflammatory Il1b expression by 80% at 2h and then over 500% at 16h; TcdB causes no such change. In addition to Il1b, concomitant increases in the IL-1 receptor antagonist, Il1rn, suggest a natural feedback mechanism. These findings are in line with a previous study demonstrating that recombinant IL1RN pretreatment attenuated TcdA+B-induced inflammation [278]. Expression of Il33, an IL-1 family cytokine involved in mucosal signaling, also dramatically increases in response to TcdA (28- and 95-fold at 6 and 16h, respectively). Similarly, in mice infected with *C. difficile* (VPI10463), intestinal levels of IL-33 increase at the peak of infection (data not shown), suggesting that this cytokine is responsive in part to toxin effects. In another study, Hirota et al. measured cytokine levels in colonic tissue lysates four hours after intrarectal instillation of TcdA+TcdB. The data published by Hirota et al. are correlated to our measured cecal, epithelial-layer gene expression (r=0.5, TcdA+B at 6h) and intracellular protein expression (r=0.36, TcdA at 6h, Figure 6.10). Six hours after cecal injection of TcdA, serum cytokine concentrations correlate even more strongly with Hirota et al.'s data (r=0.68). Hence, our data from cecal cells and serum after cecal injection of TcdA and/or TcdB are in agreement with findings from colonic tissue after intrarectal instillation of TcdA+TcdB. Additionally, our data show the expression changes of many other genes over a 16h time course for each toxin individually.

Although the expression and/or release of chemokines and cytokines are known responses to *C. difficile* toxins, the full profile of the transcription of cytokines in response to toxins has not been investigated. Previously, the role of many chemokines and proinflammatory mediators in TcdA-induced enteritis has been studied individually with ileal loops or in vitro [153]. For example, Morteau et al. found increased Ccl3 and Ccl5 transcription in whole tissue one hour after TcdA injection, and showed that Ccl3 knockout mice were less susceptible to TcdA [254]. Castagliuolo et al. identified increased expression of Cxcl2 in rat epithelial cells after injection of TcdA into ligated ileal loops [257]. Our results identify additional chemokines which are transiently expressed and provide insight into the response of the epithelial layer over a time course covering the development of toxin-mediated pathogenesis. Additionally, our data includes the expression of all cytokines in response to TcdA and TcdB separately and in combination. We found that overall cytokine expression in response to TcdA and TcdB is correlated, yet TcdA-induced changes are more pronounced. However, TcdB does not increase the expression of several inflammation-associated chemokines as TcdA does. This difference between toxins is particularly interesting in light of the fact that TcdB cecal injection causes less tissue damage and inflammation than injection of TcdA. Our data also show that the chemokine expression in response to TcdA is transient, yet many other cytokines continue to be expressed even after chemokine expression returns towards basal levels. The early chemokine expression may be involved in the acute toxin effects. However, since *C. difficile* infection typically last several days, the continued expression of several other cytokines is potentially interesting and an unexplored area of research.

In order to characterize the timing and the effects of the acute response after toxin exposure, we investigated the early effects of CXCL1 and CXCL2 in the same cecal injection system. The increased expression of chemokine genes involved in neutrophil recruitment (e.g. Cxcl1 and Cxcl2) was coincident with neutrophil infiltration. Local epithelial damage and neutrophil infiltration were not attenuated by neutralization of CXCL1 and CXCL2. Similar findings in pathology between neutralizing antibodies and isotype controls could be due to insufficient levels of antibody near the site of toxin injection or the method of antibody administration. In another neutralization study, Castagliuolo et al. injected anti-CXCL2 intravenously into fasted rats 15 minutes prior to injection of TcdA into ileal loops; this neutralization attenuated TcdA-induced fluid secretion, mucosal permeability, and MPO activity [257]. Other ileal loop experiments with TcdA have revealed that pathology and neutrophil infiltration become evident one to three hours after intoxication [256, 257]. Hence, it is unlikely the effects we measured in this study would have been discernible prior to our earliest 2h time point. On the other hand, few studies have examined the host responses after the initial acute response; most have focused on responses within the first 6 hours [181, 254–256, 258, 259, 279]. Our latest time point, 16h, did reveal attenuation of the TcdA-induced increase in systemic neutrophils for anti-CXCL1 and anti-CXCL2-treated animals. Moreover, serum levels of CXCL1 and CXCL2 were predictors for survival. This result also suggests that surviving mice are poor responders in terms of Cxcl1 and Cxcl2 expression and production. Related to this, a recent study by Feghaly et al. showed that inflammatory markers in stool, not the number of *C. difficile* colony forming units, correlated with clinical outcomes [154]. In a hamster infection model, Steele et al. showed that serum levels of CXCL1, IL6, TNF , and IL1 are increased in cases of severe, systemic infection [253]. Our results demonstrating that high CXCL1 and CXCL2 correlate with mortality are supportive of these infection studies and suggest that the release of these and perhaps other inflammatory markers in serum is primarily toxin-mediated. Our experiments with anti-CXCL1 and anti-CXCL2 thus emphasize the importance of the locale of toxin effects and chemokine expression systemically and/or throughout the intestine.

The multilevel measurements and our analysis have revealed important aspects of the relative host responses to TcdA versus TcdB intoxication, novel changes in transcription underlying observed physiological changes, and many aspects of the early time course and dynamics of the host response near the site of injection and in circulating blood. These extensive data and experimental framework also provide a basis for comparisons and future investigations with mutant toxins and mutant mouse strains. Furthermore, these data may be used to identify diagnostic markers or novel targets to attenuate host responses to TcdA and TcdB.

6.7 Acknowledgements

This chapter was taken from D'Auria, K. M., Kolling, G. L., Donato, G. M., Warren, C. A., Gray, M. C., Hewlett, E. L. & Papin, J. A. In vivo physiological and transcriptional profiling reveals host responses to Clostridium difficile toxin A and toxin B.. *Infection and Immunity* **81,** 3814–3824 (Oct. 2013). I thank the co-primary author Glynis Kolling and all other co-authors. We thank David Bolick for his technical expertise; David Lyerly at TECHLAB, Inc., for providing purified TcdA and TcdB; and Stephen Becker and Dr. Eric Houpt for providing immortalized mouse epithelial cells.

Chapter 7

High temporal resolution of the responses of multiple cell types and the necessity of toxin glucosylation

7.1 From transcriptomics of the epithelial-layer to the roles of different cell types in the epithelial layer

Localizing toxins

The gene expression changes in vitro and in vivo showed the many changes during pathogenesis, yet it is difficult to determine if specific responses are a direct reaction to toxin or a secondary response. To help elucidate this, I aimed to characterize the location of toxin within the intestine. Presumably, toxins enter epithelial cells in order to damage the epithelial barrier. However, other cell types such as macrophages, neurons, and dendritic cells drive inflammatory responses. Unfortunately, there is no antibody for TcdB that has proven to work in immunohistochemistry. Therefore, I directly labeled TcdA and TcdB with a fluor by amine conjugation. The concentration required to detect the labeled TcdB was approximately 1µm. With this limit, much of the labeled toxins would go undetected. Therefore, I here take an indirect approach, looking at the responses of different cell types to wide ranges of toxin concentrations.

Precise quantification of toxin responses

To compare the response in a reproducible and consistent manner, I decided to track broad structural changes by measuring how electrical impedance across the surface of a cell culture as described in this chapter. From this method, the potency of toxins can be determined. The "potency" and "rapidity of onset" of the toxins are linked. In the way I use the terms here, high potency means faster acting effects in cells. Since the toxins are enzymes, they can continue their activity until all Rho proteins are glucosylated. This was indeed the case for nearly all experiments. TcdA and TcdB, at all concentrations, eventually caused the same degree of cytopathic effects. The couple of exceptions where only a proportion of cells were affected may indicate limiting concentrations of toxins in which not all cells are intoxicated. This precise quantification system had the added benefit as a quality control to compare the potency of labeled versus unlabeled toxin as well as different toxin purifications.

The glucosyltransferase, the primary pathogenic activity?

The glucosyltransferase domains of TcdA and TcdB have long been considered the primary molecular mechanisms of pathogenesis. However, recent studies have challenged this line of thought. In this chapter, I take advantage of the precise assay mentioned above and the profiling of multiple cell types to undestand the necessity of glucosyltransferase activity.

7.2 Synopsis

Clostridium difficile toxins A and B (TcdA and TcdB), homologous proteins essential for *C. difficile* infection, affect the behavior and morphology of several cell types with different potency and timing. However, precise morphological changes over various time scales, which help explain the roles of cell types, are poorly characterized. The toxins' glucosyltransferase domains are critical to their deleterious effects, and cell responses to glucosyltransferase-independent activities are incompletely understood. By tracking morphological changes of multiple cell types to *C. difficile* toxins with high temporal resolution, newly characterized cellular responses to TcdA, TcdB, and a mutant, glucosyltransferase-deficient TcdB (gdTcdB) are elucidated. Human umbilical vein endothelial cells, J774 macrophage-like cells, and four epithelial cell lines were treated with TcdA, TcdB, and

gdTcdB. Impedance changes across cell cultures were measured to track changes in cell morphology. Metrics from impedance data, developed to quantify rapid and long-lasting responses, were used to build standard curves with wide dynamic ranges that defined cell line-specific toxin sensitivities. Except for T84 epithelial cells, all cell lines were more sensitive to TcdB than TcdA. Macrophages rapidly stretched and arborized, and then increased in size in response to TcdA and TcdB but not gdTcdB. High concentrations of TcdB and gdTcdB (>10 ng/ml) resulted in loss of intact macrophages. In HCT8 epithelial cells, gdTcdB (1000 ng/ml) elicited a cytopathic effect only after several days, yet it was capable of delaying TcdA and TcdB's rapid effects. gdTcdB did not delay TcdA's stimulation of macrophages. Epithelial and endothelial cells have similar responses to toxins yet differ in timing and degree. Relative potencies of TcdA and TcdB in mouse epithelial cells in vitro do not correlate with potencies in vivo. gdTcdB is not entirely benign in HCT8 cells. TcdB requires glucosyltransferase activity to stimulate macrophages, but cell death from high TcdB concentrations is glucosyltransferase-independent. Competition experiments with gdTcdB show TcdA or TcdB round HCT8 cells through common mechanisms, yet macrophages are stimulated through potentially different pathways. This first-time, precise quantification of multiple cell lines provides a comparative framework for contextualizing previous research and delineating the roles of different cell types and toxin-host interactions.

7.3 Introduction

Clostridium difficile infections, with an annual occurrence in the US of over 300,000, cause potentially fatal diarrhea and colitis [1]. These pathologies arise from the release of two potent, homologous, protein toxins—TcdA and TcdB—into the host gut. The toxins' interactions with many cell types lead to disease, yet the relative sensitivities and roles of different cell types remain poorly understood. Both toxins disrupt the epithelial barrier by causing epithelial cells to round and detach [281]. Neutrophil infiltration and activation of other immune cells, driven by inflammatory signals, are also key to toxin-induced enteritis [181]. Though several molecular mediators of disease have been identified, little is understood about the host cell dynamics and the role of each cell type involved [153, 282]. To explore the toxins' effects on different cells, facets of the host response have been studied using cell lines treated with TcdA and/or TcdB (e.g., release of cytokines [153, 257, 283], changes in cell morphology [284, 285], gene expression [230, 273], and cell death [200, 286]). Most of these assays used in previous studies are limited to few time points, and since both toxins affect cells rapidly (in less than one hour), it is unknown if either toxin has additional effects on finer time scales and if any of these effects are consistent across cell lines at comparable concentrations.

We and others have tracked temporal changes in cell morphology and attachment in response to TcdA or TcdB by continuously measuring electrical impedance across the surface of a cell culture [270, 280, 287]. When cells grow or increase their footprint or adherence, impedance rises. In contrast, cell rounding, shrinking, and/or death correspond to decreased impedance. This assay has primarily been used as a sensitive diagnostic—as a more quantitative replacement of assays that are dependent on visualization of cell rounding. In this study, we recognize that this impedance data, in addition to indirectly detecting the amount of toxin in samples, can further be analyzed to reveal previously unrecognized, dynamic responses of host cells. Our analyses and associated metrics also allow precise comparisons between the effects of TcdA and TcdB and between different cell types. Using epithelial and endothelial cells, these analyses identify characteristics such as the minimal effective toxin concentrations and the shortest time to measurable toxin effects; standard curves with wide dynamic ranges can also be derived. Impedance changes of other cells, such as macrophages, are not as easily linked to known cell functions, but the data reveal toxin effects that would not otherwise be observed at lower temporal resolution. This knowledge contextualizes the potential roles and relative abilities of different cell types to respond directly to toxin during an infection.

Impedance curves that profile cell responses also provide insight into the toxins' molecular functions. TcdA and TcdB have glucosyltransferase domains that inactivate small GTPases (see 4.1.2 for a discussion of other domains and molecular activities). With the use of engineered mutant toxins, glucosyltransferase activity has been found necessary for cell rounding [288]. However, evidence that some glucosyltransferase-deficient mutants of TcdB (gdTcdB) are cytotoxic has raised questions about whether there are other, previously unknown toxin activities [289]. The mutant in particular has two amino acids in the "DxD" motif that is important for the toxins binding to their UDP-glucose substrate [288]. Teichert et al. showed that the gluocysltransferase activity of the DxD motif in a solution with all necessary substrates was reduced 6,900-fold. In cells, no cytopathic effects could be detected [288]. In order to identify changes dependent and independent of glucosyltransferase activity, we use gdTcdB to evaluate the dynamics of the response of macrophage and epithelial cell lines to gdTcdB, elucidating changes dependent and independent of glucosyltransferase activity. We also leverage the unique response profiles to TcdA, TcdB, and gdTcdB in order to investigate synergy or antagonism between toxins.

The cell response profiles define the dynamics of basic changes in cell physiology (e.g., cell rounding) across multiple cell types in response to TcdA, TcdB, and gdTcdB. This understanding identifies those times most representative of the entire cell response, delineates the contribution of glucosyltransferase activity to overall toxin effects, and suggests the relative roles of various cell during toxin-mediated disease.

7.4 Methods

7.4.1 Cell Culture

HCT-8 cells were cultured in RPMI-1640 supplemented with 10% heat-inactivated fetal bovine serum (HI-FBS) and 1 mM sodium pyruvate. J774A.1 cells were cultured in DMEM high glucose media supplemented with 10% HI-FBS, 1 mM, and MEM nonessential amino acids (Gibco 11140). HUVEC cells (passage 3) were cultured in endothelial growth medium (EGM-Bullet Kit CC-3124, Lonza group). T84 cells were grown in an equal mixture of Ham's F12 and Dulbecco's modified Eagle's media supplemented with 2.5 mM L-glutamine and 5% HI-FBS. All cells were incubated at 37°C/5% CO_2. In our analyses, we include our previous data from immortalized, mouse, cecal epithelial cells (hereon referred to as IMCE cells) which were derived by Becker et al. and incubated at 33°C as described by Becker et al. [260, 280]. TcdA and TcdB, isolated and purified from strain VPI-10643, were a generous gift from David Lyerly (TECHLAB Inc., Blacksburg, VA). Recombinant gdTcdB and TcdB were a generous gift from the laboratory of Aimee Shen.

7.4.2 Electrical impedance assay

Impedance was measured using the xCELLigence RTCA system (ACEA Biosciences), which consists of an RTCA DP Analyzer and 16-well E-plates. PBS was added around all wells to prevent evaporation. In each well, 100 µL media was incubated at room temperature for 30 minutes, and one baseline reading was taken. Cells in 100 µL media were then added and allowed to settle at room temperature for 30 minutes. Plates were then moved inside the RTCA DP Analyzer inside a CO_2 incubator at 37°C. Subsequent readings were taken at frequencies ranging between every 4 seconds to every 10 minutes, with higher frequency measurements reserved for times directly before toxin addition to at least 6 hours after addition (complete protocols and data files available in the Supplemental Material).

Since the impedance measurements are sensitive to slight movements or vibrations, the method by which toxin was added to cells was an important consideration. In our initial experiments, mechanical agitation and replacement of media sometimes caused small, sharp spikes in electrical impedance. To minimize disturbances, plates were not removed from the RTCA Analyzer once seated. Toxins prepared in media (10x) were gently pipetted using only one to two depressions. Media was not replaced after the addition of toxin.

7.4.3 Analyses

The protocols, data, computer code, and instructions for running the code that reproduce all results and figures are provided in Appendix B.

7.5 Results

7.5.1 Quantification of the cytopathic effects elicited by TcdA and TcdB

In order to assess the cytopathic effects of TcdA and TcdB, we measured changes in impedance across the surface of electrode-embedded wells (Methods). Impedance is dependent upon cell number, adherence, and morphology. It increases as cells proliferate or spread and decreases when toxin is added and cells round up (Figure 7.1). The rate at which impedance decreases is dependent on the toxin, toxin concentration, and cell type (Figure 7.2A and Figure 7.2B). To summarize the data-rich "impedance curves", we calculated simple metrics: the area between the curves of control and toxin-treated cells (ABC, gray area in inset of Figure 7.1), the maximum slope of a curve (MaxS), and time for a curve to decrease by 50% (TD_{50}, Figure 7.1). A negative ABC indicates that the impedance curves of toxin-treated cells are below the curves of untreated cells. Blue, dashed lines in Figure 2C show the variability of the ABC of control cells from their average impedance curve. Standard curves relating TD_{50} to toxin concentration have been generated before [290], and we found that our metrics, ABC and MaxS, also produce log-linear calibration curves (Figure 7.2C). Among replicates, differences in timing translated to differences in TD_{50}, as expected, whereas MaxS values were more similar. In simpler terms, for replicates within and between experiments, the time required to observe a change in impedance was more variable than the rate of the change. For this reason, we found that MaxS, instead of TD_{50}, better quantified rapidity of the cell response to high toxin concentrations. The other metric, ABC, captures long-term effects by integrating readings over several hours. The minimal concentration to induce a change in impedance from control is denoted as the minimal cytopathic concentration (MCC; Figure 7.2C). When ABC and MaxS are considered together, toxin concentration can be determined with a dynamic range spanning six orders of magnitude or more (depending on toxin and cell type). Together, these metrics allow for millions of data points and hundreds of wells to be simultaneously visualized and summarized to dozens of numbers or fewer that can be easily interpreted (e.g., Figure 7.2D and Appendix B).

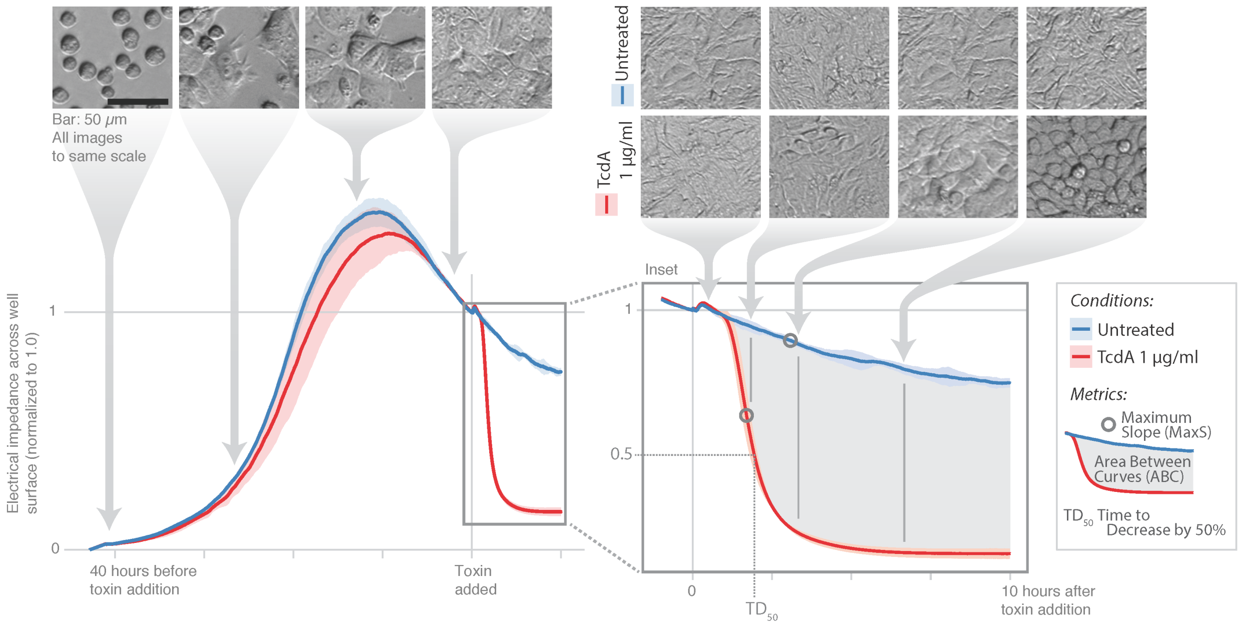

Figure 7.1: Measurement of toxins' cytopathic effects by tracking electrical impedance across the surface of a cell culture. All impedance readings were normalized to the impedance at the time toxin was added. Shaded regions above and below lines represent the standard deviation of technical replicates (n=2). Readings were taken as quickly as every four seconds (Methods). The brightness of each photograph was adjusted digitally (uniformly across an entire photograph) to make the overall brightness across all photographs similar.

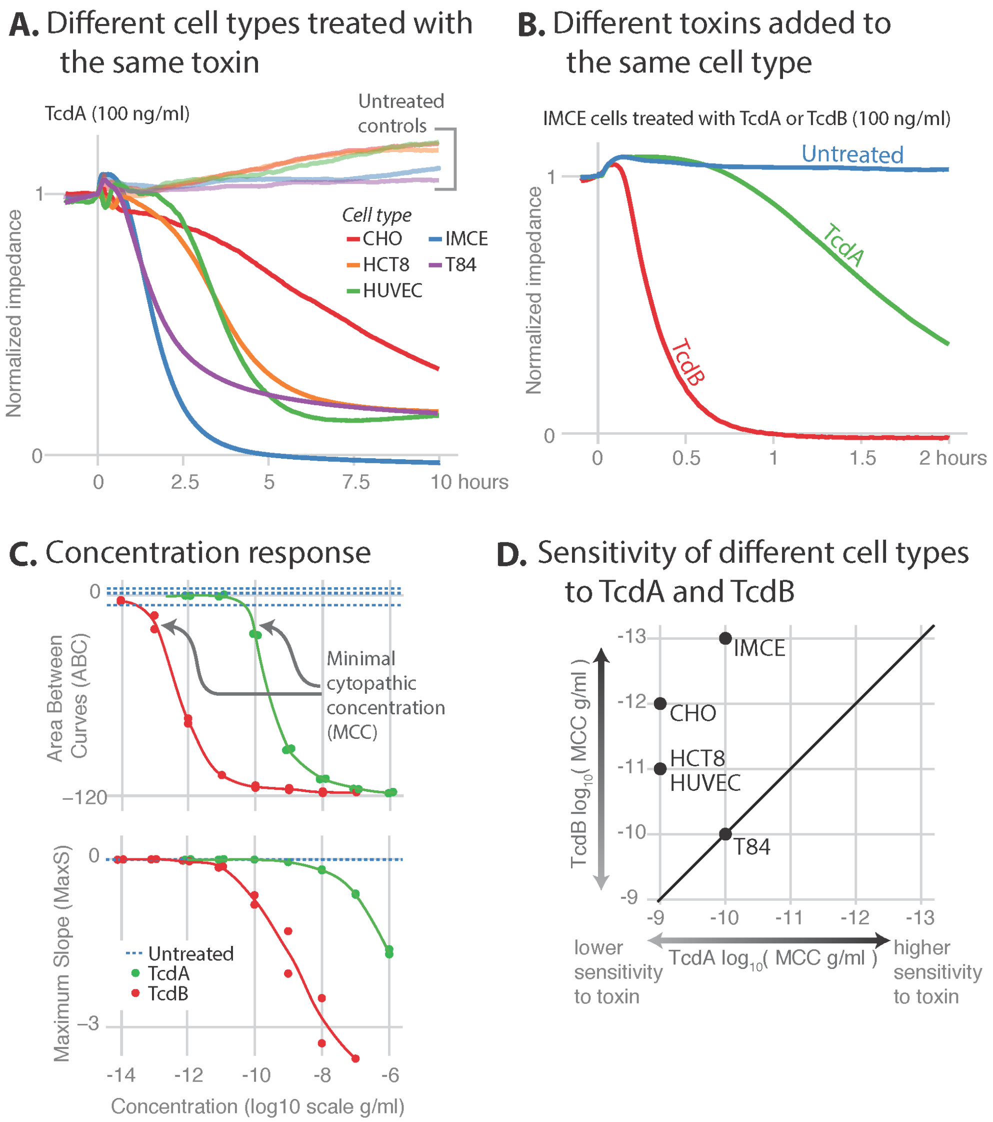

Figure 7.2: Quantification of cytopathic effects. (A and B) The cytopathic effects between cell types and toxins can easily be distinguished. **(C)** The impedance curves can be analyzed to produce two metrics, ABC and MaxS, which can then be used to define the minimal cytopathic concentration (MCC). **(D)** The MCC of TcdA and TcdB for five cell lines define cell line specific sensitivities.

7.5.2 Epithelial and endothelial cells: similar characteristic responses but different sensitivities to TcdA and TcdB

In the first set of comparisons, we chose four well-characterized cell types or cell lines—one endothelial (HUVECs) and three epithelial (CHO, HCT8, and T84)—and one immortalized, cecal, mouse epithelial cell line (IMCE, see Methods). For these five cell lines, the MCC for TcdA and TcdB varied over ranges of 0.1-1 ng/ml and 0.1-100 pg/ml, respectively (Figure 7.2D). We did not find a maximal effective concentration of either toxin (1 g/ml was the highest concentration tested). TcdB was consistently 100-1000 times more potent than TcdA, except in T84 cells, which were equally sensitive to TcdA and TcdB (as measured by MCC). The curves were largely similar in that they all consisted of a short delay followed by a sharp decrease that then leveled off (Figure 7.2A); differences were primarily in scale. Determining the time to the onset of the first toxin effects was complicated slightly by the physical process of adding toxins to wells—a process which caused disturbances that temporarily affected impedance (note the early “bump” in Figure 7.2A). Nevertheless, differences between control and toxin-treated cells can be distinguished. Across all cell types, the time required for an impedance curve to diverge from control was more than ten minutes. Nothing clearly suggested an immediate response to toxin binding. Morphological changes might not occur until after toxins enter cells and glucosylate Rho proteins. We next examined early effects of toxins on macrophages and investigated the contribution of glucosyltransferase activity to the dynamics of cell responses.

7.5.3 Macrophages: rapid, sensitive, complex concentration-dependent responses to TcdA and TcdB

J774 mouse macrophages were as sensitive and responsive to TcdA and TcdB as epithelial cells. The impedance of macrophages treated with TcdA (300 ng/ml) and TcdB (10 ng/ml) diverged from controls in 10 and 20 minutes, respectively (Appendix B). In contrast to epithelial cells, however, the impedance of macrophages increased after toxin addition (Figure 7.3), and the responses of J774 cells to TcdA and TcdB differed in shape and scale. TcdA caused a rise in impedance at 0.1 ng/ml, and the magnitude and speed of this rise increased until TcdA concentration reached 100 ng/ml (Figure 7.3A). At higher concentrations (300 and 1000 ng/ml), the slope of the rise continued to increase, yet the rise was inhibited, as if stopped prematurely before reaching its peak, and then impedance dropped below that of control cells (Figure Figure 7.3A and Appendix B). Considering now TcdB, 0.1, 1, and 10 ng/ml caused impedance to rise and stabilize at approximately double the initial value; only the slope of the rise (not the final height) was affected by toxin concentration (Figure 3A and Appendix B). These curves allowed us to resolve time points that would be of most interest for cell imaging. Increases in impedance, for TcdA and TcdB, correlated with rapid stretching and arborization of cells (appearance of many filopodia in Figure 7.3B) that suggest macrophage activation. Over the next 48 hours, cells increased in size and became more circular (Figure 7.3B). Subsequently for TcdA, decreased impedance correlated with a decrease in intact cells (Figure 7.3B). These results support complex dynamic responses of J774 cells to different toxin concentrations or a response driven by two or more cellular functions (e.g. activation and apoptosis are known to occur in monocytes and macrophages in response to TcdA and TcdB [286, 291–293].

At 100, 300, and 1000 ng/ml of TcdB, the impedance curves were entirely different than lower concentrations. Instead of rising, impedance fell (see loss of intact cells in bottom row of images of Figure 7.3B). Hence, at a concentration between 10 and 100 ng/ml, the response of macrophages to TcdB switches from cell stretching to a degradation of normal cell structure. We hypothesized that the glucosyltransferase activity of TcdB, when at or above 100 ng/ml, is not necessary to induce the loss of intact cells. To investigate this, we used gdTcdB. First, to better understand the effects of gdTcdB, we examined its ability to induce the well-known cytopathic effects of TcdA and TcdB in epithelial cells.

7.5.4 Glucosyltransferase-deficient TcdB alters the effects of TcdA and TcdB on macrophages and epithelial cells

Since the cytopathic effects of TcdA and TcdB have been attributed to their glucosyltransferase activities, we expected that gdTcdB would not cause cell rounding. Indeed, the impedances of HCT8 cells treated with gdTCB (100 and 1000 ng/ml) and untreated cells were indiscernible in the first ten hours after toxin addition (Figure 7.4A). However, gdTcdB caused an unexpected slow rise in impedance above that of control cells (Figure 7.4A). During this rise, imaging revealed continued growth, elongation, and close apposition of untreated cells, while cells treated with 100 or 1000 ng/ml of gdTcdB rounded slightly but remained attached (Figure 7.4A). The increased impedance elicited by gdTcdB was followed by a slow decrease towards that of TcdB-treated cells. This decrease, which took more than six days, was due to detachment of cells and disruption of cell morphology (Figure 7.4A). Hence, though gdTcdB does not round cells quickly as with TcdB, it still has unexplained, slow effects that alter the morphology of HCT8 epithelial cells.

To investigate if TcdA and TcdB have overlapping activity, we performed experiments with gdTcdB plus TcdA or TcdB. We anticipated that gdTcdB would attenuate or delay the effects of TcdB and perhaps TcdA. Indeed, a tenfold excess gdTcdB delayed the onset of the effects of TcdA

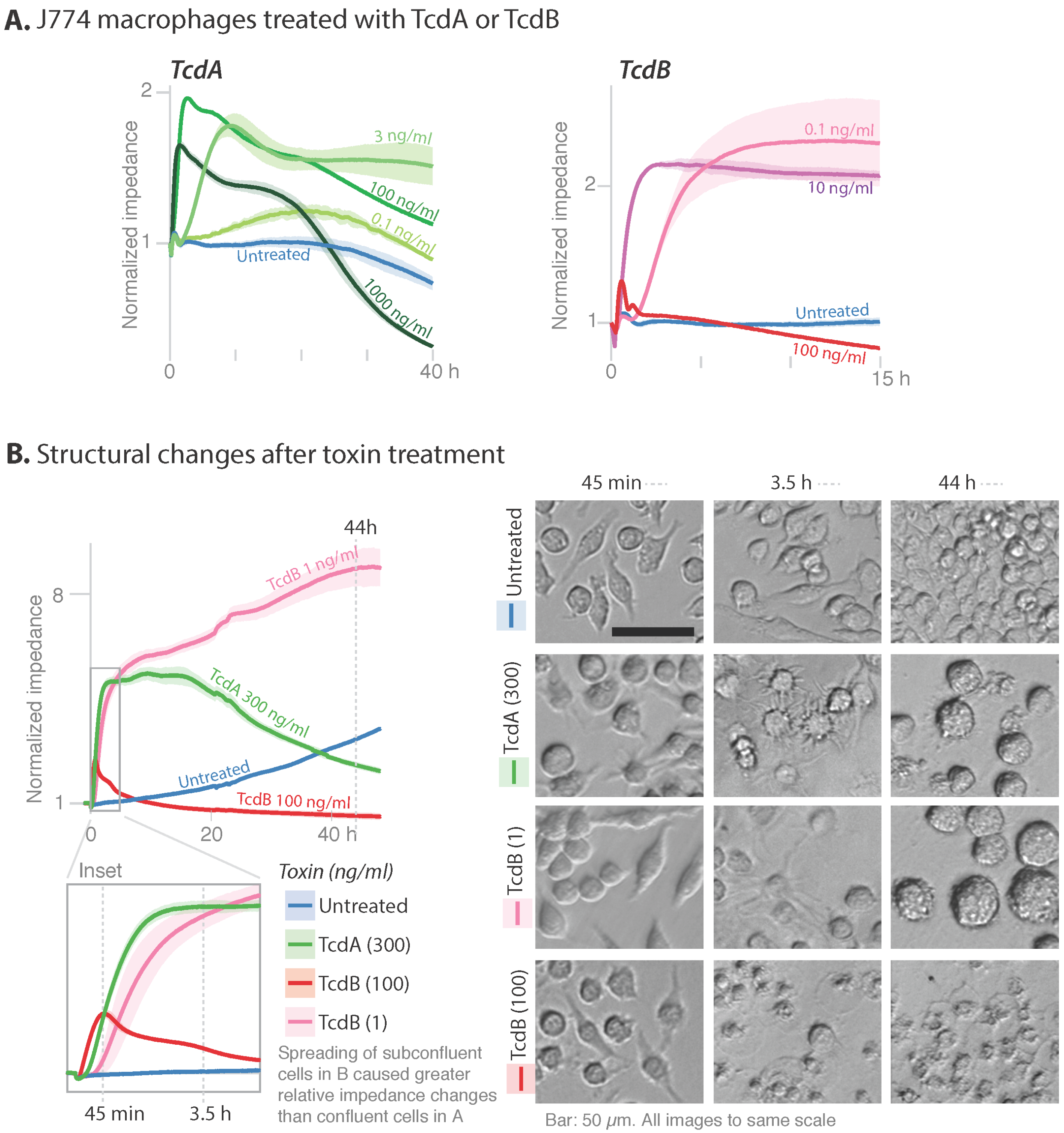

A. J774 macrophages treated with TcdA or TcdB

B. Structural changes after toxin treatment

Figure 7.3: Macrophage responses to TcdA and TcdB (A) Impedance curves from a selection of toxin concentrations for TcdA and TcdB. Both graphs represents one multi-well experiment where confluent cells were treated with toxin. **(B)** Pairing of impedance data with photographs to show the morphological changes represented in the impedance data. Since wells with electrodes are opaque, technical replicates in transparent wells were used for microscopy. Sub-confluent cultures were used so that structural changes in individual cells could more easily be observed.

and TcdB in HCT8 cells (Figure 7.4B and Figure 7.4C). Competition for shared substrates (Rho family proteins) of gdTcdB with TcdA and TcdB likely account for the delay, although other factors

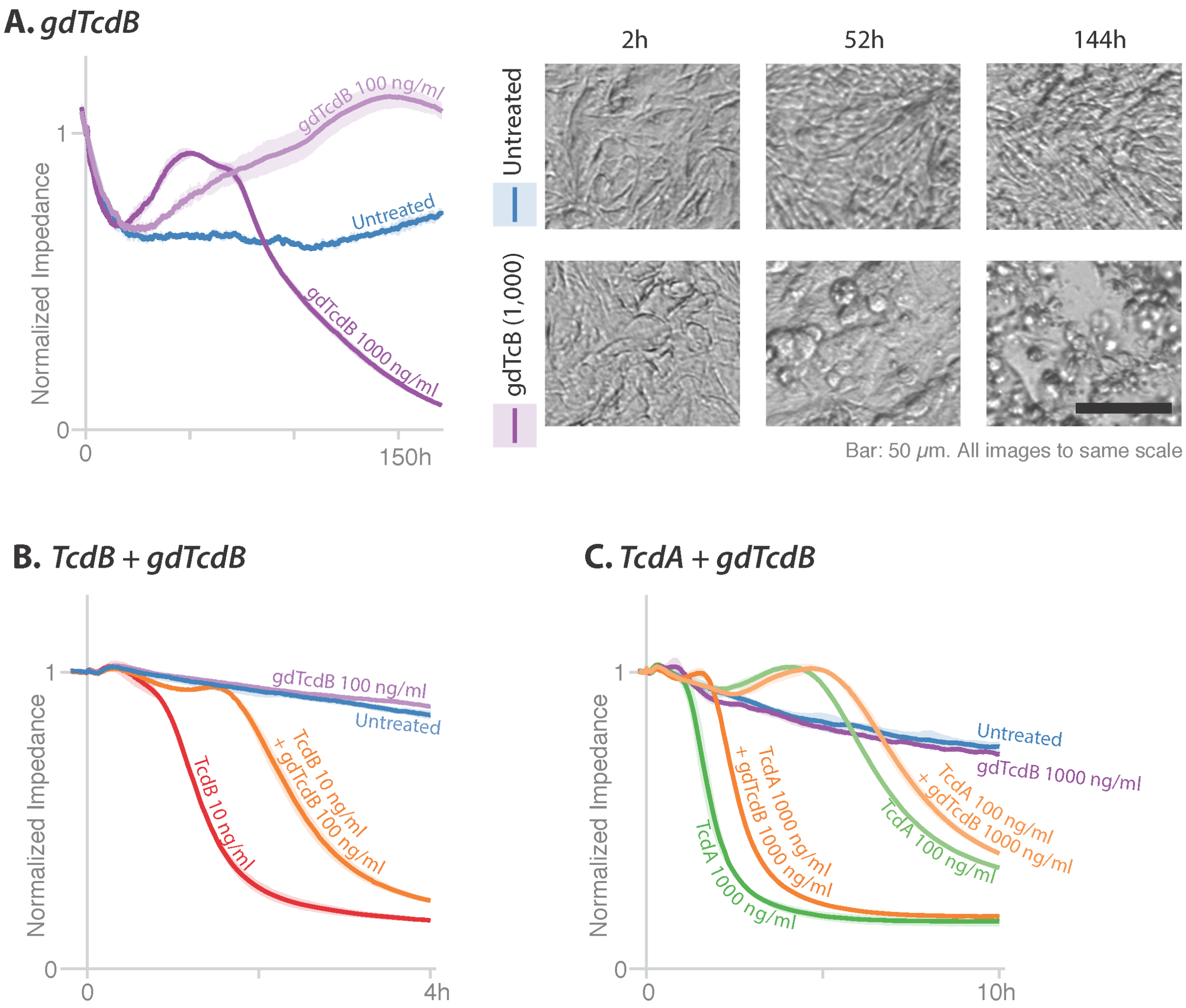

Figure 7.4: Response of HCT8 epithelial cells to gdTcdB, TcdA+gdTcdB, and TcdB+gdTcdB. **(A)** Impedance curves of HCT8 cells treated with gdTcdB and corresponding photographs. **(B)** HCT8 cells treated with TcdB or gdTcdB and TcdB in combination. **(C)** HCT8 cells treated with TcdA or gdTcdB and TcdA in combination. The three graphs are from the same multi-well experiment but are representative of three independent experiments.

such as shared receptors may be responsible.

We next determined glucosyltransferase-dependent toxin effects on J774 macrophages. Low gdTcdB concentrations did not cause macrophages change their morphology as did TcdB (Figure 7.5A). However, gdTcdB at 100 and 1000 ng/ml resulted in a loss of intact macrophages, similar to TcdB at 100 ng/ml (Figure 7.5A). Hence, glucosyltransferase activity is required for macrophage stretching and arborization but not required for the loss of intact cells for concentrations of TcdB at or above 100 ng/ml.

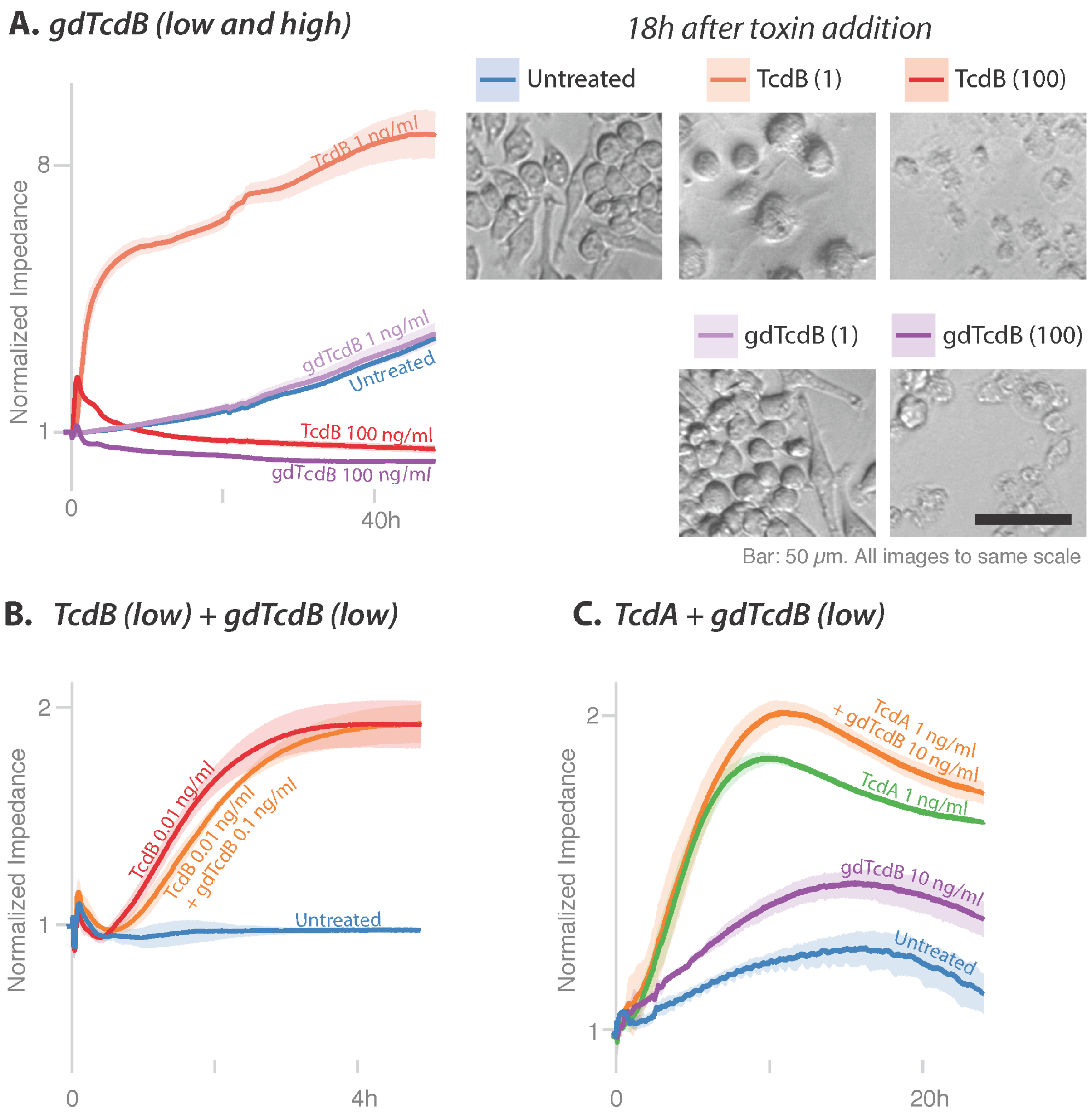

Figure 7.5: Response of J774 macrophages to gdTcdB, TcdA+gdTcdB, and TcdB+gdTcdB. **(A)** Impedance curves of J774 cells treated with gdTcdB and corresponding photographs. Concentrations at or below 10 ng/ml are denoted as "low", and other concentrations are denoted as "high". This data is derived from the same experiment shown in Figure 3B. **(B and C)** J774 cells treated with TcdB; gdTcdB and TcdB in combination; or gdTcdB and TcdA in combination. The data in the three graphs are derived from three independent experiments.

Since TcdA and TcdB caused different effects at and above 100 ng/ml, we hypothesized that TcdA and TcdB have one or more distinct activities in macrophages. As expected, gdTcdB delayed the effects of TcdB on J774 cells (Figure 7.5B). However, gdTcdB did not clearly attenuate or delay the response of J774 cells to TcdA, suggesting that the prominent responses to TcdA and TcdB in these cells are due to distinct toxin activities or substrates (Figure 7.5C).

7.6 Discussion

In this study we systematically profiled the dynamic responses of epithelial, endothelial, and macrophage cell lines to TcdA and TcdB, revealing relative sensitivities and complex concentration-dependent cell responses. While comparing results from different experimental systems is difficult, our data have allowed quantitative comparisons between cell types and between toxins under similar conditions, distinguishing which cell types may respond most quickly or most intensely when exposed directly to toxins. The impedance "response profiles" provide continuous readouts representing external changes in morphology and adherence that occur from several possible functions within the cell. We began to explore the mechanisms of these changes by using glucosyltransferase deficient TcdB (gdTcdB), revealing which molecular functions of the toxin contribute to different aspects of response profiles. The response profiles also raise many questions about the mechanisms for the novel differences we observed. Although addressing each of these in detail is beyond the scope of this study, we highlight, in the following text, the findings that bring about these questions, discuss their relevance to previous studies, and so explain how they improve our current understanding of host cell responses to TcdA and TcdB.

The cytopathic effects of TcdA and TcdB that led to their discovery are still used as the gold standard diagnostic for infection [294, 295]. Since most cytotoxicity assays are endpoint assays, the kinetics of these effects that are key to scientific research and clinical practice have not been characterized. With a continuous assay, we were better able to observe immediate effects of toxin. Although toxins may interact immediately with the toxin surface, the morphological differences (represented by impedance) occurred after a delay of ten minutes or more. Since TcdA (2.65 µg/ml) has been found to enter HT29 cells in 5-10 minutes, the delay we observed is likely because toxins must enter HCT8 cells to alter their morphology [296].

Epithelial and endothelial cell lines had the same characteristic changes in morphology, yet the rapidity of the changes distinguished different cell types, toxin concentrations, and TcdA versus TcdB. These differences could be summarized by condensing the data into metrics that represented the greatest rate of the change (MaxS) and the cumulative amount of change over several hours (ABC). When these metrics are considered together, standard curves over many orders of magnitude can be used to measure toxin concentration and determine the minimal amount of toxin necessary to induce an effect (MCC, Figure 2D). The CHO cell line was second-most sensitive to TcdB, making CHO cells a good choice for toxin detection. Indeed, a modified CHO cell line was used in the development of an ultrasensitive assay of toxin activity [270]. T84 cells, the least sensitive to TcdB, were similarly sensitive to TcdA and TcdB, as has been found previously [206]. For TcdB, the two rodent cell lines (CHO and IMCE) were more sensitive than the three human cell lines (HCT8, HUVEC, and T84), although more cell lines would be needed to confirm any species-specific sensitivity. For TcdA, cell line sensitivities were less variable than for TcdB, indicating that factors that make cells vulnerable to TcdA may be more consistent between cell lines.

Comparisons between TcdA and TcdB have often been a prominent research focus. TcdB is more cytotoxic in cell culture; TcdA is more enterotoxic in animal intoxication models [242, 280]; and there are varying results about which toxin is essential for *C. difficile* infection [223, 224]. Identifying which toxin contributes most to disease helps prioritize therapeutics. Comparisons between toxins are also valuable scientific tools. Differences in the toxins' effects provide clues about their molecular activities. Also, by correlating differences in host cell responses to differences in disease severity, particular cell types or toxin activities can be prioritized. For instance, TcdA is more enterotoxic than TcdB in mice and hamster ceca, damaging the epithelial barrier [237, 280]. This agrees with findings that TcdB binds weakly in the hamster intestine, and TcdA binds epithelial cells [244, 297]. One might then expect that cecal epithelial cells from mice of the same genetic background as those used in the aforementioned in vivo studies (IMCE cells) would be more sensitive to TcdA than TcdB. Instead, IMCE cells were over 100 times more sensitive to TcdB than TcdA, suggesting that factors in addition to the cytopathic effects on epithelial cells are important in explaining the pathologies of toxins in vivo. The extracellular environment or other cell types may be the key mediators determining disease severity.

Macrophages are likely exposed to toxin after epithelial damage and play an important part in disease, changing morphology and releasing molecules that exacerbate inflammation [292, 298]. Previous studies have quantified the viability either TcdA- or TcdB-treated macrophages at one or two time points [291, 293, 299]. We characterized the effects of both toxins on macrophages, and the other cell types already presented, over many more concentrations and time points. J774 macrophages, HUVECs, and epithelial cells had similar sensitivity to toxins, indicating that all may be affected directly by toxins during disease. TcdA or TcdB rapidly stretched and arborized macrophages, which was reflected in increased macrophage impedance. However, the timing and concentration-dependent effects of TcdA and TcdB were different, as discussed below.

TcdA increased macrophage impedance, and a subsequent decrease from the peak of the increase towards the impedance of control cells correlated with a loss of intact cells. This agrees in part with Melo Filo et al. who reported that TcdA and TcdB killed 30% and 60%, respectively, of primary mouse macrophages (1 µg/ml at 24h) [293]. The balance of activation and death may therefore account for the rise and fall of impedance of TcdA-treated macrophages. At 100 ng/ml (the concentration at which the rise in impedance was greatest), two effects appear to be balanced. At higher concentrations, the stimulatory effect that raised the impedance occurred more rapidly but did not reach the same height, indicating that higher concentrations move the balance away from stimulation towards death and decreased adherence.

TcdB caused two distinct responses in J774 macrophages: stretching (with "low" concentrations at or below 10 ng/ml) or a loss of intact structure (with "high" concentrations at or above 100 ng/ml). Siffert et al. showed TcdB-treated, human macrophages arborize with little loss of viability (1µg/ml at 3h and 24h) [291]. This arborization corresponds with the morphological responses of J774 macrophages to low TcdB concentrations. It is possible that TcdB also causes two distinct response in human macrophages, but Siffert et al. only reported results at one concentration. Although much remains to be determined about the mechanisms of these effects, we have identified new characteristics of the dynamic responses of macrophages and these effects help to explain the role of macrophages during disease. In the intestine, macrophages likely respond to several signals begun during intoxication, and given their high sensitivity, may also respond directly to toxin in the intestine. Early stimulation of macrophages may contribute to acute inflammation, while eventual death correlates with macrophage depletion and neutrophil accumulation in *C. difficile* associated diarrhea [300].

The cell responses described above prompted questions about toxin mechanisms. For instance, microinjection of TcdB's glucosyltransferase domain is sufficient to induce cytopathic effects, yet are there changes in cell structure independent of glucosyltransferase activity [301]? We found that 100 or 1,000 ng/ml of gdTcdB raised the impedance of epithelial cells above controls two days after toxin addition, and this difference was observed by tightly packed, visibly distinct control cells versus a smoother monolayer and slightly rounded gdTcdB-treated cells. The mechanisms for these differences are unclear. It is possible another toxin activity is unmasked when the strong cytopathic activity is removed or that the mutant glucosyltransferase affects substrates differently. After several days, gdTcdB causes cytotoxic or cytopathic effects. Chumbler et al. found that glucosyltransferase mutants were cytotoxic to HeLa cells after only 2.5h [289]. The different cell types (HCT8 versus HeLa) and different glucosyltransferase mutants may account for the differences in timing. It is also possible that any residual glucosyltransferase activity of the mutant toxin is not revealed until several days after treatment. The effects of mutant toxins have never been assessed over such long time scales with such great sensitivity.

The relatively benign effects of gdTcdB in the first hours after addition to HCT8 cells allowed us to investigate the effects of gdTcdB in combination with TcdA and TcdB. Since TcdA and TcdB are homologous, one might expect that gdTcdB should interfere with TcdA. Indeed, gdTcdB delayed the cytopathic effects of TcdA and TcdB. A first interpretation of this result is that TcdA and TcdB compete for cell entry. However, two studies using truncated toxins found that (1) the C-terminal domain (which is believed to be necessary for toxin internalization) of TcdA does not inhibit the effects of TcdB and (2) the TcdB C-terminus inhibits neither TcdA or TcdB-induced cell rounding [173, 302]. Hence, at the point of cell entry, TcdA and TcdB likely do not interfere with one another. Since the glucosyltransferase domains of TcdA and TcdB have many of the same Rho-family proteins as substrates, another interpretation is that the toxins compete after internalization. In this scenario, our results would indicate that gdTcdB is processed by the host cell, and its glucosyltransferase domain is still capable of binding Rho proteins or is at least close enough to interfere with TcdA. Although gdTcdB-mediated changes have the potential to reveal interesting mechanisms independent of glucosyltransferase activity, the results overall confirm the central role of the glucosyltransferase domains in eliciting the rapid, full effects of TcdA and TcdB in epithelial cells. However, as described later, glucosyltransferase activity may not be required for all toxin effects in all cell types.

gdTcdB often delayed the onset of cytopathic effects by one hour or less. Without high temporal resolution, we would have likely missed the time window in which TcdB+gTcdB was different than

TcdB alone. This has implications in other studies that wish to identify other host factors that enhance or attenuate toxin effects. Without precisely tracking changes in cell structure, several potential inhibitors of toxin effects could be missed.

Since macrophages detect a variety of antigens, one might expect that the responses to toxin might not be entirely dependent on glucosyltransferase activity. The stretching of macrophages with low TcdB concentrations required glucosyltransferase activity. However, high TcdB concentrations destroyed intact macrophage structure by an unknown, glucosyltransferase-independent mechanism.

The high sensitivity of epithelial cells, endothelial cells, and macrophages to TcdA and TcdB suggests that all of these cells could be damaged by direct toxin interaction in the host. However, the amount and location of toxin during infection is very poorly understood. With sensitivities of cells reaching as low as 100 pg/ml, tracking toxins by immunohistochemistry is technically challenging. Antibody labeling has only detected toxin on fixed, toxin-treated tissues with concentrations greater than 1 µg/ml [297]. Assessing sensitivities in vitro provides an indirect measure of the roles of different cell types in isolation. In addition to their direct effects, TcdA and TcdB initiate a cascade of deleterious events involving multiple cells. Neuronal signals have been implicated in beginning the disease process, stimulating mast cells or macrophages that may then recruit other cells [279, 303–305]. Neutrophil infiltration is a hallmark of intoxication, yet neutrophils in vitro require much higher toxin concentrations than all other cell types to be affected or recruited (>1 g/ml) [181, 285, 306–308]. Hence, it is thought that neutrophils may be primarily recruited by signals secondary to toxin damage [153, 181, 309]. To confirm the low toxin-sensitivity of neutrophils, we did attempt to measure impedance changes of neutrophils in response to toxins, yet the variability in these primarily non-adherent cells (impedance largely measures adherence) was too high to identify differences (Appendix B). Elements of the toxin responses of other cell types (e.g., mast cells [216, 310, 311], dendritic cells [312, 313], neurons [314, 315], fibroblasts [316, 317], etc.) have been studied, yet the dynamics of their responses—and in many cases concentration-dependent effects—are unknown. In the future, precisely capturing the time and concentration-dependent responses to TcdA and TcdB will better contextualize their potential roles in the host. Our analyses of endothelial cells, epithelial cells, and macrophages in the same experimental framework set a precedent for such comparisons. Furthermore, we show how data from sensitive, continuous assays, could be used to gain insight into cell function and molecular mechanisms and generate new hypotheses. The framework and simple analyses may also be used to investigate synergy, antagonism, or interactions between bacterial toxins and other host factors that affect cells over a wide range of time scales.

7.7 Acknowledgements

This chapter is a manuscript in preparation, and I would like to thank all co-authors: Meghan Bloom, Yesenia Reyes, Mary Gray, Edward van Opstal, Jason Papin, and Erik Hewlett. We are exceedingly grateful to David Lyerly and TECHLAB Inc. for providing purified TcdA and TcdB as well as Aimee Shen for providing recombinant TcdB and gdTcdB.

Chapter 8

Software for analyzing time course data from multi-well experiments

The data in the previous chapter was generated from thousands of wells in multi-well plates. For each well, thousands of data points were recorded. To manage these data, I wrote software to organize and visualize the data. This software is written in the free, open source R programming language so that it is easily accessible and extensible. Here, I briefly describe its key features.

8.1 Concise annotation of multiple wells

The meta data for all the wells can be input as a spreadsheet or table as in Table 8.1. The format and notation was chosen to minimize the amount of effort. All blank cells use the value of the next non-blank cell above it. The well identifier also allows shorthand (e.g., A-B1-2 refers to wells A1, A2, B1, and B2). Each row of the table represents an experimental action that occurred directly after the i^{th} data point. The "ID" labels that action so that it can be referenced in future data transformations and alignments. "rmVol" and "adVol" are the volume removed, respectively, during an action. "name" and "concentration" indicate the compounds in the solution being added to each well. Comma-separated values are matched with the "wells" column. In the "type" column, "final" indicates that the indicated concentration is the concentration after the action is performed; "start" indicates the concentration referse to the solution before it is added to the well.

This file is parsed and stored in an object in R.

file	wells	ID	i	rmVol	adVol	name	concentration (ng/ml)	type	solvent
T84-TcdB.txt	A-H5-6	start	1	0	100	-	-	-	media
	A-H5-6	cellSeed	2			T84	30000	total	
	B-F6, C5, E-F5	toxinAdd	1429		22.2	TcdB	1000, 300, 100, 30, 10, 3, 1, 0.1	final	
	D5					-	-	-	
CecalCells.txt	A-H3-6	start	1		100	-	-	-	
	A-H3-6	cellSeed	2			IMCE	30000	total	
	A-B3, D-H3	toxinAdd	449		22.2	TcdA	1000, 100, 10, 1, 0.1, 0.01, 0.001	final	
	C3					-	-	-	
	A-B3, D-H3		449			TcdB	100, 10, 1, 0.1, 0.01, 0.001, 0.0001	final	

Table 8.1: Example metadata file

```
# Parse and load the data
wells = parse.RTCAanalyze(metadata = "./MasterSheet2.csv", data.dir = "./Data2")

# Show a summary of the first 8 wells
print(wells[1:8])

##       file points hours well   totals    ID.soln
## 1 CHO.txt  3,461   184  A01 CHO-9000  TcdA-1000
## 2       -      -     -  B01        -
## 3       -      -     -  C01        -   TcdA-100
## 4       -      -     -  D01        -     TcdA-1
## 5       -      -     -  E01        -   TcdA-0.1
## 6       -      -     -  F01        -  TcdA-0.01
## 7       -      -     -  G01        - TcdA-0.001
## 8       -      -     -  H01        - TcdA-1e-04

# Show a summary for the first well
print(wells[[1]])

## Well: CHO.txt, A01
## 3,461 data points over 184 hours
##
##              ID  t1  t2 rmVol notes     solution       status
## 1         start   0   1     0       100, lis.... 100, lis....
## 2      cellSeed   2   3     0       100, lis.... 100, lis....
## 3         move1 285 286     0       NA, list.... 100, lis....
## 4 mediaReplace 307 308   100       100, lis.... 100, lis....
## 5     toxinAdd 611 612     0       100, lis.... 100, lis....
```

8.2 Selecting and modifying wells

Each well contains several actions. Each action contains a `solution` object.

```
# Select wells based off metadata
subset = retrieveWells(wells, file = "IMCE.txt",
                       compounds = "TcdB", max.concentrations = 50,
                       controls = TRUE )
print(subset)

##        file points hours well     totals    ID.soln
## 1  IMCE.txt  5,376 119.9  C03 IMCE-30000
## 2         -      -     -  B04          -    TcdB-10
## 3         -      -     -  C04          -     TcdB-1
## 4         -      -     -  D04          -   TcdB-0.1
## 5         -      -     -  E04          -  TcdB-0.01
## 6         -      -     -  F04          - TcdB-0.001
## 7         -      -     -  G04          - TcdB-1e-04
## 8         -      -     -  H04          - TcdB-1e-05
## 9         -      -     -  C05          -
## 10        -      -     -  A06          -    TcdB-10
## 11        -      -     -  B06          -     TcdB-1
## 12        -      -     -  C06          -   TcdB-0.1
## 13        -      -     -  D06          -  TcdB-0.01
## 14        -      -     -  E06          - TcdB-0.001
## 15        -      -     -  F06          - TcdB-1e-04
## 16        -      -     -  G06          - TcdB-1e-05
## 17        -      -     -  H06          -

# Quick look at the actions in the first well
print(subset[[1]])

## Well: IMCE.txt, C03
## 5,376 data points over 119.9 hours
##
##         ID  t1  t2 rmVol notes     solution       status
## 1    start   0   1     0       100, lis.... 100, lis....
## 2 cellSeed   2   3     0       100, lis.... 100, lis....
## 3 toxinAdd 449 450     0       100, lis.... 100, lis....

# The solution objects for each action
solutions = subset[[1]]$timeline$solution
print(solutions)

## [[1]]
## 100 uL media
##
## [[2]]
## 100 uL
## Solvent: media
## IMCE 30000 total.
##
```

```
## [[3]]
## 22.2 uL media

# Solutions have compounds and solvents
solutions[[3]]$compounds

## [1] name conc type
## <0 rows> (or 0-length row.names)

# Adding and subtracting solutions
solutions[[2]] + solutions[[3]]

## 122.2 uL
## Solvent: media
## IMCE 30000 total.

solutions[[2]] + solutions[[3]] - solutions[[1]]

## 22.2 uL
## Solvent: media
## IMCE 30000 total.
```

8.3 Visualization

Lists of well objects can be visualized and plot features can be linked to metadata.

```
plot(subset, color = "by.concentrations", linetype = "by.compounds", replicates = FALSE)
```

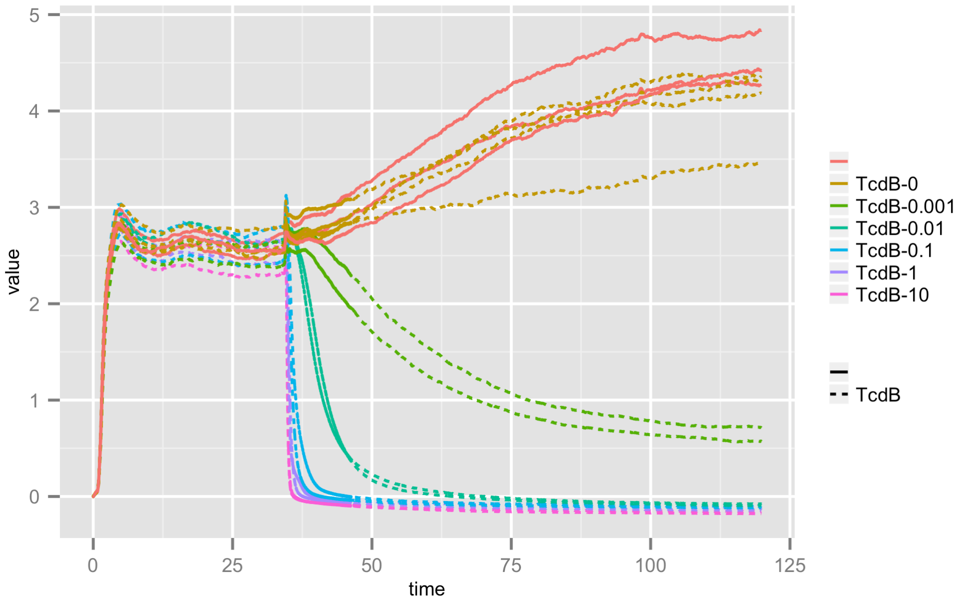

Diagnostic plots can also be made.

```
plot(subset, color = "by.concentrations", replicates = FALSE, diagnostic = 1)
```

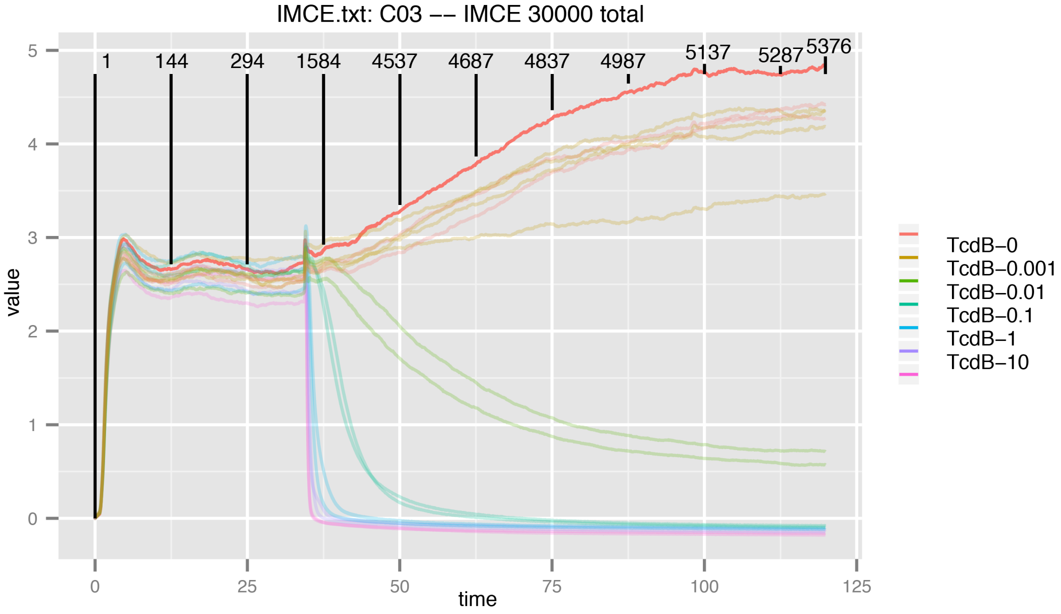

8.4 Independent wells

The software was written to be modular so that it can be easily extended. Each well is an independent object. Functions are written for well objects so they can easily be applied to a list of unrelated wells. Unless the wells in the data in a well is modified, the data is passed by reference (a copy of the data that would take more memory does *not* need to be created).

```
# Wells from any experiment can be combined. For example
well.list.1 = subset[2]
well.list.2 = subset[10:13]
new.list = c(well.list.1, well.list.2)
print(new.list)

##       file points hours well     totals   ID.soln
## 1 IMCE.txt  5,376 119.9  B04 IMCE-30000   TcdB-10
## 2        -      -     -  A06          -         -
## 3        -      -     -  B06          -    TcdB-1
## 4        -      -     -  C06          -  TcdB-0.1
## 5        -      -     -  D06          - TcdB-0.01
```

8.5 Data transformations

Replicates can be averaged, either directly or in the plot function.

```
subset.averaged = averageReplicates(subset)
print(subset.averaged)

##       file points hours        well     totals    ID.soln
## 1 IMCE.txt  5,376 119.9 C03+C05+H06 IMCE-30000
## 2        -      -     -     B04+A06          -    TcdB-10
## 3        -      -     -     C04+B06          -     TcdB-1
## 4        -      -     -     D04+C06          -   TcdB-0.1
## 5        -      -     -     E04+D06          -  TcdB-0.01
## 6        -      -     -     F04+E06          - TcdB-0.001
## 7        -      -     -     G04+F06          - TcdB-1e-04
## 8        -      -     -     H04+G06          - TcdB-1e-05

subset.transformed = transform(subset,c("tcenter","normalize"),ID="toxinAdd")
plot(subset.transformed,color="by.concentrations",xlim=c(-2,10))
```

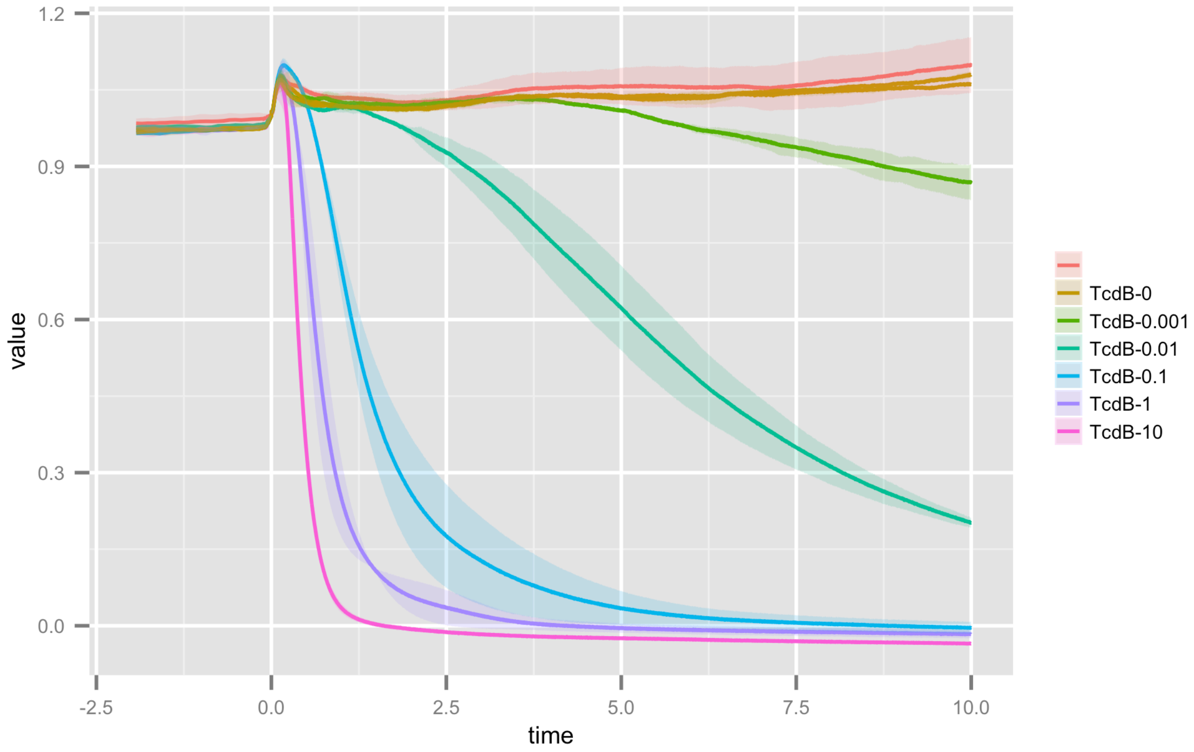

Because experimental protocols cannot be carried simultaneously on all wells, wells can be aligned according to the actions defined in the metadata. Data can then be normalized or transformed using times defined in the metadata.

```
subset2 = retrieveWells(wells,compounds="HUVEC")
new.list = c(subset[1:2],subset2[3:4])
print(new.list)

##          file points hours well     totals  ID.soln
## 1    IMCE.txt  5,376 119.9  C03 IMCE-30000
## 2           -      -     -  B04          -  TcdB-10
## 3 HUVEC-a.txt  4,979 250.5  C03 HUVEC-5000 TcdA-100
## 4           -      -     -  D03          -

# plot1 - raw data
customplot = function(...) plot(...,color="by.concentrations",
                                linetype="by.total.compounds")
plot1 = customplot(new.list)

# plot2 - aligned data
centered.wells = transform(new.list,"tcenter",ID="toxinAdd")
plot2 = customplot(centered.wells)

# plot3 - normalized data
norm.wells = transform(new.list,c("tcenter","normalize"),ID="toxinAdd")
plot3 = customplot(norm.wells)

# plot4 - take out just a slice of the time course
sliced.wells = transform(new.list,c("tcenter","normalize","slice"),
                         ID="toxinAdd",xlim=c(-1,10))
plot4 = customplot(sliced.wells)

grid.arrange(plot1,plot2,plot3,plot4,ncol=2)
```

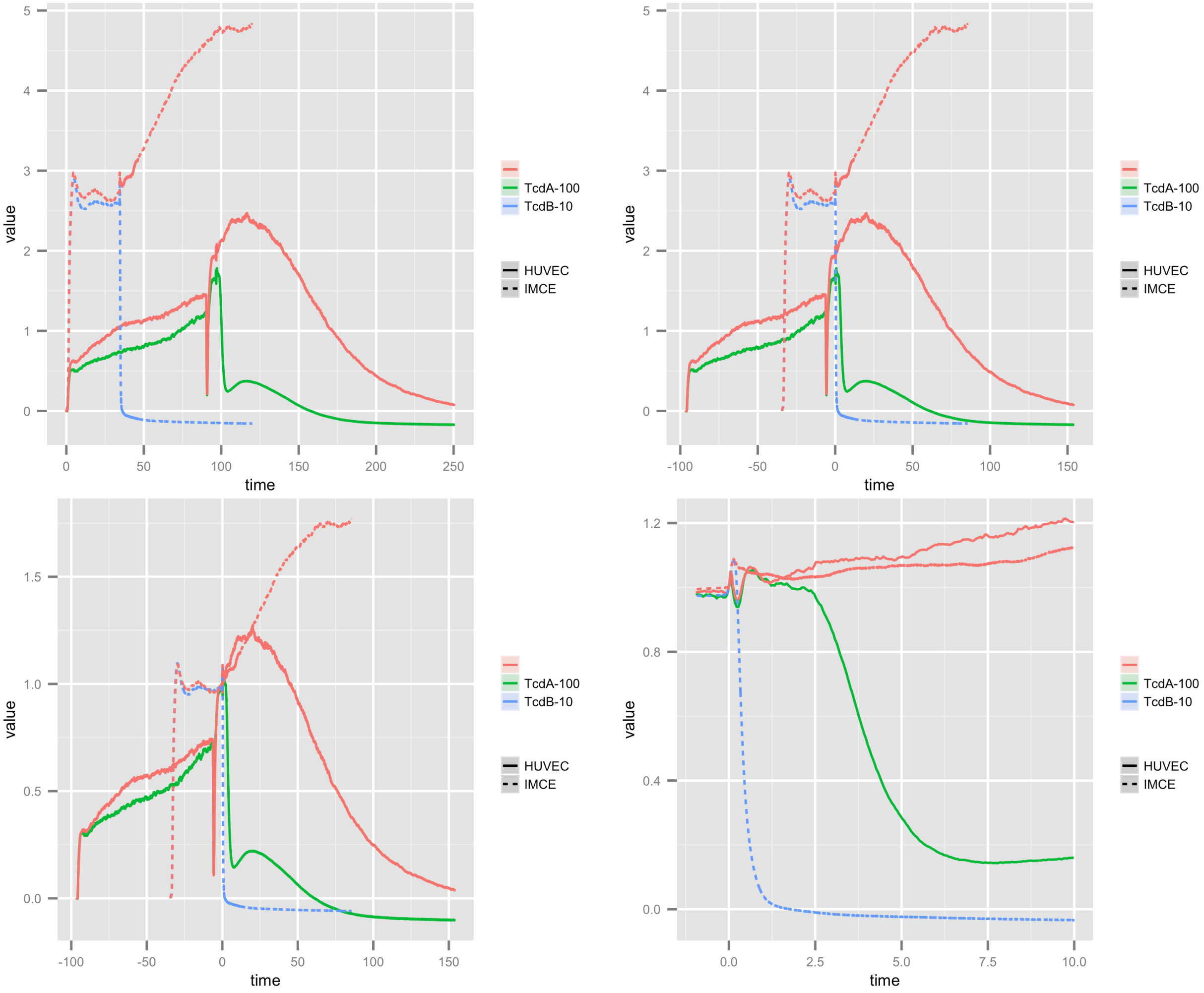

8.6 Interpolation and smoothers

Common smoothers already available in base R can be applied to multiple wells at the same time. However, because these algorithms are dependent on the number of data points and not the distance between the data points, the time courses will not be uniformly smoothed.

In many cases, different amounts of smoothing is desired at different points in a curve. For example, we do not wish to smooth the sharp drop in impedance after toxin is added. However, we do wish to smooth all other parts of the curve. In these cases, smoothing algorithms that are local (e.g., loess and kernel smoothing) may be preferred over splines that minimize the residuals along the entire curve.

In some cases, smoothing with R code took several minutes, so I wrote or attached open source C++ and Fortran functions that calculate smoothers in less than one millisecond.

- `smoother_curfit` fits a cubic spline so that the sum of the residuals matches a user-defined value (calls Fortran code from the DIERCKX package)
- `smoother_bin` bins the data and averages each bin to reduce the size of the data set
- `smoother_maverage` calculates a moving average in C++
- `smoother_smooth.spline` is the cubic smoothing spline in the R 'stats' package
- `smoother_lokern` performs "kernel regression smoothing with local plug-in bandwidth" as described by Herrman using the 'lokern' R package developed by Herrman [318].
- `interpolate_linear` performs linear interpolation
- `smooth.pchip` calculates a piecewise cubic hermitian interpolating function. This function is used when aligning two curves.
- `smoother_composite` is a multi-step smoother that I found was particularly useful for the impedance data in this chapter. First, the derivative of the curve is estimated from `smoother_bin`. `smoother_maverage` of the absolute value of the derivative is used to weight each data point so that rapidly changing parts of the curve are fit more tightly. The weights are translated to bandwidths with user-defined limits. Using these bandwidths, local polonymials are fit with `smoother_lokern` in order to estimate the residuals that are used in `smoother_curfit`. This composite smoother requires more user-defined parameters than any other, but it is very consistent between different curves and different experiments.

The polynomial smoothers can be used to calculate derivatives and integrals. Smoothers also have the added benefit of data compression, sometimes reducing 10,000+ data points to a spline with less than 20 knots.

```r
huvecs.a = retrieveWells(subset2, compounds = "TcdA")
huvecs.norm = transform(huvecs.a, c("tcenter","normalize","slice"),
                        ID="toxinAdd", xlim=c(-1,Inf))
```

```
huvecs.smth = add_smoother(huvecs.norm, method="composite", x.scale=2/3, y.scale=1,
                           noise.scale=1/60, deriv.cutoffs=c(0.05,0.25) )

plot(huvecs.smth[c(1,8,10,17)],xlim=c(-1,3),showpoints=TRUE,smoother=TRUE)
```

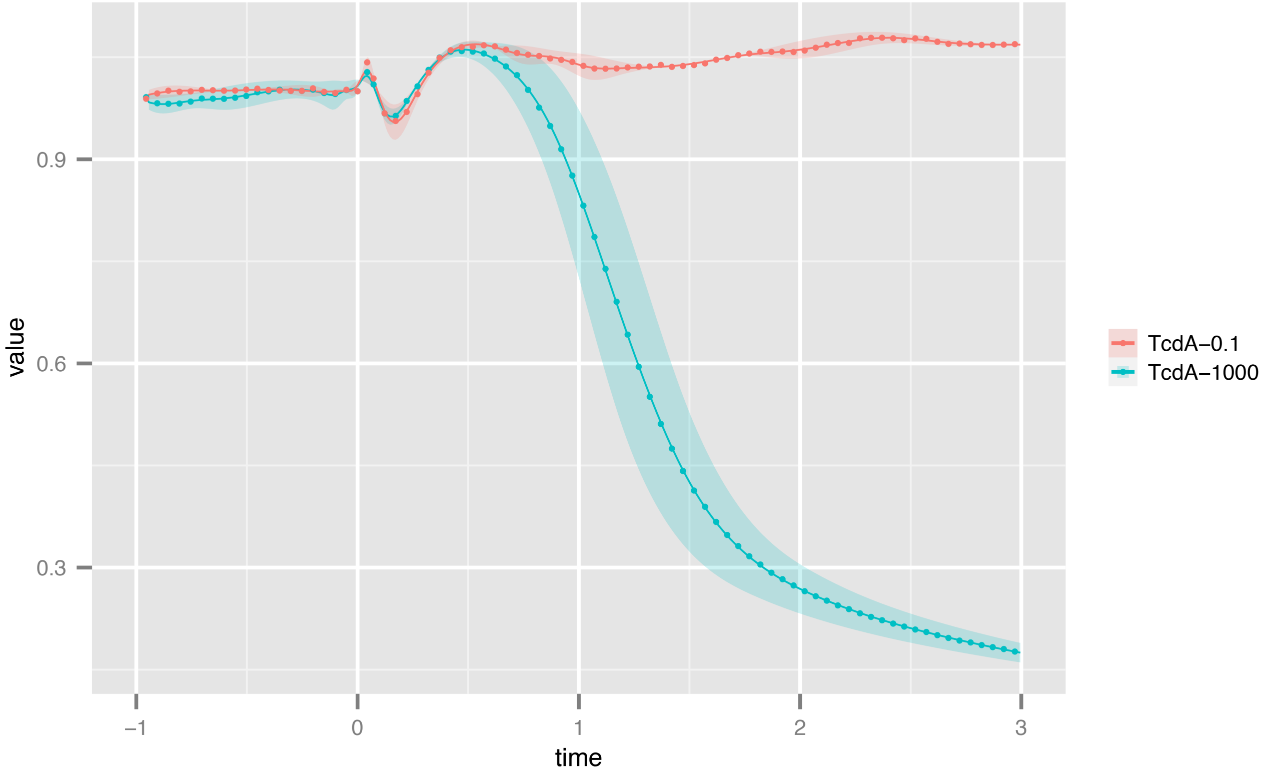

8.7 Custom metrics

With this framework, it is easy for one to define new functions that calculate metrics from the curves. Below is an example of a function (`max.rate`) that calculates the maximum slope of curves. The slopes are then plotted versus toxin concentrations.

```
subset = retrieveWells(wells, compounds="IMCE")
subset.norm = transform(subset, c("tcenter","normalize","slice"),
                        ID="toxinAdd", xlim=c(-1,Inf))
subset.smth = add_smoother(subset.norm, method="composite", x.scale=2/3, y.scale=1,
                           noise.scale=1/60, deriv.cutoffs=c(0.05,0.25) )
subset.rate = max.rate(subset.smth, ID = "toxinAdd", min.diff = 10/60/60,
                       ylim = 0.8, xlim = 2)
MaxS = groupMetric(subset.rate, ID = "toxinAdd", metric = "max.rate")
```

```
plotMetric(MaxS)
```

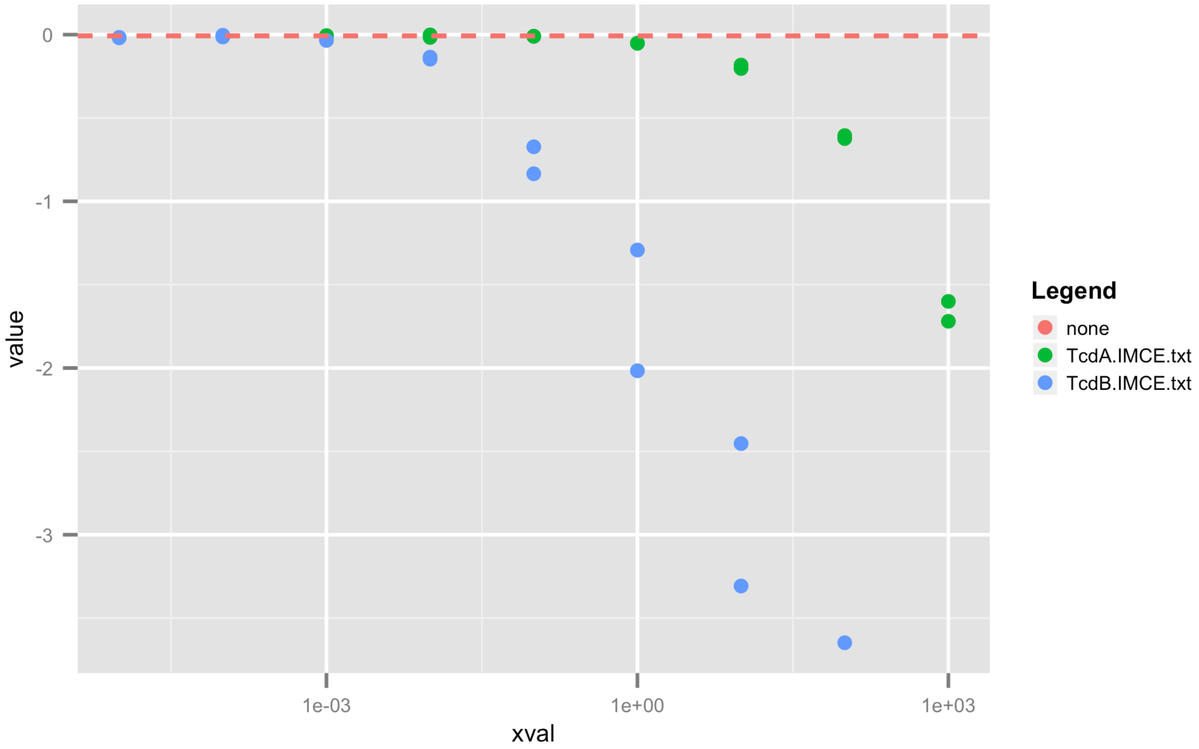

Here is the code for the function

```
print(max.rate.Well)

## function (well, ID, duration = Inf, nbw = 10, min.diff = NULL,
##     ylim = 0.75, xlim = 2, smoother = TRUE)
## {
##     dwell = spline_interpolate(well, deriv = 1, nbw = nbw, smooth = smoother,
##         min.diff = min.diff)
##     times = timesdata(dwell)
##     dm.deriv = datamat(dwell)
##     dwell = spline_interpolate(well, deriv = 0, nbw = nbw, smooth = FALSE,
##         min.diff = min.diff)
##     vals = welldata(dwell)
##     sweep = getrows.by.ID(dwell, ID)$t1
##     idx = which(sweepdata(dwell) == sweep)
##     tstart = times[idx]
##     idx.range = times > tstart & times < (tstart + duration)
##     idx.spike = times < (tstart + xlim) & vals > ylim
##     dm.deriv = dm.deriv[idx.range & !idx.spike, ]
##     id = which.min(dm.deriv$values)
##     rate = dm.deriv[id, c("time", "values")]
##     colnames(rate) = c("time", "value")
##     well$metrics$max.rate = as.data.frame(as.list(rate))
##     return(well)
## }
```

8.8 Future plans

After approval from the maintainers of R packages, this will be a standard R package accessible from the Comprehensive R Archive Network (CRAN).

Chapter 9

Future directions: toxin responses and metabolism

9.1 Toxins alter expression of many metabolic genes

As discussed in a previous chapter, many genes encoding enzymes in lipid and fatty acid pathways were differentially expressed after toxin treatment. We therefore hypothesized that metabolism of lipids and fats will alter the host responses to TcdA. To test this, we placed mice on a high fat diet and performed cecal injection experiments as described previously. When the two factors were accounted for (western diet versus regular diet and toxin-treated versus sham), there was no significant effects caused by a high fat diet 16h after toxin injection (data not shown). Nevertheless, many metabolic genes were altered. Since the greatest expression differences occurred at 16 hours, it is possible that these changes reflect upstream changes in central regulators known to control the expression of many of these genes (e.g., nuclear receptors).

9.2 Integrating and visualizing transcriptional changes within a metabolic network

Since well-curated, genome-scale networks have been constructed for human and mouse, it is possible to overlay the transcriptional data in this dissertation onto these networks to visualize modules or entire pathways that are altered. In addition, the transcription may be used to turn enzymes on or off in these models in order to determine shifts in metabolism during pathogenesis or repair from TcdA and TcdB.

Integration of transcription data with metabolic is therefore are a potential future direction that could identify novel host responses to toxin. Although this dissertation does not use metabolic models, I have had significant experience with them while working with colleagues. In this chapter, I present a review of methods for identifying drug targets from metabolic reconstructions of microbes. However, the last section is dedicated to how the host metabolism can be controlled or modified for new treatment strategies.

9.3 Synopsis

For many infectious diseases, novel treatment options are needed in order to address problems with cost, toxicity and resistance to current drugs. Systems biology tools can be used to gain valuable insight into pathogenic processes and aid in expediting drug discovery. In the past decade, constraint-based modeling of genome scale metabolic networks has become widely used. Focusing on pathogen metabolic networks, we review in silico strategies used to identify effective drug targets and highlight recent successes as well as limitations associated with such computational analyses. We further discuss how accounting for the host environment and even targeting the host may offer new therapeutic options. These systems-level approaches are beginning to provide novel avenues for drug targeting against infectious agents.

9.4 Glossary

biomass

an objective reaction consisting of important metabolites that the cell needs in order to grow (e.g. amino acids, lipids and carbohydrates). Correlated reaction sets: groups of reactions whose fluxes always change in relation to one another. 129–137, 145

exchange reaction

a reaction that transports metabolites into or out of the system. 138

flux balance analysis (FBA)

the possible combination of allowable fluxes given a defined set of constraints which bound reaction fluxes, for example reversible and irreversible reactions. 125, 126, 128–132, 134–140, 145

feasible flux space

the possible combination of allowable fluxes given a defined set of constraints which bound reaction fluxes, for example reversible and irreversible reactions. 129

flux distribution

the set of all reaction fluxes within a metabolic network. 131, 133, 134

flux variability analysis (FVA)

a linear programming-based method which determines the minimum and maximum reaction fluxes that allow for optimal or near-optimal flux through the objective reaction. 128, 137–139

gene-protein-reaction relationship (GPR)

the combination of proteins or protein components sufficient to carry out an enzymatic reaction and the combination of genes sufficient to express each of the protein components. 125, 128, 129, 134, 136

in silico

in contrast to in vivo or in vitro, the term indicates a computational process in a simulated environment. 123, 129, 135, 140

linear programming

also termed linear optimization, an area of mathematics developed for maximizing a linear combination of variables (e.g. $Av_1 + Bv_2 + Cv_3$), such that the variables are constrained by many linear equalities and inequalities (e.g. the constraint $v_1 - v_2 = 0$ implies that flux v_1 is constrained to be twice flux v_2). 124, 129, 131

mass balance

a requirement that the mass entering the system or any pathway within the system equals the mass exiting the system or pathway; a crucial characteristic of metabolic reconstructions from which functional mathematical models can be derived. 129, 134

metabolic network reconstruction

a manually-curated computational network of the metabolism of an organism with all the gene-protein-reaction relationships(GPRs) assembled from a functionally annotated genome, biochemical data, and literature, that are compiled into a stoichiometric matrix, which serves as the framework for further computational analysis. 125, 126, 128–130, 134, 136–142, 144–146

objective flux

the flux through the objective reaction. 131, 132, 137–139

objective reaction

a reaction which sets a demand for particular metabolites in the network. The typical goal in formulating this reaction is to simulate a biological objective, whether it be growth, energy, virulence, or a combination of other factors. 125, 129–131, 133, 134, 136–142

reaction flux

moles consumed in a reaction per unit time. 123–125, 129–131, 133–139, 141, 142, 144

steady state

with respect to flux, a key assumption in flux balance analysis (FBA) that the reaction fluxes within the system, and therefore the amounts of each metabolite, do not change over time, an assumption often justified by the very short time-scale of metabolic reactions compared to the time necessary for changes in cell phenotype. 130

stoichiometric matrix (S matrix)

a mathematical formalization of a metabolic reconstruction; a matrix in which each element contains the stoichiometric coefficient for a metabolite (row) participating in the corresponding reaction (column). 125, 129, 130, 140

Clicking on a glossary term within this chapter returns you to its definition in this section.

9.5 Systems biology and pathogen metabolism

Systems biology methods have been applied extensively to the study of infectious diseases across multiple scales of biological organization to generate predictions ranging from pathogen gene lethality in particular microenvironments [319, 320] to dynamics involved in the host immune response to infection [321]. Utilizing the predictive power of computational modeling and systems analysis, wideranging questions related to pathogen virulence, disease progression and host response can be explored to generate hypotheses for more thorough experimental investigation.

The increasing availability of high-quality genome-scale metabolic reconstructions [322] presents an opportunity for the rational and systematic identification of metabolic drug targets in a pathogen of interest. Built bottom-up from functional genome annotations (and a variety of other data sources) and analyzed with computational methods such as FBA, these biochemical networks can account for hundreds to thousands of metabolites participating in enzymatic reactions across a range of metabolic subsystems (e.g. carbohydrate, amino acid, lipid, nucleotide and energy metabolism) and cellular localizations (e.g. extracellular space, cytosol and compartments specific to particular organisms) (Figure 9.1A) [323]. Since the initial genome-scale reconstructions of *Escherichia coli* [324, 325] and *Haemophilus influenzae* [326, 327], the metabolic networks of over 50 organisms (bacteria, archaea and eukaryotes) have been reconstructed (reviewed in [322]). Elements of this network reconstruction process have been automated, allowing the preliminary analysis of hundreds of draft network reconstructions [328]. Among these, metabolic networks have been reconstructed for several pathogenic organisms (Table 9.1). Indeed, the study of pathogen metabolism-for the elucidation of highpriority drug targets and metabolic factors contributing to pathogenicity—is an exciting application for metabolic network modeling and systems biology.

In this review, we explore several techniques and approaches used to predict antimicrobial drug targets from metabolic network modeling using FBA. Where possible we present examples that have led to novel data, drug targets, or drugs. Metabolic network modeling is still in its infancy, but has allowed for predictions that align with previous data and has provided many hypotheses that

	Drug target-related analysis								Valid-ation				
Pathogen	Gene/reaction essentiality	Minimal media prediction	Conditional essentiality	Synthetic lethality	Flux variability analysis	Enzyme robustness	Metabolite essentiality	Correlated reaction sets	Literature derived	Novel experimental validation	Novel compounds identified	**Disease**	**Refs**
Acinetobacter baumannii	■						■		■			Opportunistic; cepacia syndrome	[329]
Burkholderia cenocepacia	■		■						■			Opportunistic; nosocomial infection	[330]
Francisella tularensis	■		■		■	■			■	■		Tularemia	[331]
Haemophilus influenzae	■	■		■					■			Otitis media and respiratory infections	[326, 327]
Helicobacter pylori	■	■	■	■					■			Gastritis; peptic ulceration; gastric cancer	[332, 333]
Klebsiella pneumoniae										■		Klebsiella pneumonia; urinary tract infection	[334]
Mycobacterium tuberculosis	■		■	■	■	■		■	■	■		Meningitis; meningococcal septicemia	[319, 320, 335]
Neisseria meningitidis		■								■		Opportunistic; cepacia syndrome	[336]
Porphyromonas gingivalis	■	■							■			Periodontal disease	[337]
Pseudomonas aeruginosa	■								■			Opportunistic; nosocomial infection	[338]
Salmonella Typhimurium	■			■	■				■	■		Gastroenteritis; diarrhea	[339–341]
Staphylococcus aureus	■	■		■					■	■		Opportunistic; nosocomial infection	[342–344]
Vibrio vulnificus							■		■	■	■	Bubonic, pneumonic, and septicemic plague	[345]
Yersinia pestis	■	■		■					■			Opportunistic; nosocomial infection	[346]
Cryptosporidium hominis	■								■			Cryptosporidiosis	[347]
Leishmania major	■	■		■		■			■			Leishmaniasis	[348]
Plasmodium falciparum	■			■					■	■	■	Malaria	[349, 350]
Trypanosoma cruzi	■				■				■			Chagas disease	[351]

Table 9.1: Drug targeting-related analysis of pathogen metabolic networks

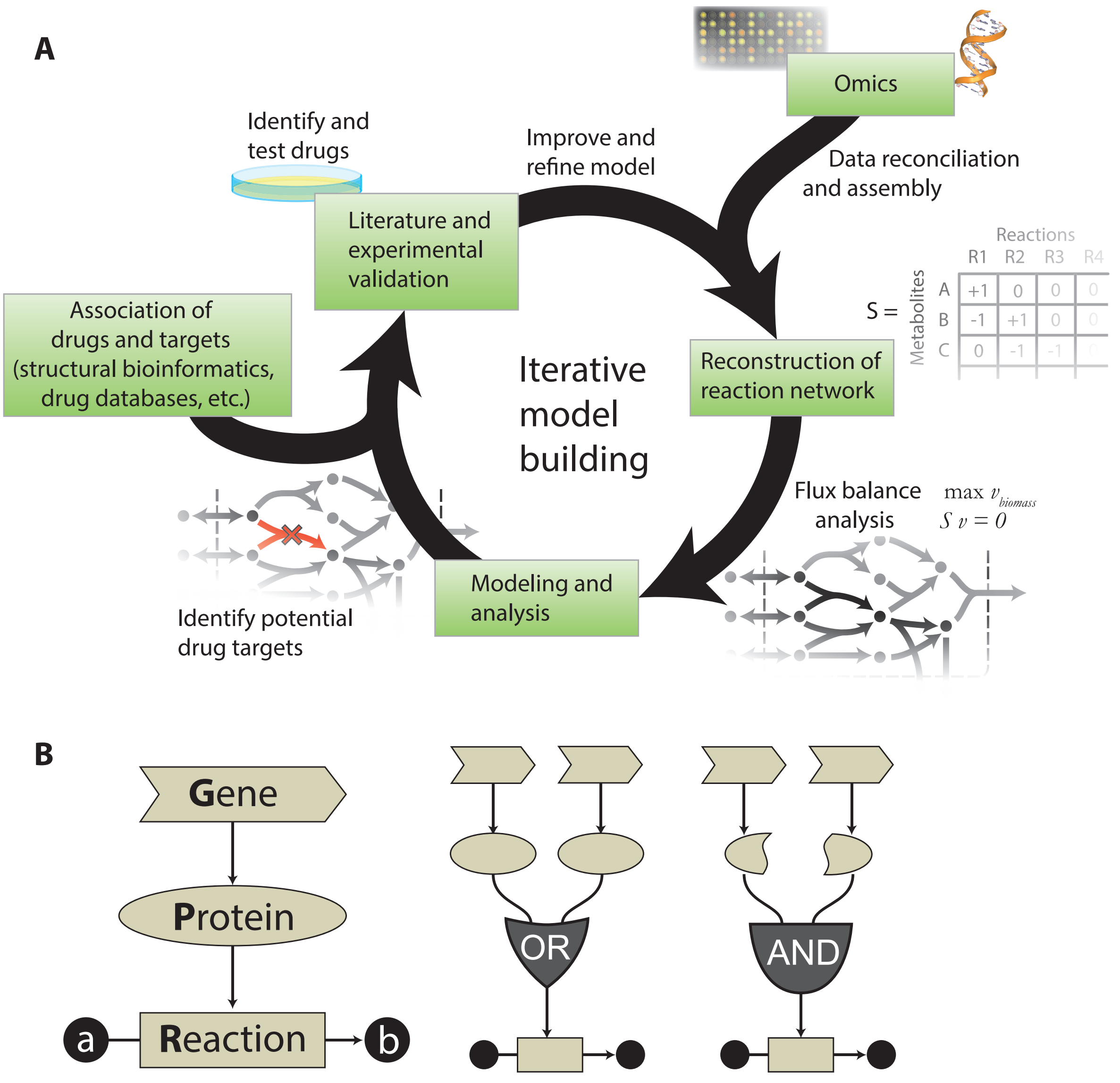

Figure 9.1: The iterative process of model building and refinement. **(A)** A functionally annotated genome together with data from the biochemical literature are used to assemble a network reconstruction. FBA allows for modeling and simulation of the reconstructed network. Advanced network analyses (such as gene essentiality or flux variability) allow for identifying potential antimicrobial drug targets. These targets can then be associated with drugs using bioinformatics approaches and obtaining target drug information from a variety of publicly available databases (e.g. STITCH or DrugBank). Predictions involving targets and drugs can be experimentally validated. Any discrepancies between computational predictions and experimental validation can be informative to improving upon and refining the original reconstruction and modeling platform. **(B)** GPRs, central to the assembly of a metabolic reconstruction, define the genes and gene products needed for each enzymatic reaction. Isozymes can be represented with 'OR' statements, whereas enzyme subunits required to function together to catalyze a particular reaction can be represented with 'AND' statements.

continue to be developed. We first discuss the fundamental aspects of network analysis and FBA in particular. Subsequently, we delve into how computational metabolic reconstructions can be used to prioritize drug target predictions. Furthermore, we review recent developments on model-guided pipelines for drug target discovery against pathogens. Finally, we extend the discussion to include host cell metabolism and propose directions for future modeling efforts in infectious disease.

9.6 Reconstructing the metabolic network and defining an objective

A metabolic network reconstruction is assembled piece-by-piece by compiling data on known enzymes, genes encoding these enzymes, and the stoichiometry of the reactions catalyzed by these enzymes (see [352] for a list of databases containing such data). GPRs, in the form of Boolean logic statements, define which genes are necessary for each enzyme and which enzymes are necessary for each reaction [323] (Figure 9.1B). The information for all the reactions in a network reconstruction with m metabolites and n reactions can be stored in an m by n table or matrix, the stoichiometric matrix. Each element or cell in this matrix corresponds to the stoichiometric coefficient of one particular metabolite in one particular reaction [323, 353]. The stoichiometric matrix enables strict accounting for the underlying biochemistry and allows a quantitative description of complex interactions between metabolites that are responsible for driving a cellular phenotype. This matrix formalism facilitates interrogation of the structural and functional properties of the network.

The application of FBA to a network reconstruction results in the identification of combinations of reaction fluxes that correspond to a maximum flux through a targeted reaction (an objective) while requiring that constraints are satisfied, for example that the mass entering the network is equal to the mass exiting the network (mass balance). In more mathematical terms, FBA involves the use of a linear programming formulation wherein an objective is optimized subject to a set of governing constraints (Box 1) [322, 353, 354]. In addition to requiring mass balance for every reaction, thermodynamic, topological, environmental, and regulatory data may provide additional constraints that dictate the feasible flux space [355]. An objective often used with FBA is biomass production, which is represented in silico as a drain capturing crucial metabolites necessary for growth of the organism [356, 357]. With the ultimate goal of identifying antimicrobial drug targets (and associated drugs) to slow or stop the growth of a pathogen, a biomass objective is often very appropriate for computational modeling efforts. Network reconstructions of most pathogenic organisms have incorporated biomass reactions as their objectives (Table 9.1).

Box 1. A brief primer on FBA

Nutrient availability, restrictions on surrounding environmental pH, and temperature are examples of basic constraints that, when imposed upon cells, can affect the resulting phenotypes [353]. Such constraints can be mathematically described, and they serve to narrow the operating range of the cell and yield a set of feasible reaction fluxes for a metabolic network. In other words, the constraints (which can be physicochemical, topological, environmental and regulatory) restrict the number of possible phenotypes, which then allows the function of the biochemical network to be characterized [353, 355].

FBA is one constraint-based method that has been extensively applied in the study of prokaryotic and eukaryotic metabolic networks [338, 358]. First, reactions of a metabolic network are assembled into a stoichiometric matrix, whose elements correspond to the stoichiometric coefficients describing the conversions from reactants to products (see figure below) [323, 353]. This simple matrix formalism permits quantitative description of the complex interactions between metabolites. Following network reconstruction, the concentrations of metabolites and fluxes through reactions can be represented as follows:

$$\frac{dC}{dt} = Sv \tag{9.1}$$

Here, C is a vector of concentrations of metabolites, t is time, S is the stoichiometric matrix consisting of m rows of metabolites and n columns of reactions, and v is a vector of fluxes through the corresponding reactions. Invoking the steady state assumption so that the rate of production of every metabolite equals its rate of consumption yields the following:

$$Sv = 0 \tag{9.2}$$

Limits can be applied to individual fluxes as follows:

$$v_{min} \leq v \leq v_{max}$$

Particular reactions can have set upper limits (v_{max}) that may align closely with experimental enzyme capacity measurements, whereas other irreversible reactions will have v_{min} set to 0.

The principle physicochemical constraints in Equation 9.2 represents a set of m linear equations. Because there are typically more unknown variables (m reaction fluxes) than equations (n steady state equations for each metabolite), the system of equations is "indeterminate" [353]. In other words, there may be many sets of fluxes (many flux distributions) that can satisfy the steady state constraints as well as the v_{min} and v_{max} of each reaction. The goal then is to use linear programming to identify which of these feasible flux distributions allow for the greatest flux through the objective reaction.

Traditionally, maximization of biomass has been chosen as the objective of choice in FBA [353]. A set of metabolites (e.g. amino acids, lipids, nucleotides and carbohydrates) that are necessary for the cell or organism to grow are typically included in the biomass reaction. Therefore, the optimization problem can be summarized as simply:

$$\begin{aligned} &\text{maximize } v_{biomass} \\ &\text{subject to } Sv = 0 \\ &\qquad\qquad v_{min} \leq v_i \leq v_{max} \text{ for } i = 1...n \end{aligned}$$

Even with these constraints, linear programming does not guarantee that the set of fluxes that allow for the maximal objective flux are unique. What is guaranteed is that the objective flux ($v_{biomass}$) found is the highest possible flux through the objective reaction that the network can allow, under any state. There are often are many possible flux distributions that achieve the maximal objective flux. See Box 4 for a method that helps investigate the many possible solutions.

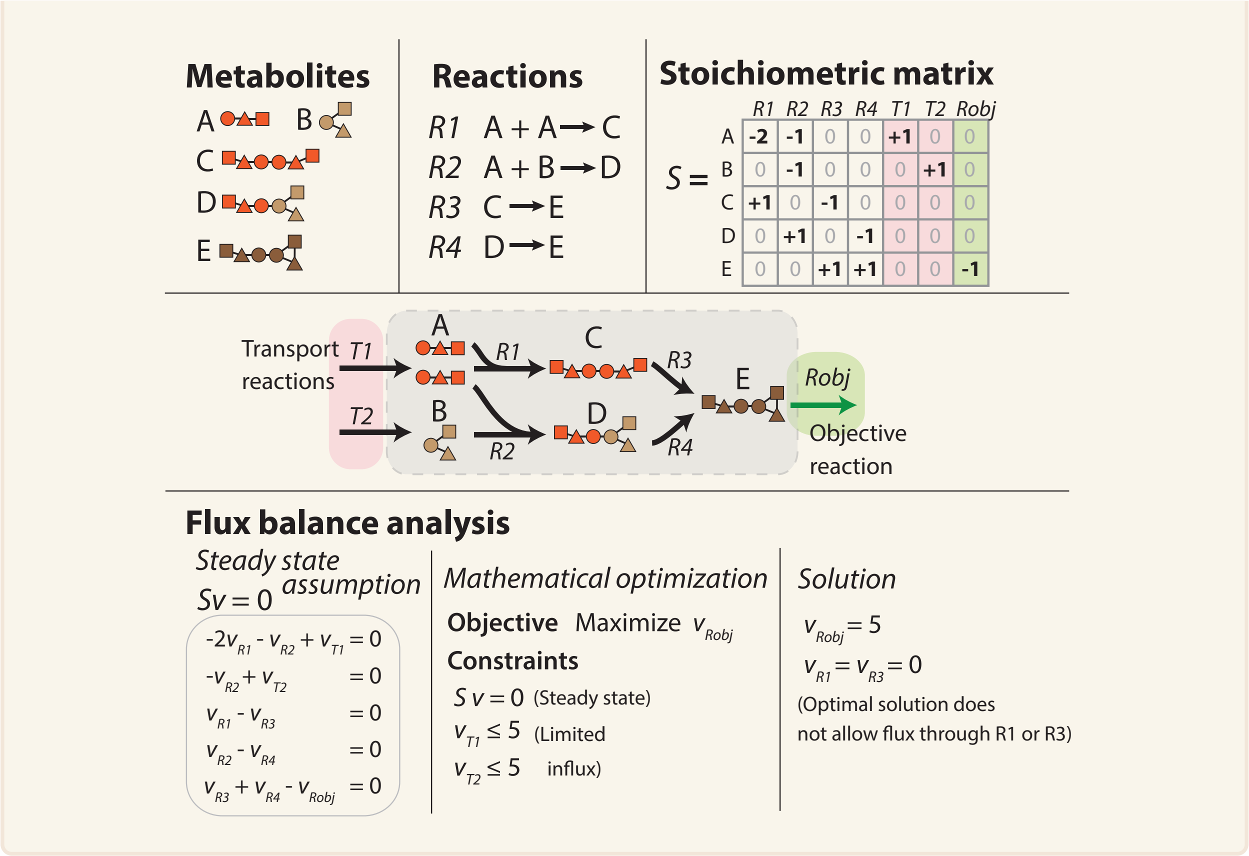

The inability of the metabolic network model to synthesize even one metabolite of the biomass reaction will result in a predicted value of zero for the objective flux (biomass), and analogously no growth. Therefore, growth predictions are sensitive to metabolites that are placed in the biomass reaction reaction. FBA can be used to investigate the ability of the model to produce each metabolite within biomass. In the *Porphyromonas gingivalis* metabolic network, the ability of the model to produce each of the 52 metabolites within the biomass reaction was evaluated after systematic reaction deletions [337]. Crucial groups of reactions were identified that were responsible for lipopolysaccharide (LPS) production, coenzyme A production, glycolysis, or purine and pyrimidine biosynthesis [337]. Corresponding enzymes that are essential for growth, as well as for the production of important bacterial components such as LPS, could serve as potential drug targets. In addition, in a study of *Leishmania major* metabolism, the contribution of minimal media components to the synthesis of individual biomass reaction constituents was analyzed [348]. The study found that the absence of cysteine and oxygen in the minimal media had a drastic impact on the overall metabolic network, limiting the generation of 30 of the 40 biomass constituents [348].

Network analyses as delineated in these examples of *P. gingivalis* and *L. major* may permit the formulation of a hypothesis for the role of specific metabolites and their influence on growth. Therefore, defining an appropriate biomass reaction (Box 2 and Box 3) is crucial for useful predictions and identification of vulnerable parts of the metabolism of a pathogen.

Box 2. Cellular objectives of pathogenic organisms

A biomass reaction is not applicable under all conditions, and very often growth alone may not be a realistic objective. Other objective such as maximizing or minimizing ATP or maximizing the production of particular cellular by-products (e.g. lactate or pyruvate) can also be used.

The metabolism of an organism may be adapted for increased virulence or pathogenicity. Pathogens and host cells may also temporarily opt for alternative objectives while under selective pressures (e.g. changes in nutrients or environmental influences of secreted toxins). In addition, different morphological stages of a pathogen (e.g. the sporozoite stage of Plasmodium falciparum in mosquitoes vs the merozoite stage in humans) may be characterized by varying metabolic requirements. Consequently, the objective function must be appropriately defined to find relevant enzyme targets crucial in particular stages of infection and/or environmental conditions.

To explore the effects of targeted perturbations (pharmacological or genetic), different objectives can be explored. It may be that the evolutionary pressures that dictate wild-type cells are different for knockout mutants. Additionally, mutants may not have the ability for immediate regulation of fluxes that allow for optimal growth. Based on these ideas, an approach termed minimization of metabolic adjustment (MOMA) was developed. The requirement for optimal growth is relaxed for gene deletions in MOMA. Instead, MOMA assumes that the overall flux distribution of a gene-knockout mutant will probably not change significantly from that of the corresponding wild type [359]. In terms of flux values, the gene-knockout mutant will remain as close as possible (in Euclidean distance) to the wild-type optimal flux distribution. MOMA aided in correcting gene essentiality predictions associated with knockouts of fructose-1,6-bisphosphatate aldolase, triosephosphate isomerase and phosphofructokinase in the *E. coli* central metabolic model [359]. These genes were predicted to be nonessential when biomass was used as the objective for *E. coli* growth on glucose, which was inconsistent with supporting literature evidence. MOMA yielded a suboptimal flux distribution for a knockout mutant that would not necessarily equal the optimum as dictated by traditional FBA [359].

Approaches such as MOMA that consider alternate hypotheses for the objective of metabolic networks provide a basis for understanding a potential biological goal for pathogenic organisms, especially considering the complexity of the environment surrounding the pathogen of interest.

Box 3. Knowledge gaps and caveats to metabolic network analysis

Multiple steps in the model-building process and subsequent analyses are prone to errors that may greatly affect flux and growth predictions and, consequently, predicted drug targets. FBA provides a quality-assurance check that ensures mass balance. Growth rates and gene essentiality predictions are validated against experimental data to ensure the model truly reflects biological processes. Gene essentiality predictions (commonly between 55% and 90%) provide confidence that downstream analyses are based on a high-quality model [319, 360]. To ensure the usefulness of any computational pipeline, drug target predictions should be compared to known targets from the literature. Below we discuss more of the particular difficulties and limitations encountered when using metabolic models to identify drug targets.

Genome annotation

In any metabolic reconstruction, there may be hundreds of putative metabolic enzymes with no experimentally identified function. These reactions and associated GPRs may be assembled strictly based on existing functional annotations of the genome or based on evidence from related organisms. Even some very well characterized enzymes may have other unexpected activities. In such cases, misannotated enzymes may yield incorrect model predictions leading to errors in drug targeting. For instance, an enzyme may be incorrectly predicted to be essential if the activity of another enzyme, which is not included in the network, can account for the same function. Therefore, this represents one important knowledge gap in the assembly of metabolic networks, and the inclusion of more refined enzyme annotations will directly improve drug target predictions [361, 362].

Nutrient availability

An important challenge in reconstructing and modeling metabolic networks is determining the composition of in silico media. Nutrients available in host environments are poorly characterized. In addition, for any nutrients that are identified, quantitative data on uptake rates are unavailable. Knowledge of the transporters of an organism elucidates which metabolites are transported into the cell. However, information on transporters is particularly limited and, in general, transport reactions lack any experimental evidence or gene associations supporting their presence. Instead, transport reactions are added for proper functioning of the computational model. Because model predictions are dependent on the media environment, nutrients and transporters must be carefully defined.

Objective function

As stated previously, in FBA-based modeling of microbial organisms, a biomass reaction has often been used. The purpose of the reaction is to ensure a drain of metabolites that are deemed essential to support the growth of the organism. Starting with the estimated weight fraction of important macromolecular components of the cell (e.g. protein, lipid, RNA, DNA and carbohydrate), the relative abundance of metabolites comprised in each group (e.g. amino acids, phospholipids, nucleotides) can be computed [356]. Among several available, a few experimental methods to measure biomass components include chloroform–methanol extraction (lipids), colorimetric protein assays, and gas chromatography–mass spectrometry (protein content) [363]. Fluxes measured directly by metabolic flux analysis, which tracks the movement of 13C from an initial 13C-labeled substrate, may also help to define the objective function [364, 365].

An objective function is most likely to cause errors if metabolites are entirely missing or incorrectly included; the relative amounts of each metabolite in the objective reaction (i.e. the stoichiometric coefficients) do not greatly affect FBA results [357, 366]. Therefore, logically deducing a biomass reaction is often adequate to estimate the growth of an organism. However, additional experimental data can reveal interesting peculiarities that may be used to design a specific biomass reaction for a particular organism. Data on growth- and non-growth-associated ATP maintenance can be included in the biomass reaction [367]. Under in vivo conditions when a pathogen is interacting with its host, an aspect that is often unclear is which biomass component(s) to include in the reaction. The composition of the biomass reaction is likely to vary under different physiological conditions, and the choice of metabolites can directly influence model predictions regarding drug targets. For example, failure to include a particular cell-wall component will not necessarily direct flux through reactions that may be crucial in vivo, and therefore the associated enzymes will not be targeted.

9.7 The quest for drug targets in metabolic networks of pathogens

Gene essentiality analysis

The most common method to identify potential drug targets has been through the prediction of essential genes (Table 9.1). The enzymes encoded by essential genes are typically hypothesized as drug targets. Gene knockouts might lead to a redistribution of flux through the network if the perturbed gene or gene product affects the removal of a particular flux-carrying reaction [322]. A GPR aids in mapping the effects of a genetic (or pharmacological) perturbation on the associated reactions, and thus the network. Gene-level perturbations that result in reduced or zero flux through a biomass reaction correspond to growth-reducing or lethal gene knockouts, respectively (Figure 9.2). For example, in a reconstruction of *Mycobacterium tuberculosis*, five previously known drug targets were encoded by genes predicted to be essential from computational analysis [335]. For metabolic reconstructions of pathogens, enzymes that are predicted to be essential will offer new experimental hypotheses and avenues for drug discovery. In the following subsections we discuss several other approaches for drug targeting using metabolic network analysis. These other approaches may provide a separate list of potential targets; however, they can also be used in tandem with gene essentiality analysis for step-by-step prioritization of drug targets.

Enzyme robustness and flux variability

In addition to an analysis of gene essentiality, assessing enzyme robustness could identify vulnerable or sensitive portions of a metabolic network suitable for drug targeting. To determine the robustness of a metabolic network to the inhibition of an enzyme-catalyzed reaction, the flux of a reaction may be constrained to a fraction of its wild type flux (simulating partial to complete inhibition), and the effects on an objective flux (e.g. biomass production) can be evaluated [368] (Figure 9.2). Such an approach was used in analyzing the network reconstruction of *Francisella tularensis*, which revealed that the growth rate was sensitive to changes in H^+ and NH_4 flux in a simulated in vitro medium but not in a simulated in vivo medium that mimicked the environment during infection [331]. Analyzing enzyme robustness with different constraints provides a detailed view of possibly nonlethal reactions whose change in flux has a strong effect on the objective of a network under different environmental conditions, therefore suggesting important reactions during an infection or perturbations for drug targeting.

Alternatively, the objective function could be constrained to a fixed percentage of its wild type flux and the allowable range of flux for each reaction can be determined using an approach termed flux variance analysis (FVA) (Box 4) [369]. A recognized shortcoming of FBA is that the typical implementation calculates only one of many possible solutions that optimize flux through the objective reaction. Consequently, there may be many possible routes through the network that achieve the same optimal flux for a given objective [355, 369]. In an effort to circumvent this shortcoming, FVA was developed to determine the range of fluxes over which a particular reaction operates, while still allowing for optimal, or near-optimal, objective flux [369]. FVA also identifies blocked reactions (reactions incapable of carrying any flux in a given model under specified constraints) or reactions with different flux ranges in various media. Enzymes that catalyze

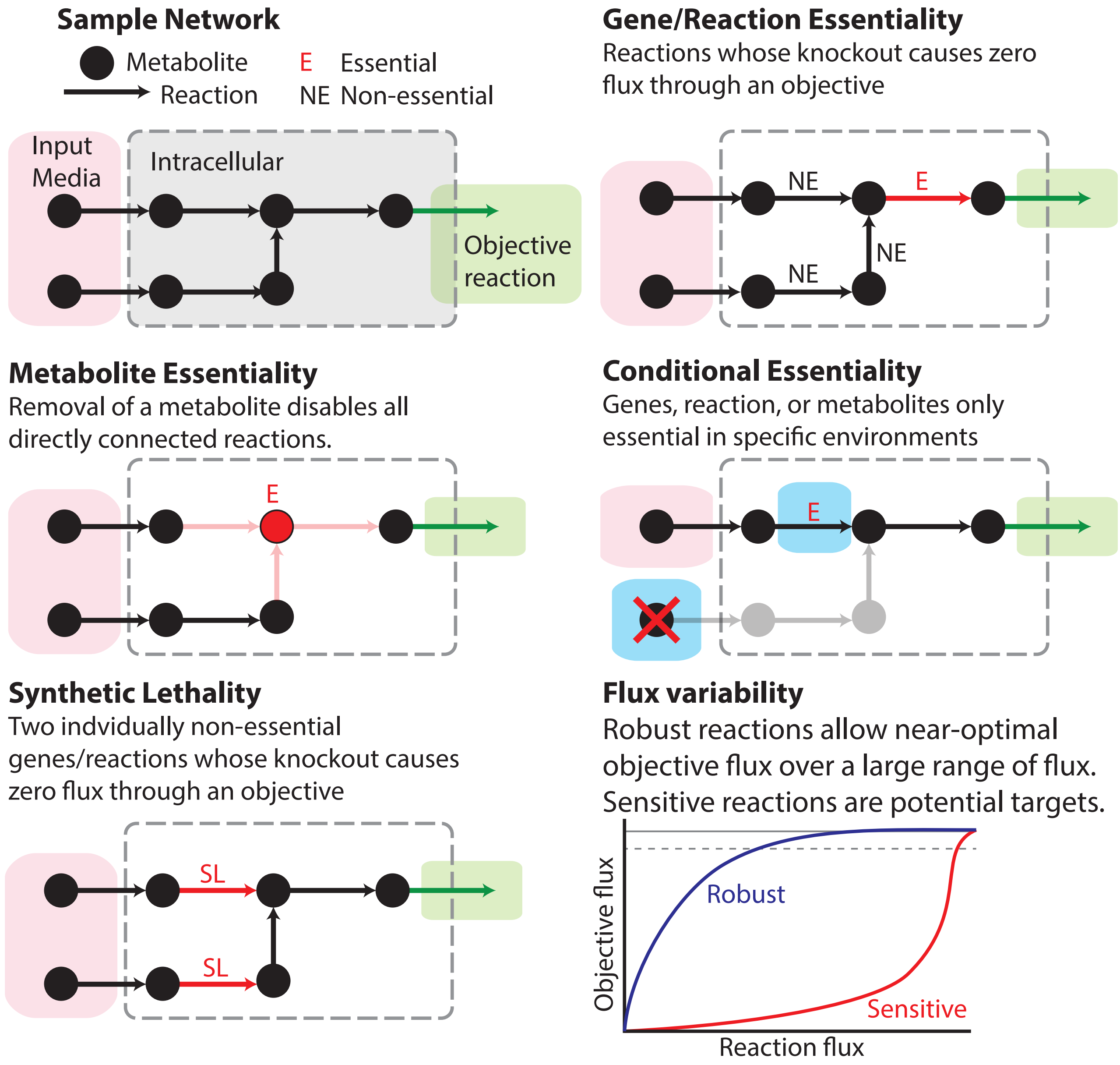
Sample Network
● Metabolite
Reaction
E Essential
NE Non-essential
Input Media
Intracellular
Objective reaction
Gene/Reaction Essentiality
Reactions whose knockout causes zero flux through an objective
NE
E
NE
NE
Metabolite Essentiality
Removal of a metabolite disables all directly connected reactions.
E
Conditional Essentiality
Genes, reaction, or metabolites only essential in specific environments
E
Synthetic Lethality
Two indvidually non-essential genes/reactions whose knockout causes zero flux through an objective
SL
SL
Flux variability
Robust reactions allow near-optimal objective flux over a large range of flux. Sensitive reactions are potential targets.
Objective flux
Robust
Sensitive
Reaction flux

Figure 9.2: Drug targeting in metabolic networks. Various strategies are illustrated for identifying drug targets by performing FBA on metabolic reconstructions. The sample network shows an input media that represents the environment and exchange reactions, intracellular reactions, and an objective reaction that drains metabolites out of the system. An essential reaction and metabolite that, when removed, block any flux through the objective are highlighted in red. In the conditionally essential panel, the absence of the metabolite highlighted in blue causes the highlighted reaction to become essential in the selected media. One of the synthetic lethal pairs of the network is denoted by 'SL'. The dashed line in the flux variability illustration may represent 'near-optimal' objective flux. A robust reaction maintains near-optimal objective flux over a larger range of reaction fluxes.

reactions with little to no variability in flux for a given objective could be selected as potential drug targets given that the network may be sensitive to even modest inhibition of its activity. In analyzing the reconstruction of *M. tuberculosis*, the average of the highest and lowest allowable flux for each reaction was used as a point of comparison for the model under constraints for two growth rates [335]. In the study, the reaction catalyzed by isocitrate lyase—an enzyme important for persistence in a host—was predicted to have increased flux during slow growth, and the activity of the enzyme was experimentally confirmed to be greater in slow-growing cells of the closely related *Mycobacterium bovis* [335]. Hence, flux variability and enzyme robustness aid in further prioritizing drug targets identified from other methods such as gene essentiality.

Box 4. A brief primer on FVA

After the application of various constraints on the biochemical network, the number of allowable network states (or possible phenotypes) is typically large. Depending on the size and interconnectedness of the cellular network, there may be several alternative optimal phenotypes [355]. FBA calculates one of many feasible solutions that result in the same optimal value of the cellular objective.

FVA calculates the range of flux in each reaction that allows for the same optimal flux through the objective reaction. The objective flux of the reaction is specified as an additional constraint and multiple optimizations are performed to compute the maximum and minimum flux for every reaction in the network:

$$\begin{aligned} &\text{Max/Min } v_i \\ &\text{subject to } Sv = 0 \\ &\qquad\qquad v_{biomass} = Z_{obj} \\ &\qquad\qquad v_{min} \leq v_i \leq v_{max} \text{ for } i = 1...n \end{aligned}$$

Here, n refers to the number of reactions in the biochemical network, and Zobj is the optimal value of the cellular objective ($v_{biomass}$) as obtained by FBA [369].

9.7.1 Metabolite essentiality

Many current drugs have high similarity to natural metabolites and compete for and/or inhibit normal enzymatic activity [370]. Therefore, another very interesting avenue towards identifying drug targets in metabolic networks is via the prediction of essential metabolites. In contrast to the more traditional individual gene knockouts mentioned previously, metabolites in the stoichiometric matrix can also be systematically removed. Consequently, all reactions in which a given metabolite participates are removed, and the resultant effects on the objective are assessed (Figure 9.2). A total of 211 essential metabolites in the *Acinetobacter baumanii* reconstruction were narrowed to 9 following removal of (i) currency metabolites (ATP, NADH, H_2O, etc.); (ii) metabolites present in the human metabolic network; and (iii) metabolites participating in reactions catalyzed by enzymes with human homologs [329]. Enzymes that catalyze reactions involved in the consumption or production of these essential metabolites may be considered as drug targets. Moreover, structural analogs of essential metabolites may be considered as test compounds for experimental evaluation, thus sidestepping extensive screening or computational predictions [345].

9.7.2 Combination gene and reaction perturbations

Many anti-infectives on the market act on multiple targets. This multiplicity of targets was exemplified in a network analysis of 890 FDA-approved drugs targeting 394 human proteins (derived from the DrugBank database), where approximately 38% of the drugs were associated with more than one protein target, and a few drugs were associated with as many as 14 targets [371]. In that regard, a drug discovery strategy incorporating compounds known to act simultaneously on multiple targets can be adopted for microbial pathogens. FBA allows predictions involving the perturbation of multiple genes or reactions in a rapid timeframe (minutes or hours)—a single in silico combination taking only a fraction of a second [372]. In a reconstruction of *M. tuberculosis* that accounted for features specific to an in vivo environment, all non-trivial double-deletion mutants (synthetic lethal pairs) were tested for in silico growth using FBA [320]. Of two experimentally-characterized double gene deletions, the model accurately predicted reduced in silico growth in both in vitro and in vivo environmental conditions [320]. A combination of drugs that affect synthetic lethal targets may act synergistically to inhibit growth of a pathogen, thereby paving the way for model-guided predictions of drug synergy. Experimentally screening for all possible drug combinations against a particular pathogen is costly and is often not feasible. Therefore, predicted combinations of drugs associated with synthetic lethal targets can direct more specific experiments and perhaps reveal entirely novel treatment strategies.

9.7.3 Groups of targets and network topology

Other approaches characterizing the structure of a genome-scale network reconstruction identify sets of reactions that act together and therefore may be targeted as an entire pathway. Sets of correlated reactions (or Co-sets) consist of groups of reactions whose fluxes are linked, and which represent functional modules within a biochemical network [373]. Co-sets, which can aid in suggesting alternative drug targets by identifying reactions that are functionally related to each other, can be divided into several categories. A perfect Co-set consists of a group of reactions such that, for any given pair in the group, a non-zero flux in one reaction implies a non-zero flux in the other, with a fixed ratio . Other categories include partial Co-sets (pairs of linked reactions, but with a variable flux ratio) and directional Co-sets (a non-zero flux in one reaction implies a nonzero flux in the other, but the converse is not true) [374]. By calculating hard-coupled reaction (HCR) sets—a subgroup of perfect Co-sets where sets of reactions are defined by participating metabolites sharing a consumption to production connectivity of 1:1 (i.e. two reactions are linked by a metabolite that is connected to no other reaction)—one study found 25 of 147 HCR sets contained previously identified drug targets in *M. tuberculosis* [319]. Because an altered flux in one reaction results in an altered flux of all reactions within a HCR set, only one enzyme needs to be targeted. This approach aids in prioritizing the list of potential drug targets by identifying linked enzymatic reactions. Hence, analyses of the topology of a metabolic network can reveal key local and structural features that may be important drug targets when data related to environment fluxes or appropriate objective are not necessarily available.

9.7.4 Environment and conditional essentiality

Finally, the metabolic phenotype is dependent on the media environment and the exchange of metabolites into and out of the system (see Box 3 for discussion of knowledge gaps associated with nutrient availability). By constraining uptake or secretion fluxes, a minimal set of metabolites that allows flux through the objective can be computed [348]. Moreover, enzymes or metabolites that are necessary for growth in various environments (e.g. minimal media, defined media, or rich media with an abundance of nutrients and carbon sources) can be predicted. In the reconstruction of *F. tularensis*, genes that were essential in a simulated macrophage environment and five other environmental conditions were considered to be unconditionally essential genes (in other words, they represented a core set of genes that were essential regardless of the medium). Of the 17 virulence factors cataloged from previous literature, eight were unconditionally essential genes [331]. By contrast, enzymes that may be necessary for growth under one condition, but not another, are conditionally essential (Figure 9.2). With a careful consideration of an objective and appropriate nutrient uptake, gene essentiality analysis may reveal new drug targets specific to particular growth conditions and environments in which a pathogen must survive. Such an analysis can also inform strategies for manipulating the environment of the pathogen that could be effective as a treatment option.

9.8 From target to drug and the development of model guided pipelines for drug discovery

Computational analysis of metabolic processes in pathogens can yield a ranking of predicted drug targets. Bioinformatics and network analyses were performed to yield a high-confidence list of targets against *M. tuberculosis* [375]. By implementing a multilayered approach, targets that did not pass sequential cut-off values were removed (e.g. elimination of enzymes with human homologs or targets with no computationally predicted binding pocket) [375]. In another proof-of-concept study it was noted that essential type II fatty acid biosynthesis (FAS II) reactions in the *E. coli* MG1655 metabolic network were also essential in several *Staphylococcus aureus* strains [376]. Following network analysis, a virtual screening strategy was employed whereby small molecules from a library of approximately 106 compounds were docked to enzymes catalyzing essential reactions, and 41 inhibitors of FAS II enzymes were selected for experimental validation [376]. In cell viability assays, six of the inhibitors had growth-retarding effects against *E. coli* and *S. aureus* strains in standard LB agar plates [376]. Finally, following the identification of 163 essential metabolites, a third study used a layered approach to prioritize five essential metabolites in the metabolic network of the opportunistic pathogen *Vibrio vulnificus* [345]. Currency metabolites, metabolites consumed by a single reaction, metabolites present in the human metabolic network, and metabolites associated with enzymes with human homologs were removed. The study screened 352 compounds found to be structurally similar to one of the five essential metabolites and identified one compound that most potently inhibited growth, more so than a currently used drug [345]. These studies provide various examples of model-guided pipelines to drug discovery by primarily using network analyses to identify and prioritize drug targets. Additional constraints such as enzyme druggability and elevated gene expression can also be used to prioritize drug targets, which can then guide the screening and selection of compounds.

A common approach in proposing drug targets using metabolic networks has been to rule out targets that overlap with host cell metabolism—the idea being that offtargets can be minimized and drug interference plus subsequent complications with the host can be avoided. However, there are arguments to be made in favor of retaining targets that overlap with human metabolism. First, accounting for the drug selectivity between host and pathogen targets at the respective binding sites may preclude off-target influences [377]. Second, if the goal is to discover drugs against infectious diseases quickly, then the best option may be to focus on finding new clinical indications for existing FDA-approved drugs (i.e. pursuing drug repurposing strategies) instead of developing new investigational compounds that are subject to regulatory hurdles [378]. Also, the majority of FDA-approved drugs target human proteins. Hence, eliminating pathogen targets that overlap with human proteins reduces the number of potential drugs that could be evaluated experimentally.

9.9 A host cell perspective

Interaction with a host cell is often crucial to the metabolism and survival of a pathogen. For instance, the kinetoplastid parasite *L. major* is unable to synthesize several essential amino acids and therefore obtains them from the host macrophage [379]. As another example, Legionella pneumophila, the bacterium responsible for Legionnaire's disease, ceases to replicate inside a host macrophage when it cannot access or process threonine [380]. Consequently, identifying the particular niche of nutrients and resources in the host cell required by a pathogen is vital to discovering treatment options that specifically target host-pathogen interactions [381].

A systems-level analysis of pathogen metabolism interfaced with cell type-specific host metabolic networks can also be conducted. Because *P. falciparum* invades mature erythrocytes to establish infection in its human host, a metabolic model of the human erythrocyte was built in conjunction with the *P. falciparum* reconstruction to make predictions which aligned closer to known conditions in the infected erythrocyte [349]. This model, modifying an existing approach from Shlomi et al. [382], integrated previous gene expression data where several enzymes were constrained to be 'on' and 'off' during specific life-cycle stages. The combined erythrocyte-blood stage *P. falciparum* network correctly predicted metabolite exchanges between the microbe and host [349]. A recently active area of research has been the development of algorithms to create cell type-specific metabolic networks by integrating gene and protein expression data with existing human metabolic reconstructions [382–384]. Inclusion of host-specific factors into pathogen metabolic-network reconstructions or developing systems-level models of host and pathogen networks will continue to enable investigations into the complexities of the host-pathogen interplay.

Finally, inhibiting host pathways and perturbing the flux of metabolites in the host cell may alter the ambient environment and require pathogens to adapt their metabolic needs. Therefore, targeting the machinery of a host cell at the host-pathogen interface can provide new therapeutic approaches [385]. For example, host proteins hijacked for viral replication are potentially important drug targets. Recently, a high-throughput screening assay identified a lipophilic compound–NA255–that inhibits the host serine palmitoyltransferase, an enzyme needed for association of hepatitis C virus (HCV) with host lipid rafts [386]. Moreover, to characterize transformations in host functions, data specific to the host cell preand post-infection must be obtained. The analysis of transcription profiles is one approach that has been successfully implemented to identify genes in the host cell that are differentially regulated due to pathogenic infection [387, 388]. Similarly, profiling the proteome and lipidome of a hepatocyte over the time-course of infection and integrating these data with protein-protein interaction networks revealed multiple lipids and enzymes differentially regulated in HCV-infected cells [389]. A third approach for identifying factors in the host necessary for establishing infection involves the use of genetic screens in which largescale insertional mutagenesis is performed to develop null mutants in a human cell line [390]. Ultimately, the use of new experimental technologies along with metabolic modeling will be vital to discovering host components crucial to the survival of a pathogen.

9.10 Next steps

Advanced meta-network analyses, such as comparative modeling of metabolic reconstructions across multiple strains and species or community-based modeling of metabolism across differing pathogenic organisms, have broad implications for understanding and investigating infectious diseases. Below, we highlight several future directions in this realm and provide a few examples of efforts already underway.

The recent completion of metabolic reconstructions of the pathogen *Pseudomonas aeruginosa* [338] and the related nonpathogen *Pseudomonas putida* [391] creates new opportunities for investigating species-specific differences in metabolism and the metabolic basis for virulence of *P. aeruginosa*. Towards that end, a reconciliation of the two reconstructions was completed such that any differences in the metabolic networks of *P. aeruginosa* and *P. putida* would be indicative of true biological variations as opposed to artifacts of the reconstruction and modeling process [392]. In the reconciliation study, the model for each organism was analyzed to characterize the tradeoffs of producing biomass versus the production of individual metabolites. Compared to *P. putida*, *P. aeruginosa* was able to produce a small proportion of the shared virulence factor precursors with only a slight decrease in biomass production. In general, the metabolic flexibility analysis suggested that the virulence of *P. aeruginosa* is complex and highly multifactorial, and has more flexibility than *P. putida* in many metabolic pathways. This computational analysis paves the way for future modeling efforts of other infectious disease-causing agents and their basis for establishing virulence.

As another example, syntrophic mutualism between a sulfate-reducing bacterium, Desulfovibrio vulgaris, and a methanogen, *Methanococcus maripaludis*, was investigated by performing FBA on a compartment-based model involving the metabolic reconstructions of both organisms and a culture medium [393]. In another study, gene expression data were integrated with the genome-scale metabolic reconstruction of *P. aeruginosa* in the context of a chronic cystic fibrosis lung infection over a 44-month time-course [394]. This analysis provided a systems-level view of bacterial adaptations in a cystic fibrotic lung environment over time. Subsequent studies can shed light on the interactions between multiple organisms over the time course of an infection.

Finally, automated reconstruction platforms such as ModelSEED permit the rapid reconstruction of hundreds of draft bacterial metabolic networks [395, 396]. Integration of many such reconstructed networks may help elucidate interactions within the host microbiome and partially explain the development of opportunistic infections that occur primarily because of an altered bacterial flora and environment. For example, an integrative metabolic analysis of organisms in the human gut microbiome could aid understanding of the intricate balance between non-pathogenic and potentially pathogenic organisms during healthy and infectious states in the gastrointestinal tract. An expected outcome of such analyses could result in the selection of drugs or drug cocktails that specifically target pathogens without eliminating non-pathogenic members.

9.11 Concluding remarks

As reconstructions of metabolic networks become more standard and automated [323], the need for computational tools to characterize these networks becomes more apparent. In addition, the generation and management of large datasets pertaining to both host cell and pathogen intracellular processes of metabolism, signal transduction or regulation has necessitated a systems approach and, therefore, the computational methods used to analyze these data are becoming increasingly important. Experimental methods will continue to improve, thereby generating data that have so far been either impossible or prohibitively laborious to obtain, and which have constrained the value of some model predictions. For example, TraDIS (a new experimental method used to identify all essential genes simultaneously) directly measures gene essentiality that the model could only predict [397]. However, the iterative relationship between modeling and experiment will always permit the generation of novel hypotheses and the contextualization of large datasets, often in a quicker and more cost-efficient manner (e.g. rapid essentiality prediction of all double gene knockouts). Network-based approaches such as genome-scale metabolic reconstructions have been effective in drug target prediction and will continue to expand in scope and applicability. In addition, integration of networks and data into more standard pipelines that traverse the spectrum from computational prediction to experimental evaluation and back again will speed the process dramatically. By including many types of data sources that have yet to be coupled, entirely new classes of drug targets or treatment strategies may be found. The already enormous amount of data is only increasing, and the use of systems biology approaches will be vital to driving future research of drug and drug target discovery against infectious diseases.

9.12 Acknowledgements

The majority of this chapter was taken from Chavali, A. K., D'Auria, K. M., Hewlett, E. L., Pearson, R. D. & Papin, J. A. A metabolic network approach for the identification and prioritization of antimicrobial drug targets. *Trends in Microbiology* **20,** 113–123 (Mar. 2012). I was co-primary author on this paper and would like to thank Dr. Chavali, the other primary author, and all other co-authors. We would like to thanks Glynis Kolling and Erwin Gianchandani for reading the manuscript and providing insightful feedback.

Bibliography

1. Lucado, J., Gould, C. & Elixhauser, A. *Clostridium Difficile Infections (CDI) in Hospital Stays, 2009: Statistical Brief #124* (Agency for Health Care Policy and Research (US), Rockville (MD), Feb. 2012) (cit. on pp. 1, 29, 31, 54, 93).

2. Johnson, D. L., Lander, E. S., Bailey, J. A., Linton, L. M., Birren, B., Nusbaum, C., Zody, M. C., Baldwin, J., Devon, K., Dewar, K., Doyle, M., FitzHugh, W., Funke, R., Gage, D., Harris, K., Heaford, A., Howland, J., Kann, L., Lehoczky, J., LeVine, R., McEwan, P., McKernan, K., Meldrim, J., Mesirov, J. P., Miranda, C., Morris, W., Naylor, J., Raymond, C., Rosetti, M., Santos, R., Sheridan, A., Sougnez, C., Stange-Thomann, N., Stojanovic, N., Subramanian, A., Wyman, D., Rogers, J., Sulston, J., Ainscough, R., Beck, S., Bentley, D., Burton, J., Clee, C., Carter, N., Coulson, A., Deadman, R., Deloukas, P., Dunham, A., Dunham, I., Durbin, R., French, L., Grafham, D., Gregory, S., Hubbard, T., Humphray, S., Hunt, A., Jones, M., Lloyd, C., McMurray, A., Matthews, L., Mercer, S., Milne, S., Mullikin, J. C., Mungall, A., Plumb, R., Ross, M., Shownkeen, R., Sims, S., Waterston, R. H., Wilson, R. K., Hillier, L. W., McPherson, J. D., Marra, M. A., Mardis, E. R., Fulton, L. A., Chinwalla, A. T., Pepin, K. H., Gish, W. R., Chissoe, S. L., Wendl, M. C., Delehaunty, K. D., Miner, T. L., Delehaunty, A., Kramer, J. B., Cook, L. L., Fulton, R. S., Minx, P. J., Clifton, S. W., Hawkins, T., Branscomb, E., Predki, P., Richardson, P., Wenning, S., Slezak, T., Doggett, N., Cheng, J. F., Olsen, A., Lucas, S., Elkin, C., Uberbacher, E., Frazier, M., Gibbs, R. A., Muzny, D. M., Scherer, S. E., Bouck, J. B., Sodergren, E. J., Worley, K. C., Rives, C. M., Gorrell, J. H., Metzker, M. L., Naylor, S. L., Kucherlapati, R. S., Nelson, D. L., Weinstock, G. M., Sakaki, Y., Fujiyama, A., Hattori, M., Yada, T., Toyoda, A., Itoh, T., Kawagoe, C., Watanabe, H., Totoki, Y., Taylor, T., Weissenbach, J., Heilig, R., Saurin, W., Artiguenave, F., Brottier, P., Bruls, T., Pelletier, E., Robert, C., Wincker, P., Smith, D. R., Doucette-Stamm, L., Rubenfield, M., Weinstock, K., Lee, H. M., Dubois, J., Rosenthal, A., Platzer, M., Nyakatura, G., Taudien, S., Rump, A., Yang, H., Yu, J., Wang, J., Huang, G., Gu, J., Hood, L., Rowen, L., Madan, A., Qin, S., Davis, R. W., Federspiel, N. A., Abola, A. P., Proctor, M. J., Myers, R. M., Schmutz, J., Dickson, M., Grimwood, J., Cox, D. R., Olson, M. V., Kaul, R., Shimizu, N., Kawasaki, K., Minoshima, S., Evans, G. A., Athanasiou, M., Schultz, R., Roe, B. A., Chen, F., Pan, H., Ramser, J., Lehrach, H., Reinhardt, R., McCombie, W. R., de la Bastide, M., Dedhia, N., Blocker, H., Hornischer, K., Nordsiek, G., Agarwala, R., Aravind, L., Bateman, A., Batzoglou, S., Birney, E., Bork, P., Brown, D. G., Burge, C. B., Cerutti, L., Chen, H. C., Church, D., Clamp, M., Copley, R. R., Doerks, T., Eddy, S. R., Eichler, E. E., Furey, T. S., Galagan, J., Gilbert, J. G., Harmon, C., Hayashizaki, Y., Haussler, D., Hermjakob, H., Hokamp, K., Jang, W., Johnson, L. S., Jones, T. A., Kasif, S., Kaspryzk, A., Kennedy, S., Kent, W. J., Kitts, P., Koonin, E. V., Korf, I., Kulp, D., Lancet, D., Lowe, T. M., McLysaght, A., Mikkelsen, T., Moran, J. V., Mulder, N., Pollara, V. J., Ponting, C. P., Schuler, G., Schultz, J., Slater, G., Smit, A. F.,

Stupka, E., Szustakowski, J., Thierry-Mieg, D., Thierry-Mieg, J., Wagner, L., Wallis, J., Wheeler, R., Williams, A., Wolf, Y. I., Wolfe, K. H., Yang, S. P., Yeh, R. F., Collins, F., Guyer, M. S., Peterson, J., Felsenfeld, A., Wetterstrand, K. A., Patrinos, A., Morgan, M. J., de Jong, P., Catanese, J. J., Osoegawa, K., Shizuya, H., Choi, S., Chen, Y. J., Szustakowki, J. & International Human Genome Sequencing Consortium. Initial sequencing and analysis of the human genome. *Nature* **409,** 860–921 (Feb. 2001) (cit. on p. 4).

3. Michael, D. & Manyuan, L. Intron—exon structures of eukaryotic model organisms. *Nucleic Acids Research* (1999) (cit. on p. 4).

4. Crick, F. Central dogma of molecular biology. *Nature* **227,** 561–563 (Aug. 1970) (cit. on p. 4).

5. International Human Genome Sequencing Consortium. Finishing the euchromatic sequence of the human genome. *Nature* **431,** 931–945 (Oct. 2004) (cit. on p. 5).

6. Grafham, D., Hunt, A., Bentley, D., Carter, N., Jones, M., Gregory, S., Barlow, K. F., McLay, K. E., Kaul, R., Swarbreck, D., Dunham, A., Scott, C. E., Howe, K. L., Woodfine, K., Spencer, C. C. A., Gillson, C., Searle, S., Zhou, Y., Kokocinski, F., McDonald, L., Evans, R., Phillips, K., Atkinson, A., Cooper, R., Jones, C., Hall, R. E., Andrews, T. D., Lloyd, C., Ainscough, R., Almeida, J. P., Ambrose, K. D., Anderson, F., Andrew, R. W., Ashwell, R. I. S., Aubin, K., Babbage, A. K., Bagguley, C. L., Bailey, J. A., Beasley, H., Bethel, G., Bird, C. P., Bray-Allen, S., Brown, J. Y., Brown, A. J., Buckley, D., Burton, J., Bye, J., Carder, C., Chapman, J. C., Clark, S. Y., Clarke, G., Clee, C., Cobley, V., Collier, R. E., Corby, N., Coville, G. J., Davies, J., Deadman, R., Dunn, M., Earthrowl, M., Ellington, A. G., Errington, H., Frankish, A., Frankland, J., French, L., Garner, P., Garnett, J., Gay, L., Ghori, M. R. J., Gibson, R., Gilby, L. M., Gillett, W., Glithero, R. J., Griffiths, C., Griffiths-Jones, S., Grocock, R., Hammond, S., Harrison, E. S. I., Hart, E., Haugen, E., Heath, P. D., Holmes, S., Holt, K., Howden, P. J., Hunt, S. E., Hunter, G., Isherwood, J., James, R., Johnson, C., Johnson, D. L., Joy, A., Kay, M., Kershaw, J. K., Kibukawa, M., Kimberley, A. M., King, A., Knights, A. J., Lad, H., Laird, G., Lawlor, S., Leongamornlert, D. A., Lloyd, D. M., Loveland, J., Lovell, J., Lush, M. J., Lyne, R., Martin, S., Mashreghi-Mohammadi, M., Matthews, L., Matthews, N. S. W., McLaren, S., Milne, S., Mistry, S., Moore, M. J. F., Nickerson, T., O'Dell, C. N., Oliver, K., Palmeiri, A., Palmer, S. A., Parker, A., Patel, D., Pearce, A. V., Peck, A. I., Pelan, S., Phelps, K., Phillimore, B. J., Plumb, R., Rajan, J., Raymond, C., Rouse, G., Saenphimmachak, C., Sehra, H. K., Sheridan, E., Shownkeen, R., Sims, S., Skuce, C. D., Smith, M., Steward, C., Subramanian, S., Sycamore, N., Tracey, A., Tromans, A., Van Helmond, Z., Wall, M., Wallis, J. M., White, S., Whitehead, S. L., Wilkinson, J. E., Willey, D. L., Williams, H., Wilming, L., Wray, P. W., Wu, Z., Coulson, A., Vaudin, M., Sulston, J. E., Durbin, R., Hubbard, T., Wooster, R., Dunham, I., McVean, G., Ross, M. T., Harrow, J., Olson, M. V., Beck, S., Rogers, J., Banerjee, R., Bryant, S. P., Burford, D. C., Burrill, W. D. H., Clegg, S. M., Dhami, P., Dovey, O., Faulkner, L. M., Gribble, S. M., Langford, C. F., Pandian, R. D., Porter, K. M. & Prigmore, E. The DNA sequence and biological annotation of human chromosome 1. *Nature* **441,** 315–321 (May 2006) (cit. on p. 5).

7. Augenlicht, L. H. & Kobrin, D. Cloning and screening of sequences expressed in a mouse colon tumor. *Cancer Research* **42,** 1088–1093 (Mar. 1982) (cit. on p. 5).

8. Maskos, U. & Southern, E. M. Oligonucleotide hybridisations on glass supports: a novel linker for oligonucleotide synthesis and hybridisation properties of oligonucleotides synthesised in situ. *Nucleic Acids Research* **20,** 1679–1684 (Apr. 1992) (cit. on p. 5).

9. Schena, M., Shalon, D., Davis, R. W. & Brown, P. O. Quantitative monitoring of gene expression patterns with a complementary DNA microarray. *Science* **270,** 467–470 (Oct. 1995) (cit. on p. 6).

10. Irizarry, R. a., Hobbs, B., Collin, F., Beazer-Barclay, Y. D., Antonellis, K. J., Scherf, U. & Speed, T. P. Exploration, normalization, and summaries of high density oligonucleotide array probe level data. *Biostatistics* **4,** 249–264 (Apr. 2003) (cit. on pp. 6–9, 61).

11. Li, C. & Wong, W. H. Model-based analysis of oligonucleotide arrays: expression index computation and outlier detection. *Proceedings of the National Academy of Sciences of the United States of America* **98,** 31–36 (Jan. 2001) (cit. on p. 7).

12. Milo, M., Fazeli, A., Niranjan, M. & Lawrence, N. D. A probabilistic model for the extraction of expression levels from oligonucleotide arrays. *Biochemical Society Transactions* **31,** 1510–1512 (Dec. 2003) (cit. on pp. 7, 10).

13. Liu, X., Milo, M., Lawrence, N. D. & Rattray, M. A tractable probabilistic model for Affymetrix probe-level analysis across multiple chips. *Bioinformatics* **21,** 3637–3644 (Sept. 2005) (cit. on pp. 7, 8, 10).

14. Ambler, G. K., Hein, A.-M. K., Richardson, S., Causton, H. C. & Green, P. J. BGX: a fully Bayesian integrated approach to the analysis of Affymetrix GeneChip data. *Biostatistics* **6,** 349–373 (July 2005) (cit. on p. 7).

15. Chen, Z., McGee, M., Liu, Q. & Scheuermann, R. H. A distribution free summarization method for Affymetrix GeneChip arrays. *Bioinformatics* **23,** 321–327 (Feb. 2007) (cit. on pp. 7, 8).

16. Hochreiter, S., Clevert, D.-A. & Obermayer, K. A new summarization method for Affymetrix probe level data. *Bioinformatics* **22,** 943–949 (Apr. 2006) (cit. on pp. 7, 8).

17. Wu, Z., Gentleman, R. C., Irizarry, R. A., Murillo, F. M. & Spencer, F. *A model based background adjustment for oligonucleotide expression arrays* tech. rep. (2004) (cit. on pp. 7, 9, 38, 61).

18. Li, C. & Wong, W. Model-based analysis of oligonucleotide arrays: model validation, design issues and standard error application. *Genome Biology* **2,** RESEARCH0032 (2001) (cit. on pp. 7, 8, 61).

19. Mosteller, F. & Tukey, J. W. *Data analysis and regression* (Addison-Wesley, 1977) (cit. on p. 8).

20. Zhang, L., Aldape, K. D. & Miles, M. F. A model of molecular interactions on short oligonucleotide microarrays. *Nature Biotechnology* **21,** 818–821 (July 2003) (cit. on pp. 8, 9, 11).

21. Bolstad, B. M., Irizarry, R. A., Astrand, M. & Speed, T. P. A comparison of normalization methods for high density oligonucleotide array data based on variance and bias. *Bioinformatics* **19,** 185–193 (Jan. 2003) (cit. on pp. 8, 183).

22. Huber, W., von Heydebreck, A., Sueltmann, H., Poustka, A. & Vingron, M. Parameter estimation for the calibration and variance stabilization of microarray data. *Statistical Applications in Genetics and Molecular Biology* **2,** Article3 (2003) (cit. on p. 8).

23. Pozhitkov, A. E., Tautz, D. & Noble, P. A. Oligonucleotide microarrays: widely applied–poorly understood. *Briefings in Functional Genomics & Proteomics* **6,** 141–148 (June 2007) (cit. on p. 9).

24. Loven, J., Burge, C. B., Orlando, D. A., Sigova, A. A., Lin, C. Y., Rahl, P. B., Levens, D. L., Lee, T. I. & Young, R. A. Revisiting global gene expression analysis. *Cell* **151,** 476–482 (Oct. 2012) (cit. on p. 10).

25. Wu, Z. & Irizarry, R. a. Preprocessing of oligonucleotide array data. *Nature Biotechnology* **22,** pages (June 2004) (cit. on p. 11).

26. Zhang, L., Baggerly, K., Wu, C., Carta, R. & Coombes, K. R. Response to Preprocessing of oligonucleotide array data. *Nature Biotechnology* **22,** 658 (June 2004) (cit. on p. 11).

27. Califano, A., Lim, W. K., Wang, K. & Lefebvre, C. Comparative analysis of microarray normalization procedures: effects on reverse engineering gene networks. *Bioinformatics* **23,** i282–8 (July 2007) (cit. on pp. 11, 61).

28. Bolger, A. M., Giorgi, F. M., Lohse, M. & Usadel, B. Algorithm-driven artifacts in median Polish summarization of microarray data. *BMC Bioinformatics* **11,** 553 (2010) (cit. on p. 11).

29. Choe, S. E., Boutros, M., Michelson, A. M., Church, G. M. & Halfon, M. S. Preferred analysis methods for Affymetrix GeneChips revealed by a wholly defined control dataset. *Genome Biology* **6,** R16 (2005) (cit. on p. 11).

30. Pearson, R. D. A comprehensive re-analysis of the Golden Spike data: towards a benchmark for differential expression methods. *BMC Bioinformatics* **9,** 164 (2008) (cit. on p. 11).

31. Schuster, E. F., Blanc, E., Partridge, L. & Thornton, J. M. Estimation and correction of non-specific binding in a large-scale spike-in experiment. *Genome Biology* **8,** R126 (2007) (cit. on p. 11).

32. Storey, J. D. & Dabney, A. R. A reanalysis of a published Affymetrix GeneChip control dataset. *Genome Biology* **7,** 401 (2006) (cit. on p. 11).

33. Irizarry, R. a., Cope, L. M. & Wu, Z. Feature-level exploration of a published Affymetrix GeneChip control dataset. *Genome Biology* **7,** 404 (2006) (cit. on p. 11).

34. Gaile, D. P. & Miecznikowski, J. C. Putative null distributions corresponding to tests of differential expression in the Golden Spike dataset are intensity dependent. *BMC Genomics* **8,** 105 (2007) (cit. on p. 11).

35. Fodor, A. A., Tickle, T. L. & Richardson, C. Towards the uniform distribution of null P values on Affymetrix microarrays. *Genome Biology* **8,** R69 (2007) (cit. on p. 11).

36. Zhu, Q., Miecznikowski, J. C. & Halfon, M. S. Preferred analysis methods for Affymetrix GeneChips. II. An expanded, balanced, wholly-defined spike-in dataset. *BMC Bioinformatics* **11,** 285 (2010) (cit. on p. 12).

37. Cui, X., Churchill, G. A. & Churchill, G. A. Statistical tests for differential expression in cDNA microarray experiments. *Genome Biology* **4,** 210 (2003) (cit. on pp. 12, 14).

38. Murie, C., Woody, O., Lee, A. Y. & Nadon, R. Comparison of small n statistical tests of differential expression applied to microarrays. *BMC Bioinformatics* **10,** 45 (2009) (cit. on p. 12).

39. Storey, J. D. & Tibshirani, R. Statistical methods for identifying differentially expressed genes in DNA microarrays. *Methods in Molecular Biology* **224,** 149–157 (2003) (cit. on p. 12).

40. Sreekumar, J. & Jose, K. K. Statistical tests for identification of differentially expressed genes in cDNA microarray experiments. *Indian Journal of Biotechnology* (2008) (cit. on p. 12).

41. Pan, W. A comparative review of statistical methods for discovering differentially expressed genes in replicated microarray experiments. *Bioinformatics* **18,** 546–554 (Apr. 2002) (cit. on p. 12).

42. Hong, F. & Breitling, R. A comparison of meta-analysis methods for detecting differentially expressed genes in microarray experiments. *Bioinformatics* **24,** 374–382 (Feb. 2008) (cit. on p. 12).

43. Bickel, D. R. & Yanofsky, C. M. Validation of differential gene expression algorithms: application comparing fold-change estimation to hypothesis testing. *BMC Bioinformatics* **11,** 63 (2010) (cit. on pp. 12, 16).

44. Kadota, K. & Shimizu, K. Evaluating methods for ranking differentially expressed genes applied to microArray quality control data. *BMC Bioinformatics* **12,** 227 (2011) (cit. on p. 12).

45. Jeffery, I. B., Higgins, D. G. & Culhane, A. C. Comparison and evaluation of methods for generating differentially expressed gene lists from microarray data. *BMC Bioinformatics* **7,** 359 (2006) (cit. on p. 12).

46. Tusher, V. G., Tibshirani, R. & Chu, G. Significance analysis of microarrays applied to the ionizing radiation response. *Proceedings of the National Academy of Sciences* **98,** 5116–5121 (Apr. 2001) (cit. on pp. 13, 15, 61).

47. Tusher, V. G., Tibshirani, R. & Chu, G. Significance analysis of microarrays applied to the ionizing radiation response. *Proceedings of the National Academy of Sciences* **98,** 5116–5121 (Apr. 2001) (cit. on p. 13).

48. Efron, B., Tibshirani, R. & Storey, J. D. Empirical Bayes analysis of a microarray experiment. *Journal of the American Statistical Association* (2001) (cit. on pp. 13–15).

49. Long, A. D. A Bayesian framework for the analysis of microarray expression data: regularized t-test and statistical inferences of gene changes. *Bioinformatics* (2001) (cit. on pp. 13, 62, 63, 190).

50. Fox, R. J. & Dimmic, M. W. A two-sample Bayesian t-test for microarray data. *BMC Bioinformatics* **7,** 126 (2006) (cit. on p. 13).

51. Demissie, M., Calza, S., Mascialino, B. & Pawitan, Y. Unequal group variances in microarray data analyses. *Bioinformatics* **24,** 1168–1174 (May 2008) (cit. on p. 13).

52. Lonnstedt, I. & Speed, T. P. Replicated microarray data. *Statistica Sinica,* 31–46 (2002) (cit. on p. 14).

53. Newton, M. A., Kendziorski, C. M., Richmond, C. S., Blattner, F. R. & Tsui, K. W. On differential variability of expression ratios: improving statistical inference about gene expression changes from microarray data. *Journal of Computational Biology* **8,** 37–52 (2001) (cit. on p. 14).

54. Murie, C. & Nadon, R. A correction for estimating error when using the Local Pooled Error Statistical Test. *Bioinformatics* **24,** 1735–1736 (Aug. 2008) (cit. on p. 14).

55. Jain, N., Thatte, J., Braciale, T., Ley, K. & O'Connell, M. Local-pooled-error test for identifying differentially expressed genes with a small number of replicated microarrays. *Journal of Bacteriology* (2003) (cit. on p. 14).

56. Yu, L., Gulati, P., Fernandez, S., Pennell, M., Kirschner, L. & Jarjoura, D. Fully moderated T-statistic for small sample size gene expression arrays. *Statistical Applications in Genetics and Molecular Biology* **10** (2011) (cit. on p. 14).

57. Astrand, M., Mostad, P. & Rudemo, M. Empirical Bayes models for multiple probe type microarrays at the probe level. *BMC Bioinformatics* **9,** 156 (2008) (cit. on p. 14).

58. Newton, M. A., Noueiry, A., Sarkar, D. & Ahlquist, P. Detecting differential gene expression with a semiparametric hierarchical mixture method. *Biostatistics* **5,** 155–176 (Apr. 2004) (cit. on p. 14).

59. Gottardo, R., Pannucci, J. A., Kuske, C. R. & Brettin, T. Statistical analysis of microarray data: a Bayesian approach. *Biostatistics* **4,** 597–620 (Oct. 2003) (cit. on p. 14).

60. Efron, B. & Tibshirani, R. Empirical bayes methods and false discovery rates for microarrays. *Genetic Epidemiology* **23,** 70–86 (June 2002) (cit. on p. 14).

61. Townsend, J. P. & Hartl, D. L. Bayesian analysis of gene expression levels: statistical quantification of relative mRNA level across multiple strains or treatments. *Genome Biology* (2002) (cit. on p. 14).

62. Sartor, M. A., Tomlinson, C. R., Wesselkamper, S. C., Sivaganesan, S., Leikauf, G. D. & Medvedovic, M. Intensity-based hierarchical Bayes method improves testing for differentially expressed genes in microarray experiments. *BMC Bioinformatics* **7,** 538 (2006) (cit. on p. 14).

63. Smyth, G. K. in *Bioinformatics and Computational Biology Solutions Using R and Bioconductor* (Springer, New York, Jan. 2006) (cit. on pp. 14, 38, 183).

64. Smyth, G. K. Linear models and empirical bayes methods for assessing differential expression in microarray experiments. *Statistical Applications in Genetics and Molecular Biology* **3,** Article3 (2004) (cit. on pp. 14, 38, 62, 63).

65. Qi, Y., Sun, H., Sun, Q. & Pan, L. Ranking analysis for identifying differentially expressed genes. *Genomics* **97,** 326–329 (May 2011) (cit. on p. 15).

66. Breitling, R., Amtmann, A., Armengaud, P. & Herzyk, P. Rank products: a simple, yet powerful, new method to detect differentially regulated genes in replicated microarray experiments. *FEBS Letters* **573,** 83–92 (Aug. 2004) (cit. on p. 15).

67. Breitling, R. & Herzyk, P. Rank-based methods as a non-parametric alternative of the T-statistic for the analysis of biological microarray data. *Journal of Bioinformatics and Computational Biology* **3,** 1171–1189 (Oct. 2005) (cit. on p. 15).

68. Hong, F., Breitling, R., McEntee, C. W., Wittner, B. S., Nemhauser, J. L. & Chory, J. RankProd: a bioconductor package for detecting differentially expressed genes in meta-analysis. *Bioinformatics* **22,** 2825–2827 (Nov. 2006) (cit. on p. 15).

69. Yan, X., Deng, M., Fung, W. K. & Qian, M. Detecting differentially expressed genes by relative entropy. *Journal of Theoretical Biology* **234,** 395–402 (June 2005) (cit. on p. 15).

70. Lu, J., Bushel, P. R., Kerns, R. T. & Peddada, S. D. Principal component analysis-based filtering improves detection for Affymetrix gene expression arrays. *Nucleic Acids Research* **39,** e86–e86 (July 2011) (cit. on p. 16).

71. Clark, N. R., Hu, K. S., Feldmann, A. S., Kou, Y., Chen, E. Y., Duan, Q. & Ma'ayan, A. The characteristic direction: a geometrical approach to identify differentially expressed genes. *BMC Bioinformatics* **15,** 79 (2014) (cit. on p. 16).

72. MAQC Consortium, Schena, M., Frueh, F. W., Thierry-Mieg, D., Canales, R. D., Puri, R., Kawasaki, E., Shi, L., Reid, L. H., Jones, W. D., Shippy, R., Warrington, J. A., Baker, S. C., Collins, P. J., de Longueville, F., Lee, K. Y., Luo, Y., Sun, Y. A., Willey, J. C., Setterquist, R. A., Fischer, G. M., Tong, W., Dragan, Y. P., Dix, D. J., Herman, D., Jensen, R. V., Johnson, C. D., Lobenhofer, E. K., Schrf, U., Thierry-Mieg, J., Wang, C., Wilson, M., Wolber, P. K., Zhang, L., Amur, S., Bao, W., Barbacioru, C. C., Lucas, A. B., Bertholet, V., Boysen, C., Bromley, B., Brown, D., Brunner, A., Cao, X. M., Cebula, T. A., Chen, J. J., Cheng, J., Chu, T.-M., Chudin, E., Corson, J., Corton, J. C., Croner, L. J., Davies, C., Davison, T. S., Delenstarr, G., Deng, X., Dorris, D., Eklund, A. C., Fan, X.-h., Fang, H., Fulmer-Smentek, S. B., Fuscoe, J. C., Gallagher, K., Ge, W., Guo, L., Guo, X., Hager, J., Haje, P. K., Han, J., Han, T., Harbottle, H. C., Harris, S. C., Hatchwell, E., Hauser, C. A., Hester, S., Hong, H., Hurban, P., Jackson, S. A., Ji, H., Knight, C. R., Kuo, W. P., LeClerc, J. E., Levy, S., Li, Q.-Z., Liu, C., Liu, Y., Lombardi, M. J., Ma, Y., Magnuson, S. R., Maqsodi, B., McDaniel, T., Mei, N., Myklebost, O., Ning, B., Novoradovskaya, N., Orr, M. S., Osborn, T. W., Papallo, A., Patterson, T. A., Perkins, R. G., Peters, E. H., Peterson, R., Philips, K. L., Pine, P. S., Pusztai, L., Qian, F., Ren, H., Rosen, M., Rosenzweig, B. A., Samaha, R. R., Schroth, G. P., Shchegrova, S., Smith, D. D., Staedtler, F., Su, Z., Sun, H., Szallasi, Z., Tezak, Z., Thompson, K. L., Tikhonova, I., Turpaz, Y., Vallanat, B., Van, C., Walker, S. J., Wang, S.-J., Wang, Y., Wolfinger, R., Wong, A., Wu, J., Xiao, C., Xie, Q., Xu, J., Yang, W., Zhang, L., Zhong, S., Zong, Y. & Slikker, W. The MicroArray Quality Control (MAQC) project shows inter- and intraplatform reproducibility of gene expression measurements. *Nature Biotechnology* **24,** 1151–1161 (Sept. 2006) (cit. on p. 16).

73. Dembele, D. & Kastner, P. Fold change rank ordering statistics: a new method for detecting differentially expressed genes. *BMC Bioinformatics* **15,** 14 (2014) (cit. on p. 16).

74. Farztdinov, V. & McDyer, F. Distributional fold change test - a statistical approach for detecting differential expression in microarray experiments. *Algorithms for Molecular Biology* **7,** 29 (2012) (cit. on p. 16).

75. Theilhaber, J., Bushnell, S., Jackson, A. & Fuchs, R. Bayesian estimation of fold-changes in the analysis of gene expression: the PFOLD algorithm. *Journal of Computational Biology* **8,** 585–614 (2001) (cit. on p. 16).

76. McCarthy, D. J. & Smyth, G. K. Testing significance relative to a fold-change threshold is a TREAT. *Bioinformatics* **25,** 765–771 (Mar. 2009) (cit. on p. 16).

77. Aston, K. I., Bell, J. L., Stevens, J. R. & White, K. L. A comparison of probe-level and probeset models for small-sample gene expression data. *BMC Bioinformatics* **11,** 281 (2010) (cit. on p. 16).

78. Deng, X., Xu, J., Hui, J. & Wang, C. Probability fold change: a robust computational approach for identifying differentially expressed gene lists. *Computer Methods and Programs in Biomedicine* **93,** 124–139 (Feb. 2009) (cit. on p. 16).

79. Hein, A.-M. K. & Richardson, S. A powerful method for detecting differentially expressed genes from GeneChip arrays that does not require replicates. *BMC Bioinformatics* **7,** 353 (July 2006) (cit. on p. 16).

80. Dave, S. S., Greiner, T. C., Armitage, J. O., Wright, G., Tan, B., Rosenwald, A., Gascoyne, R. D., Chan, W. C., Fisher, R. I., Braziel, R. M., Rimsza, L. M., Grogan, T. M., Miller, T. P., LeBlanc, M., Weisenburger, D. D., Lynch, J. C., Vose, J., Smeland, E. B., Kvaloy, S., Holte, H., Delabie, J., Connors, J. M., Lansdorp, P. M., Ouyang, Q., Lister, T. A., Davies,

A. J., Norton, A. J., Muller-Hermelink, H. K., Ott, G., Campo, E., Montserrat, E., Wilson, W. H., Jaffe, E. S., Simon, R., Yang, L., Powell, J., Zhao, H., Goldschmidt, N., Chiorazzi, M. & Staudt, L. M. Prediction of survival in follicular lymphoma based on molecular features of tumor-infiltrating immune cells. *New England Journal of Medicine* **351,** 2159–2169 (Nov. 2004) (cit. on p. 17).

81. Tibshirani, R. Immune signatures in follicular lymphoma. *New England Journal of Medicine* **352,** pages (Apr. 2005) (cit. on p. 17).

82. Evsikov, A. V. & Solter, D. Comment on " 'Stemness': transcriptional profiling of embryonic and adult stem cells" and "a stem cell molecular signature". *Science* **302,** 393–author reply 393 (Oct. 2003) (cit. on p. 18).

83. Comment on " 'Stemness': transcriptional profiling of embryonic and adult stem cells" and "a stem cell molecular signature". *Science* **302,** 393–author reply 393 (Oct. 2003) (cit. on p. 18).

84. Ivanova, N. B., Dimos, J. T., Schaniel, C., Hackney, J. A., Moore, K. A., Ramalho-Santos, M., Yoon, S., Matsuzaki, Y., Mulligan, R. C., Melton, D. A. & Lemischka, I. R. Response to Comments on " 'Stemness': Transcriptional Profiling of Embryonic and Adult Stem Cells" and "A Stem Cell Molecular Signature". **302,** 393d–393 (Oct. 2003) (cit. on p. 18).

85. Mulligan, R. C., Ramalho-Santos, M., Yoon, S., Matsuzaki, Y. & Melton, D. A. "Stemness": transcriptional profiling of embryonic and adult stem cells. *Science* **298,** 597–600 (Oct. 2002) (cit. on p. 18).

86. Van 't Veer, L. J., Dai, H., van de Vijver, M. J., He, Y. D., Hart, A. A. M., Mao, M., Peterse, H. L., van der Kooy, K., Marton, M. J., Witteveen, A. T., Schreiber, G. J., Kerkhoven, R. M., Roberts, C., Linsley, P. S., Bernards, R. & Friend, S. H. Gene expression profiling predicts clinical outcome of breast cancer. *Nature* **415,** 530–536 (Jan. 2002) (cit. on p. 18).

87. Yeoh, E.-J., Ross, M. E., Shurtleff, S. A., Williams, W. K., Patel, D., Mahfouz, R., Behm, F. G., Raimondi, S. C., Relling, M. V., Patel, A., Cheng, C., Campana, D., Wilkins, D., Zhou, X., Li, J., Liu, H., Pui, C.-H., Evans, W. E., Naeve, C., Wong, L. & Downing, J. R. Classification, subtype discovery, and prediction of outcome in pediatric acute lymphoblastic leukemia by gene expression profiling. *Cancer Cell* **1,** 133–143 (Mar. 2002) (cit. on p. 18).

88. Alizadeh, A. A., Eisen, M. B., Davis, R. E., Ma, C., Lossos, I. S., Rosenwald, A., Boldrick, J. C., Sabet, H., Tran, T., Yu, X., Powell, J. I., Yang, L., Marti, G. E., Moore, T., Hudson, J., Lu, L., Lewis, D. B., Tibshirani, R., Sherlock, G., Chan, W. C., Greiner, T. C., Weisenburger, D. D., Armitage, J. O., Warnke, R., Levy, R., Wilson, W., Grever, M. R., Byrd, J. C., Botstein, D., Brown, P. O. & Staudt, L. M. Distinct types of diffuse large B-cell lymphoma identified by gene expression profiling. *Nature* **403,** 503–511 (Feb. 2000) (cit. on p. 18).

89. Golub, T. R., Slonim, D. K., Tamayo, P., Huard, C., Gaasenbeek, M., Mesirov, J. P., Coller, H., Loh, M. L., Downing, J. R., Caligiuri, M. A., Bloomfield, C. D. & Lander, E. S. Molecular classification of cancer: class discovery and class prediction by gene expression monitoring. *Science* **286,** 531–537 (Oct. 1999) (cit. on p. 18).

90. Perou, C. M., Jeffrey, S. S., Van De Rijn, M., Rees, C. A., Eisen, M. B., Ross, D. T., Pergamenschikov, A., Williams, C. F., Zhu, S. X., Lee, J. C., Lashkari, D., Shalon, D., Brown, P. O. & Botstein, D. Distinctive gene expression patterns in human mammary epithelial cells and breast cancers. *Proceedings of the National Academy of Sciences* **96,** 9212–9217 (Aug. 1999) (cit. on p. 18).

91. Wang, Y., Klijn, J. G. M., Zhang, Y., Sieuwerts, A. M., Look, M. P., Yang, F., Talantov, D., Timmermans, M., Meijer-van Gelder, M. E., Yu, J., Jatkoe, T., Berns, E. M. J. J., Atkins, D. & Foekens, J. A. Gene-expression profiles to predict distant metastasis of lymph-node-negative primary breast cancer. *Lancet* **365,** 671–679 (Feb. 2005) (cit. on p. 18).

92. Van de Vijver, M. J., He, Y. D., van't Veer, L. J., Dai, H., Hart, A. A. M., Voskuil, D. W., Schreiber, G. J., Peterse, J. L., Roberts, C., Marton, M. J., Parrish, M., Atsma, D., Witteveen, A., Glas, A., Delahaye, L., van der Velde, T., Bartelink, H., Rodenhuis, S., Rutgers, E. T., Friend, S. H. & Bernards, R. A gene-expression signature as a predictor of survival in breast cancer. *New England Journal of Medicine* **347,** 1999–2009 (Dec. 2002) (cit. on p. 18).

93. Rosenwald, A., Armitage, J. O., Greiner, T. C., Wright, G., Chan, W. C., Connors, J. M., Campo, E., Fisher, R. I., Gascoyne, R. D., Muller-Hermelink, H. K., Smeland, E. B., Giltnane, J. M., Hurt, E. M., Zhao, H., Averett, L., Yang, L., Wilson, W. H., Jaffe, E. S., Simon, R., Klausner, R. D., Powell, J., Duffey, P. L., Longo, D. L., Weisenburger, D. D., Sanger, W. G., Dave, B. J., Lynch, J. C., Vose, J., Montserrat, E., Lopez-Guillermo, A., Grogan, T. M., Miller, T. P., LeBlanc, M., Ott, G., Kvaloy, S., Delabie, J., Holte, H., Krajci, P., Stokke, T., Staudt, L. M. & Lymphoma/Leukemia Molecular Profiling Project. The use of molecular profiling to predict survival after chemotherapy for diffuse large-B-cell lymphoma. *New England Journal of Medicine* **346,** 1937–1947 (June 2002) (cit. on p. 18).

94. Beer, D. G., Kardia, S. L. R., Huang, C.-C., Giordano, T. J., Levin, A. M., Misek, D. E., Lin, L., Chen, G., Gharib, T. G., Thomas, D. G., Lizyness, M. L., Kuick, R., Hayasaka, S., Taylor, J. M. G., Iannettoni, M. D., Orringer, M. B. & Hanash, S. Gene-expression profiles predict survival of patients with lung adenocarcinoma. *Nature medicine* **8,** 816–824 (Aug. 2002) (cit. on p. 18).

95. Bhattacharjee, A., Richards, W. G., Staunton, J., Li, C., Monti, S., Vasa, P., Ladd, C., Beheshti, J., Bueno, R., Gillette, M., Loda, M., Weber, G., Lander, E. S., Wong, W., Johnson, B. E., Golub, T. R., Sugarbaker, D. J. & Meyerson, M. Classification of human lung carcinomas by mRNA expression profiling reveals distinct adenocarcinoma subclasses. *Proceedings of the National Academy of Sciences of the United States of America* **98,** 13790–13795 (Nov. 2001) (cit. on p. 18).

96. Ramaswamy, S., Ross, K. N., Lander, E. S. & Golub, T. R. A molecular signature of metastasis in primary solid tumors. *Nature genetics* **33,** 49–54 (Jan. 2003) (cit. on p. 18).

97. Mukherjee, S., Califano, A., Pomeroy, S. L., Tamayo, P., Gaasenbeek, M., Sturla, L. M., Angelo, M., McLaughlin, M. E., Kim, J. Y. H., Goumnerova, L. C., Black, P. M., Lau, C., Allen, J. C., Zagzag, D., Olson, J. M., Curran, T., Wetmore, C., Biegel, J. A., Poggio, T., Rifkin, R., Stolovitzky, G., Louis, D. N., Mesirov, J. P., Lander, E. S. & Golub, T. R. Prediction of central nervous system embryonal tumour outcome based on gene expression. *Nature* **415,** 436–442 (Jan. 2002) (cit. on p. 18).

98. Iizuka, N., Oka, M., Yamada-Okabe, H., Nishida, M., Maeda, Y., Mori, N., Takao, T., Tamesa, T., Tangoku, A., Tabuchi, H., Hamada, K., Nakayama, H., Ishitsuka, H., Miyamoto, T., Hirabayashi, A., Uchimura, S. & Hamamoto, Y. Oligonucleotide microarray for prediction of early intrahepatic recurrence of hepatocellular carcinoma after curative resection. *Lancet* **361,** 923–929 (Mar. 2003) (cit. on p. 18).

99. Miklos, G. L. G. & Maleszka, R. Microarray reality checks in the context of a complex disease. *Nature Biotechnology* **22,** 615–621 (May 2004) (cit. on p. 18).

100. Michiels, S., Koscielny, S. & Hill, C. Interpretation of microarray data in cancer. *British Journal of Cancer* **96,** 1155–1158 (Apr. 2007) (cit. on p. 18).

101. Koscielny, S. Why most gene expression signatures of tumors have not been useful in the clinic. *Science translational medicine* **2,** 14ps2–14ps2 (Jan. 2010) (cit. on p. 18).

102. Eden, P., Ritz, C., Rose, C., Ferno, M. & Peterson, C. "Good Old" clinical markers have similar power in breast cancer prognosis as microarray gene expression profilers. *European Journal of Cancer* **40,** 1837–1841 (Aug. 2004) (cit. on p. 18).

103. Ioannidis, J. P. A. Microarrays and molecular research: noise discovery? *Lancet* **365,** 454–455 (Feb. 2005) (cit. on p. 18).

104. Koscielny, S., Michiels, S. & Hill, C. Prediction of cancer outcome with microarrays: a multiple random validation strategy. *Lancet* **365,** 488–492 (Feb. 2005) (cit. on p. 18).

105. Ein-Dor, L., Zuk, O. & Domany, E. Thousands of samples are needed to generate a robust gene list for predicting outcome in cancer. *Proceedings of the National Academy of Sciences of the United States of America* **103,** 5923–5928 (Apr. 2006) (cit. on p. 18).

106. Frantz, S. An array of problems. *Nature Reviews Drug Discovery* **4,** 362–363 (May 2005) (cit. on p. 18).

107. Fan, X., Shi, L., Fang, H., Cheng, Y., Perkins, R. & Tong, W. DNA microarrays are predictive of cancer prognosis: a re-evaluation. *Clinical Cancer Research* **16,** 629–636 (Jan. 2010) (cit. on p. 18).

108. Tong, W. & Fan, X. Statistical Evaluation of Clinical Usefulness of Microarrays for Cancer Prognosis Needs to be Placed in the Context of Clinical Reality—Response. *Clinical Cancer Research* (2010) (cit. on p. 18).

109. Koscielny, S. & Michiels, S. Clinical usefulness of microarrays for cancer prognosis in 2010–letter. *Clinical Cancer Research* **16,** 6180–author reply 6181 (Dec. 2010) (cit. on p. 18).

110. Zhang, M., Yao, C., Guo, Z., Zou, J., Zhang, L., Xiao, H., Wang, D., Yang, D., Gong, X., Zhu, J., Li, Y. & Li, X. Apparently low reproducibility of true differential expression discoveries in microarray studies. *Bioinformatics* **24,** 2057–2063 (Sept. 2008) (cit. on p. 18).

111. Zhang, M., Zhang, L., Zou, J., Yao, C., Xiao, H., Liu, Q., Wang, J., Wang, D., Wang, C. & Guo, Z. Evaluating reproducibility of differential expression discoveries in microarray studies by considering correlated molecular changes. *Bioinformatics* **25,** 1662–1668 (July 2009) (cit. on p. 18).

112. Tan, P. K., Downey, T. J., Spitznagel, E. L., Xu, P., Fu, D., Dimitrov, D. S., Lempicki, R. A., Raaka, B. M. & Cam, M. C. Evaluation of gene expression measurements from commercial microarray platforms. *Nucleic Acids Research* **31,** 5676–5684 (Oct. 2003) (cit. on p. 18).

113. Kuo, W. P., Jenssen, T.-K., Butte, A. J., Ohno-Machado, L. & Kohane, I. S. Analysis of matched mRNA measurements from two different microarray technologies. *Bioinformatics* **18,** 405–412 (Mar. 2002) (cit. on p. 18).

114. Mah, N., Thelin, A., Lu, T., Nikolaus, S., Kuhbacher, T., Gurbuz, Y., Eickhoff, H., Kloppel, G., Lehrach, H., Mellgard, B., Costello, C. M. & Schreiber, S. A comparison of oligonucleotide and cDNA-based microarray systems. *Physiological genomics* **16,** 361–370 (Feb. 2004) (cit. on p. 18).

115. Rogojina, A. T., Orr, W. E., Song, B. K. & Geisert, E. E. Comparing the use of Affymetrix to spotted oligonucleotide microarrays using two retinal pigment epithelium cell lines. *Molecular Vision* **9,** 482–496 (Oct. 2003) (cit. on p. 18).

116. A comparison of cDNA, oligonucleotide, and Affymetrix GeneChip gene expression microarray platforms. *Journal of Biomolecular Techniques* **15,** 276–284 (Dec. 2004) (cit. on p. 18).

117. Li, J., Pankratz, M. & Johnson, J. A. Differential gene expression patterns revealed by oligonucleotide versus long cDNA arrays. *Toxicological Sciences* (2002) (cit. on p. 18).

118. Kothapalli, R., Yoder, S. J. & Mane, S. Microarray results: how accurate are they? *BMC Bioinformatics* (2002) (cit. on p. 18).

119. Shi, L., Goodsaid, F., Frueh, F. W., Puri, R., Tong, W., Fang, H., Scherf, U., Han, J., Guo, L., Su, Z., Han, T., Fuscoe, J. C., Xu, Z. A., Patterson, T. A., Hong, H., Xie, Q., Perkins, R. G., Chen, J. J. & Casciano, D. A. Cross-platform comparability of microarray technology: intra-platform consistency and appropriate data analysis procedures are essential. *BMC Bioinformatics* **6 Suppl 2,** S12 (July 2005) (cit. on p. 18).

120. Lesko, L. J. & Woodcock, J. Translation of pharmacogenomics and pharmacogenetics: a regulatory perspective. *Nature Reviews Drug Discovery* **3,** 763–769 (Sept. 2004) (cit. on p. 18).

121. Frueh, F. W. Impact of microarray data quality on genomic data submissions to the FDA. *Nature Biotechnology* **24,** 1105–1107 (Sept. 2006) (cit. on p. 18).

122. Dix, D. J., Benson, W. H., Gallagher, K., Groskinsky, B. L., McClintock, J. T., Dearfield, K. L. & Farland, W. H. A framework for the use of genomics data at the EPA. *Nature Biotechnology* **24,** 1108–1111 (Sept. 2006) (cit. on p. 18).

123. Shi, L., Tong, W., Goodsaid, F. & Frueh, F. W. QA/QC: challenges and pitfalls facing the microarray community and regulatory agencies. *Expert Review of Molecular Diagnostics* (2004) (cit. on p. 18).

124. Beer, D. G., Dobbin, K. K., Meyerson, M., Yeatman, T. J., Gerald, W. L., Jacobson, J. W., Conley, B., Buetow, K. H., Heiskanen, M., Simon, R. M., Minna, J. D., Girard, L., Misek, D. E., Taylor, J. M. G., Hanash, S., Naoki, K., Hayes, D. N., Ladd-Acosta, C., Enkemann, S. A., Viale, A. & Giordano, T. J. Interlaboratory comparability study of cancer gene expression analysis using oligonucleotide microarrays. *Clinical Cancer Research* **11,** 565–572 (Jan. 2005) (cit. on p. 18).

125. Irizarry, R. a., Warren, D., Spencer, F., Kim, I. F., Biswal, S., Frank, B. C., Gabrielson, E., Garcia, J. G. N., Geoghegan, J., Germino, G., Griffin, C., Hilmer, S. C., Hoffman, E., Jedlicka, A. E., Kawasaki, E., Martinez-Murillo, F., Morsberger, L., Lee, H., Petersen, D., Quackenbush, J., Scott, A., Wilson, M., Yang, Y., Ye, S. Q. & Yu, W. Multiple-laboratory comparison of microarray platforms. *Nature Methods* **2,** 345–350 (May 2005) (cit. on p. 18).

126. Larkin, J. E., Frank, B. C., Gavras, H., Sultana, R. & Quackenbush, J. Independence and reproducibility across microarray platforms. *Nature Methods* **2,** 337–344 (May 2005) (cit. on p. 18).

127. Ulrich, R. G., Rockett, J. C., Gibson, G. G. & Pettit, S. D. Overview of an interlaboratory collaboration on evaluating the effects of model hepatotoxicants on hepatic gene expression. *Environmental Health Perspectives* **112,** 423–427 (Mar. 2004) (cit. on p. 18).

128. Beekman, J. M., Waring, J. F., Ulrich, R. G., Flint, N., Morfitt, D., Kalkuhl, A., Staedtler, F., Lawton, M. & Suter, L. Interlaboratory evaluation of rat hepatic gene expression changes induced by methapyrilene. *Environmental Health Perspectives* **112,** 439–448 (Mar. 2004) (cit. on p. 18).

129. Bammler, T., Bushel, P. R., Beyer, R. P., Bhattacharya, S., Boorman, G. A., Boyles, A., Bradford, B. U., Bumgarner, R. E., Chaturvedi, K., Choi, D., Cunningham, M. L., Deng, S., Dressman, H. K., Fannin, R. D., Farin, F. M., Freedman, J. H., Fry, R. C., Harper, A., Humble, M. C., Hurban, P., Kavanagh, T. J., Kaufmann, W. K., Kerr, K. F., Jing, L., Lapidus, J. A., Lasarev, M. R., Li, J., Li, Y.-J., Lobenhofer, E. K., Lu, X., Malek, R. L., Milton, S., Nagalla, S. R., O'malley, J. P., Palmer, V. S., Pattee, P., Paules, R. S., Perou, C. M., Phillips, K., Qin, L.-X., Qiu, Y., Quigley, S. D., Rodland, M., Rusyn, I., Samson, L. D., Schwartz, D. A., Shi, Y., Shin, J.-L., Sieber, S. O., Slifer, S., Speer, M. C., Spencer, P. S., Sproles, D. I., Swenberg, J. A., Suk, W. A., Sullivan, R. C., Tian, R., Tennant, R. W., Todd, S. A., Tucker, C. J., Van Houten, B., Weis, B. K., Xuan, S., Zarbl, H. & Members of the Toxicogenomics Research Consortium. Standardizing global gene expression analysis between laboratories and across platforms. *Nature Methods* **2,** 351–356 (May 2005) (cit. on p. 18).

130. Kawasaki, E., Petersen, D., Chandramouli, G. V. R., Geoghegan, J., Hilburn, J., Paarlberg, J., Kim, C. H., Munroe, D., Gangi, L., Han, J., Puri, R., Staudt, L., Weinstein, J., Barrett, J. C. & Green, J. Three microarray platforms: an analysis of their concordance in profiling gene expression. *BMC Genomics* **6,** 63 (2005) (cit. on p. 18).

131. Yauk, C. L., Berndt, M. L., Williams, A. & Douglas, G. R. Comprehensive comparison of six microarray technologies. *Nucleic Acids Research* **32,** e124–e124 (2004) (cit. on p. 18).

132. Park, P. J., Cao, Y. A., Lee, S. Y., Kim, J.-W., Chang, M. S., Hart, R. & Choi, S. Current issues for DNA microarrays: platform comparison, double linear amplification, and universal RNA reference. *Journal of Biotechnology* **112,** 225–245 (Sept. 2004) (cit. on p. 18).

133. Yuen, T., Wurmbach, E., Pfeffer, R. L., Ebersole, B. J. & Sealfon, S. C. Accuracy and calibration of commercial oligonucleotide and custom cDNA microarrays. *Nucleic Acids Research* **30,** e48 (May 2002) (cit. on p. 18).

134. Goodsaid, F., Austermiller, B., Canales, R. D., Luo, Y., Willey, J. C., Barbacioru, C. C., Boysen, C., Hunkapiller, K., Jensen, R. V., Knight, C. R., Lee, K. Y., Ma, Y., Maqsodi, B., Papallo, A., Peters, E. H., Poulter, K., Ruppel, P. L., Samaha, R. R., Shi, L., Yang, W. & Zhang, L. Evaluation of DNA microarray results with quantitative gene expression platforms. *Nature Biotechnology* **24,** 1115–1122 (Sept. 2006) (cit. on p. 18).

135. Shippy, R., Thierry-Mieg, D., Fulmer-Smentek, S. B., Jensen, R. V., Jones, W. D., Wolber, P. K., Johnson, C. D., Pine, P. S., Boysen, C., Guo, X., Chudin, E., Sun, Y. A., Willey, J. C., Thierry-Mieg, J., Setterquist, R. A., Wilson, M., Lucas, A. B., Novoradovskaya, N., Papallo, A., Turpaz, Y., Baker, S. C., Warrington, J. A., Shi, L. & Herman, D. Using RNA sample titrations to assess microarray platform performance and normalization techniques. *Nature Biotechnology* **24,** 1123–1131 (Sept. 2006) (cit. on p. 18).

136. Patterson, T. A., Tikhonova, I., Fulmer-Smentek, S. B., Kawasaki, E., Lobenhofer, E. K., Collins, P. J., Chu, T.-M., Bao, W., Fang, H., Hager, J., Walker, S. J., Zhang, L., Hurban, P., de Longueville, F., Fuscoe, J. C., Tong, W., Shi, L. & Wolfinger, R. D. Performance comparison of one-color and two-color platforms within the MicroArray Quality Control (MAQC) project. *Nature Biotechnology* **24,** 1140–1150 (Sept. 2006) (cit. on p. 18).

137. Tong, W., Fan, X., Lucas, A. B., Shippy, R., Fang, H., Hong, H., Orr, M. S., Chu, T.-M., Guo, X., Collins, P. J., Sun, Y. A., Wang, S.-J., Bao, W., Wolfinger, R. D., Shchegrova, S., Guo, L., Warrington, J. A. & Shi, L. Evaluation of external RNA controls for the assessment of microarray performance. *Nature Biotechnology* **24,** 1132–1139 (Sept. 2006) (cit. on p. 18).

138. Guo, L., Goodsaid, F., Lobenhofer, E. K., Wang, C., Shippy, R., Harris, S. C., Zhang, L., Mei, N., Chen, T., Herman, D., Hurban, P., Phillips, K. L., Xu, J., Deng, X., Sun, Y. A., Tong, W., Dragan, Y. P. & Shi, L. Rat toxicogenomic study reveals analytical consistency across microarray platforms. *Nature Biotechnology* **24,** 1162–1169 (Sept. 2006) (cit. on p. 18).

139. Wagenseller, A. G., Shada, A., D'Auria, K. M., Murphy, C., Sun, D., Molhoek, K. R., Papin, J. A., Dutta, A. & Slingluff, C. L. MicroRNAs induced in melanoma treated with combination targeted therapy of Temsirolimus and Bevacizumab. *Journal of Translational Medicine* **11,** 218 (2013) (cit. on pp. 20, 23, 25).

140. Robert, C., Thomas, L., Bondarenko, I., O'Day, S., M D, J. W., Garbe, C., Lebbe, C., Baurain, J.-F., Testori, A., Grob, J.-J., Davidson, N., Richards, J., Maio, M., Hauschild, A., Miller, W. H., Gascon, P., Lotem, M., Harmankaya, K., Ibrahim, R., Francis, S., Chen, T.-T., Humphrey, R., Hoos, A. & Wolchok, J. D. Ipilimumab plus dacarbazine for previously untreated metastatic melanoma. *New England Journal of Medicine* **364,** 2517–2526 (June 2011) (cit. on p. 21).

141. Hodi, F. S., O'Day, S., McDermott, D. F., Weber, R. W., Sosman, J. A., Haanen, J. B., Gonzalez, R., Robert, C., Schadendorf, D., Hassel, J. C., Akerley, W., van den Eertwegh, A. J. M., Lutzky, J., Lorigan, P., Vaubel, J. M., Linette, G. P., Hogg, D., Ottensmeier, C. H., Lebbe, C., Peschel, C., Quirt, I., Clark, J. I., Wolchok, J. D., Weber, J. S., Tian, J., Yellin, M. J., Nichol, G. M., Hoos, A. & Urba, W. J. Improved survival with ipilimumab in patients with metastatic melanoma. *New England Journal of Medicine* **363,** 711–723 (Aug. 2010) (cit. on p. 21).

142. Ko, J. M. & Fisher, D. E. A new era: melanoma genetics and therapeutics. *The Journal of Pathology* **223,** 241–250 (Jan. 2011) (cit. on p. 21).

143. Margolin, K., Baratta, T., Margolin, K. A., Longmate, J., Longmate, J., Synold, T., Synold, T., Christensen, S., Weber, J., Gajewski, T., Quirt, I. & Doroshow, J. H. CCI-779 in metastatic melanoma: a phase II trial of the California Cancer Consortium. *Cancer …* **104,** 1045–1048 (Sept. 2005) (cit. on p. 21).

144. Biber, J. E., Varker, K. A., Kefauver, C., Jensen, R., Lehman, A., Young, D., Wu, H., Lesinski, G. B., Kendra, K., Chen, H. X., Walker, M. J. & Carson, W. E. A randomized phase 2 trial of bevacizumab with or without daily low-dose interferon alfa-2b in metastatic malignant melanoma. *Annals of Surgical Oncology* **14,** 2367–2376 (Aug. 2007) (cit. on p. 21).

145. Schuster, C., Eikesdal, H. P., Puntervoll, H., Geisler, J., Geisler, S., Heinrich, D., Molven, A., Lonning, P. E., Akslen, L. A. & Straume, O. Clinical efficacy and safety of bevacizumab monotherapy in patients with metastatic melanoma: predictive importance of induced early hypertension. *PLoS ONE* **7,** e38364 (2012) (cit. on p. 21).

146. Molhoek, K. R., Griesemann, H., Shu, J., Gershenwald, J. E., Brautigan, D. L. & Slingluff, C. L. Human melanoma cytolysis by combined inhibition of mammalian target of rapamycin and vascular endothelial growth factor/vascular endothelial growth factor receptor-2. *Cancer Research* **68,** 4392–4397 (June 2008) (cit. on pp. 21, 28).

147. Slingluff, C. L., Petroni, G. R., Molhoek, K. R., Brautigan, D. L., Chianese-Bullock, K. A., Shada, A. L., Smolkin, M. E., Olson, W. C., Gaucher, A., Chase, C. M., Grosh, W. W., Weiss, G. R., Wagenseller, A. G., Olszanski, A. J., Martin, L., Shea, S. M., Erdag, G., Ram, P., Gershenwald, J. E. & Weber, M. J. Clinical activity and safety of combination therapy with temsirolimus and bevacizumab for advanced melanoma: a phase II trial (CTEP 7190/Mel47). *Clinical Cancer Research* **19,** 3611–3620 (July 2013) (cit. on p. 21).

148. Pruitt, R. N., Chambers, M. G., Ng, K. K. S., Ohi, M. D. & Lacy, D. B. Structural organization of the functional domains of Clostridium difficile toxins A and B. *Proceedings of the National Academy of Sciences* **107,** 13467–13472 (July 2010) (cit. on p. 29).

149. Pruitt, R. N., Chumbler, N. M., Rutherford, S. A., Farrow, M. A., Friedman, D. B., Spiller, B. & Lacy, D. B. Structural determinants of Clostridium difficile toxin A glucosyltransferase activity. *The Journal of Biological Chemistry* **287,** 8013–8020 (Mar. 2012) (cit. on p. 29).

150. Genisyuerek, S., Aktories, K., Papatheodorou, P., Guttenberg, G., Schubert, R. & Benz, R. Structural determinants for membrane insertion, pore formation and translocation of Clostridium difficile toxin B. *Molecular Microbiology* **79,** 1643–1654 (Mar. 2011) (cit. on pp. 29, 31).

151. Wilm, M., Eichel-Streiber, C. v., Selzer, J. & Rex, G. The enterotoxin from Clostridium difficile (ToxA) monoglucosylates the Rho proteins. *The Journal of Biological Chemistry* (1995) (cit. on pp. 29, 31).

152. Just, I., Eichel-Streiber, C. v., Selzer, J., Wilm, M., Mann, M. & Aktories, K. Glucosylation of Rho proteins by Clostridium difficile toxin B. *Nature* **375,** 500–503 (June 1995) (cit. on pp. 29, 31).

153. Savidge, T., Sun, X. & Feng, H. The enterotoxicity of Clostridium difficile toxins. *Toxins* **2,** 1848–1880 (July 2010) (cit. on pp. 29, 56, 88, 93, 94, 108).

154. El Feghaly, R. E., Haslam, D., Stauber, J. L., Deych, E., Gonzalez, C. & Tarr, P. I. Markers of intestinal inflammation, not bacterial burden, correlate with clinical outcomes in Clostridium difficile infection. *Clinical Infectious Diseases* **56,** 1713–1721 (June 2013) (cit. on pp. 29, 89).

155. Hamre, D. M., Rake, G. & McKee, C. M. The toxicity of penicillin as prepared for clinical use. *The American Journal of Medical Sciences* (1943) (cit. on p. 30).

156. Bartlett, J. G. Historical perspectives on studies of Clostridium difficile and C. difficile infection. *Clinical Infectious Diseases* **46 Suppl 1,** S4–11 (Jan. 2008) (cit. on p. 30).

157. Tedesco, F. J., Barton, R. W. & Alpers, D. H. Clindamycin-associated colitisa prospective study. *Annals of Internal Medicine* (1974) (cit. on pp. 30, 32).

158. Lusk, R. H., Fekety, R., Silva, J., Browne, R. A., Ringler, D. H. & Abrams, G. D. Clindamycin-induced enterocolitis in hamsters. *The Journal of Infectious Diseases* **137,** 464–475 (Apr. 1978) (cit. on p. 31).

159. Chang, T. W., Bartlett, J. G., Gorbach, S. L. & Onderdonk, A. B. Clindamycin-induced enterocolitis in hamsters as a model of pseudomembranous colitis in patients. *Infection and Immunity* **20,** 526–529 (May 1978) (cit. on p. 31).

160. Browne, R. A., Fekety, R., Silva, J., Boyd, D. I., Work, C. O. & Abrams, G. D. The protective effect of vancomycin on clindamycin-induced colitis in hamsters. *The Johns Hopkins Medical Journal* **141,** 183–192 (Oct. 1977) (cit. on p. 31).

161. Fekety, R., Silva, J., Toshniwal, R., Allo, M., Armstrong, J., Browne, R., Ebright, J. & Rifkin, G. Antibiotic-associated colitis: effects of antibiotics on Clostridium difficile and the disease in hamsters. *Reviews of infectious diseases* **1,** 386–397 (Mar. 1979) (cit. on p. 31).

162. Ebright, J., Fekety, R. & Silva, J. Evaluation of eight cephalosporins in hamster colitis model. *Antimicrobial Agents and Chemotherapy* (1981) (cit. on p. 31).

163. Taylor, N. S., Thorne, G. M. & Bartlett, J. G. Comparison of two toxins produced by Clostridium difficile. *Infection and Immunity* **34,** 1036–1043 (Dec. 1981) (cit. on pp. 31, 55, 56).

164. Bartlett, J. G., Chang, T. W., Gurwith, M., Gorbach, S. L. & Onderdonk, A. B. Antibiotic-associated pseudomembranous colitis due to toxin-producing clostridia. *New England Journal of Medicine* **298,** 531–534 (Mar. 1978) (cit. on p. 31).

165. Bartlett, J. G., Onderdonk, A. B., Cisneros, R. L. & Kasper, D. L. Clindamycin-associated colitis due to a toxin-producing species of Clostridium in hamsters. *The Journal of Infectious Diseases* **136,** 701–705 (Nov. 1977) (cit. on pp. 31, 55).

166. Lusk, R. H., Fekety, F. R., Silva, J., Bodendorfer, T., Devine, B. J., Kawanishi, H., Korff, L., Nakauchi, D., Rogers, S. & Siskin, S. B. Gastrointestinal side effects of clindamycin and ampicillin therapy. *The Journal of Infectious Diseases* **135 Suppl,** S111–9 (Mar. 1977) (cit. on p. 31).

167. Keighley, M. R., Burdon, D. W., Arabi, Y., Williams, J. A., Thompson, H., Youngs, D., Johnson, M., Bentley, S., George, R. H. & Mogg, G. A. Randomised controlled trial of vancomycin for pseudomembranous colitis and postoperative diarrhoea. *British Medical Journal* **2,** 1667–1669 (Dec. 1978) (cit. on p. 31).

168. Eichel-Streiber, C. v., Laufenberg-Feldmann, R., Sartingen, S., Schulze, J. & Sauerborn, M. Comparative sequence analysis of the Clostridium difficile toxins A and B. *Molecular and General Genetics* **233,** 260–268 (May 1992) (cit. on pp. 31, 55).

169. Eichel-Streiber, C. v. & Sauerborn, M. Clostridium difficile toxin A carries a C-terminal repetitive structure homologous to the carbohydrate binding region of streptococcal glycosyltransferases. *Gene* **96,** 107–113 (Nov. 1990) (cit. on p. 31).

170. Eichel-Streiber, C. v., Sauerborn, M. & Kuramitsu, H. K. Evidence for a modular structure of the homologous repetitive C-terminal carbohydrate-binding sites of Clostridium difficile toxins and Streptococcus mutans glucosyltransferases. *Journal of Bacteriology* **174,** 6707–6710 (Oct. 1992) (cit. on p. 31).

171. Ho, J. G. S., Greco, A., Rupnik, M. & Ng, K. K. S. Crystal structure of receptor-binding C-terminal repeats from Clostridium difficile toxin A. *Proceedings of the National Academy of Sciences of the United States of America* **102,** 18373–18378 (Dec. 2005) (cit. on p. 31).

172. Greco, A., Ho, J. G. S., Lin, S.-J., Palcic, M. M., Rupnik, M. & Ng, K. K. S. Carbohydrate recognition by Clostridium difficile toxin A. *Nature Structural & Molecular Biology* **13,** 460–461 (May 2006) (cit. on p. 31).

173. Frisch, C., Hoffmann, F., Gerhard, R. & Aktories, K. The complete receptor-binding domain of Clostridium difficile toxin A is required for endocytosis. *Biochemical and Biophysical Research Communications* (2003) (cit. on pp. 31, 36, 107).

174. Yeh, C.-Y., Lin, C.-N., Chang, C.-F., Lin, C.-H., Lien, H.-T., Chen, J.-Y. & Chia, J.-S. C-terminal repeats of Clostridium difficile toxin A induce production of chemokine and adhesion molecules in endothelial cells and promote migration of leukocytes. *Infection and Immunity* **76,** 1170–1178 (Mar. 2008) (cit. on p. 31).

175. Castagliuolo, I., Anderluh, G., Zemljic, M., Rupnik, M., Scarpa, M. & Palu, G. Repetitive domain of Clostridium difficile toxin B exhibits cytotoxic effects on human intestinal epithelial cells and decreases epithelial barrier function. *Anaerobe* **16,** 527–532 (Oct. 2010) (cit. on p. 31).

176. Aktories, K., Papatheodorou, P., Zamboglou, C., Genisyuerek, S. & Guttenberg, G. Clostridial glucosylating toxins enter cells via clathrin-mediated endocytosis. *PLoS ONE* **5,** e10673 (2010) (cit. on pp. 31, 36).

177. Qa'Dan, M., Spyres, L. M. & Ballard, J. D. pH-Induced Conformational Changes inClostridium difficile Toxin B. *Infection and Immunity* (2000) (cit. on p. 31).

178. Egerer, M., Aktories, K., Giesemann, T., Jank, T. & Satchell, K. J. F. Auto-catalytic cleavage of Clostridium difficile toxins A and B depends on cysteine protease activity. *The Journal of Biological Chemistry* **282,** 25314–25321 (Aug. 2007) (cit. on pp. 31, 36).

179. Barth, H., Pfeifer, G., Busch, C., Aktories, K., Schirmer, J., Leemhuis, J. & Meyer, D. K. Cellular uptake of Clostridium difficile toxin B. Translocation of the N-terminal catalytic domain into the cytosol of eukaryotic cells. *The Journal of Biological Chemistry* **278,** 44535–44541 (Nov. 2003) (cit. on p. 31).

180. Lyerly, D. M., Krivan, H. C. & Wilkins, T. D. Clostridium difficile: its disease and toxins. *Clinical Microbiology Reviews* (1988) (cit. on p. 32).

181. Kelly, C., Becker, S., Linevsky, J. K., Joshi, M. A., O'Keane, J. C., Dickey, B. F., LaMont, J. T. & Pothoulakis, C. Neutrophil recruitment in Clostridium difficile toxin A enteritis in the rabbit. *Journal of Clinical Investigation* **93,** 1257–1265 (Mar. 1994) (cit. on pp. 32, 57, 89, 93, 108).

182. Ackermann, M. & Strimmer, K. A general modular framework for gene set enrichment analysis. *BMC Bioinformatics* **10,** 47 (2009) (cit. on pp. 33, 63).

183. Huang, D. W., Sherman, B. T. & Lempicki, R. A. Bioinformatics enrichment tools: paths toward the comprehensive functional analysis of large gene lists. *Nucleic Acids Research* **37,** 1–13 (Jan. 2009) (cit. on p. 33).

184. Abatangelo, L., Maglietta, R., Distaso, A., D'Addabbo, A., Creanza, T. M., Mukherjee, S. & Ancona, N. Comparative study of gene set enrichment methods. *BMC Bioinformatics* **10,** 275 (2009) (cit. on p. 33).

185. Van den Berg, B. H. J., Thanthiriwatte, C., Manda, P. & Bridges, S. M. Comparing gene annotation enrichment tools for functional modeling of agricultural microarray data. *BMC Bioinformatics* **10 Suppl 11,** S9 (2009) (cit. on p. 33).

186. Adewale, A. J., Dinu, I., Liu, Q., Potter, J. D., Jhangri, G. S., Mueller, T., Einecke, G., Famulsky, K., Halloran, P. & Yasui, Y. A biological evaluation of six gene set analysis methods for identification of differentially expressed pathways in microarray data. *Cancer Informatics* **6,** 357–368 (2008) (cit. on p. 33).

187. Freeman, J., Bauer, M. P., Baines, S. D., Corver, J., Fawley, W. N., Goorhuis, B., Kuijper, E. J. & Wilcox, M. H. The changing epidemiology of Clostridium difficile infections. *Clinical Microbiology Reviews* **23,** 529–549 (July 2010) (cit. on p. 36).

188. Warny, M., Pepin, J., Fang, A., Killgore, G. E., Thompson, A., Brazier, J., Frost, E. & Mcdonald, L. C. Toxin production by an emerging strain of Clostridium difficile associated with outbreaks of severe disease in North America and Europe. *Lancet* **366,** 1079–1084 (Sept. 2005) (cit. on p. 36).

189. Zilberberg, M. D., Shorr, A. F. & Kollef, M. H. Increase in adult Clostridium difficile-related hospitalizations and case-fatality rate, United States, 2000-2005. *Emerging Infectious Diseases* **14,** 929–931 (June 2008) (cit. on p. 36).

190. Dubberke, E. R. & Wertheimer, A. I. Review of current literature on the economic burden of Clostridium difficile infection. *Infection Control and Hospital Epidemiology* **30,** 57–66 (Jan. 2009) (cit. on p. 36).

191. Eichel-Streiber, C. v., Nusrat, A., Turner, J. R., Verkade, P., Madara, J. L. & Parkos, C. A. Clostridium difficile toxins disrupt epithelial barrier function by altering membrane microdomain localization of tight junction proteins. *Infection and Immunity* **69,** 1329–1336 (Mar. 2001) (cit. on pp. 36, 45).

192. Tompkins, W. A., Watrach, A. M., Schmale, J. D., Schultz, R. M. & Harris, J. A. Cultural and antigenic properties of newly established cell strains derived from adenocarcinomas of the human colon and rectum. *Journal of the National Cancer Institute* **52,** 1101–1110 (Apr. 1974) (cit. on p. 36).

193. Comer, J. E., Galindo, C. L., Chopra, A. K. & Peterson, J. W. GeneChip analyses of global transcriptional responses of murine macrophages to the lethal toxin of Bacillus anthracis. *Infection and Immunity* **73,** 1879–1885 (Mar. 2005) (cit. on p. 36).

194. Bush, K. L., Comer, J. E., Galindo, C. L., Zhang, F., Wenglikowski, A. M., Garner, H. R., Peterson, J. W. & Chopra, A. K. Murine macrophage transcriptional and functional responses to Bacillus anthracis edema toxin. *Microbial Pathogenesis* **41,** 96–110 (Aug. 2006) (cit. on p. 36).

195. Blankenhorn, E. P., Lu, C., Pelech, S., Zhang, H., Bond, J., Spach, K., Noubade, R. & Teuscher, C. Pertussis toxin induces angiogenesis in brain microvascular endothelial cells. *Journal of Neuroscience Research* **86,** 2624–2640 (Sept. 2008) (cit. on p. 36).

196. Leyva-Illades, D., Cherla, R. P., Galindo, C. L., Chopra, A. K. & Tesh, V. L. Global transcriptional response of macrophage-like THP-1 cells to Shiga toxin type 1. *Infection and Immunity* **78,** 2454–2465 (June 2010) (cit. on p. 36).

197. Nougayrede, J.-P., Taieb, F., De Rycke, J. & Oswald, E. Cyclomodulins: bacterial effectors that modulate the eukaryotic cell cycle. *Trends in Microbiology* **13,** 103–110 (Mar. 2005) (cit. on p. 37).

198. Fiorentini, C., Fabbri, A., Falzano, L., Fattorossi, A., Matarrese, P., Rivabene, R. & Donelli, G. Clostridium difficile toxin B induces apoptosis in intestinal cultured cells. *Infection and Immunity* **66,** 2660–2665 (June 1998) (cit. on pp. 37, 50).

199. Kim, H., Pothoulakis, C., LaMont, J. T., Savidge, T., Rhee, S. H., Kokkotou, E., Na, X. & Moyer, M. P. Clostridium difficile toxin A regulates inducible cyclooxygenase-2 and prostaglandin E2 synthesis in colonocytes via reactive oxygen species and activation of p38 MAPK. *The Journal of Biological Chemistry* **280,** 21237–21245 (June 2005) (cit. on pp. 37, 48, 50).

200. Just, I., Gerhard, R., Nottrott, S., Schoentaube, J., Tatge, H. & Olling, A. Glucosylation of Rho GTPases by Clostridium difficile toxin A triggers apoptosis in intestinal epithelial cells. *Journal of Medical Microbiology* **57,** 765–770 (June 2008) (cit. on pp. 37, 45, 48, 50, 94).

201. Nottrott, S., Just, I., Gerhard, R., Schoentaube, J. & Genth, H. Clostridium difficile toxin A-induced apoptosis is p53-independent but depends on glucosylation of Rho GTPases. *Apoptosis* **12,** 1443–1453 (Aug. 2007) (cit. on pp. 37, 48, 50).

202. Apweiler, R., Binns, D., Barrell, D., Dimmer, E., Huntley, R. P. & O'Donovan, C. The GOA database in 2009–an integrated Gene Ontology Annotation resource. *Nucleic Acids Research* **37,** D396–403 (Jan. 2009) (cit. on p. 38).

203. Alexa, A., Rahnenfuhrer, J. & Lengauer, T. Improved scoring of functional groups from gene expression data by decorrelating GO graph structure. *Bioinformatics* **22,** 1600–1607 (July 2006) (cit. on pp. 38, 43).

204. Basiji, D., Hall, B. E., George, T. C., Lynch, D. H., Ortyn, W. E., Perry, D. J., Seo, M. J., Zimmerman, C. A. & Morrissey, P. J. Distinguishing modes of cell death using the ImageStream multispectral imaging flow cytometer. *Cytometry. Part A.* **59,** 237–245 (June 2004) (cit. on p. 38).

205. George, T. C., Henery, S., Basiji, D., Hall, B. E., Ortyn, W. & Morrissey, P. Quantitative image based apoptotic index measurement using multispectral imaging flow cytometry: a comparison with standard photometric methods. *Apoptosis* **13,** 1054–1063 (Aug. 2008) (cit. on p. 38).

206. Eichel-Streiber, C. v., Chaves-Olarte, E., Weidmann, M. & Thelestam, M. Toxins A and B from Clostridium difficile differ with respect to enzymatic potencies, cellular substrate specificities, and surface binding to cultured cells. *Journal of Clinical Investigation* **100,** 1734–1741 (Oct. 1997) (cit. on pp. 40, 50, 55, 105).

207. Resnik, P. Semantic similarity in a taxonomy: An information-based measure and its application to problems of ambiguity in natural language. *Journal of Artificial Intelligence Research* **11,** 95–130 (1999) (cit. on p. 43).

208. Ballard, J. D., Qa'Dan, M., Ramsey, M., Daniel, J., Spyres, L. M., Safiejko-Mroczka, B. & Ortiz-Leduc, W. Clostridium difficile toxin B activates dual caspase-dependent and caspase-independent apoptosis in intoxicated cells. *Cellular Microbiology* **4,** 425–434 (2002) (cit. on p. 45).

209. Alcantara-Warren, C., Brito, G. A. C., Carneiro, B. A., Fujii, J., Oria, R. B., Lima, A. A. M., Obrig, T. & Guerrant, R. L. Caspase and bid involvement in Clostridium difficile toxin A-induced apoptosis and modulation of toxin A effects by glutamine and alanyl-glutamine in vivo and in vitro. *Infection and Immunity* **74,** 81–87 (Jan. 2006) (cit. on p. 45).

210. Brito, G. A. C., Carneiro-Filho, B. A., Fujji, J., Lima, A. A. M., Obrig, T. & Guerrant, R. L. Mechanism of Clostridium difficile toxin A-induced apoptosis in T84 cells. *The Journal of Infectious Diseases* **186,** 1438–1447 (Nov. 2002) (cit. on p. 45).

211. Falzano, L., Matarrese, P., Popoff, M. R., Fabbri, A., Gambardella, L., Frank, C., Geny, B., Malorni, W. & Fiorentini, C. Clostridium difficile toxin B causes apoptosis in epithelial cells by thrilling mitochondria. Involvement of ATP-sensitive mitochondrial potassium channels. *The Journal of Biological Chemistry* **282,** 9029–9041 (Mar. 2007) (cit. on p. 45).

212. Hagen, S., He, D., Pothoulakis, C., Chen, M., Medina, N. D., Warny, M. & LaMont, J. T. Clostridium difficile toxin A causes early damage to mitochondria in cultured cells. *Gastroenterology* **119,** 139–150 (July 2000) (cit. on p. 45).

213. He, D., Sougioultzis, S., Hagen, S., Liu, J. & Keates, S. Clostridium difficile toxin A triggers human colonocyte IL-8 release via mitochondrial oxygen radical generation. *Gastroenterology* (2002) (cit. on p. 45).

214. Qiu, B., Pothoulakis, C., Castagliuolo, I., Nikulasson, S. & LaMont, J. T. Participation of reactive oxygen metabolites in Clostridium difficile toxin A-induced enteritis in rats. *The American Journal of Physiology* **276,** G485–90 (Feb. 1999) (cit. on p. 45).

215. Flegel, W. A., Muller, F., Daubener, W., Fischer, H. G., Hadding, U. & Northoff, H. Cytokine response by human monocytes to Clostridium difficile toxin A and toxin B. *Infection and Immunity* **59,** 3659–3666 (Oct. 1991) (cit. on p. 45).

216. Gerhard, R., Meyer, G. K. A., Just, I., Neetz, A., Brandes, G., Tsikas, D. & Butterfield, J. H. Clostridium difficile toxins A and B directly stimulate human mast cells. *Infection and Immunity* **75,** 3868–3876 (Aug. 2007) (cit. on pp. 45, 108).

217. Lee, J. Y., Park, H. R., Oh, Y.-K., Kim, Y.-J., Youn, J., Han, J.-S. & Kim, J. M. Effects of transcription factor activator protein-1 on interleukin-8 expression and enteritis in response to Clostridium difficile toxin A. *Journal of Molecular Medicine* **85,** 1393–1404 (Dec. 2007) (cit. on p. 45).

218. Na, X., Zhao, D., Koon, H. W., Kim, H., Husmark, J. & Moyer, M. P. Clostridium difficile toxin B activates the EGF receptor and the ERK/MAP kinase pathway in human colonocytes. *Gastroenterology* (2005) (cit. on p. 45).

219. Murray, A. W. Recycling the cell cycle: cyclins revisited. *Cell* **116,** 221–234 (Jan. 2004) (cit. on p. 45).

220. Denicourt, C. & Dowdy, S. F. Cip/Kip proteins: more than just CDKs inhibitors. *Genes & Development* **18,** 851–855 (Apr. 2004) (cit. on p. 45).

221. Inhibition of cytokinesis by Clostridium difficile toxin B and cytotoxic necrotizing factors–reinforcing the critical role of RhoA in cytokinesis. *Cell Motility and the Cytoskeleton* **66,** 967–975 (Nov. 2009) (cit. on pp. 48, 50).

222. Riegler, M., Sedivy, R., Pothoulakis, C., Hamilton, G., Zacherl, J., Bischof, G., Cosentini, E., Feil, W., Schiessel, R. & LaMont, J. T. Clostridium difficile toxin B is more potent than toxin A in damaging human colonic epithelium in vitro. *Journal of Clinical Investigation* **95,** 2004–2011 (May 1995) (cit. on p. 50).

223. Kuehne, S. A., Cartman, S. T., Heap, J. T., Kelly, M. L., Cockayne, A. & Minton, N. P. The role of toxin A and toxin B in Clostridium difficile infection. *Nature* **467,** 711–713 (Oct. 2010) (cit. on pp. 50, 55, 105).

224. Lyras, D., O'Connor, J. R., Howarth, P. M., Sambol, S. P., Carter, G. P., Phumoonna, T., Poon, R., Adams, V., Vedantam, G., Johnson, S., Gerding, D. N. & Rood, J. I. Toxin B is essential for virulence of Clostridium difficile. *Nature* **458,** 1176–1179 (Apr. 2009) (cit. on pp. 50, 55, 56, 105).

225. Janvilisri, T., Scaria, J. & Chang, Y.-F. Transcriptional profiling of Clostridium difficile and Caco-2 cells during infection. *Journal of Infectious Diseases* **202,** 282–290 (July 2010) (cit. on p. 50).

226. Ameyar, M., Wisniewska, M. & Weitzman, J. B. A role for AP-1 in apoptosis: the case for and against. *Biochimie* **85,** 747–752 (Aug. 2003) (cit. on p. 51).

227. Welsh, C. F., Roovers, K., Villanueva, J., Liu, Y., Schwartz, M. A. & Assoian, R. K. Timing of cyclin D1 expression within G1 phase is controlled by Rho. *Nature Cell Biology* **3,** 950–957 (Nov. 2001) (cit. on p. 51).

228. Huelsenbeck, J., Just, I., Gerhard, R., Barth, H., Dreger, S. & Genth, H. Difference in the cytotoxic effects of toxin B from Clostridium difficile strain VPI 10463 and toxin B from variant Clostridium difficile strain 1470. *Infection and Immunity* **75,** 801–809 (Feb. 2007) (cit. on p. 51).

229. Kim, M., Ashida, H., Ogawa, M., Yoshikawa, Y., Mimuro, H. & Sasakawa, C. Bacterial interactions with the host epithelium. *Cell Host & Microbe* **8,** 20–35 (July 2010) (cit. on p. 52).

230. Kolling, G. L., D'Auria, K. M., Donato, G. M., Gray, M. C., Warren, C. A., Cave, L. M., Solga, M. D., Lannigan, J. A., Papin, J. A. & Hewlett, E. L. Systems analysis of the transcriptional response of human ileocecal epithelial cells to Clostridium difficile toxins and effects on cell cycle control. *BMC Systems Biology* **6,** 2 (2012) (cit. on pp. 52, 56, 66, 73, 82, 94, 193).

231. Blanpain, C. & Simons, B. D. Unravelling stem cell dynamics by lineage tracing. *Nature Reviews Molecular Cell Biology* **14,** 489–502 (Aug. 2013) (cit. on p. 53).

232. Barker, N., van Oudenaarden, A. & Clevers, H. Identifying the stem cell of the intestinal crypt: strategies and pitfalls. *Cell Stem Cell* **11,** 452–460 (Oct. 2012) (cit. on p. 53).

233. Sakaue-Sawano, A., Kurokawa, H., Morimura, T., Hanyu, A., Hama, H., Osawa, H., Kashiwagi, S., Fukami, K., Miyata, T., Miyoshi, H., Imamura, T., Ogawa, M., Masai, H. & Miyawaki, A. Visualizing spatiotemporal dynamics of multicellular cell-cycle progression. *Cell* **132,** 487–498 (Feb. 2008) (cit. on p. 53).

234. Ghantoji, S. S., Sail, K., Lairson, D. R., DuPont, H. L. & Garey, K. W. Economic healthcare costs of Clostridium difficile infection: a systematic review. *The Journal of Hospital Infection* **74,** 309–318 (Apr. 2010) (cit. on p. 54).

235. McGlone, S. M., Bailey, R. R., Zimmer, S. M., Popovich, M. J., Tian, Y., Ufberg, P., Muder, R. R. & Lee, B. Y. The economic burden of Clostridium difficile. *Clinical Microbiology and Infection* **18,** 282–289 (Mar. 2012) (cit. on p. 54).

236. Dubberke, E. R. & Olsen, M. A. Burden of Clostridium difficile on the healthcare system. *Clinical Infectious Diseases* **55 Suppl 2,** S88–92 (Aug. 2012) (cit. on p. 54).

237. Libby, J. M., Jortner, B. S. & Wilkins, T. D. Effects of the two toxins of Clostridium difficile in antibiotic-associated cecitis in hamsters. *Infection and Immunity* **36,** 822–829 (May 1982) (cit. on pp. 55, 56, 84, 105).

238. Jank, T. & Aktories, K. Structure and mode of action of clostridial glucosylating toxins: the ABCD model. *Trends in Microbiology* **16,** 222–229 (May 2008) (cit. on p. 55).

239. Carter, G. P., Rood, J. I. & Lyras, D. The role of toxin A and toxin B in the virulence of Clostridium difficile. *Trends in Microbiology* **20,** 21–29 (Jan. 2012) (cit. on p. 55).

240. Drudy, D., Fanning, S. & Kyne, L. Toxin A-negative, toxin B-positive Clostridium difficile. *International Journal of Infectious Diseases* **11,** 5–10 (Jan. 2007) (cit. on p. 55).

241. Small, J. D. Fatal enterocolitis in hamsters given lincomycin hydrochloride. *Laboratory Animal Care* **18,** 411–420 (Aug. 1968) (cit. on p. 55).

242. Lyerly, D. M., Saum, K. E., MacDonald, D. K. & Wilkins, T. D. Effects of Clostridium difficile toxins given intragastrically to animals. *Infection and Immunity* **47,** 349–352 (Feb. 1985) (cit. on pp. 56, 84, 105).

243. Savidge, T., Pothoulakis, C., O'Brien, M., Pan, W.-H., Newman, P. & Anton, P. M. Clostridium difficile toxin B is an inflammatory enterotoxin in human intestine. *Gastroenterology* **125,** 413–420 (Aug. 2003) (cit. on p. 56).

244. Rolfe, R. D. Binding kinetics of Clostridium difficile toxins A and B to intestinal brush border membranes from infant and adult hamsters. *Infection and Immunity* **59,** 1223–1230 (Apr. 1991) (cit. on pp. 56, 84, 86, 105).

245. Krivan, H. C., Clark, G. F., Smith, D. F. & Wilkins, T. D. Cell surface binding site for Clostridium difficile enterotoxin: evidence for a glycoconjugate containing the sequence Gal alpha 1-3Gal beta 1-4GlcNAc. *Infection and Immunity* **53,** 573–581 (Sept. 1986) (cit. on p. 56).

246. Tucker, K. D. & Wilkins, T. D. Toxin A of Clostridium difficile binds to the human carbohydrate antigens I, X, and Y. *Infection and Immunity* **59,** 73–78 (Jan. 1991) (cit. on p. 56).

247. Rolfe, R. D. & Song, W. Immunoglobulin and non-immunoglobulin components of human milk inhibit Clostridium difficile toxin A-receptor binding. *Journal of Medical Microbiology* **42,** 10–19 (Jan. 1995) (cit. on p. 56).

248. Kelly, C., Pothoulakis, C., Gilbert, R. J., Cladaras, C., Castagliuolo, I., Semenza, G., Hitti, Y., Montcrief, J. S., Linevsky, J., Nikulasson, S., Desai, H. P., Wilkins, T. D. & LaMont, J. T. Rabbit sucrase-isomaltase contains a functional intestinal receptor for Clostridium difficile toxin A. *Journal of Clinical Investigation* **98,** 641–649 (Aug. 1996) (cit. on p. 56).

249. Kelly, C., Pothoulakis, C., Galili, U. & Castagliuolo, I. A human antibody binds to alpha-galactose receptors and mimics the effects of Clostridium difficile toxin A in rat colon. *Gastroenterology* (1996) (cit. on p. 56).

250. Na, X., LaMont, J. T., Pothoulakis, C., Kim, H. & Moyer, M. P. gp96 is a human colonocyte plasma membrane binding protein for Clostridium difficile toxin A. *Infection and Immunity* **76,** 2862–2871 (July 2008) (cit. on pp. 56, 87).

251. Armstrong, J., El-Hawiet, A., Kitova, E. N., Kitov, P. I., Eugenio, L., Ng, K. K. S., Mulvey, G. L., Dingle, T. C., Szpacenko, A. & Klassen, J. S. Binding of Clostridium difficile toxins to human milk oligosaccharides. *Glycobiology* **21,** 1217–1227 (Sept. 2011) (cit. on p. 56).

252. Madan, R. & Jr, W. A. P. Immune responses to Clostridium difficile infection. *Trends in Molecular Medicine* **18,** 658–666 (Nov. 2012) (cit. on p. 56).

253. Steele, J., Chen, K., Sun, X., Zhang, Y., Wang, H., Tzipori, S. & Feng, H. Systemic dissemination of Clostridium difficile toxins A and B is associated with severe, fatal disease in animal models. *Journal of Infectious Diseases* **205,** 384–391 (Feb. 2012) (cit. on pp. 57, 86, 89).

254. Morteau, O., Pothoulakis, C., Gerard, N. P., Castagliuolo, I., Gerard, C., Mykoniatis, A., Zacks, J., Wlk, M. & Lu, B. Genetic deficiency in the chemokine receptor CCR1 protects against acute Clostridium difficile toxin A enteritis in mice. *Gastroenterology* **122,** 725–733 (Mar. 2002) (cit. on pp. 57, 88, 89).

255. Kokkotou, E., Espinoza, D. O., Torres, D., Karagiannides, I., Kosteletos, S., Savidge, T., O'Brien, M. & Pothoulakis, C. Melanin-concentrating hormone (MCH) modulates C difficile toxin A-mediated enteritis in mice. *Gut* **58,** 34–40 (Jan. 2009) (cit. on pp. 57, 89).

256. Ishida, Y., Maegawa, T., Kondo, T., Kimura, A., Iwakura, Y., Nakamura, S. & Mukaida, N. Essential involvement of IFN-gamma in Clostridium difficile toxin A-induced enteritis. *Journal of Immunology* **172,** 3018–3025 (Mar. 2004) (cit. on pp. 57, 86, 89).

257. Kelly, C., Castagliuolo, I., Keates, A. C., Wang, C. C., Pasha, A., Valenick, L., Nikulasson, S. T., LaMont, J. T. & Pothoulakis, C. Clostridium difficile toxin A stimulates macrophage-inflammatory protein-2 production in rat intestinal epithelial cells. *Journal of Immunology* **160,** 6039–6045 (June 1998) (cit. on pp. 57, 88, 89, 94).

258. Kelly, C., Warny, M., Keates, A. C., Keates, S., Castagliuolo, I., Zacks, J. K., Aboudola, S., Qamar, A., Pothoulakis, C. & LaMont, J. T. p38 MAP kinase activation by Clostridium difficile toxin A mediates monocyte necrosis, IL-8 production, and enteritis. *Journal of Clinical Investigation* **105,** 1147–1156 (Apr. 2000) (cit. on pp. 57, 89).

259. Brito, G. A. C., Alcantara-Warren, C., Carneiro-Filho, B. A., Jin, X. H., Barrett, L. J., Carey, R. M. & Guerrant, R. L. Angiotensin II subtype 1 receptor blockade inhibits Clostridium difficile toxin A-induced intestinal secretion in a rabbit model. *Journal of Infectious Diseases* **191,** 2090–2096 (June 2005) (cit. on pp. 57, 89).

260. Becker, S. M., Cho, K.-N., Guo, X., Fendig, K., Oosman, M. N., Whitehead, R., Cohn, S. M. & Houpt, E. R. Epithelial cell apoptosis facilitates Entamoeba histolytica infection in the gut. *The American Journal of Pathology* **176,** 1316–1322 (Mar. 2010) (cit. on pp. 58, 95).

261. Pawlowski, S. W., Calabrese, G., Kolling, G. L., Platts-Mills, J., Freire, R., Alcantara-Warren, C., Liu, B., Sartor, R. B. & Guerrant, R. L. Murine model of Clostridium difficile infection with aged gnotobiotic C57BL/6 mice and a BI/NAP1 strain. *Journal of Infectious Diseases* **202,** 1708–1712 (Dec. 2010) (cit. on p. 58).

262. Albert, E. J., Duplisea, J., Dawicki, W., Haidl, I. D. & Marshall, J. S. Tissue eosinophilia in a mouse model of colitis is highly dependent on TLR2 and independent of mast cells. *The American Journal of Pathology* **178,** 150–160 (Jan. 2011) (cit. on p. 58).

263. Ballman, K. V., Grill, D. E., Oberg, A. L. & Therneau, T. M. Faster cyclic loess: normalizing RNA arrays via linear models. *Bioinformatics* **20,** 2778–2786 (Nov. 2004) (cit. on p. 61).

264. Wang, Y., Kawasaki, E., Miao, Z.-H., Pommier, Y. & Player, A. Characterization of mismatch and high-signal intensity probes associated with Affymetrix genechips. *Bioinformatics* **23,** 2088–2095 (Aug. 2007) (cit. on pp. 61, 184).

265. Tukey, J. W. *Exploratory Data Analysis* 1977 (cit. on p. 61).

266. Affymetrix. *Statistical Algorithms Description Document* tech. rep. (Santa Clara, 2002) (cit. on p. 61).

267. Benjamini, Y. & Hochberg, Y. Controlling the false discovery rate: a practical and powerful approach to multiple testing. *Journal of the Royal Statistical Society* (1995) (cit. on p. 62).

268. Wu, D. & Smyth, G. K. Camera: a competitive gene set test accounting for inter-gene correlation. *Nucleic Acids Research* **40,** e133–e133 (Sept. 2012) (cit. on pp. 63, 74, 191).

269. Kim, S.-Y. & Volsky, D. J. PAGE: parametric analysis of gene set enrichment. *BMC Bioinformatics* **6,** 144 (2005) (cit. on p. 64).

270. He, X., Wang, J., Steele, J., Sun, X., Nie, W., Tzipori, S. & Feng, H. An ultrasensitive rapid immunocytotoxicity assay for detecting Clostridium difficile toxins. *Journal of Microbiological Methods* **78,** 97–100 (July 2009) (cit. on pp. 65, 94, 105).

271. Bradbury, E. J., Starkey, M. L., Davies, M., Yip, P. K., Carter, L. M., Wong, D. J. N. & McMahon, S. B. Expression of the regeneration-associated protein SPRR1A in primary sensory neurons and spinal cord of the adult mouse following peripheral and central injury. *The Journal of Comparative Neurology* **513,** 51–68 (Mar. 2009) (cit. on p. 71).

272. Linhoff, M. W., Lauren, J., Cassidy, R. M., Dobie, F. A., Takahashi, H., Nygaard, H. B., Airaksinen, M. S., Strittmatter, S. M. & Craig, A. M. An unbiased expression screen for synaptogenic proteins identifies the LRRTM protein family as synaptic organizers. *Neuron* **61,** 734–749 (Mar. 2009) (cit. on p. 71).

273. Just, I., Gerhard, R., Tatge, H., Genth, H., Thum, T., Borlak, J. & Fritz, G. Clostridium difficile toxin A induces expression of the stress-induced early gene product RhoB. *The Journal of Biological Chemistry* **280,** 1499–1505 (Jan. 2005) (cit. on pp. 73, 94).

274. Hirota, S. A., Al Bashir, S., Becker, H., Armstrong, J., Iablokov, V., Tulk, S. E., Schenck, L. P., Nguyen, J., Dingle, T. C., Laing, A., Liu, J., Li, Y., Bolstad, J., Mulvey, G. L., MacNaughton, W. K., Muruve, D. A., Macdonald, J. A. & Beck, P. L. Intrarectal instillation of Clostridium difficile toxin A triggers colonic inflammation and tissue damage: development of a novel and efficient mouse model of Clostridium difficile toxin exposure. *Infection and Immunity* **80,** 4474–4484 (Dec. 2012) (cit. on pp. 78, 84).

275. Gerhard, R., Zeiser, J., Just, I. & Pich, A. Substrate specificity of clostridial glucosylating toxins and their function on colonocytes analyzed by proteomics techniques. *Journal of Proteome Research* **12,** 1604–1618 (Apr. 2013) (cit. on pp. 82, 85, 193).

276. Kim, B.-H., Shenoy, A. R., Kumar, P., Bradfield, C. J. & Macmicking, J. D. IFN-inducible GTPases in host cell defense. *Cell Host & Microbe* **12,** 432–444 (Oct. 2012) (cit. on p. 86).

277. Ahn, K. J., Pothoulakis, C., Nam, H. J., Kang, J. K., Kim, S.-K., Seok, H., Park, S. J., Chang, J. S., Lamont, J. T. & Kim, H. Clostridium difficile toxin A decreases acetylation of tubulin, leading to microtubule depolymerization through activation of histone deacetylase 6, and this mediates acute inflammation. *The Journal of Biological Chemistry* **285,** 32888–32896 (Oct. 2010) (cit. on p. 87).

278. Ng, J., Armstrong, J., Hirota, S. A., Gross, O., Li, Y., Ulke-Lemee, A., Potentier, M. S., Schenck, L. P., Vilaysane, A., Seamone, M. E., Feng, H., Tschopp, J., Macdonald, J. A., Muruve, D. A. & Beck, P. L. Clostridium difficile toxin-induced inflammation and intestinal injury are mediated by the inflammasome. *Gastroenterology* **139,** pages (Aug. 2010) (cit. on p. 87).

279. Castagliuolo, I., LaMont, J. T., Letourneau, R., Kelly, C., O'Keane, J. C., Jaffer, A., Theoharides, T. C. & Pothoulakis, C. Neuronal involvement in the intestinal effects of Clostridium difficile toxin A and Vibrio cholerae enterotoxin in rat ileum. *Gastroenterology* **107,** 657–665 (Sept. 1994) (cit. on pp. 89, 108).

280. D'Auria, K. M., Kolling, G. L., Donato, G. M., Warren, C. A., Gray, M. C., Hewlett, E. L. & Papin, J. A. In vivo physiological and transcriptional profiling reveals host responses to Clostridium difficile toxin A and toxin B. *Infection and Immunity* **81,** 3814–3824 (Oct. 2013) (cit. on pp. 89, 94, 95, 105, 195).

281. Pothoulakis, C. Effects of Clostridium difficile toxins on epithelial cell barrier. *Annals of the New York Academy of Sciences* **915,** 347–356 (2000) (cit. on p. 93).

282. Shen, A. Clostridium difficile toxins: mediators of inflammation. *Journal of Innate Immunity* **4,** 149–158 (2012) (cit. on p. 93).

283. Kelly, C., Keates, S., Siegenberg, D., Linevsky, J. K., Pothoulakis, C. & Brady, H. R. IL-8 secretion and neutrophil activation by HT-29 colonic epithelial cells. *The American Journal of Physiology* **267,** G991–7 (Dec. 1994) (cit. on p. 94).

284. Grossmann, E. M., Longo, W. E., Kaminski, D. L., Smith, G. S., Murphy, C. E., Durham, R. L., Shapiro, M. J., Norman, J. G. & Mazuski, J. E. Clostridium difficile toxin: cytoskeletal changes and lactate dehydrogenase release in hepatocytes. *The Journal of Surgical Research* **88,** 165–172 (Feb. 2000) (cit. on p. 94).

285. Brito, G. A. C., Sullivan, G. W., Ciesla, W. P., Carper, H. T., Mandell, G. L. & Guerrant, R. L. Clostridium difficile toxin A alters in vitro-adherent neutrophil morphology and function. *The Journal of Infectious Diseases* **185,** 1297–1306 (May 2002) (cit. on pp. 94, 108).

286. Solomon, K., Webb, J., Ali, N., Robins, R. A. & Mahida, Y. R. Monocytes are highly sensitive to clostridium difficile toxin A-induced apoptotic and nonapoptotic cell death. *Infection and Immunity* **73,** 1625–1634 (Mar. 2005) (cit. on pp. 94, 100).

287. Ryder, A. B., Huang, Y., Li, H., Zheng, M., Wang, X., Stratton, C. W., Xu, X. & Tang, Y.-W. Assessment of Clostridium difficile infections by quantitative detection of tcdB toxin by use of a real-time cell analysis system. *Journal of Clinical Microbiology* **48,** 4129–4134 (Nov. 2010) (cit. on p. 94).

288. Teichert, M., Gerhard, R., Just, I., Tatge, H. & Schoentaube, J. Application of mutated Clostridium difficile toxin A for determination of glucosyltransferase-dependent effects. *Infection and Immunity* **74,** 6006–6010 (Oct. 2006) (cit. on pp. 94, 95).

289. Haslam, D., Chumbler, N. M., Farrow, M. A., Lapierre, L. A., Franklin, J. L., Goldenring, J. R. & Lacy, D. B. Clostridium difficile Toxin B causes epithelial cell necrosis through an autoprocessing-independent mechanism. *PLoS pathogens* **8,** e1003072 (2012) (cit. on pp. 94, 107).

290. Xu, X. & Zheng, M. in, 151–175 (Springer US, Boston, MA, Aug. 2012) (cit. on p. 97).

291. Siffert, J. C., Baldacini, O., Kuhry, J. G., Wachsmann, D., Benabdelmoumene, S., Faradji, A., Monteil, H. & Poindron, P. Effects of Clostridium difficile toxin B on human monocytes and macrophages: possible relationship with cytoskeletal rearrangement. *Infection and Immunity* **61,** 1082–1090 (Mar. 1993) (cit. on pp. 100, 105, 106).

292. Linevsky, J. K., Kelly, C., Pothoulakis, C., Keates, S., Warny, M., Keates, A. C. & LaMont, J. T. IL-8 release and neutrophil activation by Clostridium difficile toxin-exposed human monocytes. *The American Journal of Physiology* **273,** G1333–40 (Dec. 1997) (cit. on pp. 100, 105).

293. Melo-Filho, A. A., Souza, M. H., Lyerly, D. M., Cunha, F. Q., Lima, A. A. & Ribeiro, R. A. Role of tumor necrosis factor and nitric oxide in the cytotoxic effects of Clostridium difficile toxin A and toxin B on macrophages. *Toxicon* **35,** 743–752 (May 1997) (cit. on pp. 100, 105, 106).

294. Larson, H. E., Parry, J. V., Price, A. B., Davies, D. R., Dolby, J. & Tyrrell, D. A. Undescribed toxin in pseudomembranous colitis. *British Medical Journal* **1,** 1246–1248 (May 1977) (cit. on p. 104).

295. Planche, T. & Wilcox, M. Reference assays for Clostridium difficile infection: one or two gold standards? *Journal of Clinical Pathology,* 1 (Jan. 2011) (cit. on p. 104).

296. Just, I., Olling, A., Goy, S., Hoffmann, F., Tatge, H. & Gerhard, R. The repetitive oligopeptide sequences modulate cytopathic potency but are not crucial for cellular uptake of Clostridium difficile toxin A. *PLoS ONE* **6,** e17623 (2011) (cit. on p. 104).

297. Keel, M. K. & Songer, J. G. The distribution and density of Clostridium difficile toxin receptors on the intestinal mucosa of neonatal pigs. *Veterinary Pathology* **44,** 814–822 (Nov. 2007) (cit. on pp. 105, 108).

298. Rocha, M. F., Soares, A. M., Flores, C. A., Steiner, T. S., Lyerly, D. M., Guerrant, R. L., Ribeiro, R. A. & Lima, A. A. Intestinal secretory factor released by macrophages stimulated with Clostridium difficile toxin A: role of interleukin 1beta. *Infection and Immunity* **66,** 4910–4916 (Oct. 1998) (cit. on p. 105).

299. He, X., Sun, X., Wang, J., Wang, X., Zhang, Q., Tzipori, S. & Feng, H. Antibody-enhanced, Fc gamma receptor-mediated endocytosis of Clostridium difficile toxin A. *Infection and Immunity* **77,** 2294–2303 (June 2009) (cit. on p. 105).

300. Johal, S. S., Lambert, C. P., Hammond, J., James, P. D., Borriello, S. P. & Mahida, Y. R. Colonic IgA producing cells and macrophages are reduced in recurrent and non-recurrent Clostridium difficile associated diarrhoea. *Journal of Clinical Pathology* **57,** 973–979 (Sept. 2004) (cit. on p. 106).

301. Eichel-Streiber, C. v., Rupnik, M., Pabst, S., Rupnik, M., Urlaub, H. & Soling, H.-D. Characterization of the cleavage site and function of resulting cleavage fragments after limited proteolysis of Clostridium difficile toxin B (TcdB) by host cells. *Microbiology* **151,** 199–208 (Jan. 2005) (cit. on p. 106).

302. Armstrong, J., Dingle, T., Wee, S., Mulvey, G. L., Greco, A., Kitova, E. N., Sun, J., Lin, S., Klassen, J. S., Palcic, M. M. & Ng, K. K. S. Functional properties of the carboxy-terminal host cell-binding domains of the two toxins, TcdA and TcdB, expressed by Clostridium difficile. *Glycobiology* **18,** 698–706 (Sept. 2008) (cit. on p. 107).

303. Sorensson, J., Jodal, M. & Lundgren, O. Involvement of nerves and calcium channels in the intestinal response to Clostridium difficile toxin A: an experimental study in rats in vivo. *Gut* (2001) (cit. on p. 108).

304. Castagliuolo, I., LaMont, J. T. & Pothoulakis, C. Nerves and Intestinal Mast Cells Modulate Responses to Enterotoxins. *News in Physiological Sciences* **13,** 58–63 (Apr. 1998) (cit. on p. 108).

305. Gerard, N. P., Castagliuolo, I., Riegler, M., Pasha, A., Nikulasson, S., Lu, B., Gerard, C. & Pothoulakis, C. Neurokinin-1 (NK-1) receptor is required in Clostridium difficile- induced enteritis. *Journal of Clinical Investigation* **101,** 1547–1550 (Apr. 1998) (cit. on p. 108).

306. Triadafilopoulos, G., Shah, M. H. & Pothoulakis, C. The chemotactic response of human granulocytes to Clostridium difficile toxin A is age dependent. *The American Journal of Gastroenterology* **86,** 1461–1465 (Oct. 1991) (cit. on p. 108).

307. Pothoulakis, C., Sullivan, R., Melnick, D. A., Triadafilopoulos, G., Gadenne, A. S., Meshulam, T. & LaMont, J. T. Clostridium difficile toxin A stimulates intracellular calcium release and chemotactic response in human granulocytes. *Journal of Clinical Investigation* **81,** 1741–1745 (June 1988) (cit. on p. 108).

308. Dailey, D. C., Kaiser, A. & Schloemer, R. H. Factors influencing the phagocytosis of Clostridium difficile by human polymorphonuclear leukocytes. *Infection and Immunity* **55,** 1541–1546 (July 1987) (cit. on p. 108).

309. Voth, D. E. & Ballard, J. D. Clostridium difficile toxins: mechanism of action and role in disease. *Clinical Microbiology Reviews* **18,** 247–263 (Apr. 2005) (cit. on p. 108).

310. Calderon, G. M., Torres-Lopez, J., Lin, T. J., Chavez, B., Hernandez, M., Munoz, O., Befus, A. D. & Enciso, J. A. Effects of toxin A from Clostridium difficile on mast cell activation and survival. *Infection and Immunity* **66,** 2755–2761 (June 1998) (cit. on p. 108).

311. Gerhard, R., Just, I., Queisser, S., Tatge, H., Meyer, G., Dittrich-Breiholz, O., Kracht, M. & Feng, H. Down-regulation of interleukin-16 in human mast cells HMC-1 by Clostridium difficile toxins A and B. *Naunyn-Schmiedeberg's archives of pharmacology* **383,** 285–295 (Mar. 2011) (cit. on p. 108).

312. Kim, Y.-J., Lee, J. Y., Kim, H., Cha, M. Y., Park, H. G., Kim, I. Y. & Kim, J. M. Clostridium difficile toxin A promotes dendritic cell maturation and chemokine CXCL2 expression through p38, IKK, and the NF-kappaB signaling pathway. *Journal of Molecular Medicine* **87,** 169–180 (Feb. 2009) (cit. on p. 108).

313. Jafari, N. V., Kuehne, S. A., Bryant, C. E., Elawad, M., Wren, B. W., Minton, N. P., Allan, E. & Bajaj-Elliott, M. Clostridium difficile modulates host innate immunity via toxin-independent and dependent mechanism(s). *PLoS ONE* **8,** e69846 (2013) (cit. on p. 108).

314. Xia, Y., Hu, H. Z., Liu, S., Pothoulakis, C. & Wood, J. D. Clostridium difficile toxin A excites enteric neurones and suppresses sympathetic neurotransmission in the guinea pig. *Gut* (2000) (cit. on p. 108).

315. Neunlist, M., Barouk, J., Michel, K., Just, I., Oreshkova, T., Schemann, M. & Galmiche, J. P. Toxin B of Clostridium difficile activates human VIP submucosal neurons, in part via an IL-1beta-dependent pathway. *American Journal of Physiology. Gastrointestinal and Liver Physiology* **285,** G1049–55 (Nov. 2003) (cit. on p. 108).

316. Wedel, N., LaMont, J. T., Toselli, P., Pothoulakis, C., Faris, B., Oliver, P. & Franzblau, C. Ultrastructural effects of Clostridium difficile toxin B on smooth muscle cells and fibroblasts. *Experimental Cell Research* **148,** 413–422 (Oct. 1983) (cit. on p. 108).

317. Chaves-Olarte, E., Popoff, M. R., Eichel-Streiber, C. v., Florin, I. & Thelestam, M. UDP-Glucose Deficiency in a Mutant Cell Line Protects against Glucosyltransferase Toxins from Clostridium difficile and Clostridium sordellii. *The Journal of Biological Chemistry* **271,** 6925–6932 (Mar. 1996) (cit. on p. 108).

318. Herrmann, E. Local bandwidth choice in kernel regression estimation. *Journal of Computational and Graphical Statistics* (1997) (cit. on p. 118).

319. Jamshidi, N. & Palsson, B. O. Investigating the metabolic capabilities of Mycobacterium tuberculosis H37Rv using the in silico strain iNJ661 and proposing alternative drug targets. *BMC Systems Biology* **1,** 26 (2007) (cit. on pp. 126, 127, 134, 141).

320. Fang, X., Wallqvist, A. & Reifman, J. Development and analysis of an in vivo-compatible metabolic network of Mycobacterium tuberculosis. *BMC Systems Biology* **4,** 160 (2010) (cit. on pp. 126, 127, 140).

321. Segovia-Juarez, J. L., Ganguli, S. & Kirschner, D. Identifying control mechanisms of granuloma formation during M. tuberculosis infection using an agent-based model. *Journal of Theoretical Biology* **231,** 357–376 (Dec. 2004) (cit. on p. 126).

322. Oberhardt, M. A., Palsson, B. O. & Papin, J. A. Applications of genome-scale metabolic reconstructions. *Molecular Systems Biology* **5,** 320 (2009) (cit. on pp. 126, 129, 136).

323. Thiele, I. & Palsson, B. O. A protocol for generating a high-quality genome-scale metabolic reconstruction. *Nature Protocols* **5,** 93–121 (Jan. 2010) (cit. on pp. 126, 129, 130, 146).

324. Edwards, J. S. & Palsson, B. O. The Escherichia coli MG1655 in silico metabolic genotype: Its definition, characteristics, and capabilities. *Proceedings of the National Academy of Sciences* **97,** 5528–5533 (May 2000) (cit. on p. 126).

325. Reed, J. L., Vo, T. D., Schilling, C. H. & Palsson, B. O. An expanded genome-scale model of Escherichia coli K-12 (iJR904 GSM/GPR). *Genome Biology* **4,** R54 (2003) (cit. on p. 126).

326. Edwards, J. S. & Palsson, B. O. Systems properties of the Haemophilus influenzaeRd metabolic genotype. *The Journal of Biological Chemistry* (1999) (cit. on pp. 126, 127).

327. Schilling, C. H. & Palsson, B. O. Assessment of the metabolic capabilities of Haemophilus influenzae Rd through a genome-scale pathway analysis. *Journal of Theoretical Biology* **203,** 249–283 (Apr. 2000) (cit. on pp. 126, 127).

328. Henry, C. S., DeJongh, M., Best, A. A., Frybarger, P. M., Linsay, B. & Stevens, R. L. High-throughput generation, optimization and analysis of genome-scale metabolic models. *Nature Biotechnology* **28,** 977–982 (Sept. 2010) (cit. on p. 126).

329. Kim, H. U., Kim, T. Y. & Lee, S. Y. Genome-scale metabolic network analysis and drug targeting of multi-drug resistant pathogen Acinetobacter baumannii AYE. *Molecular BioSystems* **6,** 339–348 (Feb. 2010) (cit. on pp. 127, 140).

330. Fang, K., Zhao, H., Sun, C., Lam, C. M. C., Chang, S., Zhang, K., Panda, G., Godinho, M., Martins dos Santos, V. A. P. & Wang, J. Exploring the metabolic network of the epidemic pathogen Burkholderia cenocepacia J2315 via genome-scale reconstruction. *BMC Systems Biology* **5,** 83 (2011) (cit. on p. 127).

331. Raghunathan, A., Shin, S. & Daefler, S. Systems approach to investigating host-pathogen interactions in infections with the biothreat agent Francisella. Constraints-based model of Francisella tularensis. *BMC Systems Biology* **4,** 118 (2010) (cit. on pp. 127, 137, 142).

332. Thiele, I., Vo, T. D., Price, N. D. & Palsson, B. O. Expanded metabolic reconstruction of Helicobacter pylori (iIT341 GSM/GPR): an in silico genome-scale characterization of single- and double-deletion mutants. *Journal of Bacteriology* **187,** 5818–5830 (Aug. 2005) (cit. on p. 127).

333. Schilling, C. H., Covert, M. W., Famili, I., Church, G. M., Edwards, J. S. & Palsson, B. O. Genome-scale metabolic model of Helicobacter pylori 26695. *Journal of Bacteriology* **184,** 4582–4593 (Aug. 2002) (cit. on p. 127).

334. Liao, Y.-C., Huang, T.-W., Chen, F.-C., Charusanti, P., Hong, J. S. J., Chang, H.-Y., Tsai, S.-F., Palsson, B. O. & Hsiung, C. A. An experimentally validated genome-scale metabolic reconstruction of Klebsiella pneumoniae MGH 78578, iYL1228. *Journal of Bacteriology* **193,** 1710–1717 (Apr. 2011) (cit. on p. 127).

335. Beste, D. J. V., Hooper, T., Stewart, G., Bonde, B., Avignone-Rossa, C., Bushell, M. E., Wheeler, P., Klamt, S., Kierzek, A. M. & McFadden, J. GSMN-TB: a web-based genome-scale network model of Mycobacterium tuberculosis metabolism. *Genome Biology* **8,** R89 (2007) (cit. on pp. 127, 137, 139).

336. Baart, G. J. E., Zomer, B., de Haan, A., van der Pol, L. A., Beuvery, E. C., Tramper, J. & Martens, D. E. Modeling Neisseria meningitidis metabolism: from genome to metabolic fluxes. *Genome Biology* **8,** R136 (2007) (cit. on p. 127).

337. Mazumdar, V., Snitkin, E. S., Amar, S. & Segre, D. Metabolic network model of a human oral pathogen. *Journal of Bacteriology* **191,** 74–90 (Jan. 2009) (cit. on pp. 127, 132).

338. Oberhardt, M. A., Puchalka, J., Fryer, K. E., Martins dos Santos, V. A. P. & Papin, J. A. Genome-scale metabolic network analysis of the opportunistic pathogen Pseudomonas aeruginosa PAO1. *Journal of Bacteriology* **190,** 2790–2803 (Apr. 2008) (cit. on pp. 127, 130, 145).

339. AbuOun, M., Suthers, P. F., Jones, G. I., Carter, B. R., Saunders, M. P., Maranas, C. D., Woodward, M. J. & Anjum, M. F. Genome scale reconstruction of a Salmonella metabolic model: comparison of similarity and differences with a commensal Escherichia coli strain. *The Journal of Biological Chemistry* **284,** 29480–29488 (Oct. 2009) (cit. on p. 127).

340. Allen, D. K., Thiele, I., Hyduke, D. R., Steeb, B., Fankam, G., Bazzani, S., Charusanti, P., Chen, F.-C., Fleming, R. M. T., Hsiung, C. A., De Keersmaecker, S. C. J., Liao, Y.-C., Marchal, K., Mo, M. L., Ozdemir, E., Raghunathan, A., Reed, J. L., Shin, S.-I., Sigurbjornsdottir, S., Steinmann, J., Sudarsan, S., Swainston, N., Thijs, I. M., Zengler, K., Palsson, B. O., Adkins, J. N. & Bumann, D. A community effort towards a knowledge-base and mathematical model of the human pathogen Salmonella Typhimurium LT2. *BMC Systems Biology* **5,** 8 (2011) (cit. on p. 127).

341. Raghunathan, A., Reed, J., Shin, S., Palsson, B. & Daefler, S. Constraint-based analysis of metabolic capacity of Salmonella typhimurium during host-pathogen interaction. *BMC Systems Biology* **3,** 38 (2009) (cit. on p. 127).

342. Almaas, E., Lee, D.-S., Oltvai, Z. N., Barabasi, A.-L., Burd, H., Liu, J., Wiest, O. & Kapatral, V. Comparative genome-scale metabolic reconstruction and flux balance analysis of multiple Staphylococcus aureus genomes identify novel antimicrobial drug targets. *Journal of Bacteriology* **191,** 4015–4024 (June 2009) (cit. on p. 127).

343. Heinemann, M., Kummel, A., Ruinatscha, R. & Panke, S. In silico genome-scale reconstruction and validation of the Staphylococcus aureus metabolic network. *Biotechnology and Bioengineering* **92,** 850–864 (Dec. 2005) (cit. on p. 127).

344. Becker, S. A. & Palsson, B. O. Genome-scale reconstruction of the metabolic network in Staphylococcus aureus N315: an initial draft to the two-dimensional annotation. *BMC Microbiology* (2005) (cit. on p. 127).

345. Kim, H. U., Kim, S. Y., Jeong, H., Kim, T. Y., Kim, J. J., Choy, H. E., Yi, K. Y., Rhee, J. H. & Lee, S. Y. Integrative genome-scale metabolic analysis of Vibrio vulnificus for drug targeting and discovery. *Molecular Systems Biology* **7,** 460–460 (Jan. 2011) (cit. on pp. 127, 140, 143).

346. Almaas, E. & Navid, A. Genome-scale reconstruction of the metabolic network in Yersinia pestis, strain 91001. *Molecular BioSystems* **5,** 368–375 (Apr. 2009) (cit. on p. 127).

347. Vanee, N., Roberts, S. B., Fong, S. S., Manque, P. & Buck, G. A. A genome-scale metabolic model of Cryptosporidium hominis. *Chemistry & Biodiversity* **7,** 1026–1039 (May 2010) (cit. on p. 127).

348. Chavali, A. K., Whittemore, J. D., Eddy, J. A., Williams, K. T. & Papin, J. A. Systems analysis of metabolism in the pathogenic trypanosomatid Leishmania major. *Molecular Systems Biology* **4,** 177 (2008) (cit. on pp. 127, 132, 142).

349. Huthmacher, C., Hoppe, A., Bulik, S. & Holzhutter, H.-G. Antimalarial drug targets in Plasmodium falciparum predicted by stage-specific metabolic network analysis. *BMC Systems Biology* **4,** 120 (2010) (cit. on pp. 127, 144).

350. Plata, G., Hsiao, T.-L., Olszewski, K. L., Llinas, M. & Vitkup, D. Reconstruction and flux-balance analysis of the Plasmodium falciparum metabolic network. *Molecular Systems Biology* **6,** 408 (Sept. 2010) (cit. on p. 127).

351. Roberts, S. B., Robichaux, J. L., Chavali, A. K., Manque, P. A., Lee, V., Lara, A. M., Papin, J. A. & Buck, G. A. Proteomic and network analysis characterize stage-specific metabolism in Trypanosoma cruzi. *BMC Systems Biology* **3,** 52 (2009) (cit. on p. 127).

352. Durot, M., Bourguignon, P.-Y. & Schachter, V. Genome-scale models of bacterial metabolism: reconstruction and applications. *FEMS Microbiology Reviews* **33,** 164–190 (Jan. 2009) (cit. on p. 129).

353. Lee, J. M., Gianchandani, E. P. & Papin, J. A. Flux balance analysis in the era of metabolomics. *Briefings in Bioinformatics* **7,** 140–150 (June 2006) (cit. on pp. 129–131).

354. Gianchandani, E. P., Chavali, A. K. & Papin, J. A. The application of flux balance analysis in systems biology. *Wiley Interdisciplinary Reviews. Systems Biology and Medicine* **2,** 372–382 (May 2010) (cit. on p. 129).

355. Price, N. D., Reed, J. L. & Palsson, B. O. Genome-scale models of microbial cells: evaluating the consequences of constraints. *Nature Reviews Microbiology* **2,** 886–897 (Nov. 2004) (cit. on pp. 129, 130, 137, 139).

356. Feist, A. M. & Palsson, B. O. The biomass objective function. *Current Opinion in Microbiology* **13,** 344–349 (June 2010) (cit. on pp. 129, 135).

357. Varma, A. & Palsson, B. O. Metabolic Capabilities of Escherichia coli: I. Synthesis of Biosynthetic Precursors and Cofactors. *Journal of Theoretical Biology* (1993) (cit. on pp. 129, 136).

358. Duarte, N. C., Becker, S. A., Jamshidi, N., Thiele, I., Mo, M. L., Vo, T. D., Srivas, R. & Palsson, B. O. Global reconstruction of the human metabolic network based on genomic and bibliomic data. *Proceedings of the National Academy of Sciences of the United States of America* **104,** 1777–1782 (Feb. 2007) (cit. on p. 130).

359. Segre, D., Vitkup, D. & Church, G. M. Analysis of optimality in natural and perturbed metabolic networks. *Proceedings of the National Academy of Sciences of the United States of America* **99,** 15112–15117 (Nov. 2002) (cit. on pp. 133, 134).

360. Feist, A. M., Henry, C. S., Reed, J. L., Krummenacker, M., Joyce, A. R., Karp, P. D., Broadbelt, L. J., Hatzimanikatis, V. & Palsson, B. O. A genome-scale metabolic reconstruction for Escherichia coli K-12 MG1655 that accounts for 1260 ORFs and thermodynamic information. *Molecular Systems Biology* **3,** 121 (2007) (cit. on p. 134).

361. Hsiao, T.-L., Revelles, O., Chen, L., Sauer, U. & Vitkup, D. Automatic policing of biochemical annotations using genomic correlations. *Nature Chemical Biology* **6,** 34–40 (Jan. 2010) (cit. on p. 135).

362. Szappanos, B., Kovacs, K., Szamecz, B., Honti, F., Costanzo, M., Baryshnikova, A., Gelius-Dietrich, G., Lercher, M. J., Jelasity, M., Myers, C. L., Andrews, B. J., Boone, C., Oliver, S. G., Pal, C. & Papp, B. An integrated approach to characterize genetic interaction networks in yeast metabolism. *Nature genetics* **43,** 656–662 (July 2011) (cit. on p. 135).

363. Boyle, N. R. & Morgan, J. A. Flux balance analysis of primary metabolism in Chlamydomonas reinhardtii. *BMC Systems Biology* **3,** 4 (2009) (cit. on p. 135).

364. Chen, X., Alonso, A. P., Allen, D. K., Reed, J. L. & Shachar-Hill, Y. Synergy between (13)C-metabolic flux analysis and flux balance analysis for understanding metabolic adaptation to anaerobiosis in E. coli. *Metabolic Engineering* **13,** 38–48 (Jan. 2011) (cit. on p. 136).

365. Blank, L. M., Kuepfer, L. & Sauer, U. Large-scale 13C-flux analysis reveals mechanistic principles of metabolic network robustness to null mutations in yeast. *Genome Biology* **6,** R49 (2005) (cit. on p. 136).

366. Varma, A. & Palsson, B. O. Stoichiometric flux balance models quantitatively predict growth and metabolic by-product secretion in wild-type Escherichia coli W3110. *Applied and Environmental Microbiology* **60,** 3724–3731 (Oct. 1994) (cit. on p. 136).

367. Forster, J., Famili, I., Fu, P., Palsson, B. O. & Nielsen, J. Genome-scale reconstruction of the Saccharomyces cerevisiae metabolic network. *Genome Research* **13,** 244–253 (Feb. 2003) (cit. on p. 136).

368. Edwards, J. S. & Palsson, B. O. Robustness analysis of the Escherichia coli metabolic network. *Biotechnology Progress* **16,** 927–939 (Nov. 2000) (cit. on p. 137).

369. Mahadevan, R. & Schilling, C. H. The effects of alternate optimal solutions in constraint-based genome-scale metabolic models. *Metabolic Engineering* **5,** 264–276 (Oct. 2003) (cit. on pp. 137, 139).

370. Dobson, P. D., Patel, Y. & Kell, D. B. 'Metabolite-likeness' as a criterion in the design and selection of pharmaceutical drug libraries. *Drug Discovery Today* **14,** 31–40 (Jan. 2009) (cit. on p. 140).

371. Yildirim, M. A., Barabasi, A.-L., Goh, K.-I., Cusick, M. E. & Vidal, M. Drug-target network. *Nature Biotechnology* **25,** 1119–1126 (Oct. 2007) (cit. on p. 140).

372. Becker, S. A., Feist, A. M., Mo, M. L., Hannum, G., Palsson, B. O. & Herrgard, M. J. Quantitative prediction of cellular metabolism with constraint-based models: the COBRA Toolbox. *Nature Protocols* **2,** 727–738 (2007) (cit. on p. 140).

373. Papin, J. A., Reed, J. L. & Palsson, B. O. Hierarchical thinking in network biology: the unbiased modularization of biochemical networks. *Trends in Biochemical Sciences* **29,** 641–647 (Dec. 2004) (cit. on p. 141).

374. Xi, Y., Chen, Y.-P. P., Qian, C. & Wang, F. Comparative study of computational methods to detect the correlated reaction sets in biochemical networks. *Briefings in Bioinformatics* **12,** 132–150 (Mar. 2011) (cit. on p. 141).

375. Raman, K., Yeturu, K. & Chandra, N. targetTB: a target identification pipeline for Mycobacterium tuberculosis through an interactome, reactome and genome-scale structural analysis. *BMC Systems Biology* **2,** 109 (2008) (cit. on p. 142).

376. Shen, Y., Liu, J., Estiu, G., Isin, B., Ahn, Y.-Y., Lee, D.-S., Barabasi, A.-L., Kapatral, V., Wiest, O. & Oltvai, Z. N. Blueprint for antimicrobial hit discovery targeting metabolic networks. *Proceedings of the National Academy of Sciences* **107,** 1082–1087 (Jan. 2010) (cit. on p. 142).

377. Hopkins, A. L. Network pharmacology: the next paradigm in drug discovery. *Nature Chemical Biology* **4,** 682–690 (Nov. 2008) (cit. on p. 143).

378. Chong, C. R. & Sullivan, D. J. New uses for old drugs. *Nature* **448,** 645–646 (Aug. 2007) (cit. on p. 143).

379. McConville, M. J., de Souza, D., Saunders, E., Likic, V. A. & Naderer, T. Living in a phagolysosome; metabolism of Leishmania amastigotes. *Trends in Parisitology* **23,** 368–375 (Aug. 2007) (cit. on p. 143).

380. Sauer, J.-D., Bachman, M. A. & Swanson, M. S. The phagosomal transporter A couples threonine acquisition to differentiation and replication of Legionella pneumophila in macrophages. *Proceedings of the National Academy of Sciences of the United States of America* **102,** 9924–9929 (July 2005) (cit. on p. 143).

381. Brown, S. A., Palmer, K. L. & Whiteley, M. Revisiting the host as a growth medium. *Nature Reviews Microbiology* **6,** 657–666 (Sept. 2008) (cit. on p. 143).

382. Shlomi, T., Cabili, M. N., Herrgard, M. J., Palsson, B. O. & Ruppin, E. Network-based prediction of human tissue-specific metabolism. *Nature Biotechnology* **26,** 1003–1010 (Sept. 2008) (cit. on p. 144).

383. Context-specific metabolic networks are consistent with experiments. *PLoS Computational Biology* **4,** e1000082 (May 2008) (cit. on p. 144).

384. Jensen, P. A. & Papin, J. A. Functional integration of a metabolic network model and expression data without arbitrary thresholding. *Bioinformatics* **27,** 541–547 (Feb. 2011) (cit. on p. 144).

385. Schwegmann, A. & Brombacher, F. Host-directed drug targeting of factors hijacked by pathogens. *Science Signaling* **1,** re8–re8 (2008) (cit. on p. 144).

386. Aoki, M., Sakamoto, H., Arisawa, M., Okamoto, K., Kato, H., Katsume, A., Ohta, A., Tsukuda, T., Shimma, N., Aoki, Y., Kohara, M. & Sudoh, M. Host sphingolipid biosynthesis as a target for hepatitis C virus therapy. *Nature Chemical Biology* **1,** 333–337 (Nov. 2005) (cit. on p. 144).

387. Handley, S. A., Dube, P. H. & Miller, V. L. Histamine signaling through the H(2) receptor in the Peyer's patch is important for controlling Yersinia enterocolitica infection. *Proceedings of the National Academy of Sciences of the United States of America* **103,** 9268–9273 (June 2006) (cit. on p. 144).

388. Hossain, H., Tchatalbachev, S. & Chakraborty, T. Host gene expression profiling in pathogen-host interactions. *Current Opinion in Immunology* **18,** 422–429 (Aug. 2006) (cit. on p. 144).

389. Diamond, D. L., Syder, A. J., Jacobs, J. M., Sorensen, C. M., Walters, K.-A., Proll, S. C., McDermott, J. E., Gritsenko, M. A., Zhang, Q., Zhao, R., Metz, T. O., Camp, D. G., Waters, K. M., Smith, R. D., Rice, C. M. & Katze, M. G. Temporal proteome and lipidome profiles reveal hepatitis C virus-associated reprogramming of hepatocellular metabolism and bioenergetics. *PLoS pathogens* **6,** e1000719 (Jan. 2010) (cit. on p. 144).

390. Carette, J. E., Guimaraes, C. P., Varadarajan, M., Park, A. S., Wuethrich, I., Godarova, A., Kotecki, M., Cochran, B. H., Spooner, E., Ploegh, H. L. & Brummelkamp, T. R. Haploid genetic screens in human cells identify host factors used by pathogens. *Science* **326,** 1231–1235 (Nov. 2009) (cit. on p. 144).

391. Puchalka, J., Oberhardt, M. A., Godinho, M., Bielecka, A., Regenhardt, D., Timmis, K. N., Papin, J. A. & Martins dos Santos, V. A. P. Genome-scale reconstruction and analysis of the Pseudomonas putida KT2440 metabolic network facilitates applications in biotechnology. *PLoS Computational Biology* **4,** e1000210 (Oct. 2008) (cit. on p. 145).

392. Oberhardt, M. A., Puchalka, J., Martins dos Santos, V. A. P. & Papin, J. A. Reconciliation of genome-scale metabolic reconstructions for comparative systems analysis. *PLoS Computational Biology* **7,** e1001116 (Mar. 2011) (cit. on p. 145).

393. Stolyar, S., Van Dien, S., Hillesland, K. L., Pinel, N., Lie, T. J., Leigh, J. A. & Stahl, D. A. Metabolic modeling of a mutualistic microbial community. *Molecular Systems Biology* **3,** 92 (2007) (cit. on p. 145).

394. Oberhardt, M. A., Goldberg, J. B., Hogardt, M. & Papin, J. A. Metabolic network analysis of Pseudomonas aeruginosa during chronic cystic fibrosis lung infection. *Journal of Bacteriology* **192,** 5534–5548 (Oct. 2010) (cit. on p. 145).

395. Begley, T., Overbeek, R., Butler, R. M., Choudhuri, J. V., Chuang, H.-Y., Cohoon, M., de Crecy-Lagard, V., Diaz, N., Disz, T., Edwards, R., Fonstein, M., Frank, E. D., Gerdes, S., Glass, E. M., Goesmann, A., Hanson, A., Iwata-Reuyl, D., Jensen, R., Jamshidi, N., Krause, L., Kubal, M., Larsen, N., Linke, B., McHardy, A. C., Meyer, F., Neuweger, H., Olsen, G., Olson, R., Osterman, A., Portnoy, V., Pusch, G. D., Rodionov, D. A., Ruckert, C., Steiner, J., Stevens, R., Thiele, I., Vassieva, O., Ye, Y., Zagnitko, O. & Vonstein, V. The subsystems approach to genome annotation and its use in the project to annotate 1000 genomes. *Nucleic Acids Research* **33,** 5691–5702 (2005) (cit. on p. 145).

396. Olsen, G., Aziz, R. K., Bartels, D., Best, A. A., DeJongh, M., Disz, T., Edwards, R. A., Formsma, K., Gerdes, S., Glass, E. M., Kubal, M., Meyer, F., Olson, R., Osterman, A. L., Overbeek, R. A., McNeil, L. K., Paarmann, D., Paczian, T., Parrello, B., Pusch, G. D., Reich, C., Stevens, R., Vassieva, O., Vonstein, V., Wilke, A. & Zagnitko, O. The RAST Server: rapid annotations using subsystems technology. *BMC Genomics* **9,** 75 (2008) (cit. on p. 145).

397. Langridge, G. C., Phan, M.-D., Turner, D. J., Perkins, T. T., Parts, L., Haase, J., Charles, I., Maskell, D. J., Peters, S. E., Dougan, G., Wain, J., Parkhill, J. & Turner, A. K. Simultaneous assay of every Salmonella Typhi gene using one million transposon mutants. *Genome Research* **19,** 2308–2316 (Dec. 2009) (cit. on p. 146).

398. Chavali, A. K., D'Auria, K. M., Hewlett, E. L., Pearson, R. D. & Papin, J. A. A metabolic network approach for the identification and prioritization of antimicrobial drug targets. *Trends in Microbiology* **20,** 113–123 (Mar. 2012) (cit. on p. 147).

399. Bolstad, B. M., Gentleman, R. C., Carey, V., Bates, D. M., Dettling, M., Dudoit, S., Ellis, B., Gautier, L., Ge, Y., Gentry, J., Hornik, K., Hothorn, T., Huber, W., Iacus, S., Irizarry, R., Leisch, F., Li, C., Maechler, M., Rossini, A. J., Sawitzki, G., Smith, C., Smyth, G., Tierney, L., Yang, J. Y. H. & Zhang, J. Bioconductor: open software development for computational biology and bioinformatics. *Genome Biology* **5,** R80 (2004) (cit. on p. 182).

400. Bolstad, B. M., Gautier, L., Cope, L. & Irizarry, R. a. affy–analysis of Affymetrix GeneChip data at the probe level. *Bioinformatics* **20,** 307–315 (Feb. 2004) (cit. on p. 183).

401. Durinck, S., Spellman, P. T., Birney, E. & Huber, W. Mapping identifiers for the integration of genomic datasets with the R/Bioconductor package biomaRt. *Nature Protocols* **4,** 1184–1191 (2009) (cit. on p. 183).

402. Wickham, H. *ggplot2* (Springer New York, New York, NY, 2009) (cit. on p. 183).

403. Wickham, H. Reshaping Data with the reshape Package. *Journal of Statistical Software* (2007) (cit. on p. 183).

404. Huang, D. W., Sherman, B. T. & Lempicki, R. A. Systematic and integrative analysis of large gene lists using DAVID bioinformatics resources. *Nature Protocols* **4,** 44–57 (2009) (cit. on p. 185).

405. Kasprzyk, A. BioMart: driving a paradigm change in biological data management. *Database* **2011,** bar049 (2011) (cit. on p. 185).

406. Ashburner, M., Ball, C. A., Blake, J. A., Botstein, D., Butler, H., Cherry, J. M., Davis, A. P., Dolinski, K., Dwight, S. S., Harris, M. A., Hill, D. P., Issel-Tarver, L., Kasarskis, A., Lewis, S., Matese, J. C., Richardson, J. E., Ringwald, M., Rubin, G. M. & Sherlock, G. Gene ontology: tool for the unification of biology. The Gene Ontology Consortium. *Nature genetics* **25,** 25–29 (May 2000) (cit. on p. 185).

407. Hermjakob, H., Matthews, L., Gopinath, G., Gillespie, M., Caudy, M., Croft, D., de Bono, B., Garapati, P., Hemish, J., Jassal, B., Kanapin, A., Lewis, S., Mahajan, S., May, B., Schmidt, E., Vastrik, I., Wu, G., Birney, E., Stein, L. & D'Eustachio, P. Reactome knowledgebase of human biological pathways and processes. *Nucleic Acids Research* **37,** D619–22 (Jan. 2009) (cit. on p. 185).

408. Blake, J. A., Bult, C. J., Kadin, J. A., Richardson, J. E. & Mouse Genome Database Group. The Mouse Genome Database (MGD): comprehensive resource for genetics and genomics of the laboratory mouse. *Nucleic Acids Research* **40,** D881–6 (Jan. 2012) (cit. on p. 185).

409. Harrow, J., Barrell, D., Kahari, A. K., Birney, E. & Fernandez-Suarez, X. M. Ensembl 2012. *Nucleic Acids Research* **40,** D84–90 (Jan. 2012) (cit. on p. 186).

410. Xie, Y. knitr: A General-Purpose Tool for Dynamic Report Generation in R (2013) (cit. on p. 194).

Appendices

Appendix A

Instructions for reproducing in vivo transcriptomics analysis

A.1 Introduction

To ensure that all computational analyses, tables, and figures presented are reproducible, we have provided the necessary data files, scripts, and accompanying explanations. All analyses were performed with the free, open source R programming language and R software packages within the Bioconductor project [399]. In addition to the instructions included in this document, every script file is well commented, providing further details. The supplemental figures and associated text are in a separate document.

A.2 Preparing software, files, and folders

A.2.1 Directory structure

All of the scripts and data, except for the microarray data, are stored in a compressed folder that can be accessed at `http://bme.virginia.edu/csbl/downloads-cdiff`. The scripts, without the large annotation and data files in the `./data` folder, are also accessible from an online version control system at bitbucket.org.

Once extracted, this root folder serves as the working directory for all scripts. The folder is heretofore referred to with the path `./` . Note that for path names on Windows operating systems, backslashes are used instead of forward slashes. Several physiological measurements are included in the tab delimited text file `./PhysiologyMeasurements.csv`. Files associated with different steps of the analysis are included in subfolders corresponding to subsequent sections of this document.

A.2.2 R and R packages

Version 2.15.2 of R was run on a `x86_64-pc-linux-gnu` platform. The following R packages were used [21, 63, 400–403] :

```
affy_1.36.1
affyio_1.26.0
affyPLM_1.34.0
AnnotationDbi_1.20.3
Biobase_2.18.0
BiocGenerics_0.4.0
BiocInstaller_1.8.3
biomaRt_2.14.0
Biostrings_2.26.3
bitops_1.0-5
caTools_1.14
colorspace_1.2-1
DBI_0.2-5
dichromat_2.0-0
digest_0.6.2
gcrma_2.30.0
gdata_2.12.0
ggplot2_0.9.3
GO.db
gplots_2.11.0
grid_2.15.2
gtable_0.1.2
gtools_2.7.0
IRanges_1.16.4
KernSmooth_2.23-8
labeling_0.1
lattice_0.20-13
limma_3.14.4
MASS_7.3-23
Matrix_1.0-11
mouse4302cdf_2.11.0
mouse4302.db_2.8.1
mouse4302probe_2.11.0
munsell_0.4
org.Mm.eg.db_2.8.0
parallel_2.15.2
plyr_1.8
preprocessCore_1.20.0
proto_0.3-10
qvalue_1.32.0
RColorBrewer_1.0-5
RCurl_1.95-3
reshape_0.8.4
reshape2_1.2.2
RSQLite_0.11.2
scales_0.2.3
splines_2.15.2
stats4_2.15.2
stringr_0.6.2
tcltk_2.15.2
tools_2.15.2
XML_3.95-0.1
zlibbioc_1.4.0
```

A.2.3 Downloading the microarray data

The microarray data files are deposited in the NCBI GEO database as a data series with the accession number `GSE44091`. The matrix of preprocessed data is also uploaded to GEO. However, for the purposes of this analysis, the compressed folder of `.CEL` files must be downloaded. On the GEO web page for `GSE44091`, there should be a link to download the compressed folder which is probably in a `tar` format (i.e. with a `tar` file extension). Once extracted, all of the `.CEL` files should be placed in the `./data/CEL.files/` folder. Each of the 32 files is approximately ten megabytes.

A.3 Loading and organizing microarray data

The script `./A-LoadingData/loadData.R` parses the `.CEL` files into `AffyBatch` objects and and saves them in the `./data/RData/abatches.RData` file. There are four `AffyBatch` objects for four groupings of the microarrays: 2hr, 6hr, 16hr, and all arrays. The endpoint and toxin injection associated with each array are also labeled and can be accessed using the `pData` function on each `AffyBatch`.

A.4 Preprocessing microarray data

`./B-Preprocessing/preprocessData.R` preprocesses the `AffyBatch` objects. Once preprocessed, each `AffyBatch` object leads to an `ExpressionSet` object which contains the signal intensities for every probe set on each microarray. The `ExpressionSet` objects are stored in `./data/RData/esets.RData`.

A.5 Microarray and gene annotation

A.5.1 Background

On the Mouse 430 2.0 Affymetrix array used here, there are approximately $1002 \times 1002 = 1{,}004{,}004$ probes, each of which has a different 25 base pair oligomer. Affymetrix used the GenBank and Unigene databases to choose the probe sequences that align with all the genes in the mouse genome. Approximately half of the probes are "mismatch" probes, probes for which the sequence differs by one nucleotide from the corresponding "perfect-match" probe. These mismatch probes are intended to measure nonspecific binding. However, how to best use the readings from mismatch probes is still unclear [264]. Several processing techniques successfully use only the "perfect match" probes; we do the same here.

Affymetrix arranged probes into probe sets. Each probe set includes approximately 10-20 probes and is intended to represent the sequence of a specific gene or transcript. The Affymetrix probe set IDs can in turn be linked to databases of other identifiers (e.g. Entrez gene, Ensembl, MGI, etc.). In order to understand and interpret the signal intensities of the probes in reference to commonly used gene names (e.g. Jun, Rhob, etc.), the annotations from probe to probe set to gene name are exceedingly important. Multiple databases, which we employ here, have arisen to address this need.

A.5.2 Annotation sources

Sequence annotations are constantly updated as new experimental findings come to light. To ensure our annotations and subsequent analyses using these annotations are repeatable, we have either provided the version number of annotation packages used or downloaded annotation files from public databases. All downloaded annotation files are in the `./data/RData/annotation.files` folder; the file names are made to be self explanatory. The parsed annotations files resulted in R variables used in all further analyses. These variables are stored in the `./data/RData/annotation.RData` folder. One could therefore skip this section of the ths document and simply load these variables into the R workspace.

Affymetrix probe set IDs

The Affymetrix probe to probe set mappings were taken from the `mouse4302.db` and `mouse4302cdf` packages, version 2.8.1 and 2.11.0, respectively. The DAVID [404] and Biomart [405] databases were used for linking Affymetrix probe set IDs to gene symbols (e.g. Rhob), gene names (e.g. Ras homolog gene family, member B), MGI IDs (e.g. MGI:107949), and Entrez IDs (e.g. 11852). Version 2.4.1 of the `org.Mm.eg.db` package was also used. The `biomaRt` package, version 2.14.0, was used to access version 0.8 of the BioMart database.

Gene set annotations

Gene ontology gene associations with MGI gene IDs were downloaded from geneontology.org and are saved in the annotation folder [406]. Gene assocations from the Reactome database (reactome.org) with human Entrez gene IDs were also downloaded [407].

Orthology annotations

The Reactome database is built using Human Entrez IDs. To be able to use Reactome and other databases with human data, annotations were downloaded from NCBI homologene and MGI's flat files in order to map mouse genes to their human orthologs [408]. In order to compare mouse and human transcriptional date sets, Ensembl transcript IDs and gene IDs were mapped using the Biomart database.

Additional annotations

The relationship between Affymetrix probe sets and gene IDs is typically *many-to-many*. In other words, there are probe sets that map to *many* genes, and there are genes that map to *many* probe sets. For example, there are two microarray probe sets (`1418652_at` and `1456907_at`) that map to *Cxcl9*. Which probe set should then be used to show the data for *Cxcl9*, or how should these probe sets be combined into a single probe set? We address this selection/summarization problem with functions described in section A.5.5 of this document.

As an alternative, we also aligned probe sequences to gene sequences from Ensembl [409] in order to define custom probe sets with *one-to-one* mappings to Ensembl gene IDs. These Ensembl-defined probe sets then made MGI-defined probe sets possible using a mapping from Ensembl to MGI gene IDs. To map MGI IDs to Ensembl Gene IDs, the Biomart database was used and a mapping file from MGI was also downloaded. Mappings from Ensembl transcript IDs to Ensembl Gene IDs were downloaded from Ensembl. Probe sequences were taken from version 2.11.0 of the `mouse4302probe` Bioconductor package and written to a FASTA file. NCBI BLAST-2.2.27+ was used to map probes which aligned 100% with Ensembl transcript IDs which then mapped to Ensembl Gene IDs.

The strict requirements we set reduced the number of probes (310,467 from ~450,000) and probe sets (21,288 from 45,101). Redifining probe sets thus lost ~30% of the microarray data. Since this probe set redefinition did not greatly affect our overall analyses, we continued with the Affymetrix defined probe sets. A parallel analysis to the one presented in this document (but with our redefined probe sets) is contained in the `./DiffProbeSets` folder yet is not discussed further.

A.5.3 Generating annotation lists in R

Several scripts generate the mappings from one type of ID to another. These mappings are contained in nested `list` objects (hereon referred to as annotation lists).

```r
# Examples of annotation lists
load("./data/annotation.RData/MsAnn.RData")
load("./data/annotation.RData/MsAnnGO.RData")
head(MsAnn$MGI$Affy, 3)

## $`101757`
## [1] "1448346_at"   "1455138_x_at"
##
## $`101758`
## [1] "1421566_at"
##
## $`101759`
## [1] "1415844_at" "1415845_at"

head(MsAnnGO$MGI$BP, 3)

## $`101757`
##  [1] "GO:0007010" "GO:0006928" "GO:0030010" "GO:0007015" "GO:0030030"
##  [6] "GO:0045792" "GO:0006468" "GO:0006606" "GO:0022604" "GO:0043200"
## [11] "GO:0000910" "GO:0001755" "GO:0030836" "GO:0001842"
##
## $`101759`
## [1] "GO:0006810" "GO:0007269" "GO:0048489" "GO:0017158"
##
## $`101760`
## [1] "GO:0006396" "GO:0006355" "GO:0006397" "GO:0008380" "GO:0006351"
## [6] "GO:0048025"
```

The scripts which parse annotation files and access annotation databases are within the `../C-Annotations/` folder. The script names, the mappings the scripts generate, and in what variable the mappings (i.e. the annotation lists) are stored are shown in Table A.1. The variables are saved in similarly named `.RData` files in the `./data/annotation.RData` folder.

Script	R variable	ID mappings
`ProbeSetToOthers.R`	`MsAnn`	Affy ↔ MGI, Entrez, Gene Symbol, Gene Name
`GOAnnotations.R`	`MsAnnGO`	MGI ↔ Gene Ontology Term
`OtherGenesetAnnotations.R`	`GSAnn`	Human Entrez ↔ REACTOME
`OrthologAnnotations.R`	`MsAnn`	Human Entrez ↔ Entrez, Affy
		Human Ensembl ↔ Ensembl
`EnsemblToOthers.R`	`MsAnn`	Ensembl gene ↔ MGI
`NewProbeSets.R`	`CustomPS`	Affy probe ↔ Ensembl, MGI
`GeneSymbols.R`	`MsAnn`	MGI ↔ Gene Symbol

Table A.1: Annotation scripts and variables. “Affy”=Affymetrix Mouse 430 2.0 probeset ID. “Entrez”=Entrez gene ID, “Ensembl”=Ensembl gene ID

The data from our previous study of the HCT8 cell transcriptional response to TcdA and TcdB was reanalyzed in the same way this *in vivo* data is analyzed. The annotation files are given in Table A.2. The scripts are located in the `./InVitro/C-Annotations/` folder and the R variables are saved to the `./InVitro/data/annotation.RData/` folder.

Script	R variable	ID mappings
`makeAnnotations.R`	`HsAnn`	Affy ↔ Gene Symbol, Entrez, Gene Name
	`HsAnnGO`	Symbol ↔ Gene Ontology Term
`NewProbeSetsHS.R`	`HsAnn`	Ensembl ↔ Probe, Entrez, Gene Symbol

Table A.2: Annotation scripts and variables for Hgu133 Plus 2.0 chip

A.5.4 Transitive mapping

Not all gene, probe, and probe set identifiers have direct mappings available. However, it is sometimes possible to map one identifier to another using intermediate mappings. In symbolic terms, for IDs a,b, and c, if there are mappings $a \to b$ and $b \to c$, then an $a \to c$ mapping can be made. The `TransitiveMapping` function in the `./C-Annotations/TransitiveMapping.R` script generates such "transitive mappings" when given two mappings related by one common ID. Annotation lists or two-column matrices are taken as input. The function uses simple matrix multiplication for efficient mapping, typically taking <5s for many genome-wide mappings.

```
# An example of transitive mapping
source("./C-Annotations/TransitiveMapping.R")
head(TransitiveMapping(MsAnn$MGI$Affy, MsAnnGO$MGI$BP), 4)

## $`1415670_at`
## [1] "GO:0006810" "GO:0006886" "GO:0015031" "GO:0016192" "GO:0072384"
## [6] "GO:0051683"
##
## $`1415671_at`
## [1] "GO:0006810" "GO:0006811" "GO:0006200" "GO:0015992" "GO:0034220"
## [6] "GO:0015991"
##
## $`1415672_at`
## [1] "GO:0006893"
##
## $`1415673_at`
## [1] "GO:0008152" "GO:0008652" "GO:0006564" "GO:0006563"
```

A.5.5 Many probes to many genes mapping

As introduced in section A.5.2, the relationship between Affymetrix probe sets and gene IDs is typically many-to-many. For example, one usually wants to report the expression of gene A, not the expression of probe set 1, probe set 2, and probe set 3 that map to gene A. There are two solutions to this *many probe set to gene* problem: (1) selecting only one of the several probe sets for each gene (selection), and (2) combining all of the probe sets into a new probe set (gene summarization).

Continuing with this example, a further problem may be that probe set 2 also maps to gene B. Hence, it is possible that one probe set may represent or contribute to the measured expression of many different genes. This *probe set to many gene* problem is more difficult to resolve. Perhaps the most straightforward solution is complete reannotation of the microarray as discussed in section A.5.2. We reannotated the microarray to contain only one-to-one relationships, yet found that reducing the many-to-many relationship to only a many-to-one (not one-to-one) relationship led to similar results. The many-to-one relationship also kept the data for many microarray probes that must be discarded in the generation of one-to-one mappings.

The script `./C-Annotation/CollapseIDs.R` contains functions which will "collapse" genes with multiple probe sets into a single measurement, either by selection of a probe set or by gene summarization. In other words, data with probe set IDs is converted to data with commonly used and understandable gene IDs, even when given a many-to-many probe set to gene mapping. The criteria for selecting which probe set represents a gene or the criteria by which several probe sets are summarized into a gene are inputs to the `collapseExprMatrix` and `collapseExprVector` functions defined in the `CollapseIDs.R` script. By default, the probe set with the largest interquartile range is selected. For gene summarization, the mean of probe sets is taken to represent the expression for a gene.

```r
# An example of 'collapsing' an expression matrix
library(affy)
source("./C-Annotations/CollapseIDs.R")
load("./data/RData/esets.RData")
data = exprs(esets[["6hr"]])
head(data, 3)
```

```
##              213   214   215   216   217   218    221   223   224   232
## 1415670_at 8.514 8.752 8.630 8.317 8.468 8.504  8.647 8.593 8.564 8.414
## 1415671_at 9.748 9.626 9.627 9.763 9.804 9.859  9.668 9.823 9.929 9.950
## 1415672_at 9.892 9.910 9.993 9.635 9.682 9.588 10.079 9.551 9.609 9.566

head(collapseExprMatrix(data, MsAnn$MGI$Affy, type = "select"), 3)

##          213   214   215   216   217   218   221   223   224   232
## 101757 8.570 8.732 8.784 8.652 8.465 8.411 8.698 8.582 8.522 8.091
## 101758 2.025 1.844 1.720 2.214 1.491 2.178 1.844 1.654 1.992 1.832
## 101759 1.838 1.993 2.089 1.840 1.921 2.012 1.913 1.981 2.128 1.780
```

A.6 Analyzing differential expression

The CyberT statistical test [49] was used to generate p-values for the differential expression of probe sets after toxin injection relative to sham injection. The CyberT R source code was downloaded from http://cybert.ics.uci.edu; this source code is in the ./D-DiffExpression/bayesreg.R script. We wrote the cybertWrapper function to automatically format ExpressionSet objects for the bayesT function in the bayesreg.R script. The wrapper function automatically sets up toxin versus sham comparisons according to the phenotype data within each ExpressionSet. Hence, the wrapper function is highly customized for this study. The wrapper function outputs a list containing matrices of parameters and p-values; the columns of each matrix represent the different two-class comparisons. The ./D-DiffExpression/cybertRun.R script applies the cybertWrapper for all of the toxin-sham comparisons and saves the results to ./data/RData/cyberT.results.RData.

```
# Part of the output from CyberT test for differential expression
load("./data/RData/cyberT.results.RData")
head(cyberT.results$pval, 3)

##            A2-Sham2 B2-Sham2 AB2-Sham2  A6-Sham6 B6-Sham6 AB6-Sham6
## 1415670_at   0.1456   0.6577    0.2659 0.3397942   0.4228 2.696e-01
## 1415671_at   0.4098   0.8156    0.4063 0.0174292   0.3247 9.285e-03
## 1415672_at   0.0409   0.8617    0.2724 0.0007157   0.6105 3.125e-05
##            A16-Sham16 B16-Sham16
## 1415670_at  0.0003463    0.08325
## 1415671_at  0.2354018    0.79854
## 1415672_at  0.3446540    0.16402

head(cyberT.results$tstats, 3)
```

```
##            A2-Sham2 B2-Sham2 AB2-Sham2 A6-Sham6 B6-Sham6 AB6-Sham6
## 1415670_at   1.5087   0.4492    1.1417   0.9758  -0.8169     1.136
## 1415671_at  -0.8402  -0.2361   -0.8466  -2.5710  -1.0073    -2.879
## 1415672_at  -2.1721  -0.1762   -1.1257   3.9298   0.5167     5.345
##            A16-Sham16 B16-Sham16
## 1415670_at     4.1950     1.8108
## 1415671_at    -1.2185     0.2582
## 1415672_at    -0.9649    -1.4376
```

A.7 Gene set enrichment

A.7.1 Competitive

Competitive gene set enrichment was performed with the method CAMERA developed by Wu *et al.* [268]. The `camera` function, in the limma Bioconductor package, calls other functions within limma to determine t-statistics for every gene. These t-statistics are then used in gene set enrichment. We modified `camera` to be able to accept other t-statistics. Our modified function `cameraMod` is defined in the script `./DiffExpression/cameraMod.R`.

Since gene sets are made from gene-level IDs such as MGI IDs or Entrez IDs, the data with Affymetrix probe sets must be collapsed to data with gene-level IDs (see section A.5.5 for more about collapsing). Since CAMERA calculates gene-gene correlations, it must begin with the data for each microarray (the `ExpressionSet` objects). The `ExpressionSet` objects were collapsed, and CyberT was applied to obtain test statistics for each gene ID.

```
# saving the mapping when a matrix is collapsed
data = exprs(esets[["6hr"]])
result = collapseExprMatrix(data, MsAnn$MGI$Affy, type = "select", func = function(x) IQR(x),
    return.probes = TRUE)
collapsed.data = result$expMat
head(result$collapseMap, 5)

##       101757       101758       101759       101760       101761
## "1448346_at" "1421566_at" "1415844_at" "1438675_at" "1422851_at"
```

Again, there are a few complications with annotations of genes and gene sets, which we discuss using an example. Consider a gene set that includes genes A, B, ..., and K. We then find that no probe sets map to genes J or K. We then reduce the gene set to genes for which there is data, genes

A, B, ..., and I. Now consider that, in collapsing probe sets to genes, probe set 1 was selected as the probe set to represent the closely related genes E, F, G, H, and I. If probe set 1 was strongly differentially expressed, then the majority of genes in this gene set would be found to be differentially expressed, which may or may not be the case. To avoid a probe set errantly making a gene set significantly enriched, a probe set was not allowed to be repreated in a gene set. In this example, the gene set would then be genes A, B, C, D, and one gene represented by probe set 1. When gene set enrichment is performed on a collapsed matrix, it is thus necessary to save which probes map to genes (note the `return.probes` option in the previous example of the `collapseExprMatrix` function). Finally, gene sets with few genes are more likely to be enriched by one or two outliers, and gene sets with several hundred genes are often too vague for interpretation. Hence, gene sets with very few or several hundred genes were excluded. The function `indexGeneSets` accounts for all the problems mentioned above; it also converts the format of the gene set annotation lists so that they may be used with `camera` and `cameraMod`.

A wrapper function, `cameraModWrapper` in `cameraModWrapper.R`, uses the CyberT t statistic as input to `cameraMod`. The wrapper function is used in the script `runCAMERA.R` and the results are saved to `./data/RData/cameraMod.RData`.

A.7.2 Self-contained

The function for the self contained test, `cactus`, is defined in the `./E-Enrichment/cactus.R` script. The `runCactus.R` script runs `cactus` for every toxin-sham comparison and saves the p-values from each gene set enrichment in the `./data/RData/cactus.RData` file. The annotation problems mentioned for competitive gene set enrichment were addressed in the same way for self-contained gene set enrichment.

```
# Example of p-values from gene set enrichment
source("./E-Enrichment/cameraModWrapper.R")
eset = esets[["16hr"]]
result = cameraModWrapper(eset, MsAnnGO$MF$MGI, list(c("A16", "Sham16")), MsAnn$MGI$Affy)
head(sort(result, decreasing = FALSE))

## GO:0043498 GO:0005525 GO:0003924 GO:0004364 GO:0005097 GO:0047485
##  0.0002763  0.0021449  0.0022396  0.0031255  0.0038467  0.0043996
```

```
source("./E-Enrichment/cactus.R")
eset = esets[["2hr"]]
result = cactus(eset, MsAnnGO$BP$MGI, list(c("A2", "Sham2"), c("B2", "Sham2")),
    MsAnn$MGI$Affy)
head(result, 4)

##              A2-Sham2 B2-Sham2
## GO:0000038  0.53392   0.3159
## GO:0000045  0.07490   0.3596
## GO:0000060  0.04644   0.3564
## GO:0000070  0.65147   0.3277
```

A.8 Analysis of previous *in vitro* data

The analysis described in the previous sections was repeated for the transcriptional response of HCT8 cells exposed to TcdA or TcdB [230]. The scripts and files for this analysis are in the `./InVitro/` folder. The directory structure is the same as for analysis of our *in vivo* data.

Our reanalysis of the *in vitro* data uncovered a clear batch effect between different runs of microarrays. The batch effect had little effect on the ranking of genes or the gene set enrichment results we have reported previously. Nevertheless, we corrected for this batch effect using a simple linear model. Factors for the three different runs were included in the model. A principal components plot of all the microarrays before and after batch correction are shown in Figure A.1.

A.9 Comparisons to other transcriptomic and proteomic data

Proteomic data from Zeiser *et al.* was downloaded from the supplementary material of their manuscript [275]. The transcriptional data with HCT8 cells was downloaded from NCBI GEO. The scripts parsing these data are in the `./G-Comparisons` folder. In merging the data between mouse and human, only one-to-one mappings were used.

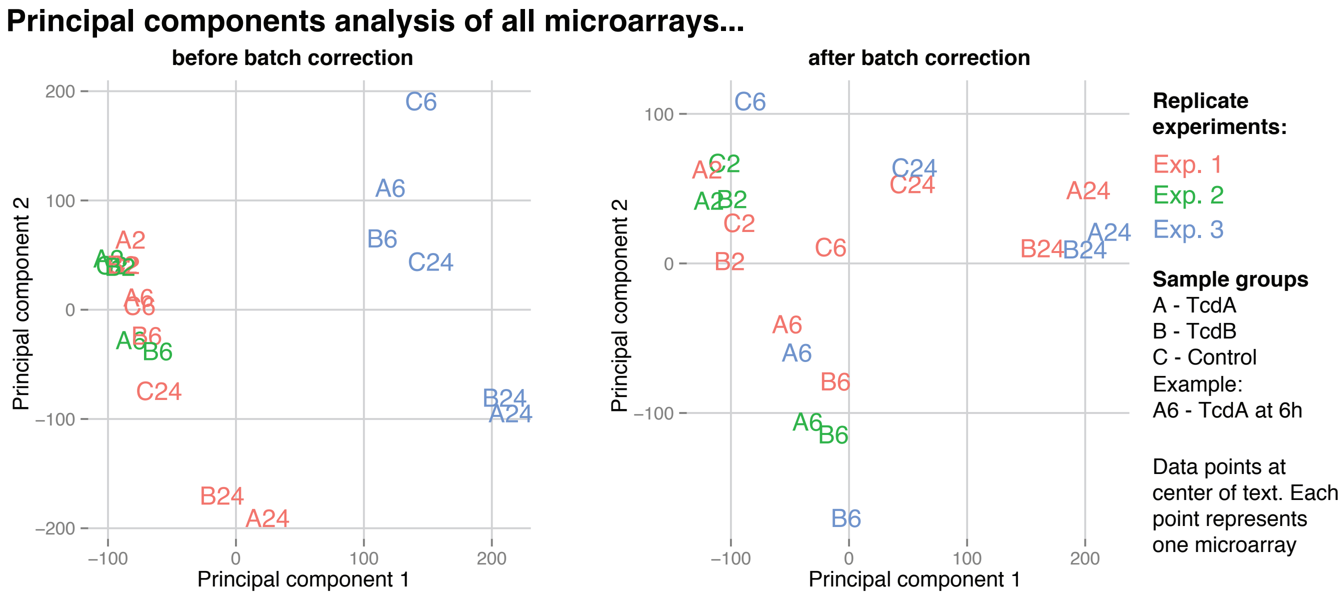

Figure A.1: Batch corrected HCT8 transcriptional data

A.10 Cytotoxicity assay

After toxin addition, measurements for the cytotoxicity assay were taken 6 times/minute. In order to have enough replicates, two plates were used. Toxin was added to the columns of each plate using a multichannel pipette. The time at which toxin was added to each column was recorded manually. This information was used to interpolate the measurements from all wells to the exact same time points. The plotting functions and calculations are in the `./F-Figures/CytotoxAssay.R` script. The data is in the `./data/CytotoxData.txt` file.

A.11 Scripts for generating figures and tables

Most figures and tables were produced from R scripts. Unless otherwise noted, the scripts in Table A.3 are in the `./F-Figures` folder. Many of these scripts depend on the scripts and results described in the previous sections.

A.12 Notes on formatting

This document is written using LaTeX and the `knitr` software package from Yihui Xie [410]; the document files are in the `./LaTeX` folder. The figures were exported to `pdf` or `svg` files and further

Figure or Table	Script
Table 1	Table1.R
Tables 2 & 3	Tables2and3.R
Figure 2	Figure2.R
Figure 3 & S6	Figure3.R
Figure 4	Figure4.R
Figure S1, S3, S7, and S8	Supplement.R
Tables S1 & S2	Manually entered
Figure S2	CytotoxAssay.R
Figure S4	flow.R
Figure S5	./G-Comparisons/Hirota-et-al/HirotaCytokines.R
Figures S9 & S10	./G-Comparisons/HCT8-cells/Sims.R & ./G-Comparisons/Proteomics/loadData.R

Table A.3: Scripts for producing tables and figures

formatted with Adobe Illustrator.

A.13 Acknowledgements

This appendix is part of the supplement for D'Auria, K. M., Kolling, G. L., Donato, G. M., Warren, C. A., Gray, M. C., Hewlett, E. L. & Papin, J. A. In vivo physiological and transcriptional profiling reveals host responses to Clostridium difficile toxin A and toxin B.. *Infection and Immunity* **81,** 3814–3824 (Oct. 2013).

Appendix B

Reproducing time-course analyses

B.1 Introduction

This document includes the supplemental data referred to in Chapter 7 as well as instructions for how to reproduce our analyses and explore the data further. This is a functional document in that scripts (written in the R programming languange with the `knitr` package) are embedded, and they were run during PDF creation to produce the figures and output shown. Thus, the analyses can be repeated by downloading the source of this document (with the data) or copy-pasting all of the code into one's own R console.

B.2 References from Chapter 7

B.2.1 Reference 1

"The impedance curves of cells treated with TcdA (300 ng/ml) and TcdB (10 ng/ml) diverged from controls in 10 and 20 minutes, respectively (Appendix B)."

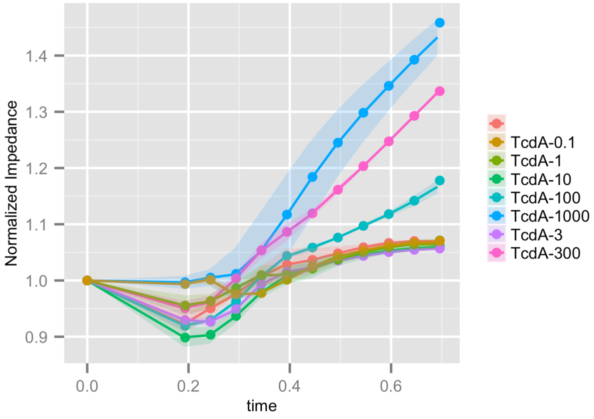

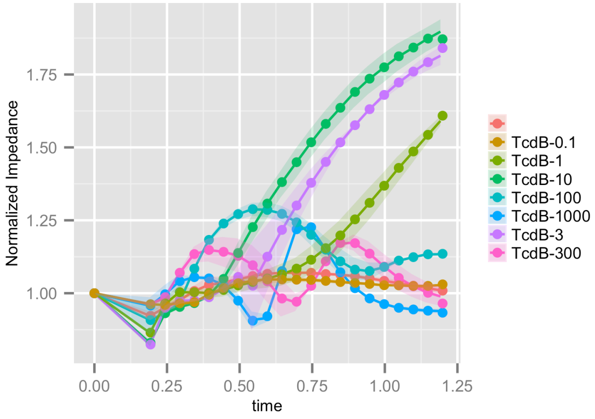

B.2.2 Reference 2

“To confirm the low toxin-sensitivity of neutrophils, we did attempt to measure impedance changes of neutrophils in response to toxins, yet the variability in these primarily non-adherent cells (impedance largely measures adherence) was too high to identify differences (Appendix B).”

See subsection B.4.8

B.3 Reproducing Figures

Below are the scripts to reproduce the figures. The data files and annotation file needed for the scripts to work are included in the supplemental data folder. The figures below were exported to PDFs. Cosmetic alterations (colors, line widths, axes labeling, legends, etc.) were made with Adobe Illustrator.

```
# A library of functions for processing multi-well data
source("./Scripts2/library.R")

# Custom 'normalize_toxin' and 'smoother_toxin' functions made for this
# LaTeX document specifically
source("./Scripts2/latexLibrary.R")

# Parse and load the data
wells = parse.RTCAanalyze(metadata = "./MasterSheet2.csv", data.dir = "./Data2")
```

B.3.1 Figure 1

```
# Process data from file HCT8-4.txt
subset = retrieveWells(wells, file = "HCT8-4.txt")
t.subset = normalize_toxin(subset, xlim = c(-Inf, 100))

# Select conditions: controls and TcdA 1000 ng/ml
conditions = groupWells(t.subset, group = "by.concentrations") %in% c("", "TcdA-1000")
f.subset = t.subset[conditions]

# Make and organize the two graphs
p1 = plot(f.subset, xlim = c(-43, 10))
p2 = plot(f.subset, xlim = c(-1, 10))
grid.arrange(p1, p2, ncol = 2)
```

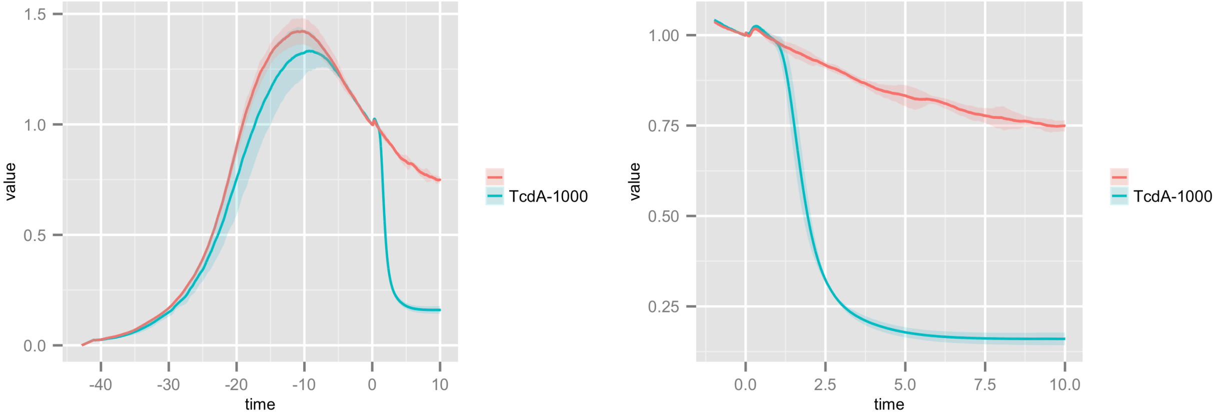

B.3.2 Figure 2

```
#### Since this figure includes data from multiple experiments and files,
#### they must all be processed first

# Only select wells seeded with at most 6,000 HCT8 cells
hct8 = retrieveWells(wells, file = "HCT8.txt", compounds = "HCT8", max.concentrations = 6000)

# The rest of the wells come from these files
files = list( "CHO.txt", "IMCE.txt", c("HUVEC-a.txt","HUVEC-b.txt"),
              c("T84-a.txt","T84-b.txt"))
subsets = lapply(files, function(f) retrieveWells(wells, file = f))
subsets = c(list(hct8), subsets)

# Normalize each subset
xlims = list(c(-0.1, 43), c(-1, Inf), c(-1, Inf), c(-1, 60), c(-1, 27))
```

```
n.subsets = mapply(normalize_toxin, subsets, xlim = xlims)

# Add a smoother to each subset
x.scales = c( 2/3, 1, 1, 2/3, 2/3 )
s.subsets = mapply( smoother_toxin, n.subsets, x.scale=x.scales )

# Calculate ABC for each subset (with different integration limits)
left = rep(0, 5)
right = c(43, 40, 80, 80, 27)
i.subsets = mapply(integrate, s.subsets, left, right)
allwells = do.call(c, i.subsets)

# Calculate MaxS for each well
allwells = max.rate(allwells, ID = "toxinAdd", min.diff = 10/60/60,
                    ylim = 0.8, xlim = 2)



######### Panel A. Different cell types. Same concentrations. #########
subset = retrieveWells(allwells, compounds = "TcdA", ID = "toxinAdd",
                       max.concentrations = 101, min.concentrations = 99)
panelA = plot(subset, xlim = c(-1, 10), se = FALSE, color = "by.total.compounds",
              linetype = "by.compounds")

######### Panel B. Same cell type. Different toxins ############
subset = retrieveWells(allwells, compounds = "IMCE")
subset2 = retrieveWells(subset, compounds = c("TcdA", "TcdB"), ID = "toxinAdd",
                  max.concentrations = c(101, 101), min.concentrations = c(99, 99))
panelB = plot(subset2, xlim = c(-0.1, 2), se = FALSE)

######## Panel C. MaxS and ABC for IMCE cells ###########
subset = retrieveWells(allwells, compounds = "IMCE")
MaxS = groupMetric(subset, ID = "toxinAdd", metric = "max.rate")
p1 = plotMetric(MaxS)
ABC = groupMetric(subset, ID = "toxinAdd", metric = "integral")
p2 = plotMetric(ABC)
panelC = arrangeGrob(p1 + theme(legend.position = "none"),
                     p2 + theme(legend.position = "none"), ncol = 2)

####### Panel D. The MCC for each cell type ##############
# The MCC was found by plotting the ABC of each cell type over
# a range of concentrations. The concentration diverging from
# controls was considered the MCC
ABC = groupMetric(allwells, ID = "toxinAdd", metric = "integral")
ABC$cells = groupWells(allwells, group = "by.total.compounds")
plotMetric(ABC, file = FALSE) + facet_wrap(~cells, scales = "free_y")
```

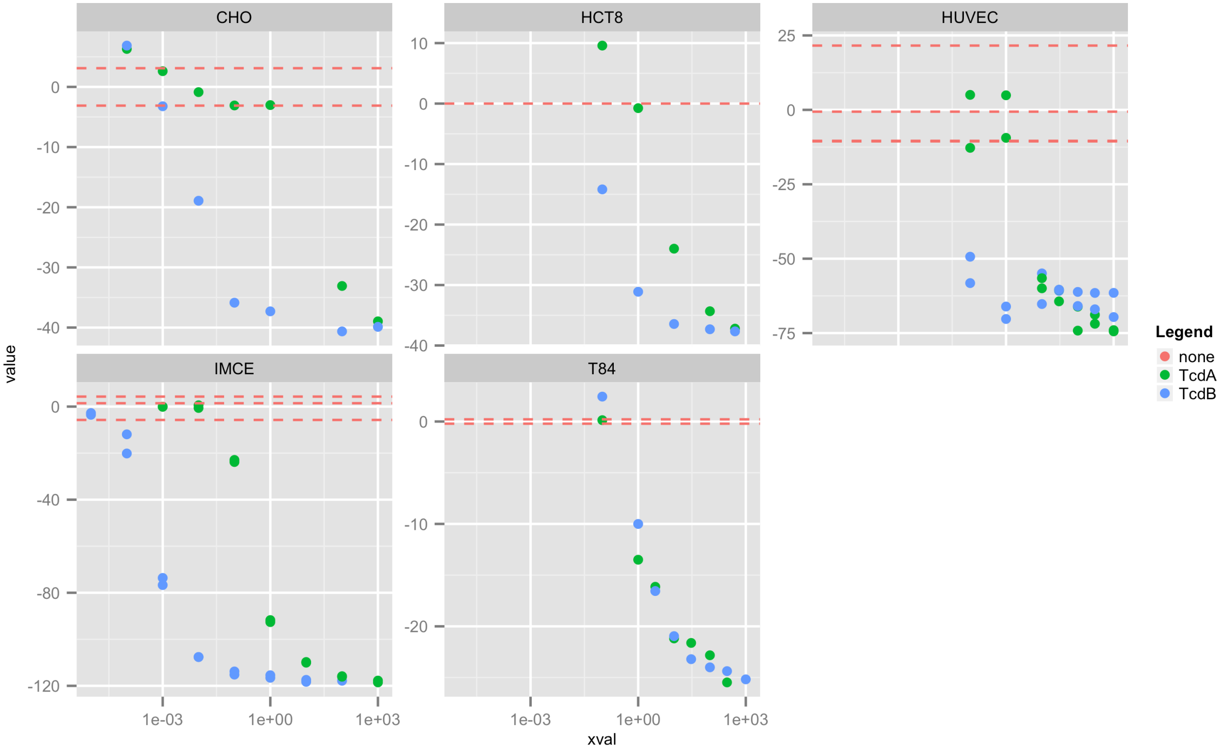

After the processing, the four panels can be combined.

```
# Manually enter the MCC for each cell type
d = data.frame(type = c("CHO", "HCT8", "HUVEC", "IMCE", "T84"), a = c(1, 1,
    1, 0.1, 0.1), b = c(0.001, 0.01, 0.01, 1e-04, 0.1))
panelD = ggplot(d, aes(x = log10(a), y = log10(b), label = type)) + geom_text() +
    scale_x_reverse(limits = c(0, -4)) + scale_y_reverse(limits = c(0, -4)) +
   geom_abline(slope = 1, intercept = 0) + coord_equal() + geom_point(color = "red")

# Show the final plot
grid.arrange(panelA, panelB, panelC, panelD, ncol = 2)
```

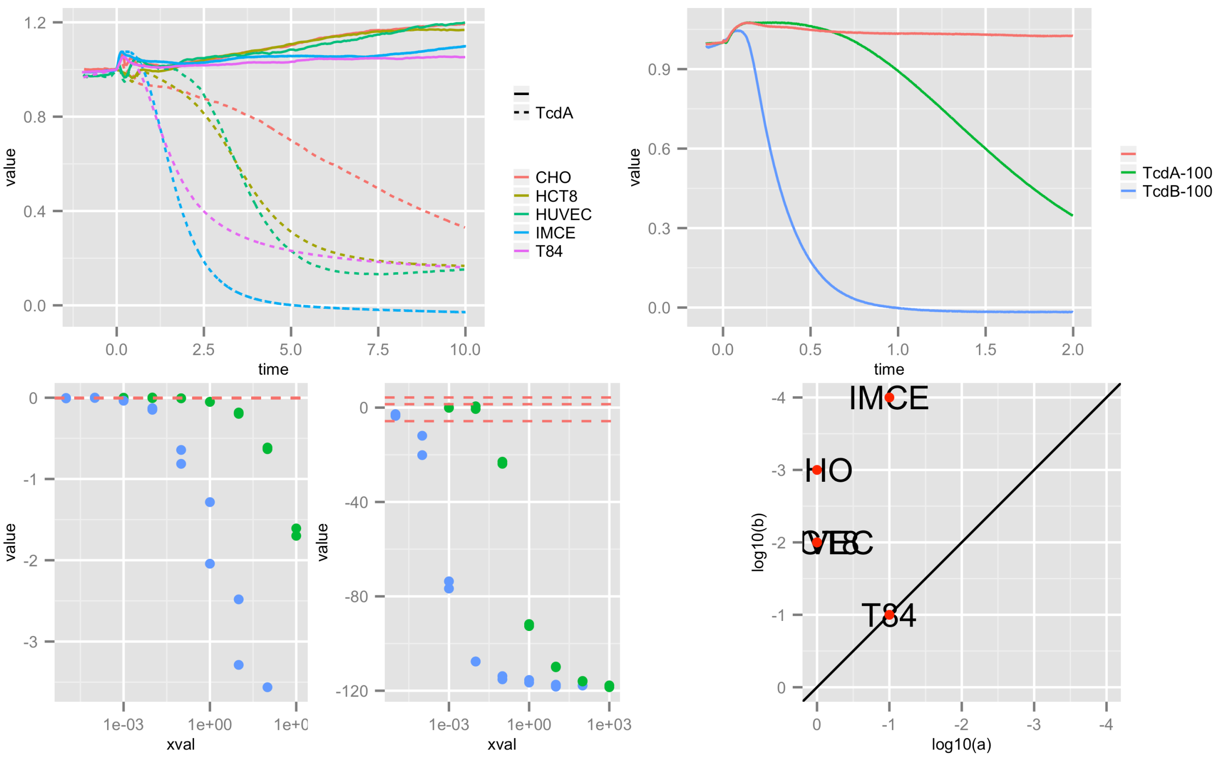

B.3.3 Figure 3

```
###### Panel A
subset = retrieveWells(wells, file = c("J774-a.txt", "J774-b.txt"))
t.subset = normalize_toxin(subset, xlim = c(-Inf, 100))

# Toxin A curves
conditions = groupWells(t.subset, group = "by.concentrations") %in%
                  c("", paste0("TcdA-", c(0.1, 3, 100, 1000)))
p1 = plot(t.subset[conditions], xlim = c(-0.01, 40))

# Toxin B curves
conditions = groupWells(t.subset, group = "by.concentrations") %in%
                  c("", paste0("TcdB-", c(0.1, 10, 100)))
p2 = plot(t.subset[conditions], xlim = c(-0.01, 15))

# TcdA and TcdB curves side by side
grid.arrange(p1, p2, ncol = 2)
```

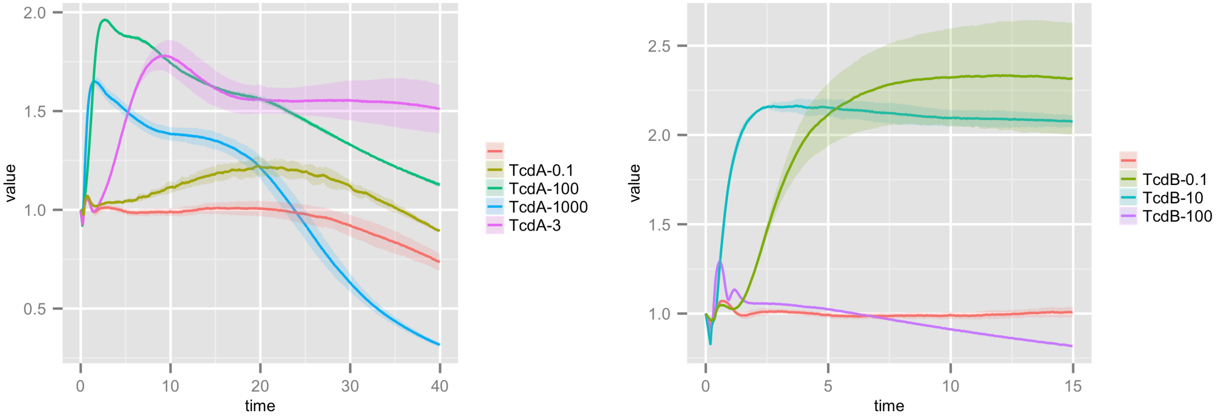

```
###### Panel B
subset = retrieveWells(wells, file = "J774-4.txt")
t.subset = normalize_toxin(subset, xlim = c(-Inf, 100))

conditions = groupWells(t.subset, group = "by.concentrations") %in% c("", "TcdA-300",
    "TcdB-100", "TcdB-1")
p3 = plot(t.subset[conditions], xlim = c(-1, 48))
p4 = plot(t.subset[conditions], xlim = c(-1, 5))
grid.arrange(p3, p4, ncol = 2)
```

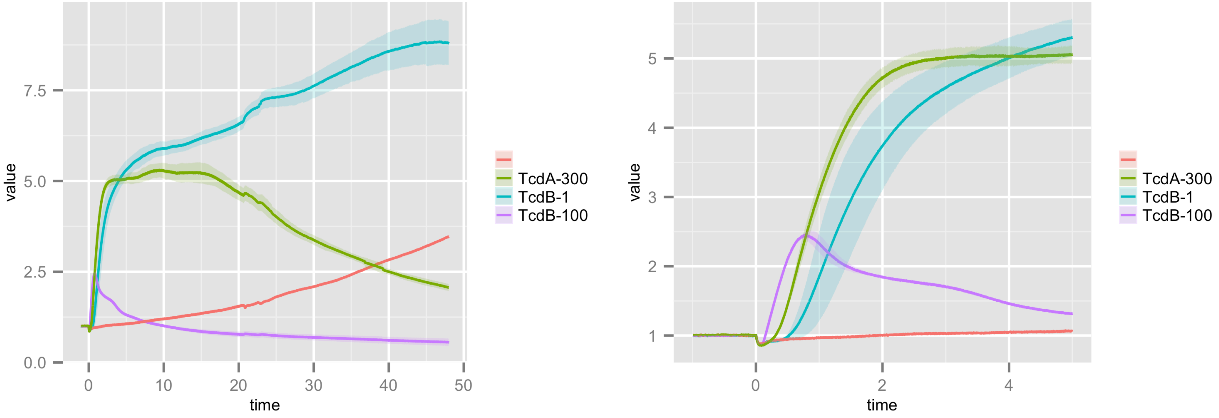

B.3.4 Figure 4

```
subset = retrieveWells(wells, file = c("HCT8-4.txt"))
t.subset = normalize_toxin(subset, xlim = c(-2, Inf))

###### Panel A
conditions = groupWells(t.subset, group = "by.compounds") %in% c("gdTcdB", "")
p1 = plot(t.subset[conditions]) + ylim(0, 1.2)
```

```
###### Panel B
conditions = groupWells(t.subset, group = "by.concentrations") %in%
                 c("", "gdTcdB-100", "TcdB-10", "gdTcdB-100.TcdB-10")
p2 = plot(t.subset[conditions], xlim = c(-0.2, 4)) + ylim(0, 1.2)

###### Panel C
conditions = groupWells(t.subset, group = "by.concentrations") %in%
                 c("", "gdTcdB-1000", "TcdA-1000", "gdTcdB-1000.TcdA-1000",
                                      "TcdA-100", "gdTcdB-1000.TcdA-100")
p3 = plot(t.subset[conditions], xlim = c(-0.2, 10)) + ylim(0, 1.2)

grid.arrange(p1,p2,p3,ncol=2)
```

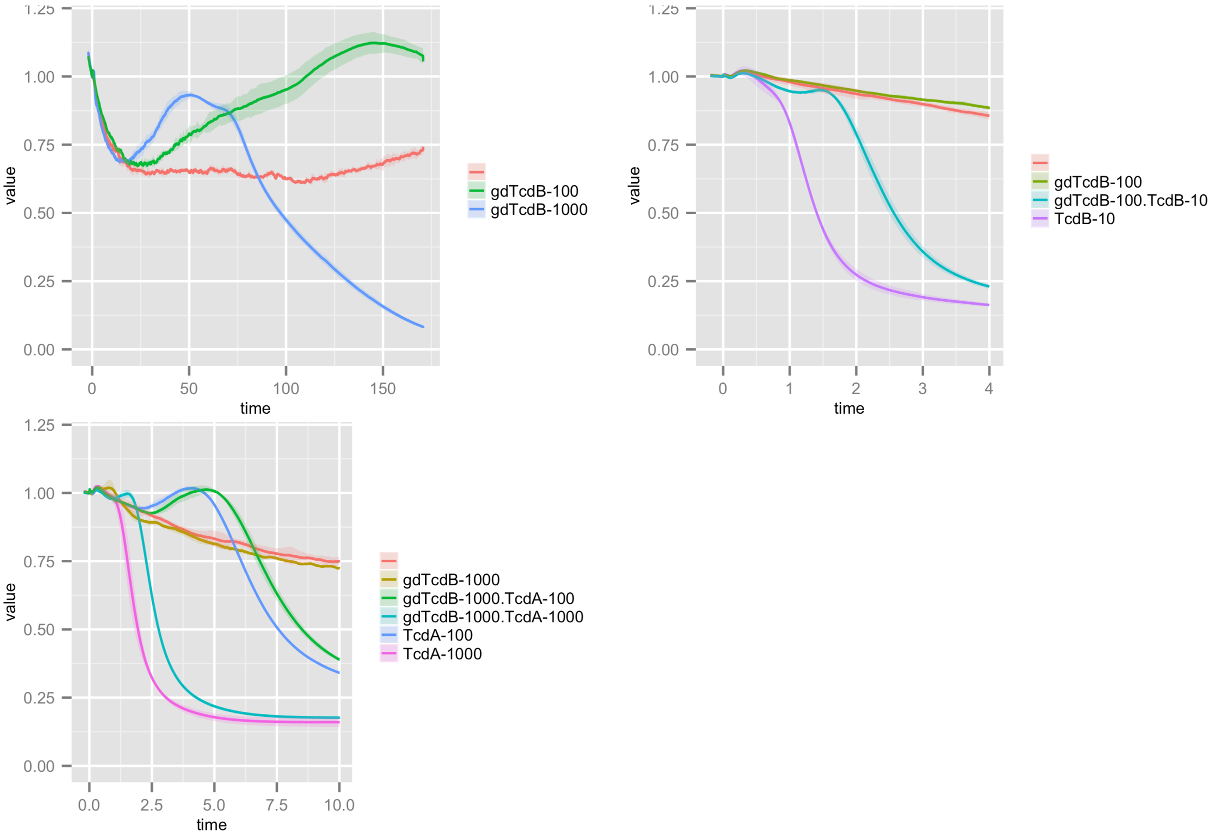

B.3.5 Figure 5

```
##### Panel A
subset = retrieveWells(wells, file = "J774-4.txt")
t.subset = normalize_toxin(subset, xlim = c(-2, Inf))
conditions = groupWells(t.subset, group = "by.compounds") %in%
                 c("", "TcdB", "gdTcdB")
p1 = plot(t.subset[conditions], xlim = c(-1, 48))
```

```
##### Panel B
subset = retrieveWells(wells, file = c("J774-3a.txt", "J774-3b.txt"))
t.subset = normalize_toxin(subset, xlim = c(-2, Inf))
conditions = groupWells(t.subset, group = "by.concentrations") %in%
                 c("", "TcdB-0.01", "gdTcdB-1.TcdB-0.01")
p2 = plot(t.subset[conditions], xlim = c(-0.2, 5))

##### Panel C
subset = retrieveWells(wells, file = c("J774-5.txt"))
t.subset = normalize_toxin(subset, xlim = c(-2, Inf))
conditions = groupWells(t.subset, group = "by.concentrations") %in%
                  c("", "gdTcdB-10", "TcdA-1", "gdTcdB-10.TcdA-1")
p3 = plot(t.subset[conditions], xlim = c(-0.2, 24))

grid.arrange(p1, p2, p3, ncol = 2)
```

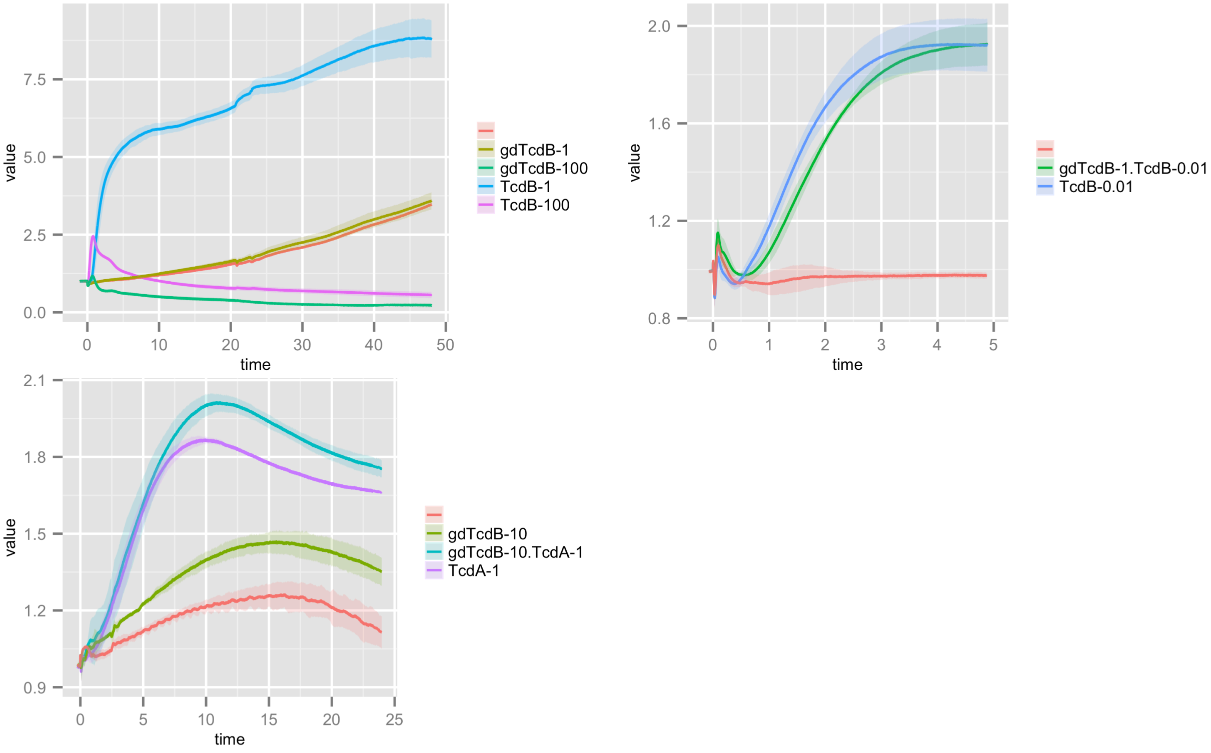

B.4 Exploring the data

All experiments, each involving several experimental conditions, are summarized in the table below. Independent experiments that occurred on different days are separated by horizontal lines. Diagrams of the physical multi-well plates are displayed in B.4.9. The number of cells seeded and all the incubation times can be found in the csv annotation file in the supplemental data or can be accessed in the **wells** variable within R (as shown in B.3).

B.4.1 Plate summaries

Cell type	File names	Toxins (ng/ml)	Notes
HCT8	HCT8.txt	A (500, 100, 10, 1, 0.1)	
		B (500, 100, 10, 1, 0.1)	
	HCT8-2a.txt HCT8-2b.txt	B (1), A (100)	toxins + gdTcdB
		gdTcdB (100, 1000)	
		B (1) + gdTcdB (100)	
		B (1) + gdTcdB(1000)	
		A (100) + gdTcdB (1000)	
	HCT8-3.txt	B (1), A (100)	toxins + gdTcdB
		gdTcdB (10, 100, 1000)	
		B (1) + gdTcdB (10)	
		B (1) + gdTcdB (100)	
		A (100) + gdTcdB (1000)	
	HCT8-4.txt	B (10, 100), A (100, 1000)	toxins + gdTcdB
		gdTcdB (100, 1000)	
		B (10) + gdTcdB (100)	
		B (10) + gdTcdB (1000)	
		B (100) + gdTcdB (100)	
		B (100) + gdTcdB (1000)	
		A (10) + gdTcdB (100)	
		A (100) + gdTcdB (100)	
		A (100) + gdTcdB (1000)	
		A (1000) + gdTcdB (1000)	
CHO	CHO.txt	A (1000, 100, 1, 0.1, 0.01, 1e-3, 1e-4)	
		B (1000, 100, 1, 0.1, 0.01, 1e-3, 1e-4)	
IMCE	IMCE.txt	A (1000, 100, 10, 1, 0.1, 0.01, 0.001)	
		B (1000, 100, 10, 1, 0.1, 0.01, 0.001)	
HUVEC	HUVEC-a.txt	A (1000, 300, 100, 30, 10, 1, 0.1)	
	HUVEC-b.txt	B (1000, 300, 100, 30, 10, 1, 0.1)	
T84	T84-a.txt	A (300, 100, 30, 10, 3, 1, 0.1)	
	T84-b.txt	B (1000, 300, 100, 30, 10, 3, 1, 0.1)	
J774	J774-a.txt	A (0.1, 1, 3, 10, 100, 300, 1000)	
	J774-b.txt	B (0.1, 1, 3, 10, 100, 300, 1000)	
	J774-2.txt	B (0.00001, 0.0001, 0.001, 0.01, 0.1, 1, 10)	
	J774-3a.txt J774-3b.txt	A (10), B (0.01)	toxins + gdTcdB
		gdTcdB (0.1, 1, 100)	
		B (0.01) + gdTcdB (1)	
		B (0.01) + gdTcdB (0.1)	
		A (10) + gdTcdB (100)	
	J774-4.txt	A (3, 300), B (1, 100)	toxins + gdTcdB
		gdTcdB (1, 100)	
		A (10) + gdTcdB (100)	

	J774-5.txt	A (1, 1000), gdTcdB (10, 100) A (1) + gdTcdB (10) A (1000) + gdTcdB (1000) B (10) + gdTcdB (100)	toxins + gdTcdB
PMN	PMN-a.txt PMN-b.txt	A (10000, 7000, 5000, 3000, 1000, 500, 100) B (10000, 7000, 5000, 3000, 1000, 500, 100)	toxins + IL8
	PMN-2a.txt PMN-2b.txt	A (1000, 100, 10, 1, 0.1, 0.01, 0.001) B (1000, 100, 10, 1, 0.1, 0.01, 0.001)	toxins alone
	PMN-3.txt	A (10, 100, 1000) B (1, 10, 100, 1000)	toxins alone and toxins + IL8
	PMN-4.txt	A (10, 100, 1000) B (10, 100, 1000)	toxins alone and toxins + IL8

B.4.2 HCT8 cells

HCT8.txt

```
subset = retrieveWells(wells, file = "HCT8.txt", compounds = "HCT8", max.concentrations = 6000)
t.subset = normalize_toxin(subset, xlim = c(-1, 10))
p1 = plot(retrieveWells(t.subset, compounds = "TcdA"))
p2 = plot(retrieveWells(t.subset, compounds = "TcdB"))
grid.arrange(p1, p2, ncol = 2)
```

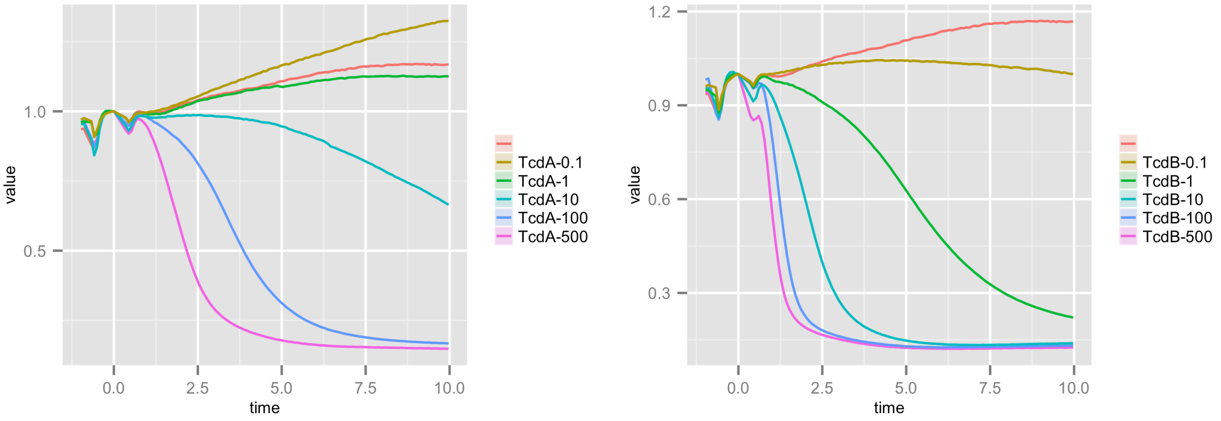

HCT8-2a.txt and HCT8-2b.txt

```
subset = retrieveWells(wells, file = c("HCT8-2a.txt", "HCT8-2b.txt"))
t.subset = normalize_toxin(subset, xlim = c(-2, Inf))
p1 = plot(t.subset, xlim = c(-2, 150))
```

```
t.subset = smoother_toxin(t.subset, x.scale = 1.1)
t.subset = max.rate(t.subset, ID = "toxinAdd", min.diff = 10/3600, ylim = 0.88,
    xlim = 2)
maxs = getMetric(t.subset, metric = "max.rate")
labels = factor(groupWells(t.subset, group = "by.concentrations", ID = "toxinAdd"),
    levels = c("", "gdTcdB-100", "gdTcdB-1000", "gdTcdB-1000.TcdA-100", "TcdA-100",
        "gdTcdB-100.TcdB-1", "gdTcdB-10.TcdB-1", "TcdB-1"))
p2 = qplot(labels, maxs$value, color = labels) + no_x_labels + labs(color = "Legend") +
    xlab("group") + ylab("MaxS")

grid.arrange(p1, p2, ncol = 2)
```

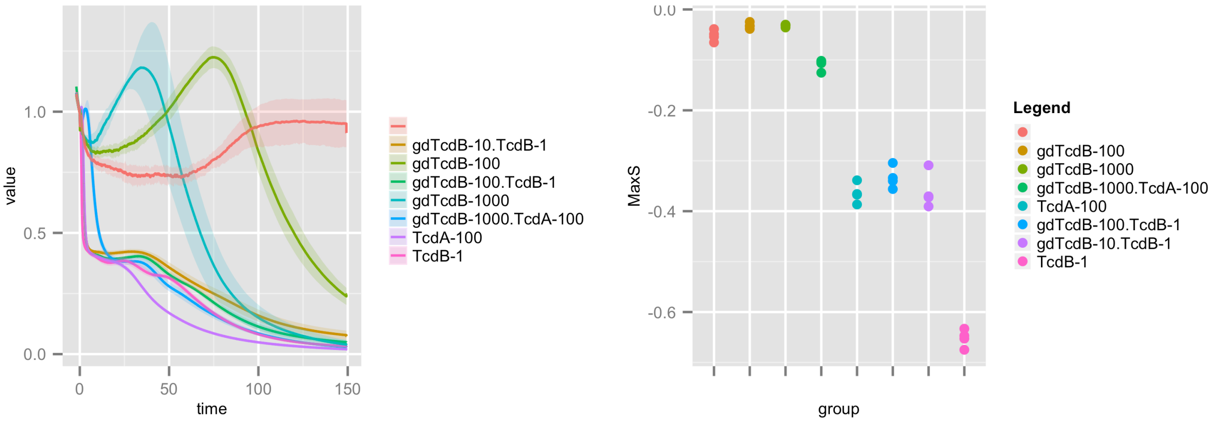

HCT8-3.txt

```
subset = retrieveWells(wells, file = c("HCT8-3.txt"))
t.subset = normalize_toxin(subset, xlim = c(-2, 58))
p1 = plot(t.subset)

t.subset = smoother_toxin(t.subset, x.scale = 1.1)
t.subset = max.rate(t.subset, ID = "toxinAdd", min.diff = 10/3600, ylim = 0.88,
    xlim = 2)
maxs = getMetric(t.subset, metric = "max.rate")
labels = factor(groupWells(t.subset, group = "by.concentrations", ID = "toxinAdd"),
    levels = c("", "gdTcdB-10", "gdTcdB-100", "gdTcdB-1000", "gdTcdB-100.TcdB-1",
      "gdTcdB-10.TcdB-1", "TcdB-1", "gdTcdB-1000.TcdA-100", "TcdA-100", "TcdAother-100",
        "TcdAup-100"))
p2 = qplot(labels, maxs$value, color = labels) + no_x_labels + labs(color = "Legend") +
    xlab("group") + ylab("MaxS")
grid.arrange(p1, p2, ncol = 2)
```

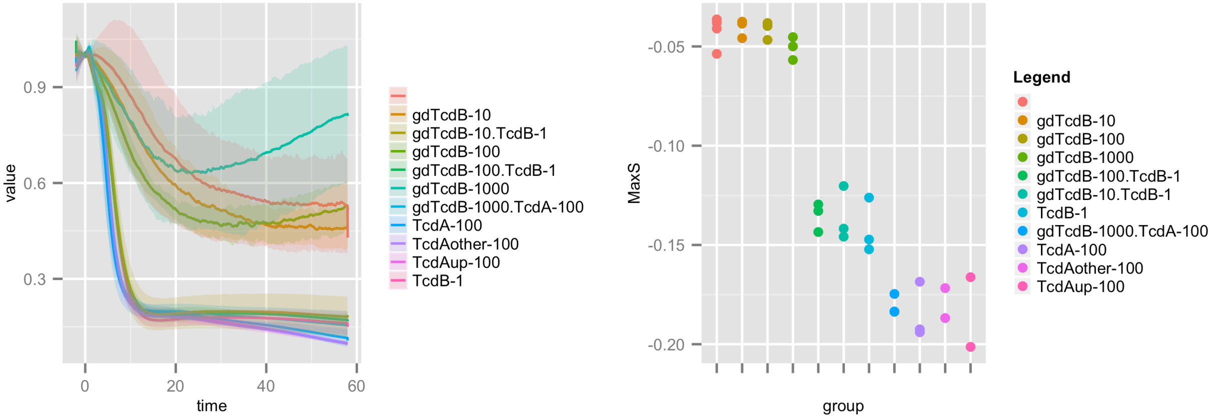

HCT8-4.txt

```
subset = retrieveWells(wells, file = c("HCT8-4.txt"))
t.subset = normalize_toxin(subset, xlim = c(-2, 155))
p1 = plot(t.subset)

t.subset = smoother_toxin(t.subset, x.scale = 1.1)
t.subset = max.rate(t.subset, ID = "toxinAdd", min.diff = 10/3600, ylim = 0.88,
    xlim = 2)
t.subset = integrate(t.subset, lower = 0, upper = 10)

maxs = getMetric(t.subset, metric = "max.rate")
labels = factor(groupWells(t.subset, group = "by.concentrations", ID = "toxinAdd"),
    levels = c("", "gdTcdB-100", "gdTcdB-1000", "gdTcdB-100.TcdA-10", "TcdA-10",
     "gdTcdB-1000.TcdA-100", "gdTcdB-100.TcdA-100", "TcdA-100", "gdTcdB-1000.TcdA-1000",
        "TcdA-1000", "gdTcdB-1000.TcdB-10", "gdTcdB-100.TcdB-10", "TcdB-10",
        "gdTcdB-1000.TcdB-100", "gdTcdB-100.TcdB-100", "TcdB-100"))
p2 = qplot(labels, maxs$value, color = labels) + no_x_labels + labs(color = "Legend") +
    xlab("group") + ylab("MaxS")

# MaxS metrics show unexpected results for TcdB at 100 ng/ml This plot shows
# that gdTcdB appears to have only been added to one of the four wells?
# Regardless, gdTcdB clearly delayed TcdB at 10 ng/ml
aa = retrieveWells(t.subset, compounds = "TcdB", max.concentrations = 101, min.concentrations = 99
p3 = plot(aa, xlim = c(-1, 7), replicates = FALSE)

grid.arrange(arrangeGrob(p1, p3, ncol = 2), p2, nrow = 2)
```

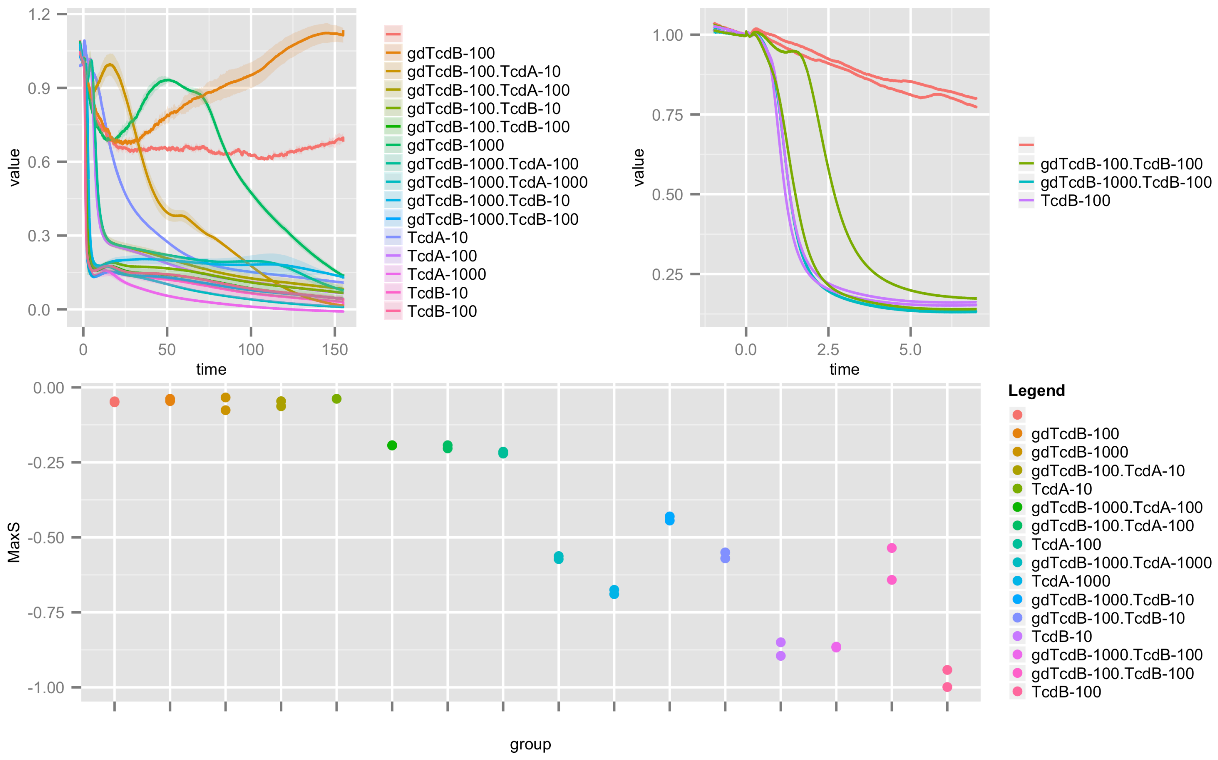

B.4.3 CHO cells

CHO.txt

```
subset = retrieveWells(wells, file = "CHO.txt")
t.subset = normalize_toxin(subset, c(-2, Inf))
p1 = plot(retrieveWells(t.subset, compounds = "TcdA"), xlim = c(-1, 40))
p2 = plot(retrieveWells(t.subset, compounds = "TcdB"), xlim = c(-1, 20))
grid.arrange(p1, p2, ncol = 2)
```

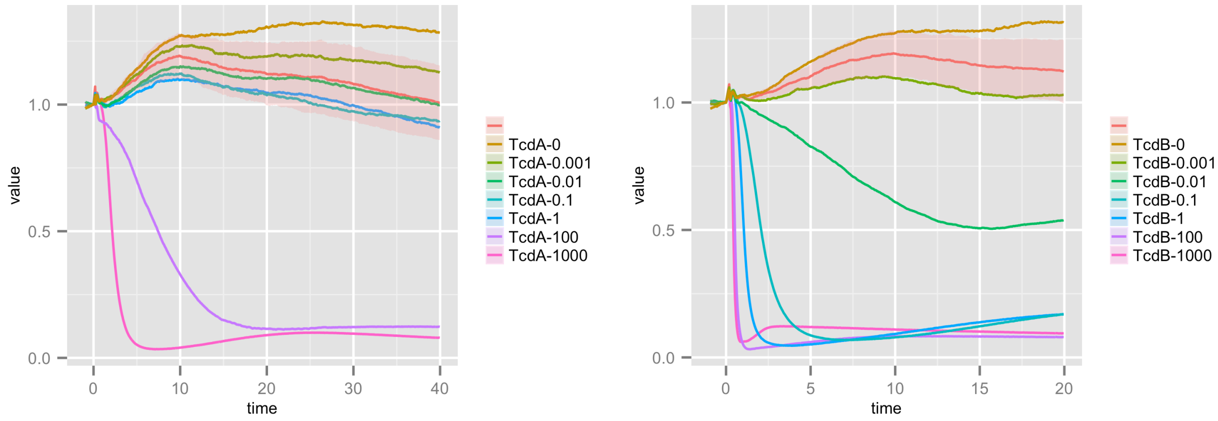

B.4.4 IMCE cells

IMCE.txt

```
subset = retrieveWells(wells, file = "IMCE.txt")
t.subset = normalize_toxin(subset, c(-2, Inf))
p1 = plot(retrieveWells(t.subset, compounds = "TcdA"), xlim = c(-1, 80))
p2 = plot(retrieveWells(t.subset, compounds = "TcdB"), xlim = c(-1, 80))
grid.arrange(p1, p2, ncol = 2)
```

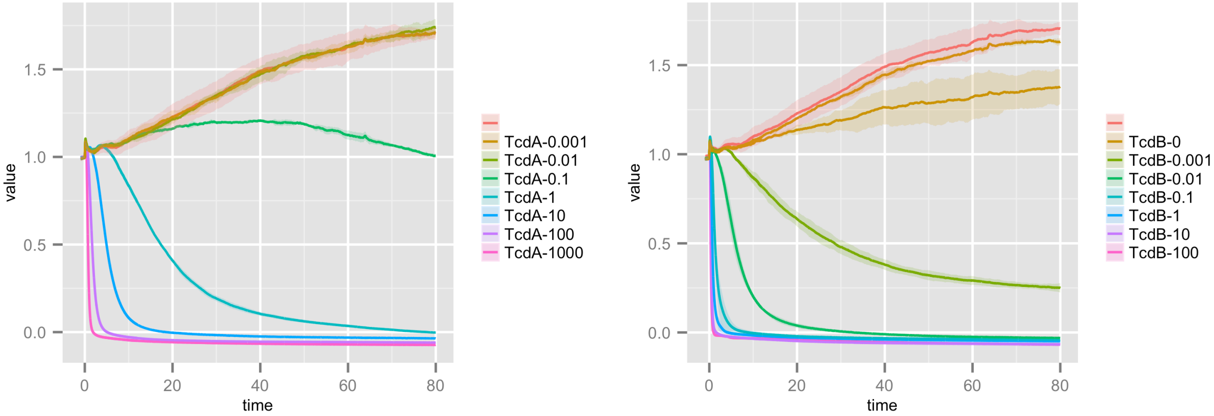

B.4.5 HUVECs

HUVEC-a.txt and HUVEC-b.txt

```
subset = retrieveWells(wells, file = c("HUVEC-a.txt", "HUVEC-b.txt"))
t.subset = normalize_toxin(subset, c(-2, Inf))
p1 = plot(retrieveWells(t.subset, compounds = "TcdA"), xlim = c(-1, 20))
p2 = plot(retrieveWells(t.subset, compounds = "TcdB"), xlim = c(-1, 20))
grid.arrange(p1, p2, ncol = 2)
```

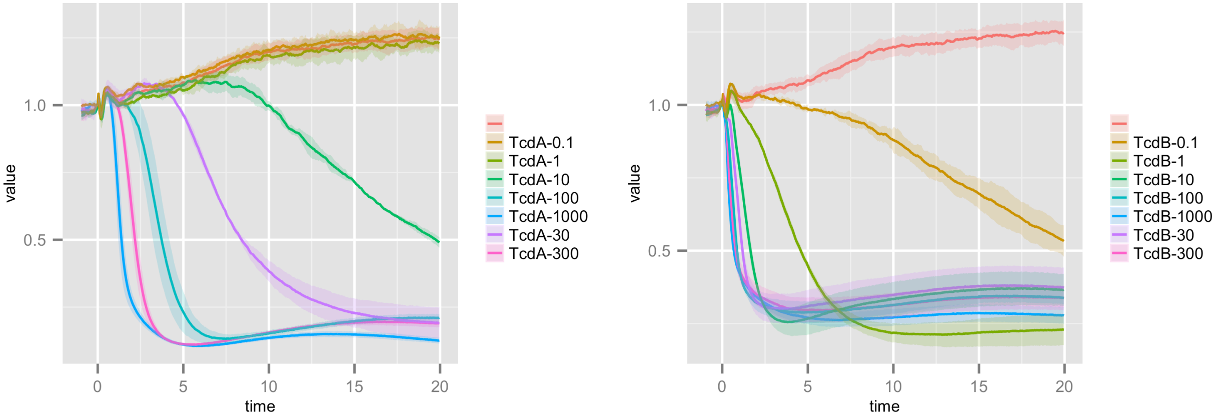

B.4.6 T84 cells

T84-a.txt and T84-b.txt

```
subset = retrieveWells(wells, file = c("T84-a.txt", "T84-b.txt"))
t.subset = normalize_toxin(subset, c(-2, Inf))
p1 = plot(retrieveWells(t.subset, compounds = "TcdA"), xlim = c(-1, 20))
p2 = plot(retrieveWells(t.subset, compounds = "TcdB"), xlim = c(-1, 20))
grid.arrange(p1, p2, ncol = 2)
```

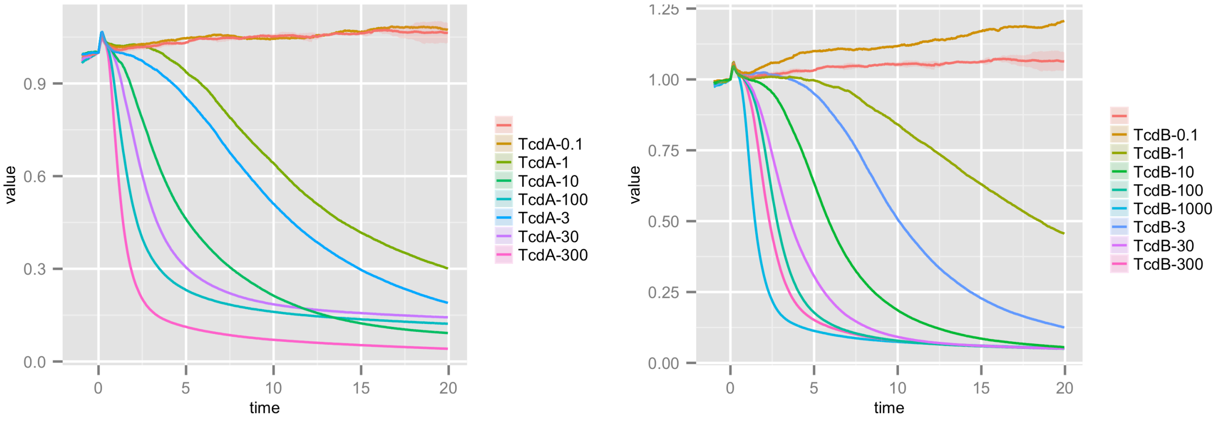

B.4.7 J774 cells

J774-a.txt and J774-b.txt

```
subset = retrieveWells(wells, file = c("J774-a.txt", "J774-b.txt"))
t.subset = normalize_toxin(subset, c(-2, Inf))
p1 = plot(retrieveWells(t.subset, compounds = "TcdA"), xlim = c(-1, 40))
p2 = plot(retrieveWells(t.subset, compounds = "TcdB"), xlim = c(-1, 40))
grid.arrange(p1, p2, ncol = 2)
```

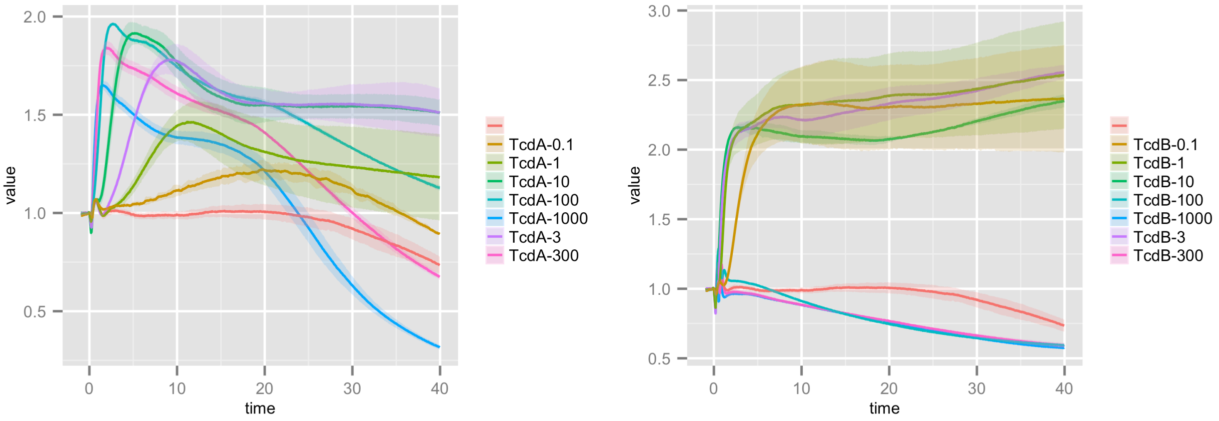

J774-2.txt

```
subset = retrieveWells(wells, file = "J774-2.txt")
t.subset = normalize_toxin(subset, c(-2, Inf))
p1 = plot(t.subset, xlim = c(-1, 40))
p2 = plot(t.subset, xlim = c(-1, 5))
grid.arrange(p1, p2, ncol = 2)
```

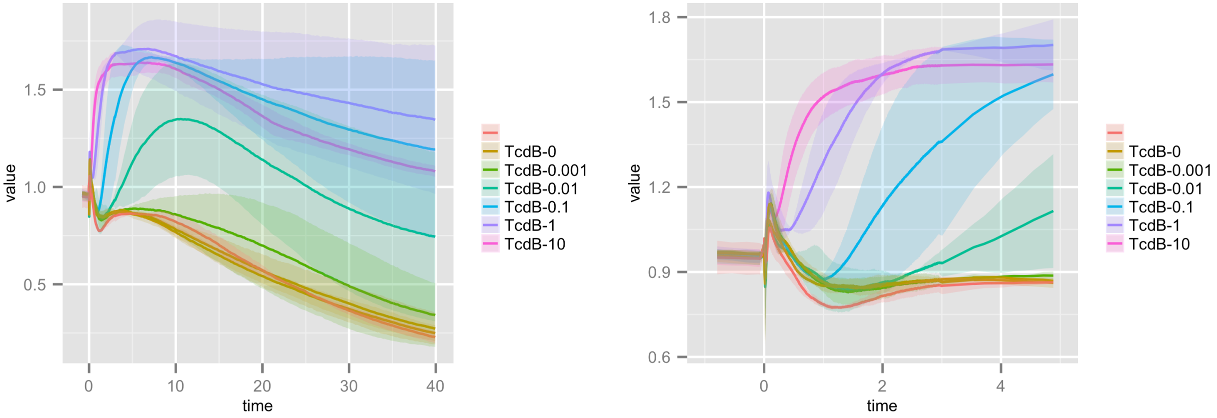

J774-3a.txt and J774-3b.txt

```
subset = retrieveWells(wells, file = c("J774-3a.txt", "J774-3b.txt"))
t.subset = normalize_toxin(subset, c(-2, Inf))
p1 = plot(t.subset, xlim = c(-1, 24))
p2 = plot(t.subset, xlim = c(-1, 5))
grid.arrange(p1, p2, ncol = 2)
```

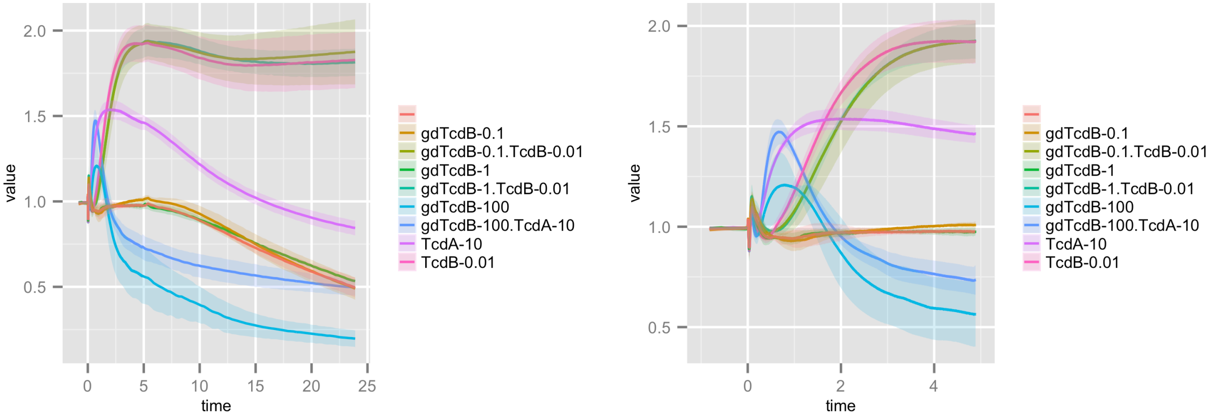

J774-4.txt

```
subset = retrieveWells(wells, file = "J774-4.txt")
t.subset = normalize_toxin(subset, c(-2, Inf))
p1 = plot(t.subset, xlim = c(-1, 48))
p2 = plot(t.subset, xlim = c(-1, 5))
grid.arrange(p1, p2, ncol = 2)
```

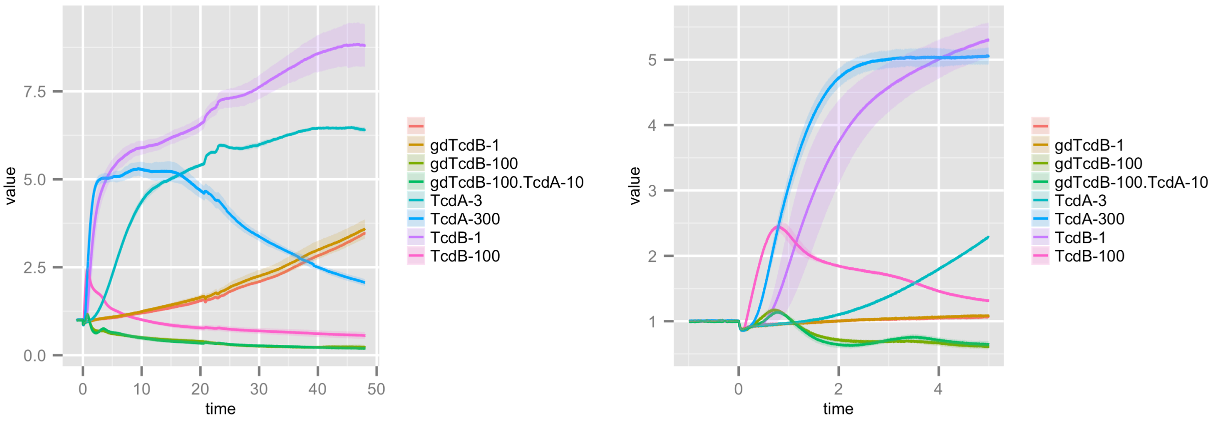

J774-5.txt

```
subset = retrieveWells(wells, file = "J774-5.txt")
t.subset = normalize_toxin(subset, c(-2, Inf))
p1 = plot(t.subset, xlim = c(-1, 48))
p2 = plot(t.subset, xlim = c(-1, 5))
grid.arrange(p1, p2, ncol = 2)
```

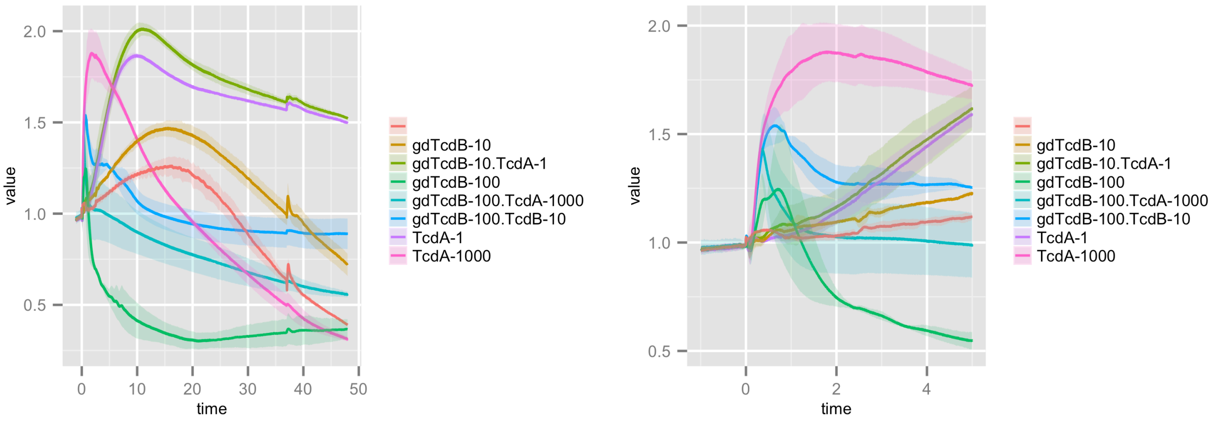

B.4.8 PMN leukocytes

Consistent response profiles of PMNs to TcdA or TcdB could not be obtained.

PMN-2a.txt and PMN-2b.txt

Only TcdA at 1,000 ng/ml was clearly different than control cells. Instead of normalizing the impedance at the time toxin was added, the change in impedance from the time of toxin addition is shown.

```r
subset = retrieveWells(wells, file = c("PMN-2a.txt", "PMN-2b.txt"))
t.subset = transform(subset, c("tcenter", "slice", "level"), xlim = c(-2, Inf),
    ID = "toxinAdd")
p1 = plot(retrieveWells(t.subset, compounds = "TcdA"), xlim = c(-1, 24))
p2 = plot(retrieveWells(t.subset, compounds = "TcdB"), xlim = c(-1, 24))
grid.arrange(p1, p2, ncol = 2)
```

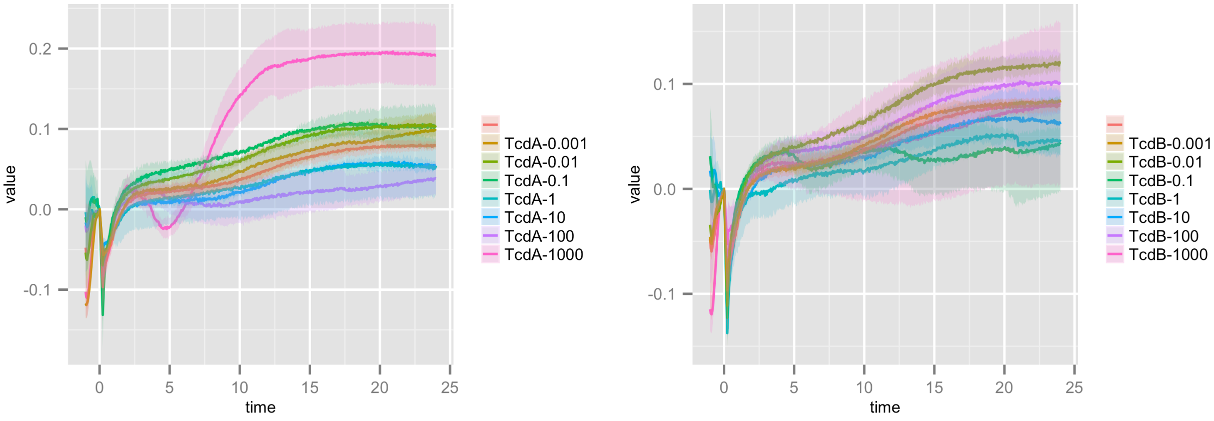

PMN-a.txt and PMN-b.txt

Cells were seeded in the presence of 100 ng/ml (9.01 nM) of human recombinant IL-8 in an attempt to increase impedance before adding toxin.

```r
subset = retrieveWells(wells, file = c("PMN-a.txt", "PMN-b.txt"))
t.subset = transform(subset, c("tcenter", "slice", "level"), xlim = c(-2, Inf),
    ID = "toxinAdd")
p1 = plot(retrieveWells(t.subset, compounds = "TcdA"), xlim = c(-1, 24))
p2 = plot(retrieveWells(t.subset, compounds = "TcdB"), xlim = c(-1, 24))
grid.arrange(p1, p2, ncol = 2)
```

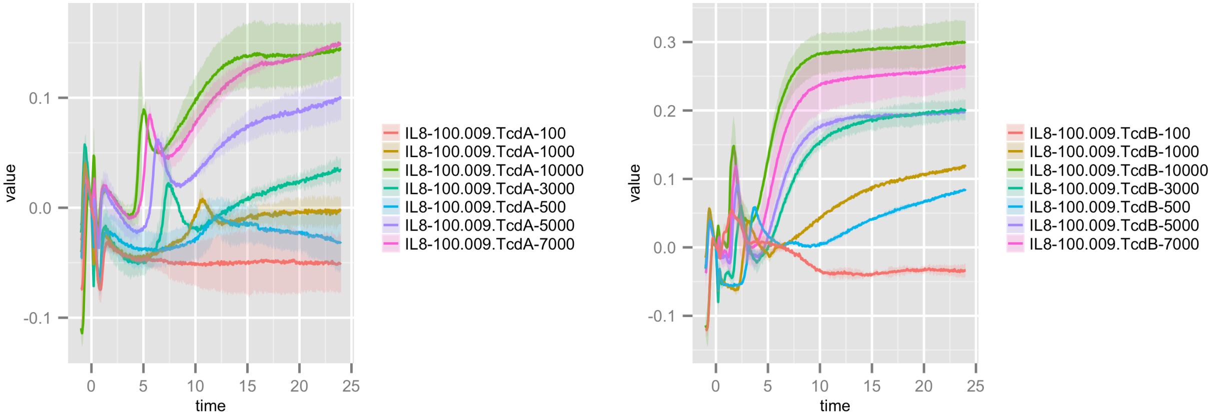

PMN-3.txt

Cells were seeded in the presence of 25 nM (277.45 ng/ml) of IL-8.

```
subset = retrieveWells(wells, file = "PMN-3.txt")
t.subset = transform(subset, c("tcenter", "slice", "level"), xlim = c(-2, Inf),
    ID = "toxinAdd")
p1 = plot(retrieveWells(t.subset, compounds = "TcdA"), xlim = c(-1, 48), replicates = FALSE)
p2 = plot(retrieveWells(t.subset, compounds = "TcdB"), xlim = c(-1, 48), replicates = FALSE)
grid.arrange(p1, p2, ncol = 2)
```

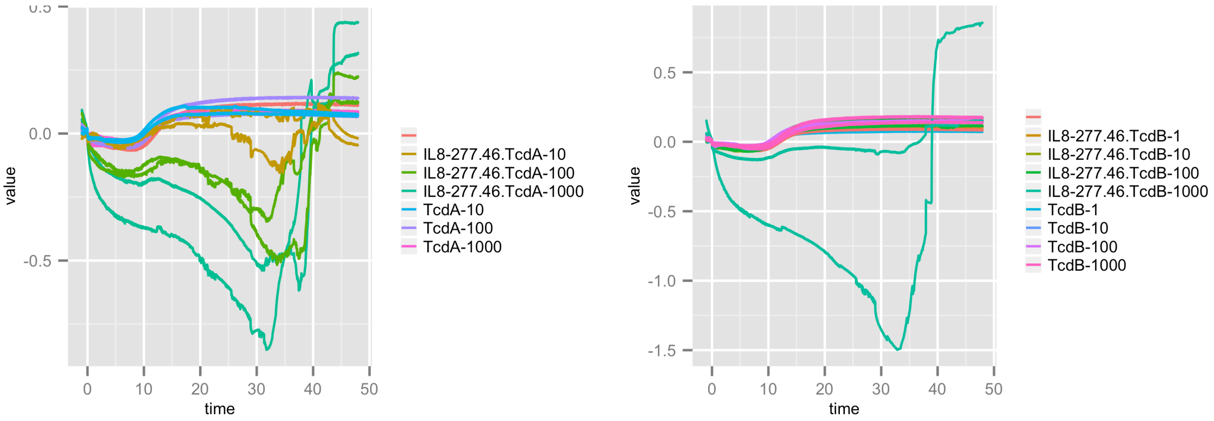

PMN-4.txt

Cells were seeded in the presence of 25 nM (277.45 ng/ml) of IL-8. The machine temporarily stopped making impedance measurements from approximately five to 20 hours.

```
subset = retrieveWells(wells, file = "PMN-4.txt")
t.subset = transform(subset, c("tcenter", "slice", "level"), xlim = c(-2, Inf),
    ID = "toxinAdd")
p1 = plot(retrieveWells(t.subset, compounds = "TcdA"), xlim = c(-1, 48))
p2 = plot(retrieveWells(t.subset, compounds = "TcdB"), xlim = c(-1, 48))
grid.arrange(p1, p2, ncol = 2)
```

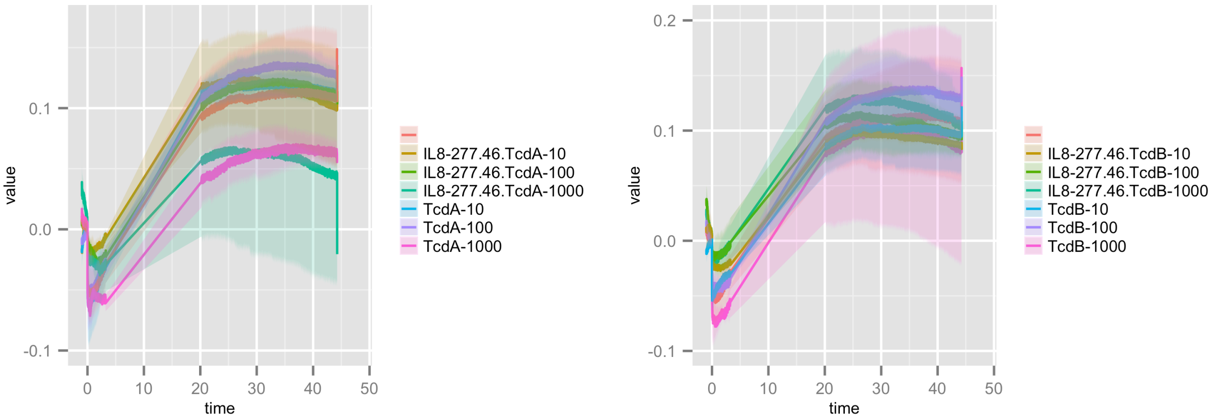

B.4.9 Plate Layouts

Below are the layouts of all of the plates used.

```
fwells = split(wells, getfiles(wells))
fwells = fwells[sort(names(fwells))]

options(xtable.print.results=FALSE)
fwt = lapply(fwells, well_table, ID="toxinAdd")
lt = lapply(fwt, print_well_table, scalebox=0.6, floating=FALSE)

do.call( cat, c("\\begin{adjustwidth}{0in}{3in}{",lt,"} \\end{adjustwidth}") )
```

	1	2
A	TcdA-1000	TcdB-1000
B		TcdB-100
C	TcdA-100	TcdB-1
D	TcdA-1	TcdB-0.1
E	TcdA-0.1	TcdB-0.01
F	TcdA-0.01	
G	TcdA-0.001	TcdB-0.001
H	TcdA-1e-04	TcdB-1e-04

CHO.txt

	1	2
A	TcdB-1, gdTcdB-100	TcdB-1, gdTcdB-100
B	TcdB-1, gdTcdB-10	TcdB-1, gdTcdB-10
C	TcdA-100, gdTcdB-1000	TcdA-100, gdTcdB-1000
D	TcdB-1	TcdB-1
E	TcdA-100	TcdA-100
F	gdTcdB-1000	gdTcdB-1000
G	gdTcdB-100	gdTcdB-100
H		

HCT8-2a.txt

	3	4
A	TcdB-1, gdTcdB-100	TcdB-1, gdTcdB-100
B	TcdB-1, gdTcdB-10	TcdB-1, gdTcdB-10
C	TcdA-100, gdTcdB-1000	TcdA-100, gdTcdB-1000
D	TcdB-1	TcdB-1
E	TcdA-100	TcdA-100
F	gdTcdB-1000	gdTcdB-1000
G	gdTcdB-100	gdTcdB-100
H		

HCT8-2b.txt

	3	4	5	6
A	TcdA-100, gdTcdB-1000		TcdA-100	gdTcdB-10
B	gdTcdB-100	TcdA-100	TcdA-100, gdTcdB-1000	TcdAup-100
C	TcdA-100	gdTcdB-100		gdTcdB-10
D		TcdA-100, gdTcdB-1000	gdTcdB-100	TcdAup-100
E	TcdB-1	gdTcdB-1000	TcdB-1, gdTcdB-10	gdTcdB-10
F	TcdB-1, gdTcdB-100	TcdB-1, gdTcdB-10	TcdB-1	TcdAother-100
G	TcdB-1, gdTcdB-10	TcdB-1, gdTcdB-100	gdTcdB-1000	TcdAother-100
H	gdTcdB-1000	TcdB-1	TcdB-1, gdTcdB-100	

HCT8-3.txt

	1	2	3	4
A	TcdA-10	TcdB-10	TcdB-100, gdTcdB-1000	TcdB-100, gdTcdB-1000
B	TcdA-1000	TcdA-1000	TcdB-100	TcdB-10
C			TcdA-10, gdTcdB-100	TcdB-100, gdTcdB-100
D	gdTcdB-1000	gdTcdB-1000	TcdA-100, gdTcdB-100	TcdA-1000, gdTcdB-1000
E	gdTcdB-100	TcdA-100	TcdA-1000, gdTcdB-1000	
F	TcdB-10, gdTcdB-100	gdTcdB-100	TcdA-10, gdTcdB-100	TcdA-100, gdTcdB-1000
G	TcdB-10, gdTcdB-100	TcdA-100	TcdB-10, gdTcdB-1000	TcdA-100, gdTcdB-1000
H	TcdB-10, gdTcdB-1000	TcdB-100	TcdA-100, gdTcdB-100	TcdB-100, gdTcdB-100

HCT8-4.txt

	3	4
A	TcdA-100	TcdA-100
B	NA-NA	NA-NA
C	TcdB-100	
D	TcdA-500	TcdB-500
E	TcdA-100	TcdB-100
F	TcdA-10	TcdB-10
G	TcdA-1	TcdB-1
H	TcdA-0.1	TcdB-0.1

HCT8.txt

	3	4
A	TcdA-1000	TcdB-1000
B	TcdA-300	TcdB-300
C	TcdA-100	TcdB-100
D		
E	TcdA-30	TcdB-30
F	TcdA-10	TcdB-10
G	TcdA-1	TcdB-1
H	TcdA-0.1	TcdB-0.1

HUVEC-a.txt

	5	6
A	TcdA-1000	TcdB-1000
B	TcdA-300	TcdB-300
C	TcdA-100	TcdB-100
D		
E	TcdA-30	TcdB-30
F	TcdA-10	TcdB-10
G	TcdA-1	TcdB-1
H	TcdA-0.1	TcdB-0.1

HUVEC-b.txt

	3	4	5	6
A	TcdA-1000	TcdB-100	TcdA-1000	TcdB-10
B	TcdA-100	TcdB-10	TcdA-100	TcdB-1
C		TcdB-1		TcdB-0.1
D	TcdA-10	TcdB-0.1	TcdA-10	TcdB-0.01
E	TcdA-1	TcdB-0.01	TcdA-1	TcdB-0.001
F	TcdA-0.1	TcdB-0.001	TcdA-0.1	TcdB-1e-04
G	TcdA-0.01	TcdB-1e-04	TcdA-0.01	TcdB-1e-05
H	TcdA-0.001	TcdB-1e-05	TcdA-0.001	

IMCE.txt

	5	6
A	TcdB-10	TcdB-10
B	TcdB-1	TcdB-1
C	TcdB-0.1	TcdB-0.1
D	TcdB-0.01	TcdB-0.01
E	TcdB-0.001	TcdB-0.001
F	TcdB-1e-04	TcdB-1e-04
G	TcdB-1e-05	TcdB-1e-05
H		

J774-2.txt

	1	2
A	TcdB-0.01, gdTcdB-1	TcdB-0.01, gdTcdB-1
B	TcdB-0.01, gdTcdB-0.1	TcdB-0.01, gdTcdB-0.1
C	TcdA-10, gdTcdB-100	TcdA-10, gdTcdB-100
D	TcdB-0.01	TcdB-0.01
E	TcdA-10	TcdA-10
F	gdTcdB-100	gdTcdB-100
G	gdTcdB-1	gdTcdB-1
H	gdTcdB-0.1	

J774-3a.txt

	3	4
A	TcdB-0.01, gdTcdB-1	TcdB-0.01, gdTcdB-1
B	TcdB-0.01, gdTcdB-0.1	TcdB-0.01, gdTcdB-0.1
C	TcdA-10, gdTcdB-100	TcdA-10, gdTcdB-100
D	TcdB-0.01	TcdB-0.01
E	TcdA-10	TcdA-10
F	gdTcdB-100	
G		gdTcdB-1
H	gdTcdB-0.1	gdTcdB-0.1

J774-3b.txt

	1	2
A	TcdB-1	TcdB-1
B	TcdB-100	TcdB-100
C		
D	gdTcdB-1	gdTcdB-1
E	gdTcdB-100	gdTcdB-100
F	TcdA-3	TcdA-3
G	TcdA-300	TcdA-300
H	gdTcdB-100, TcdA-10	gdTcdB-100, TcdA-10

J774-4.txt

	1	2
A	gdTcdB-100, TcdB-10	gdTcdB-100, TcdB-10
B	gdTcdB-10, TcdA-1	gdTcdB-10, TcdA-1
C	gdTcdB-100, TcdA-1000	gdTcdB-100, TcdA-1000
D	TcdA-1	TcdA-1
E	TcdA-1000	TcdA-1000
F	gdTcdB-10	gdTcdB-10
G	gdTcdB-100	gdTcdB-100
H		

J774-5.txt

	1	2
A	TcdA-1000	TcdB-1000
B	TcdA-300	TcdB-300
C		
D	TcdA-100	TcdB-100
E	TcdA-10	TcdB-10
F	TcdA-3	TcdB-3
G	TcdA-1	TcdB-1
H	TcdA-0.1	TcdB-0.1

J774-a.txt

	5	6
A	TcdA-1000	TcdB-1000
B	TcdA-300	TcdB-300
C		Other-100
D	TcdA-100	TcdB-100
E	TcdA-10	TcdB-10
F	TcdA-3	TcdB-3
G	TcdA-1	TcdB-1
H	TcdA-0.1	TcdB-0.1

J774-b.txt

	3	4
A	TcdA-1000	TcdB-1000
B	TcdA-100	TcdB-100
C	TcdA-10	TcdB-10
D	TcdA-1	TcdB-1
E	TcdA-0.1	TcdB-0.1
F		TcdB-0.01
G	TcdA-0.01	TcdB-0.001
H	TcdA-0.001	NA-NA

PMN-2a.txt

	5	6
A	TcdA-1000	TcdB-1000
B	TcdA-100	TcdB-100
C	TcdA-10	TcdB-10
D	TcdA-1	TcdB-1
E	TcdA-0.1	TcdB-0.1
F		TcdB-0.01
G	TcdA-0.01	TcdB-0.001
H	TcdA-0.001	

PMN-2b.txt

	3	4	5	6
A	IL8-110.98, TcdB-1	IL8-110.98, TcdB-1	TcdB-1	TcdB-1
B	IL8-110.98, TcdB-10	IL8-110.98, TcdB-10	TcdB-10	TcdB-10
C	IL8-110.98	IL8-110.98		
D	IL8-110.98, TcdB-100	IL8-110.98, TcdB-100	TcdB-100	TcdB-100
E	IL8-110.98, TcdB-1000	IL8-110.98, TcdB-1000	TcdB-1000	TcdB-1000
F	IL8-110.98, TcdA-1000	IL8-110.98, TcdA-1000	TcdA-1000	TcdA-1000
G	IL8-110.98, TcdA-100	IL8-110.98, TcdA-100	TcdA-100	TcdA-100
H	IL8-110.98, TcdA-10	IL8-110.98, TcdA-10	TcdA-10	TcdA-10

PMN-3.txt

	1	2	3	4
A	IL8-110.98, TcdA-10	IL8-110.98, TcdA-10	TcdA-10	TcdA-10
B	IL8-110.98, TcdA-100	IL8-110.98, TcdA-100	TcdA-100	TcdA-100
C	IL8-110.98	IL8-110.98		
D	IL8-110.98, TcdA-1000	IL8-110.98, TcdA-1000	TcdA-1000	TcdA-1000
E	IL8-110.98, TcdB-1000	IL8-110.98, TcdB-1000	TcdB-1000	TcdB-1000
F	IL8-110.98, TcdB-100	IL8-110.98, TcdB-100	TcdB-100	TcdB-100
G	IL8-110.98, TcdB-10	IL8-110.98, TcdB-10	TcdB-10	TcdB-10

PMN-4.txt

	1	2
A	TcdA-10000	TcdB-10000
B	TcdA-7000	TcdB-7000
C	TcdA-5000	TcdB-5000
D		
E	TcdB-3000	TcdA-3000
F	TcdB-1000	TcdA-1000
G	TcdB-500	TcdA-500
H	TcdB-100	TcdA-100

PMN-a.txt

	3	4
A	TcdA-10000	TcdB-10000
B	TcdA-7000	TcdB-7000
C	TcdA-5000	TcdB-5000
D		
E	TcdB-3000	TcdA-3000
F	TcdB-1000	TcdA-1000
G	TcdB-500	TcdA-500
H	TcdB-100	TcdA-100

PMN-b.txt

	3	4
A	NA-NA	NA-NA
B	TcdA-300	TcdA-1
C	TcdA-100	TcdA-0.1
D	TcdA-30	NA-NA
E	TcdA-10	
F	TcdA-3	NA-NA
G	NA-NA	NA-NA
H	NA-NA	NA-NA

T84-a.txt

	5	6
A	NA-NA	NA-NA
B	NA-NA	TcdB-1000
C	TcdB-3	TcdB-300
D		TcdB-100
E	TcdB-1	TcdB-30
F	TcdB-0.1	TcdB-10
G	NA-NA	NA-NA
H	NA-NA	NA-NA

T84-b.txt